BJRS

BRAZILIAN JOURNAL
OF
RADIATION SCIENCES
07-01A (2019) 01-10

# Study of dosimetry in CT using head phantom

A.M.L. Gómez[a]; A.P. Mourão[a, b]

[a] *Department of Nuclear Engineering, UFMG, 31270-901 Belo Horizonte, MG, Brazil*

[b] *Biomedical Engineering Center, CEFET-MG, 30480-000 Belo Horizonte, MG, Brazil*

*amlgphys@gmail.com*

---

## ABSTRACT

Non-invasive diagnosis methods based on x-ray attenuation, such as Computed Tomography (CT) has had since its discovery and the development of this technology, a rapid growth in radiology services. The quantity of dose deposited in patients, is still large, this type of examination is that reaches the highest levels of absorbed dose in the population. Legislation that regulates the levels of patient's dose is only limited to a maximum amount deposited, depending the body region to be irradiated. Therefore, it is necessary to determine the amount of absorbed dose on patients depending on the protocols of routine used in radiology services for propose an optimization of these based on the principles of radiation protection. Experiments were conducted to determine the profile of dose deposited in head routine exams for adult, using a cylindrical head phantom made of polymethylmethacrylate (PMMA). This standard phantom has four openings in peripheral and one central. Radiochromic film strips were introduced into each one of these openings to register the longitudinal dose profile in each region to determine the amount of deposited dose in the volume of the head phantom. A CT scanner with 64 channels of GE from the radiology department was used for scanning the head phantom. The scanning were done with voltages of 80, 100 and 120 kV, and dose index found were between 6.24 and 23.73 mGy. Analysis of image quality was performed, finding that all scan comply with the parameters acceptable in diagnosis for Brazilian legislation. It is propose an optimized protocol for exams by CT head for the voltage of 80 kV and images with 0.5% of noise index.

*Keywords:* dosimetry, computed tomography, phantom

---

ISSN: 2319-0612
Accepted 2018-05-07

## 1. INTRODUCTION

The processes of medical imaging are used in the diagnosis of the development of different lines of research in areas such as engineering, science and medicine, in order to obtain detailed information of the different tissues, organs and physiological processes present in the human body through various techniques (Dhawan, 2011). The developments of non-invasive techniques for the detection of different types of diseases, among them are X-ray attenuation techniques.

The protocols on which they are based, as a result of a series of investigations in which it is sought to maintain the improvement of the image quality in order to reduce the risks to the health of patients and workers exposed to ionizing radiation. Therefore, analyses of mass, volume, deposited dose and contrast of the acquired image are factors of great importance in the process of diagnostic optimization using protocols for obtain images with quality (Dalmazo, 2010).

The adoption of computed systems allowed a significant advance in the quality of the diagnosis processes by images, and thus, increasing the diagnostic applications. However, these principles in technology have brought with them new challenges in relation to the validation of the image acquisition processes (Andisco, et al, 2014). Computed Tomography (CT) uses the principle of X-ray attenuation for the acquisition of diagnostic images. Since its discovery in the 1970s, it has become one of the most important methods of diagnostic imaging, since it allows the observation of structures of low contrast, like soft tissues (Biester, *et al.*, 2012; Andrade, 2008; Calzado *et al.*, 2010).

The development of technologies associated with CT scanners which allows a greater speed of data acquisition, greater efficiency and precision in the representation of structures, bring with them an increase in the risks for the individuals exposed to this examination. CT test is the radio diagnostic exam was responsible for being the largest contributor in doses in the population compared to the other existing techniques (Augusto, 2009).

## 2. MATERIALS AND METHODS

### 2.1.CT scanner

The CT scan of radiodiagnostic services was used in an institution with an agreement for the development of research, in the city of Belo Horizonte (MG-BR). The scanner is of multi-slice type that allows realizing explorations in helical mode.

The experiments were performed on a head phantom in cylindrical shape of 16 cm in diameter and 15 cm in length, made of polymethylmethacrylate (PMMA). The cylinder has five openings, four at the periphery which are offset from one another by 90°, and one central. The openings are 1.25 cm in diameter and 15 cm in length. The center of the peripheral openings is 1 cm from the surface. The head phantom was placed in the isocenter of the gantry aligning the openings similarly as the positions 3, 6, 9 and 12 of an analog clock, through the help of the equipment positioning lasers. The Figure 1 shows the head phantom placed in the isocenter of the gantry of the CT scanner.

**Figure 1.** Phantom head in the isocenter gantry.

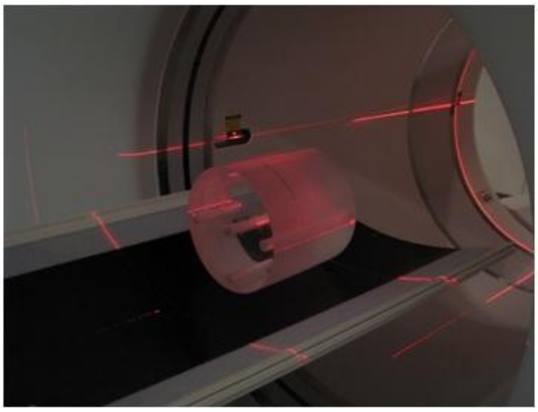

Dose measurements were performed using the GAFCRHOMIC XR-QA2 radiochromic film. The film leave was cut in strips measuring 0.5 x 12.5 cm and placed into special rods, also made of

PMMA, developed to accommodate these strips. The Figure 2 shows one of the rod loaded with one of the radiochromic film strip.

**Figure 2.** Rod charged with radiochromic film strip.

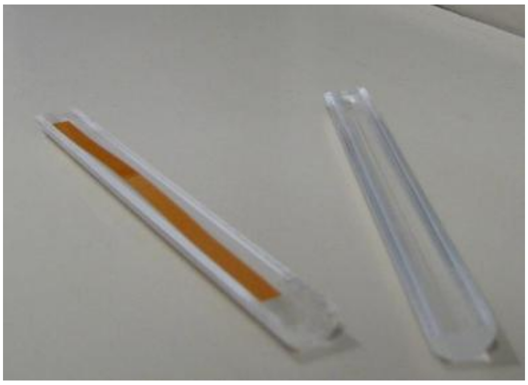

A RADCAL ACCU-GOLD, 10X6-3CT pencil ionization chamber with a range detection from 200 nGy to 1 kGy was used to obtain the dose deposited on the head phantom. This chamber has 4% uncertainty for X-rays generated with voltages up to 150 kV (Radcal, 2015).

### 2.2.Methodology

The protocols used in helical mode scans are described in the Table 1.

**Table 1.** Acquisition Protocols.

| Voltage (kV) | Charge (mA.s) | Beam thickness (mm) | Pitch |
|---|---|---|---|
| 80 | | | |
| 100 | 100 | 40 | 0.984 |
| 120 | | | |

The rods loaded with the radiochromic film strips were positioned inside the head phantom to make a scan of 10 cm in length in its central region programming the equipment in helical mode. The strips present a darkening proportional to the amount of energy deposited when exposed to radiation (Tawfik, 2012). Figure 3 shows a non-irradiated strip (a) and a radiated strip (b) digitized and processed in grayscale.

**Figure 3.** Radiochromic film strip non-irradiated (a) and irradiated (b).


After the exposition, the strips were digitized and processed to obtain the darkening intensity values and then, these values were converted to dose values in mGy. The dose values were corrected considering the coefficients of linear attenuation for X-rays with energies of 50, 60 and 80 keV (NIST, 2015). For the analysis and validation of the image quality, the image of the central slice was selected in order to study the interference of the secondary radiation that it generates. For this, four regions of interest (ROIs) were defined in the image to be compared within the parameters of diagnostic image quality.

## 3. RESULTS AND DISCUSSIONS

The volumetric CT dose index ($CTDI_{vol}$) were calculated using the average values of the central region in each of the positions where the film strips were placed. The expression by which the values of $CTDI_{vol}$ were calculated was:

$$CTDI_{vol} = \frac{1}{3}(CTDI_{100,central} + 2 * CTDI_{100,per}) \quad (1)$$

Where $CTDI_{100,\ central}$ is the dose index value found at the central position and $CTDI_{100,\ per}$ is the average dose index value at the peripheral positions of the head phantom. The dose index values calculated with equation (1) for each one voltage values are described in Table 2.

**Table 2.** Volumetric dose index values.

| **Voltage (kV)** | **CTDIvol (mGy)** |
|---|---|
| 80 | 6.24 |
| 100 | 13.25 |
| 120 | 23.73 |

For the same charge (100 mA.s) the dose index were proportional to the increase in the voltage values of the X-ray tube, experiencing an increase in dose in relation to the lowest calculated dose value of 112.33% and 280.28%, respectively.

The dose profiles found for each one of the positions were referenced to perform the calibration of the radiochromic film strips and to perform the conversion of intensity values in grayscale for absorbed dose. The absorbed dose profiles for the voltage values of 80, 100 and 120 kV are presented in Figure 4.

**Figure 4.** Absorbed dose profile for 80, 100 and 120 kV.

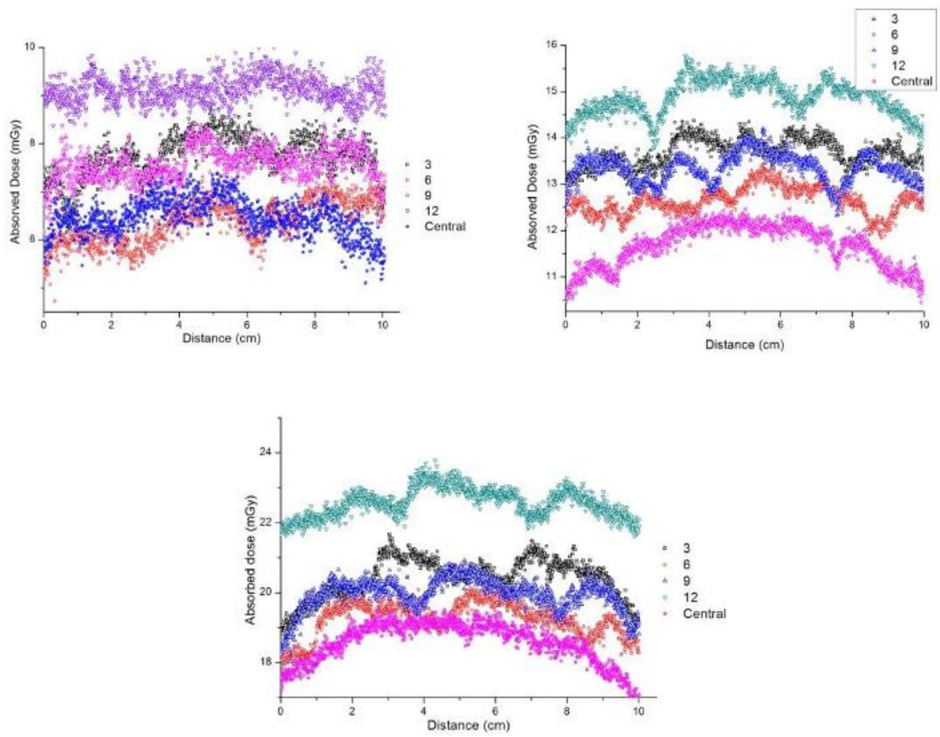


The lowest dose value recorded with a voltage value of 80 kV was 6.36 ± 0.45 mGy at position 6. At position 12 the highest dose value was recorded, which was 9.13 ± 0.28 mGy , with a difference of 43.55% between them. For the 100 kV voltage, the lowest recorded value was in the central position of 11.65 ± 0.46 mGy, with a difference of 27.47% with the highest recorded value of 14.85 ± 0.38 mGy in the position 12. With the equipment programmed at 120 kV voltage, the highest dose value was recorded at position 12 with 22.57 ± 0.41 mGy, being 21.74% higher than the lowest dose recorded in the central position with 18.54 ± 0.59 mGy.

The noise was calculated as the percentage value of the standard deviation in relation to the average value of Hounsfield (HU) scale intensity. Equation (2) defines the percentage noise value for each selected region of the image.

$$Noise(\%) = \frac{SD}{Average + 1000} * 100 (2)$$

Therefore, the calculation was performed in each of the four ROIs selected in the central slice image. The results are shown in Table 3.

**Table 3.** Percentage noise index.

| **Region** | **Noise (%)** | | |
|---|---|---|---|
| | **80 kV** | **100 kV** | **120 kV** |
| 1 | 9.31 | 6.32 | 5.03 |
| 2 | 9.48 | 6.24 | 5.04 |
| 3 | 9.56 | 6.08 | 5.29 |
| 4 | 9.65 | 6.49 | 5.30 |
| **Average** | 9.50 | 6.28 | 5.16 |
| **DS** | 0.15 | 0.17 | 0.15 |

It is possible to observe that the images present greater noise for the voltage of 80 kV than for 120 kV, verifying that, for lower voltage levels, the percentage of quantum noise recorded in CT images is higher and must be compensated by increasing of the X-ray tube current (mA). In order to corroborate the possibility of reducing the dose in head examinations in adult patients, the protocols for this type of examination were verified using optimized values of current (mA), obtaining noise smaller then 1%. For this, the automatic exposure control tool was used to determine the ideal current for a fixed noise value. Therefore, it was defined in noise index tool the of this CT scanner the value of 5.9, because that represents a noise smaller then 1% for an image reconstruction of 40 mm. Defined these electrical current values the noises were next to 0.5%. Tab. 4 shows the optimized acquisition parameters of voltage, current, tube time and charge in helical mode for a pitch 0.984, and dose index obtained for routine protocols of the radiodiagnostic service and for the optimized protocol that is proposed.

**Tab. 4** Routine and optimized protocols for head CT scans.

| Protocol | Voltage (kV) | Courrent (mA) | Rotation time (s) | Charge (mA.s) | CTDIvol (mGy) |
|---|---|---|---|---|---|
| Routine | 120 | 200 | 0.5 | 100 | 23.73 |
| Optimized | 120 | 200 | 0.8 | 160 | 37.97 |
| | 100 | 300 | 0.8 | 240 | 32.71 |
| | 80 | 450 | 0.8 | 360 | 23.40 |

As the routine protocol studied for this equipment presented a noise of about 5.16 %, it was decided to optimize that protocol both to reduce the deposited dose and to improve the image quality. When comparing the results, it can be verified that the protocol optimized for 80 kV there is a dose reduction of 1.39% in relation to the routine protocol, but this protocol has a smaller noise.

## 4. CONCLUSIONS

The irradiations of the central region of the head phantom, using radiochromic film strips, allowed to observe that when using the parameters of the radiodiagnostic service (120 kV voltage), there is a greater dose deposition in comparison to the other parameters used in this study.

Despite the increase in the percentage of noise in the images due to the reduction in the voltage values of the tube, the images were within the limits of the percentage of noise acceptable for diagnosis.

The results obtained allow us to conclude that the routine protocols defined for head examinations in adult patients still deposit high doses of radiation, regardless of whether the equipment has the automatic control system, since head examinations do not use automatic exposure control, due to the fact that the diameter of the skull does not vary considerably. However, the dose values found are within the reference value that is 50 mGy for routine headache established by Brazilian legislation.

## 5. ACKNOWLEDGMENT

The authors thank the Technology in Molecular Medicine Center (INCT-MM) of the UFMG that contributed to the development of this study.

## REFERENCES

ANDISCO, D.; BLANCO, S.; BUZZI, A. Dosimetría en tomografía computada. ***Revista Argentina de radiología***, Elsevier, v. 78, n. 3, p. 156–160, 2014.

ANDRADE, M. E. A. Avaliação da qualidade de imagem e do índice volumétrico de kerma ar em tomografia computadorizada (cvol) em recife. ***Universidade Federal de Pernambuco***, 2008.

AUGUSTO, F. M. Estudo da qualidade da imagem e índices de dose em tomografia computadorizada. Tese (Doutorado) — ***Universidade Federal do Rio de Janeiro***, 2009.

BEISTER, M.; KOLDITZ, D.; KALENDER, W. A. Iterative reconstruction methods in x-ray ct. ***Physica medica***, Elsevier, v. 28, n. 2, p. 94–108, 2012.

CALZADO, A.; GELEIJNS, J. Tomografía computarizada. evolución, principios técnicos y aplicaciones. Revista de Física Médica, v. 11, n. 3, 2010.

DALMAZO, J. *et al*. Otimização da dose em exames de rotina em tomografía computadorizada: estudo de viabilidade em um hospital universitário. ***Radiologia Brasileira***, Colégio Brasileiro de Radiologia e Diagnóstico por Imagem, v. 43, n. 4, p. 241–248, 2010.

DHAWAN, A. P. Medical Image Analysis. [S.l.]: ***IEEE***, 2011. 88-93 p.

RADCAL, C. **ACCU-GOLD** *User Guide*. [S.l.], 2015.

TAWFIK, G. et al. Characteristics of gafchromic xrqa2 films for kv image dose measurement. ***Medical Physics***, v. 39, n. 2, 2012.

National Institute of Standards and Technology. *www.nist.gov*, access January 30th. 2015.

ISSN: 2572-3235

Santos and Mourão. Int J Radiol Imaging Technol 2022, 8:099
DOI: 10.23937/2572-3235.1510099
Volume 8 | Issue 2
Open Access

International Journal of
Radiology and Imaging Technology

ORIGINAL ARTICLE

# Dose Evaluation of Head CT Scans Using Phantom for Optimization Protocols

Check for updates

***Fernanda Stephanie Santos** and Arnaldo Prata Mourão***

*Department of Nuclear Engineering, Federal University of Minas Gerais, CEP: 31270-970, Belo Horizonte, MG, Brazil*

***Corresponding author:** *Fernanda Stephanie Santos, Department of Nuclear Engineering, Federal University of Minas Gerais, CEP: 31270-970, Belo Horizonte, MG, Brazil*

**Abstract**

Computed Tomography (CT) scans promote a higher dose deposition than conventional radiology exams. These tests contribute significantly to the increase in the patient and collective dose, being a public health concern worldwide. There is a great need to improve protocols to seek lower doses while maintaining the diagnostic image quality. The development of phantoms allows the testing of different acquisition protocols. For this, the phantoms must present an absorption characteristic of the X-ray beam similar to the represented patient. In this study were tested two cylindrical head phantoms of polymethylmethacrylate (PMMA). One CT head phantom is the head standard test with 16 cm in diameter and the other head phantom developed is smaller at 12 cm in diameter. Both phantoms are 15 cm long. Different acquisition protocols were performed on a GE CT scanner, LightSpeed VCT model with 64 channels. The central slice of the phantoms was irradiated successively, and using a pencil ionization chamber, to obtain the CT air *kerma* indexes in PMMA ($C_{k,PMMA,100}$) and CT dose indexes (CTDI). From these results, the CT Dose Index values weighted and volumetric ($CTDI_w$, $CTDI_{vol}$) were obtained for 10 cm scans of the central region of the head phantoms, in helical mode. The scans were performed using different voltage values (80, 100 and 120 kV) and charge (mA.s). Absorbed dose values ($CTDI_{vol}$) using routine protocols for head scans ranged from 39.22 to 49.67 mGy. Proposed optimized protocols varied from 20.89 to 31.93 mGy and reduced the absorbed dose by up to 57.94% in the smallest phantom, with 12 cm in diameter.

**Keywords**

Computed tomography, Phantom, Dosimetry

## Introduction

Computed Tomography (CT) is one of the most used exams for radiologic diagnostic in medicine. It is a very fast test that can produce high quality images. However, the increasing demand for CT had a considerable impact on doses provided to patients and on the exposure of the population as whole, being a public health concern worldwide [1,2]. According to UNSCEAR report the use of CT contributed with 62% of the collective dose from diagnostic radiological tests [3]. Many factors collaborated to the increased demand for CT scans, including the constant technological evolution of the equipment associated to greater availability and a relative tendency to decrease exam costs [4,5].

Patients undergoing CT scans can range from neonates to oversized adults. However, radiation doses in CT are generally measured in cylindrical PMMA phantoms, that represent a standard adult patient. These phantoms are designed to simulate a head, 16 cm in diameter, and a body, 32 cm [6,7].

It is difficult to obtain reliable quantitative values of patient doses from any measurements performed in these standard phantoms, because patients have sizes and body compositions that can differ markedly from the phantoms, such as pediatric and obese patients. The development of phantoms allows testing different acquisition protocols [8,9]. For this, the phantoms must have an X-ray beam absorption characteristic similar to the represented patient.

The increasing demand for CT scans in pediatric patients is mainly due to the high rates of traumatic injuries from car accidents, falls on bicycles, blunt trauma, traumatic brain injury, as well as a significant increase in the incidence of childhood neoplasms, being the CT images used in the diagnostic process. Therefore,

CLINMED INTERNATIONAL LIBRARY

**Citation:** Santos FS, Mourão AP (2022) Dose Evaluation of Head CT Scans Using Phantom for Optimization Protocols. Int J Radiol Imaging Technol 8:099. doi.org/10.23937/2572-3235.1510099

**Accepted:** December 22, 2022; **Published:** December 24, 2022

acquisition protocols should be used that determine the reduction of the radiation dose without compromising the diagnostic quality [10,11].

The risks of stochastic effects increase in children due to the tissue radiosensitivity allied to the long-life expectancy. The dose deposited in a pediatric patient is directly related to the energy that was retained during the process of exposure to ionizing radiation [12,13].

In this study, two CT head phantoms were used, the standard head phantom and another with smaller volume to observe the dose distribution and to obtain the dose index (CTDI). Also, different acquisition protocols were tested using different values of X-ray tube supply voltage (80, 100 and 120 kV) and load (mA.s).

## Materials and Methods

The experiment was conducted using a GE CT scanner, LightSpeed VCT model with 64 channels. For the development of this work, experimental measures have been obtained using two head phantoms, both made in polymethyl-methacrylate (PMMA). These phantoms were constructed by the research team of the Center for Research in Biomedical Engineering (CENEB) of the Federal Center for Technological Education of Minas Gerais (CEFET-MG), being a representative of a standard adult and a pediatric patient's head. The standard adult head phantom is cylinder with 16 cm in diameter and 15 cm in length. This phantom is considered the default for the dose reference in head CT scans. The pediatric head phantom is cylinder and has a dimension of 12 cm in diameter and 15 cm in length, representing a smaller head, like a pediatric patient.

This cylindrical phantom has five openings for positioning the dosimeters, one central and four at the peripheral openings, which are displaced from each other by 90°. The openings are 1.27 cm in diameter and 15 cm in length. The center of the peripheral openings is 1 cm from the edge of the phantom. The Figure 1 shows an illustration with the measurements of the adult and pediatric phantoms made with PMMA.

The standard adult head phantom is considered for dose reference in head CT scans. Therefore, all head CT scans performed on a given equipment are accompanied by a report that informs an estimated value of patient absorbed dose (CTDI) based on the scan of this phantom. The Figure 2 shows the image of these phantoms placed in the isocenter of the gantry of the CT scanner.

Dose measurements have been performed by positioning the head phantom in the isocenter of the gantry and aligning the openings like as the positions 3, 6, 9 and 12 of an analog clock, through the help of the CT scanner lasers. The phantom openings are filled with PMMA rods which must be removed one by one for the positioning of the pencil chamber, targeting the dose measurements in the five regions.

A pencil ionization chamber RADCAL ACCU-GOLD model 10X6-3CT was used to measure a CT air *kerma* in PMMA ($C_{k,\ PMMA,100}$) in each opening of both phantoms. First, a scout was made in order to check the correct alignment of the phantoms as well as to demarcate the central slice position. Furthermore, the central slice of the phantoms was irradiated successively. For each chamber positioning, five measurements were performed, getting a minimum of 25 measurements for each protocol and for each phantom. In the central slice irradiations, the remaining openings were filled using PMMA rods. From these results, the CT Dose Index values, weighted and volumetric ($CTDI_w$, $CTDI_{vol}$), were obtained for 10 cm scans of the central region of the head phantoms, in helical mode. The $CTDI_w$ and $CTDI_{vol}$ were calculated according to the Eq. 1 and 2 [13,14]:

$$CTDI_w = \frac{1}{3} \cdot \left( CTDI_{100,central} + \frac{2}{3} \cdot CTDI_{100,per} \right) \quad (1)$$

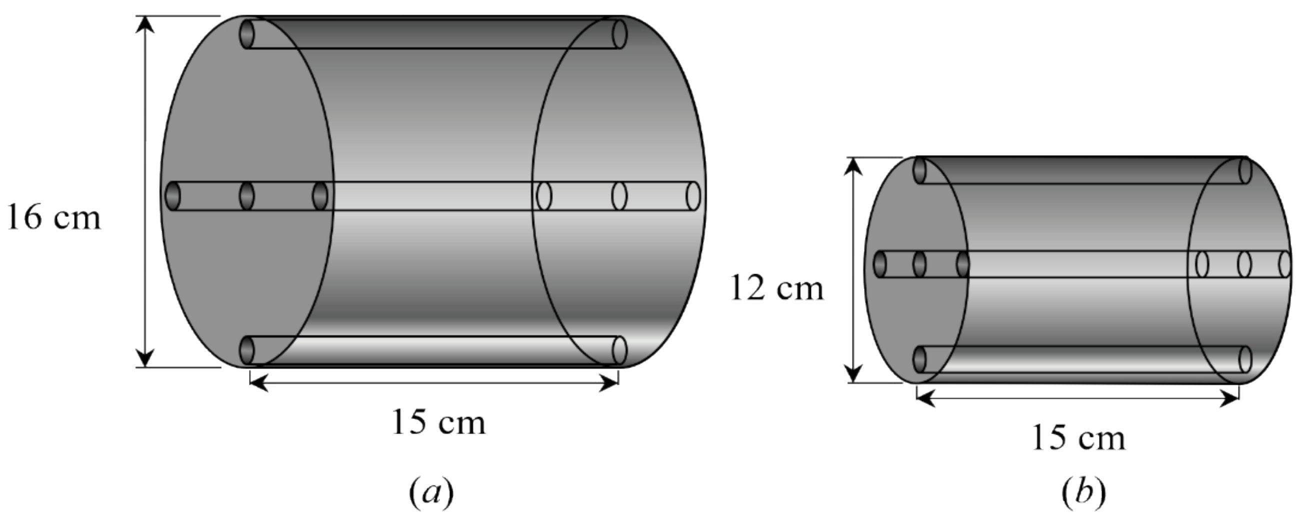


**Figure 1:** Head phantoms dimensions: (a) Adult standard and (b) Pediatric.

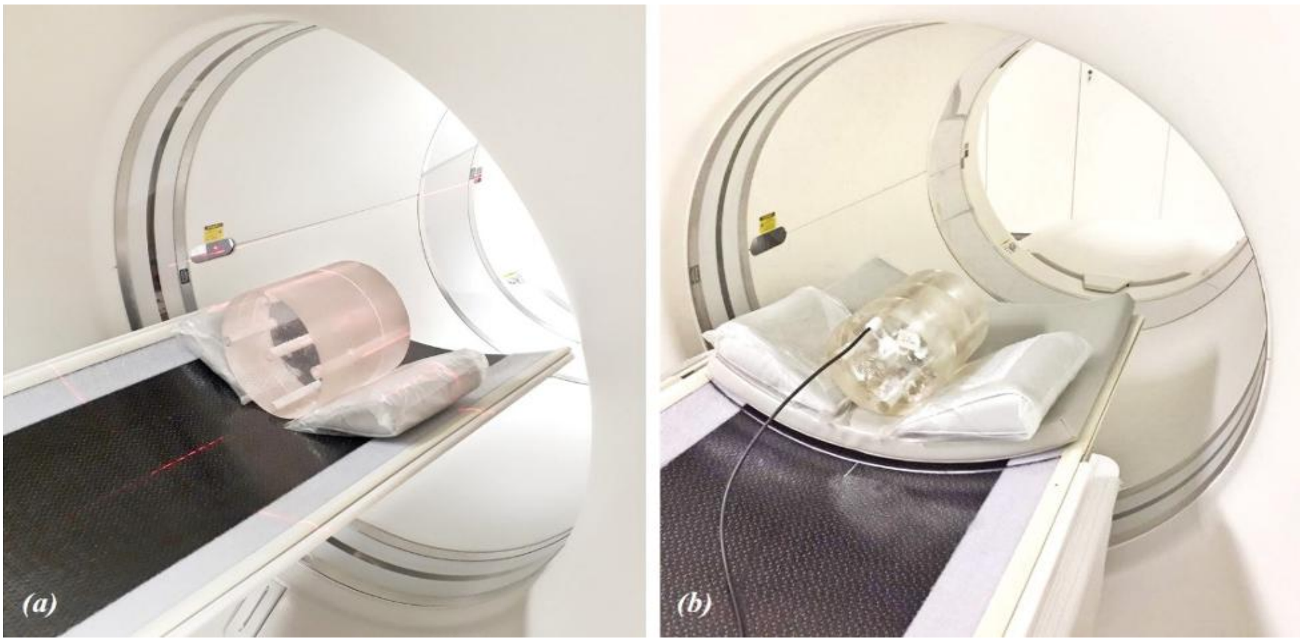


**Figure 2:** PMMA head phantom images: (a) Adult standard and (b) Pediatric.

**Table 1:** Routine protocol of CT head scan.

| Voltage (kV) | Current (mA) | Charge (mA.s) | Tube time (s) | Beam Thickness (mm) | Pitch | Reconstruction (mm) |
|---|---|---|---|---|---|---|
| 120 | 200 | 100 | 0.5 | 40 | 0.984 | 1.25 |

$$CTDI_{vol} = \frac{CTDI_w}{pitch} \quad (2)$$

where, $CTDI_{100,\ central}$ is the dose index value found at the central position and $CTDI_{100,\ per}$ is the average dose index value at the peripheral positions of the head phantom. The scans were performed using different voltage values (80, 100 and 120 kV) and charge (mA.s). In order to obtain the CT Dose Index (CTDI) values from the air kerma values the measurements were adjusted using a conversion factor ($F_c$) air/PMMA. The $F_c$ used are 1.0418, 1.0324, and 1.0106 for the X-ray beam generated with 120, 100 and 80 kV, respectively [14-16].

The protocol for irradiation the phantom central slice, in axial mode, used the following parameters: Current of 100 mA, charge of 100 mA.s, tube rotation time of 1s, beam thickness of 10 mm and three voltage values (120, 100 and 80 kV).

Helical scans of 10 cm in length were also performed in the central region of the head phantoms, aiming to define a current value adjusted by the equipment's automatic exposure control (auto mA), using the different voltage values. Usually, in the initial slices of the scan there is an adjustment in the current value (mA) in the first slices irradiated and after these adjustments the current stabilizes, since all the slices of the phantom have the same size.

With the current reference value defined based on the current recorded in the central slice, new scans were made to test fixed current values, lower than the value suggested by the automatic current control scan. For each current value tested, noise was calculated in the image of the central slice and the best current value was determined for each phantom and voltage.

The protocols used in the scans of the central region of the phantom used pitch values closest to 1, that is available in the CT equipment. Table 1 shows the CT head scanning protocol used in the service routine, regardless of the patient's size or age.

In order to validate the quality of the CT images, a noise analysis of the central slice image was performed in each helical CT scan, aiming at maintaining the diagnostic quality of the images. The noise value had its maximum acceptable limit of 1%, considering that the phantom is homogeneous [15-17]. This noise limitation, using a homogeneous material, implies in the generation of diagnostic images of the human body. Then, as a control parameter for testing new protocols, it was defined that the noise threshold in the central slice image should be 1% to guarantee the diagnostic quality of the patient's image.

Four regions of interest (ROI) were selected in the image and were analyzed. The noise (N) was calculated as the percentage value of the standard deviation in relation to the average value of the Hounsfield scale (HU) through Equation 3.

**Table 2:** Values of $C_{k,100,\ PMMA,}$ $C_w$ and $CTDI_w$ in mGy standard deviation for head phantoms.

| Position | Phantom | | | | | |
|---|---|---|---|---|---|---|
| | Adult standard (16 cm) | | | Pediatric (12 cm) | | |
| | 120 kV | 100 kV | 80 kV | 120 kV | 100 kV | 80 kV |
| Central | 17.52 ± 0.03* | 11.28 ± 0.09 | 5.94 ± 0.01 | 22.99 ± 0.07 | 14.84 ± 0.06 | 8.02 ± 0.04 |
| 3 | 19.48 ± 0.02 | 12.94 ± 0.22 | 7.10 ± 0.06 | 23.84 ± 0.24 | 15.57 ± 0.14 | 8.61 ± 0.10 |
| 6 | 18.17 ± 0.09 | 11.98 ± 0.11 | 5.84 ± 0.02 | 21.98 ± 0.18 | 14.24 ± 0.15 | 7.72 ± 0.08 |
| 9 | 19.04 ± 0.04 | 12.83 ± 0.08 | 6.94 ± 0.06 | 23.67 ± 0.22 | 15.46 ± 0.08 | 8.61 ± 0.09 |
| 12 | 21.39 ± 0.38 | 14.10 ± 0.08 | 8.93 ± 0.10 | 25.26 ± 0.54 | 17.29 ± 0.22 | 9.87 ± 0.13 |
| Cw(mGy) | 18.85 ± 0.10 | 12.40 ± 0.11 | 6.69 ± 0.04 | 23.46 ± 0.39 | 15.37 ± 0.12 | 8.47 ± 0.08 |
| $CTDI_w$(mGy) | 19.64 ± 0.10 | 12.80 ± 0.12 | 6.76 ± 0.04 | 24.44 ± 0.40 | 15.87 ± 0.12 | 8.56 ± 0.08 |

*Standard deviation

**Table 3:** Routine and optimized protocols.

| Phantom | Protocol | Voltage (kV) | Charge (mA.s) | $CTDI_{VOL}$ (mGy) |
|---|---|---|---|---|
| Adult (16 cm) | Routine | 120 | 200 | 39.92 ± 0.21* |
| | Opt. 1 | 120 | 160 | 31.93 ± 0.16 |
| | Opt. 2 | 100 | 240 | 31.22 ± 0.28 |
| | Opt. 3 | 80 | 420 | 28.87 ± 0.18 |
| Pediatric | Routine | 120 | 200 | 49.67 ± 0.82 |
| | Opt. 4 | 120 | 100 | 24.83 ± 0.41 |
| | Opt. 5 | 100 | 144 | 23.23 ± 0.18 |
| | Opt. 6 | 80 | 240 | 20.89 ± 0.20 |

*Standard deviation

$$N\% = \frac{SD}{\overline{HU} + 1000} \cdot 100 \qquad (3)$$

## Results

### Dose measurements

Table 2 shows the average values and standard deviation of punctual and weighted air kerma in PMMA ($C_{k,100,PMMA}$ and $C_w$) and absorbed dose ($CTDI_w$) that were obtained from $C_{k,100,PMMA}$ measured in the five positions of the phantoms, using the parameters defined for the central slice (10 mm) irradiation with the charge fixed in 100 mA.s.

The protocol using the voltage of 120 kV has the highest absorbed dose value recorded in position 12 of 21.39 mGy in the adult phantom and 25.26 mGy on the pediatric phantom. The minimum value happened in the position 6 for both phantoms with the 80 kV voltage, with the value of 5.84 mGy in adult and 7.72 in pediatric phantom. The proximity between the doses at points 3 and 9 indicates the good positioning of the object in the gantry isocenter.

Analyzing the measurements obtained, the pediatric phantom has dose values always higher, since the other parameters of central slice irradiation is the same. The cut area of the pediatric phantom is smaller than the adult, promoting a higher dose deposition. Also, with the voltage of 80 kV the values are always the lowest since the other parameters used were the same. Since average energy of the beam of 80 kV is lower, promoted smaller doses deposition. Although, the 120 kV voltage generates the highest dose depositions.

### Optimized CT scan protocols

Table 3 shows the results of absorbed doses ($CTDI_{vol}$) and standard deviation obtained when it was used the routine and optimized protocols in both phantoms with the use different voltage values and optimized charge in the X-ray tube during the scans of the central region of the phantoms. In optimized protocols, the optimized charge value (mA.s) was adjusted to the point where the noise in the central slice was less than 1%. The other parameters: Pitch, tube rotation time, beam thickness and image reconstruction were the same of the routine protocol (Table 1).

In the tests for new protocols, it was decided to use same pitch of 0.984 of the routine protocol, which is the closest possibility to the value 1 available in this CT machine.

The absorbed doses of the new protocols tested in the adult standard head phantom varied from 28.87 to 31.93 mGy, with the lowest dose occurring with the Opt. 3 protocol that use a voltage of 80 kV and 420 mA.s. The noise value verified in the central image of this scan was 0.978%, which is the established criterion for maintaining the diagnostic quality of the image. The Opt. 3 protocol promoted a dose reduction in the patient of 27.68%, with the absorbed dose going from 39.92 to 28.87 mGy.

In the pediatric phantom with 12 cm, the lowest absorbed dose was 20.89 mGy for the Opt. 6 protocol of 80 kV, 240 mA.s. The noise value verified in the central image of this scan was 0.929%, which is the established criterion for maintaining the diagnostic quality of the image. The Opt. 6 protocol promoted a dose reduction in the pediatric phantom of 57.94%, with the absorbed dose going from 49.67 to 20.89 mGy. Also, the absorbed dose in the routine of the pediatric phantom had a dose of 19.63% higher than the adult phantom. The Figure 3 shows a graphic with the absorbed dose values ($CTDI_{vol}$) for the adult and pediatric phantom considering the different protocols defined in Table 3.

Observing the absorbed dose values obtained for the tested protocols, it is verified that the adult and pediatric phantom had a better CT scan with the voltage of 80 kV. The optimized protocols selected with the low absorbed dose obtained noise values below 1%, being a good alternative to be used aiming the reducing of absorbed dose of the patient and maintaining the diagnostic quality of the image.

It is also worth noting that the tested protocols showed in Table 3 were selected among several others tested with the variation of the mA.s value until a noise low than 1% was obtained in the analysis of the image of the central slice. The mA.s and pitch variation cannot be chosen randomly, since there are discrete values in the CT equipment menu that are possible to be tested.

## Conclusions

Patients undergoing CT scans can range from newborns to large adults. However, CT radiation doses are usually measured on PMMA phantoms representing a standard adult patient. It is difficult to obtain reliable quantitative values of patient doses from any measurements performed on this standard head phantom because patients have body sizes and compositions that may differ from the standard phantom, as is the case for pediatric patients, small women, and patients bigger and obese. Therefore, the development of the phantoms used in this work allows representing different sizes of patients and testing different acquisition protocols for head scans.

This work highlights relevant information on dose reduction in adult and pediatric head CT scans, being of great importance to argue for the adoption of optimized protocols without losing the diagnostic image quality.

## Acknowledgments

This study was financed in part by the Coordenação de Aperfeiçoamento de Pessoal de Nível Superior - Brasil (CAPES) - Finance Code 001. Also, this work was supported by the FAPEMIG.

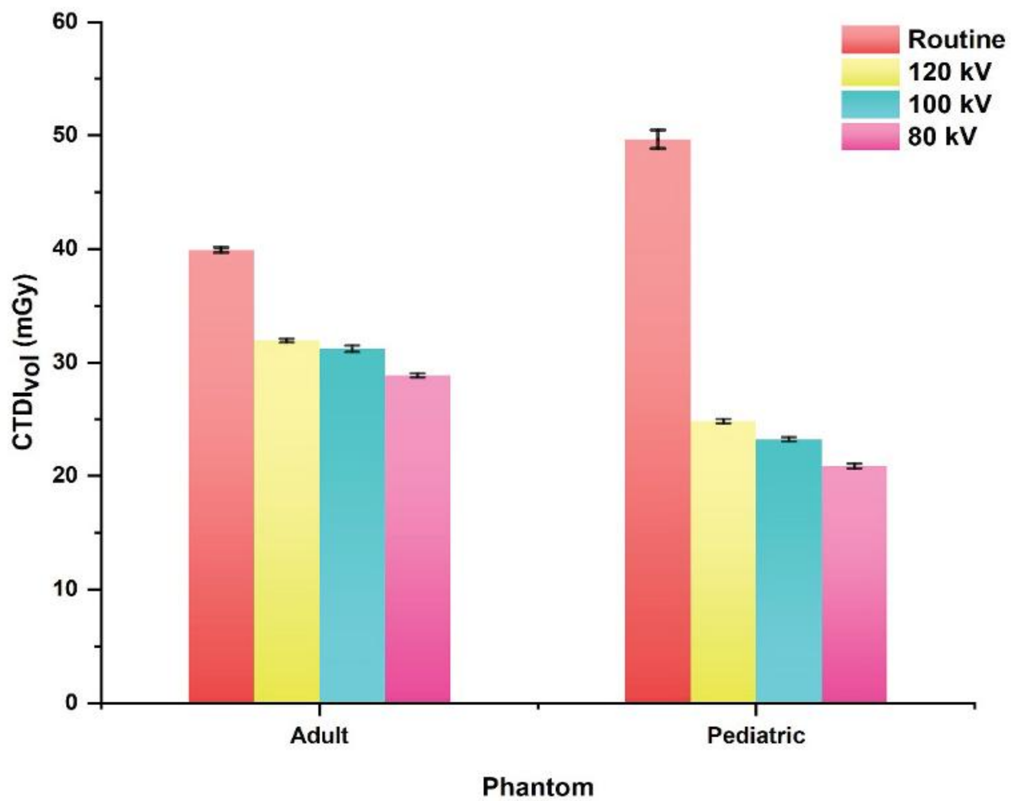


**Figure 3:** $CTD_{lvol}$ values for adults and pediatric head phantoms obtained with routine and optimized protocols.

## References


1. Aburjaile WN, Mourao AP (2017) Development of a chest phantom for testing in Computed Tomography scans. Radiation Physics and Chemistry 140: 275-277.
2. Goo HW (2012) CT radiation dose optimization and estimation: An update for radiologists. Korean J Radiol 13: 1-11.
3. (2022) UNSCEAR - United Nations Scientific Committee on the Effects of Atomic Radiation et al. Sources, Effects and Risks of Ionizing Radiation, United Nations Scientific Committee on the Effects of Atomic Radiation (UNSCEAR) 2020/2021 Report, Volume I: Report to the General Assembly, with Scientific Annex A-Evaluation of Medical Exposure to Ionizing Radiation. 354.
4. Mathews JD, Butler MW, Wallace AB, McGale P, Bickerstaffe AC (2013) Cancer riskin 680 000 people exposed to computed tomography scans in childhood or adolescence: Data linkage study of 11 million Australians. BMJ 346: 1-18.
5. Mourão AP (2018) Tomografia computadorizada: Tecnologias e aplicações. Difusão Editora.
6. Yang C-C (2020) Evaluation of impact of factors affecting CT radiation dose for optimizing patient dose levels. Diagnostics 10: 787.
7. Alonso TC, Filho APM, Da Silva TA (2018) Measurements of air kerma index in computed tomography: A comparison among methodologies. Appl Radiat Isot 138: 10-13.
8. AAPM - American Association of Physicists in Medicine (2010) Comprehensive methodology for the evaluation of radiation dose in x-ray computed tomography. Report of AAPM Task Group 111: The Future of CT Dosimetry.
9. Miglioretti DL, Johnson E, Williams A, Greenlee RT, Weinmann S, et al. (2013) The use of computed tomography in pediatrics and the associated radiation exposure and estimated cancer risk. JAMA Pediatr 167: 700-707.
10. Finatto JA, Froner APP, Pimentel J, da Silva AMM (2015) Estudo comparativo de descritor de dose em exames pediátricos de tomografia computadorizada. Brazilian Journal of Radiation Sciences 3: 24-32.
11. IAEA - International Atomic Energy Agency (2007) Dosimetry in diagnostic radiology: an international code of practice. Technical Reports Series No. 457, Viena, 359.
12. Mourão AP (2018) Tomografia computadorizada: Tecnologias e aplicações. Difusão Editora, 2018.
13. Mourão AP, Aburjaile WN, Santos FS (2019) Dosimetry and Protocol Optimization of Computed Tomography Scans using Adult Chest Phantoms. Int J Radiol Imaging Technol 5: 1-6.
14. Spampinato MV, Stalcup S, Matheus MG, Byington K, Tyler M, et al. (2018) Radiation dose and image quality in pediatric head CT. Radiat Prot Dosimetry 182: 310-316.
15. Gomez AML (2017) Estudo de dosimetria e qualidade de imagem em varreduras de tomografia computadorizada de cabeça utilizando objeto simulador. Master degree, Universidade Federal de Minas Gerais, Minas Gerais, Brasil.
16. NIST - National Institute of Standard and Tecnology (2020) Values of the mass attenuation.
17. ICRP- International Commission on Radiological Protection (2002) Diagnostic reference levels in medical imaging: review and additional advice. Oxford, 14.

Artigo Original

Revista Brasileira de Física Médica (2023) 17:706

# Study of CT Acquisition Protocols Using Two Head Phantoms

## Estudo de protocolos de aquisição de TC usando simuladores de duas cabeças

Fernanda S. Santos[1], Fernando A. Oliveira[2], Arnaldo P. Mourão[1]

[1]Departamento de Engenharia Nuclear, Universidade Federal de Minas Gerais, Belo Horizonte, Brasil
[2]Secretaria Municipal de Saúde, Prefeitura Municipal de Belo Horizonte, Belo Horizonte, Brasil

**Resumo**

Os exames de Tomografia Computadorizada (TC) promovem uma deposição de dose maior do que os exames de radiologia convencionais. Esses exames aumentaram significativamente as doses dos pacientes e a dose coletiva, se tornando uma preocupação de saúde pública global. Há uma grande necessidade de aprimorar protocolos para buscar doses menores mantendo a qualidade da imagem diagnóstica. O desenvolvimento de objetos simuladores permite testar diferentes protocolos de aquisição. Neste estudo foram testados dois objetos cilíndricos simuladores de cabeça de polimetilmetacrilato (PMMA). Um dos objetos simuladores de cabeça de TC é o modelo padrão de cabeça com 16 cm de diâmetro e o outro objeto simulador de cabeça desenvolvido é menor com 12 cm de diâmetro. Ambos os objetos simuladores têm 15 cm de comprimento. Diferentes protocolos de aquisição foram realizados num tomógrafo Philips, modelo Access com 16 canais. A fatia central dos objetos simuladores foi irradiada sucessivamente e as medições foram realizadas usando uma câmara de ionização do tipo lápis para obter os índices de *kerma* no ar em PMMA ($C_{k,PMMA,100}$) e os índices de dose de CT (CTDI). A partir desses resultados, foram obtidos os valores de índice de dose em TC ponderado e volumétrico ($CTDI_w$, $CTDI_{vol}$) para varreduras de 10 cm da região central dos objetos simuladores da cabeça, no modo helicoidal. As varreduras foram realizadas utilizando diferentes valores de tensão (80, 100 e 120 kV) e carga (mA.s). Os valores de dose variaram de 5,59 a 21,51 mGy. O maior valor de dose registrado foi de 21,51 mGy para o objeto simulador de cabeça menor e 19,25 mGy para o objeto simulador de cabeça padrão com 120 kV. Considerando a geração de imagens com o mesmo objetivo diagnóstico, os resultados obtidos mostraram que o índice de dose volumétrica ($CTDI_{vol}$) apresentou maior valor de dose no objeto simulador de 12 cm de diâmetro. Este objeto simulador tem um volume menor que o de cabeça padrão.

**Palavras-chave**: Tomografia Computadorizada; Objeto Simulador; Dosimetria; Qualidade de Imagem.

***Abstract***

*Computed Tomography (CT) scans promote a higher dose deposition than conventional radiology exams. These exams have significantly increased patient and collective doses and have become a global public health concern. There is a great need to improve protocols to seek for lower doses while maintaining the diagnostic image quality. The development of phantoms allows the testing of different acquisition protocols. In this study were tested two cylindrical head phantoms of polymethylmethacrylate (PMMA). One CT head phantom is the head standard test with 16 cm in diameter and the other head phantom developed is smaller at 12 cm in diameter. Both phantoms are 15 cm long. Different acquisition protocols were performed on a Philips CT scanner, Access model with 16 channels. The central slice of the phantoms was irradiated successively and measurements were performed using a pencil ionization chamber to obtain the CT air Kerma indexes in PMMA ($C_{k,PMMA,100}$) and CT dose indexes (CTDI). From these results, the CT Dose Index values weighted and volumetric ($CTDI_w$, $CTDI_{vol}$) were obtained to 10 cm scans of the central region of the head phantoms, in helical mode. The scans were performed using different voltage values (80, 100 and 120 kV) and charge (mA.s). Dose values varied from 5.59 to 21.51 mGy. The highest recorded dose value was 21.51 mGy for the smaller head phantom and 19.25 mGy for the standard head phantom with 120 kV. Considering the generation of images with the same diagnostic objective, the results obtained showed that the volumetric dose index ($CTDI_{vol}$) presented a higher dose value in the 12 cm diameter phantom. This phantom has smaller volume than the standard head phantom.*

**Keywords***: Computed Tomography; Phantom; Dosimetry; Image Quality.*

## 1. Introduction

Computed Tomography (CT) is one of the most used exams for radiological diagnosis in medicine. It is a very quick test and produces high quality images. However, the increasing demand for CT tests has a considerable impact on doses provided to patients and on the exposure of the population as whole, being a public health concern worldwide (2). According to UNSCEAR 2020/2021 report, the use of CT contributed with 62% of the collective dose from diagnostic radiological tests (3). Many factors collaborated to the increase in the demand for CT scans, including the constant technological evolution of the equipment associated to greater availability and a relative tendency to decrease exam costs (4,5).

Dose reduction in pediatric patients is already a concern among professionals from different areas of health, with international dose reduction programs, such as *Image Gently*, which aims to raise awareness among professionals, alert to the development of methods that can reduce the dose without compromising image quality in pediatric exams and provides specific guidelines for medical physicists (4,5). The risks of stochastic effects increase in children due to the tissue radiosensitivity allied to the long-life expectancy. The dose deposited in a pediatric patient is directly related to the energy that was retained during the process of exposure to ionizing radiation (5,6).

The increasing demand for CT scans in pediatric patients is mainly due to the high rates of traumatic injuries from car accidents, falls on bicycles, blunt trauma, traumatic brain injury, as well as a significant increase in the incidence of childhood neoplasms, being the CT images used in the diagnostic process (7,8). A retrospective study of a cohort of pediatric patients exposed to CT scans demonstrated that cumulative doses of 60 mGy to the brain may triple the risk of brain tumor (9). Therefore, acquisition protocols should be used that determine the reduction of the radiation dose without compromising the diagnostic quality.

Patients undergoing CT scans can range from neonates to oversized adults. However, radiation doses in CT are generally measured in cylindrical PMMA phantoms, that represent a standard adult patient. These phantoms are designed to simulate a head with 16 cm in diameter, and a body with 32 cm (10,11)

It is difficult to obtain reliable quantitative values of patient doses from any measurements performed on these standard phantoms, because patients have sizes and body compositions that can differ markedly from the phantoms, such as pediatric and obese patients. The development of phantoms allows testing different acquisition protocols (12,13). For this, the phantoms must have an X-ray beam absorption characteristic similar to the represented patient.

In this study, two CT head phantoms were used, the standard head phantom and another with smaller volume to observe the dose distribution and to obtain the dose index (CTDI). Different protocols were used in the phantom CT scans using three X-ray tube voltages.

## 2. Materials and Methods

The experiment was conducted using a Philips scanner, Access model with 16 channels. For the development of this work, experimental measures have been obtained using two head phantoms, both made in polymethylmethacrylate (PMMA). These phantoms were constructed by the research team of the Center for Research in Biomedical Engineering (CENEB), being a representative of a standard adult and a pediatric patient's head size. The standard adult head phantom is cylindrical with 16 cm in diameter and 15 cm in length. This phantom is considered the standard for the dose reference in head CT scans. The pediatric head phantom is also a cylinder and has a dimension of 12 cm in diameter and 15 cm in length, representing a smaller head. The Figure 1 shows the image of these phantoms placed in the isocenter of the CT scanner gantry.

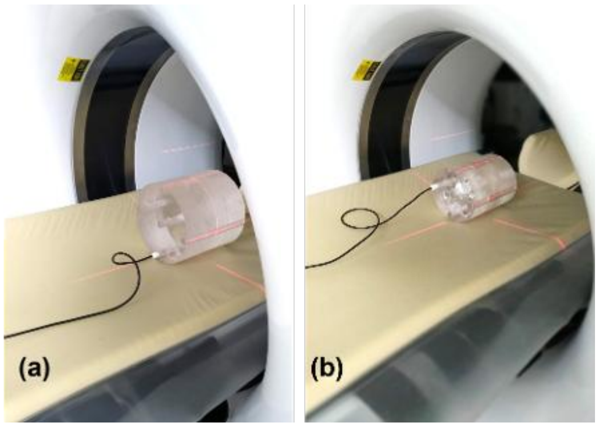


**Figure 1.** PMMA head phantom: (*a*) Adult standard; and (*b*) pediatric.

These cylindrical phantoms have five openings for positioning the dosimeters, one central and four at the peripheral openings, which are displaced from each other by 90°. The openings are 1.25 cm in diameter and 15 cm in length. The center of the peripheral openings is 1 cm from the edge of the phantom. Figure 2 shows an illustration with the dimensions of the adult and pediatric phantoms made of PMMA.

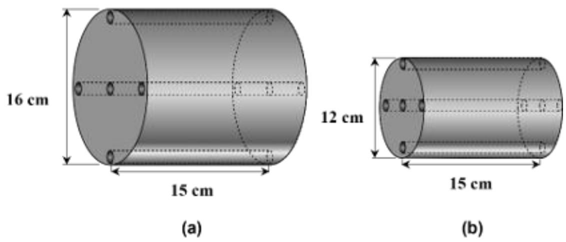


**Figure 2.** Head phantoms dimensions: (*a*) Adult standard; and *(b)* pediatric.

Dose measurements have been performed by positioning the head phantom in the isocenter of the gantry and aligning the openings like as the positions 3, 6, 9 and 12 of an analog clock, through the help of the CT scanner lasers. The phantom openings are filled with PMMA rods which must be removed one by one for the positioning of the pencil ionization chamber, targeting the dose measurements in the five positions.

A pencil ionization chamber RADCAL ACCU-GOLD model 10X6-3CT was used to measure the CT air kerma in PMMA ($C_{k,PMMA,100}$) in each opening of both phantoms. The ionization chamber was calibrated in the LABPROSAUD - Laboratory of Health Products - Calibration Laboratories Service - Ionizing Radiations. First, a scout was made in order to check the correct alignment of the phantoms as well as to demarcate the central slice position. Furthermore, the central slice of the phantoms was irradiated successively. For each chamber positioning, 5 measurements were performed, getting a minimum of 25 measurements for each protocol and for each phantom. In the central slice irradiations, the remaining openings were filled using PMMA rods. From these results, the CT Dose Index values, weighted and volumetric ($CTDI_w$, $CTDI_{vol}$), were obtained for 10 cm scans of the central region of the head phantoms, in helical mode (14,15).

The $CTDI_w$ and $CTDI_{vol}$ were calculated according to the Equations (1) and (2):

$$CTDI_w = \frac{1}{3}.(CTDI_{100,central} + \frac{2}{3}.CTDI_{100,per}) \quad (1)$$

$$CTDI_{vol} = \frac{CTDI_w}{pitch} \quad (2)$$

where $CTDI_{100,central}$ is the dose index value obtained at the central role and $CTDI_{100,per}$ is the average dose index value at the peripheral roles, in a 100 mm central axial region around the center position of the head phantom. The scans were performed using different voltage values (80, 100 and 120 kV) and charge (mA.s). To obtain the CT Dose Index (CTDI) values from the air kerma values the measurements were adjusted using a conversion factor ($F_c$) air/PMMA. The Fc used were 1.0418, 1.0324, and 1.0106 for the X-ray beam generated with 120, 100 and 80 kV, respectively (15,16).

The protocol for irradiation of the phantom central slice, in axial mode, used the following parameters: current of 100 mA, charge of 100 mA.s, tube rotation time of 1 s, beam thickness of 10 mm and three voltage values (120, 100 and 80 kV).

Helical scans of 10 cm in length were also performed in the central region of the head phantoms, aiming to define a current value adjusted by the equipment's automatic exposure control (auto mA), using the different voltage values. Usually, in the initial slices of the scan there is an adjustment in the current value (mA) in the first slices irradiated and after these adjustments the current stabilizes, since all the slices of the phantom have the same size. Head acquisition protocols often use a constant current value (mA), as the axial section of the head does not have large diameter variations.

With the current reference value defined based on the current recorded in the central slice, new scans were made to test fixed current values, lower than the value suggested by the automatic current control scan. For each current value tested, pixel noise value was calculated in the image of the central slice and the best current value was determined for each phantom and voltage.

The protocols used in the scans of the central region of the phantom used pitch values closest to 1, that is available in the CT equipment. Table 1 shows the CT head scanning protocol used in the service routine, regardless of the patient's size or age.

**Table 1.** Routine protocol of the CT scanner.

| Voltage (kV) | Current (mA) | Charge (mA.s) | Time (s) | Pitch |
|---|---|---|---|---|
| 120 | 73.7 | 110.5 | 1.5 | 1.0625 |

Source: The Author (2023).

Dose reduction in patient's CT scans was performed by increasing the pitch value to close to 1, thus decreasing patient re-irradiation and varying the charge value (mA.s). Three different values of available voltages were tested and keeping the reconstructed image in 1.25 mm, already defined in the routine protocol of the service. Both increasing the pitch and decreasing the mA.s promote an increase in the pixel noise of the image [17,18].

Unlike human organs, which are composed by the association of different tissues, PMMA is homogeneous; on the Hounsfield scale, PMMA has a value around 118.7 for images generated with an X-ray beam of 120 kV. As it is a homogeneous material it is possible to evaluate the variation of pixel noise in the images generated by different acquisition protocol tested. In acceptance tests of CT equipment during installation, the pixel noise must be less than 1% for tests with a PMMA phantom [17,18,19].

In order to validate the quality of the CT images, a noise analysis of the central slice image was performed in each helical CT scan, aiming at maintaining the diagnostic quality of the images. The noise value had its maximum acceptable limit of 1%, considering that the phantom is homogeneous [19,20]. This noise limitation, using a homogeneous material, implies in the generation of diagnostic images of the human body. Then, as a control parameter for testing new protocols, it was defined that the noise threshold in the central slice image should be 1% to guarantee the diagnostic quality of the patient's image. This value is recommended by the manufacturer when testing for acceptance of CT equipment after installation [18,19,20,21].

Four regions of interest (ROI) were selected in the image and were analyzed. The noise (N) was calculated as the percentage value of the standard deviations in relation to the average value of the Hounsfield scale (HU) through Eq.3.

$$N\% = \frac{SD}{\overline{HU}+1000}.100 \quad (3)$$

## 3. Results

### *3.1. Dose Measurements*

Table 2 shows the average values and standard deviations of punctual and weighted air *kerma* in PMMA ($C_{k,100,PMMA}$ and $C_w$) and weighted CT Dose Index ($CTDI_w$) that were obtained from $C_{k,100,PMMA}$ measured in the five positions of the phantoms, using the parameters defined in Table 1 with the charge fixed in 100 mA.s.

**Table 2.** The Values of $C_w$ and $CTDI_w$ in mGy for head phantoms.

| Phantoms | Voltage (kV) | $C_w$ (mGy) | $CTDI_w$ (mGy) |
|---|---|---|---|
| Adult (16 cm) | 120 | 18.48±0.32* | 19.25±0.33 |
| | 100 | 11.07±0.16 | 11.54±0.17 |
| | 80 | 5.36±0.10 | 5.59±0.10 |
| Pediatric (12 cm) | 120 | 20.65±0.23 | 21.51±0.24 |
| | 100 | 12.49±0.10 | 13.02±0.11 |
| | 80 | 6.15±0.06 | 6.40±0.06 |

*Standard deviations
Source: The Author (2023).

The protocol using the voltage of 120 kV has the highest absorbed dose value recorded of 19.25 mGy in the adult phantom and 21.51 mGy on the pediatric phantom. The minimum value happened in the adult and pediatric phantoms with the 80 kV voltage, with the values of 5.59 mGy and 6.40 mGy respectively.

Analyzing the measurements obtained, it is verified that with the pediatric phantom the values are always the highest, since the other parameters used were the same; the volume of the pediatric phantom is smaller than the adult, promoting a higher dose deposition.

*3.2. Optimized CT Scan Protocols*

Table 3 shows the results of volume CT Dose Index ($CTDI_{vol}$) obtained when the routine and optimized protocols were used in both phantoms with different voltage values and optimized charge in the X-ray tube during the scans of the central region of the phantoms. In optimized protocols, the optimized charge value (mA.s) was adjusted to the point where the noise in the central slice was less than 1%. The other parameters: pitch, tube time, thickness beam and image reconstruction were the same of the routine protocol (Table 1).

**Table 3.** Routine and optimized protocols.

| Phantoms | Protocol | Voltage (kV) | Charge (mA.s) | $CTDI_{VOL}$ (mGy) |
|---|---|---|---|---|
| **Adult (16cm)** | Routine | 120 | 110.5 | 20.02 ± 0.34* |
| | Opt. 1 | 120 | 35 | 6.34 ± 0.11 |
| | Opt. 2 | 100 | 60 | 6.51 ± 0.09 |
| | Opt. 3 | 80 | 130 | 6.83 ± 0.12 |
| **Pediatric (12cm)** | Routine | 120 | 110.5 | 22.87 ± 0.39 |
| | Opt. 4 | 120 | 25 | 5.06 ± 0.06 |
| | Opt. 5 | 100 | 40 | 4.90 ± 0.04 |
| | Opt. 6 | 80 | 90 | 5.43 ± 0.05 |

*Standard deviation
Source: The Author (2023).

In Table 3 it is possible to observe the variation of the absorbed dose values for both phantoms for the analysis of the protocol that presents the lowest dose for the patient, maintaining the image quality. In the adult head phantom, the absorbed dose in the routine protocol had a higher dose of 20.02 mGy and with the optimized protocols smaller doses were obtained. The optimized protocol Opt.1 with 120kV had the lowest value of 6.34 mGy with a reduced dose of 68.33% in relation with the routine protocol.

On the other hand, the pediatric head phantom presented a significant variation in the absorbed dose values. The absorbed dose in the routine of the pediatric phantom had a higher dose than the adult phantom with a dose of 22.87 mGy that is 14.23% higher. The optimized protocol Opt. 5 with 100kV reduced the dose in the pediatric phantom in 78.6% in relation with the routine protocol. Figure 4 shows a graphic with the $CTDI_{vol}$ values for adult and newborn phantoms obtained according with the average current and pitch.

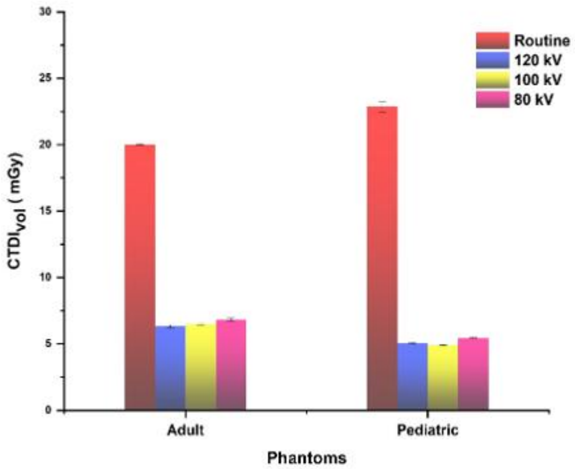


**Figure 4.** $CTDI_{vol}$ values for adult and pediatric head phantoms obtained with routine and optimized protocols.

Observing the absorbed dose values obtained for the tested protocols, it is verified that the pediatric phantom had a better CT scan with the voltage of 100 kV. The optimized protocols selected with the low absorbed dose obtained noise values below 1%, being a good alternative to be used aiming the reducing of absorbed dose of the patient and maintaining the diagnostic quality of the image.

It is also worth noting that the tested protocols showed in Table 3 were selected among several others tested with the variation of the mA.s value until a noise lower than 1% was obtained in the analysis of the image of the central slice. The mA.s and pitch variation cannot be chosen randomly, since there are discrete values in the CT equipment menu that are possible to be tested.

## 5. Conclusion

The absorbed dose index values were determined during head CT scans with the standard adult and pediatric PMMA phantoms.

This work made it possible to highlight relevant information on dose reduction in head CT scans in adults and children, which is of great importance to argue for the adoption of optimized protocols without loss of diagnostic image quality. In addition, the use of optimized protocols increases the useful life of the CT X-ray tube, generating less expenses for the radiodiagnosis service.

Dose values were significantly higher in the pediatric phantom using the same routine protocol than the adult. In the generation of images with the same diagnostic objective, the volumetric dose index showed a higher dose value in the pediatric phantom, corresponding to a head with smaller volume, compared to the value measured in the standard head phantom.

## Acknowledgment

This study was supported in part by the Coordenação de Aperfeiçoamento de Pessoal de Nível Superior - Brasil (CAPES) - Finance Code 001. Also, this work was supported by the FAPEMIG.

## References

1. Aburjaile WN, Mourao AP. Development of a chest phantom for testing in Computed Tomography scans. Radiat Phys Chem. 2017; 140:275-277.
2. Goo, HW. CT radiation dose optimization and estimation: an update for radiologists. Korean J Radiol. 2012; 13(1):1-11.
3. Unscear - United Nations Scientific Committee on the Effects of Atomic Radiation et al. Sources, Effects and Risks of Ionizing Radiation, United Nations Scientific Committee on the Effects of Atomic Radiation (UNSCEAR) 2020/2021 Report, Volume I: Report to the General Assembly, with Scientific Annex A-Evaluation of Medical Exposure to Ionizing Radiation. 2022: 354.
4. Mathews, J. D. et al. Cancer risk in 680 000 people exposed to computed tomography scans in childhood or adolescence: data linkage study of 11 million Australians. BMJ. 2013; 346:1-18.
5. Mourão, A. P. Tomografia computadorizada: tecnologias e aplicações. São Caetano do Sul: Difusão Editora. 2018.
6. Mourão AP, Aburjaile WN, Santos FS. Dosimetry and Protocol Optimization of Computed Tomography Scans using Adult Chest Phantoms. Int J Radiol Imaging Technol. 2019; 5:050.
7. Finatto J, Froner APP, Pimentel J, Silva AMM. Estudo comparativo de descritor de dose em exames pediátricos de tomografia computadorizada. Braz J Radiat Sci. 2015; 3(1A): 24-32.
8. IAEA - INTERNATIONAL ATOMIC ENERGY AGENCY. Dosimetry in diagnostic radiology: an international code of practice. Technical Reports Series No. 457, Viena, 2007.
9. Bolus NE. NCRP report 160 and what it means for medical imaging and nuclear medicine. J Nucl Med Technol. 2013; 41(4):255-260.
10. Yang CC. Evaluation of impact of factors affecting CT radiation dose for optimizing patient dose levels. Diagnostics. 2020; 10(10):787-792.
11. Alonso TC; Mourão AP; Silva TA. Measurements of air kerma index in computed tomography: A comparison among methodologies. Appl Radiat Isot. 2018; 138:10-13.
12. AAPM - American Association of Physicists in Medicine. Comprehensive methodology for the evaluation of radiation dose in x-ray computed tomography. Report of AAPM Task Group 111: The Future of CT Dosimetry, 2010.
13. Miglioretti DL, et al. The use of computed tomography in pediatrics and the associated radiation exposure and estimated cancer risk. JAMA Pediatr. 2013;167(8):700-707.
14. Spampinato MV, et al. Radiation dose and image quality in pediatric head CT. Radiat Prot Dosimetry. 2018; 182(3):310-316.
15. Gomez AML. Estudo de dosimetria e qualidade de imagem em varreduras de tomografia computadorizada de cabeça utilizando objeto simulador. Master degree, Universidade Federal de Minas Gerais, Minas Gerais, Brasil 2017.
16. Diwakar M; Kumar M. A review on CT image noise and its denoising. Biomed Signal Process Control. 2018; 42:73-88.
17. INTERNATIONAL ATOMIC ENERGY AGENCY, Diagnostic Radiology Physics, Non-serial Publications , IAEA, Vienna (2014).
18. Vásquez AC, Runz A, Echner G, Sroka-Perez G, Karger CP. Comparison of two respiration monitoring systems for 4D imaging with a Siemens CT using a new dynamic breathing phantom. Phys Med Biol. 2012; 57(9):N131-43.
19. Manson EN; Fletcher JJ; Amausi JH. Variation of noise with some scanning parameters for image quality test in 128 slice computed tomography scanner using catphan 7000 phantom. J Radiol Diagn Methods. 2018; 1: 102-115.
20. Cantera, A. C.; Tortosa, M. L. Calidad de imagen. In: Curso de Garantia de qualidad en TC. Tarragona, España. 2003; 8–12.
21. NIST - National Institute of Standard and Tecnology. Values of the mass attenuation. Available at: < http://physics.nist.gov/PhysRefData/XrayMassCoef/tab4.html >. Last accessed: 08 Sept. 2020.
22. ICRP- International Commission on Radiological Protection. Diagnostic reference levels in medical imaging: review and additional advice. Oxford. 2002; 14.
23. Huda W. Medical Radiation Dosimetry. RSNA categorical course in diagnostic radiology physics: from invisible to visible—the science and practice of x-ray imaging and radiation dose optimization. RSNA. 2006; 29–39.

## Contato:

Fernanda Stephanie Santos
Departamento de Engenharia Nuclear, Universidade Federal de Minas Gerais.
Departamento de Engenharia Nuclear, Universidade Federal de Minas Gerais, CEP:31270-970, Belo Horizonte, MG, Brasil.
fernanda.stephaniebh@yahoo.com.br

*2017 International Nuclear Atlantic Conference - INAC 2017*
*Belo Horizonte, MG, Brazil, October 22-27, 2017*
*ASSOCIAÇÃO BRASILEIRA DE ENERGIA NUCLEAR – ABEN*

Agência Brasileira do ISBN
ISBN 978-85-99141-07-6

# COMPUTED TOMOGRAPHY SCAN OPTIMIZATION USING HEAD PHANTOM AND RADIOCHROMIC FILMS

**Lorena C. Fernandes[1], P.C. Santana[2], Carlos E. Velasquez[1] and Arnaldo P. Mourão[1,3]**

[1] Departamento de Engenharia Nuclear
Universidade Federal de Minas Gerais
Avenida Presidente Antônio Carlos, 6627
31270-901 Minas Gerais, MG
lorena.cfernandes@hotmail.com, carlosvelcab@hotmail.com

[2] Centro de Imagem Molecular do INCT-MM
Faculdade de Medicina da Universidade Federal de Minas Gerais
Avenida Av. Prof. Alfredo Balena, 190
30130-100 Minas Gerais, MG
pridili@gmail.com

[3] Centro Federal de Educação Tecnológica de Minas Gerais
Av. Amazonas 5253
30421-169 Minas Gerais, MG
apmourao@gmail.com

## ABSTRACT

The research and development in technology applied to computed tomography has been improve in the image quality, resulting in the best identification of diseases, and therefore an increase in the number of exams, among them the head exams can be highlighted. In order to promote a radioprotection and reduction on the dose of the general public some international agencies have stipulated dose limits to be followed and the implementation of the principles of ALARA in all establishments that use ionizing radiation. One of these principles is the optimization that should be treated with substantial attention, because the reduction of radiation doses can be feasible as long as it does not compromise the tomographic images; such practice is difficult to perform due to the lack of proper guidance. In optimization of the CT exams, not only the lowest dose is evaluated to obtain diagnostic image, but also should be knowledge the dose distribution throughout the scanned area. In this work were used a cylindrical head phantom of PMMA, a GE Discovery CT scan with 64 channels, and radiochromic films. The films were positioned in the phantom in their central region for the dose evaluation using the automatic control for the voltages of 80, 100 and 120 kV. The images were acquired from the scan of the phantom and the film readings were obtained through digital images. The results show an evaluation of the longitudinal kerma profiles, dose delivered, and the image noise was also observed using the central slice images.

## 1. INTRODUCTION

The evolution of the technology in Computed Tomography (CT) increased the agility of the processing data, an improvement in the image quality, and time reduction and tomography exams costs. These characteristics can highlight this technique among the other methods of production in the medical image. In this context, there has been an increase in the number of examinations in recent years, for example is estimated that in the year of 2010 in the United States it was about 1 million examinations performed by CT. Therefore, this influenced by the increase of radiation dose used in these systems, the international agencies responsible for radioprotection propose protocols for dosimetry and optimization of CT exams [1, 2, 3, 4].

The CT examination protocol optimization consists in the measurement of the dosimetric quantities using a phantom, ionization camera and radiochromic films (method suggested by several other studies). In order to evaluate the dose levels obtained, these were compared with the diagnostic reference levels determined by international and national recommendations for the multiple average dose (MSAD), which is stipulated for an adult with standard measures, 50 mGy for head, 35 mGy for lumbar spine and 25 mGy for abdomen [1, 2, 5, 6].

According to the American Medical Physics Association, suggest the use of the dosimetric quantification in terms of the computed tomography dose index (CTDI), which is basically the dose measurement in a single CT slice. However, the code of practice TRS-457 published by the International Atomic Energy Agency (IAEA) present the measurement in kerma index (*C*), which measures the air kerma free in air or air kerma in PMMA in one rotation of the X-ray tube. The quantities suggested by both are acquired in an analogous way, but differ in the concepts and calculations [7, 8].

There is CT software that modulates the current in the tube according to the anatomical shape and body density. This software contributes to choose the best current parameters choice that reduces the dose in regions with higher radiosensitivity. There can be emphasized that not always the smallest dose is associated with better image and, consequently, better diagnosis [3, 7].

Therefore, the main objective of this paper is propose an optimization of the head exam protocol using automatic exposure control (AEC) and to present the feasibility associating the best image quality with the lowest dose in helical CT scanner.

## 2. MATERIAL AND METHODS

The materials used were a Gafchromic XRQA2 radiocromatic film strips (0.5 wide by 12 cm length), one scanner HP, a 64-channel GE Discovery CT scanner, a cylindrical PMMA simulator of 16 cm in diameter and 15 cm in length, which has 5 openings of 1.25 cm in diameter and their positions correspond to one central hole and four peripherals, such their locations identified as clock hours at 3am, 6am, 9am, 12pm; and one ionization pencil chamber, Accu-Gold model 10X6-0.6CT. The ionization chamber was calibrated by a standard calibration laboratory and to guarantee its reliability, the dose constancy test was performed.

### 2.1. Optimization of the head exam protocol

Using a laser orientation, the phantom was positioned in the CT isocenter region, as presented in figure 1, with the following parameters: AEC activated, fixed the noise index in 10, slice thickness of 40 mm, reconstruction image of 5 mm, tube rotation time of 0.8 s, and pitch in

0.984. Images were acquired for the voltages of 80, 100 and 120 kV. From each image acquired, the central slice current was selected; they were used in the optimized protocol.

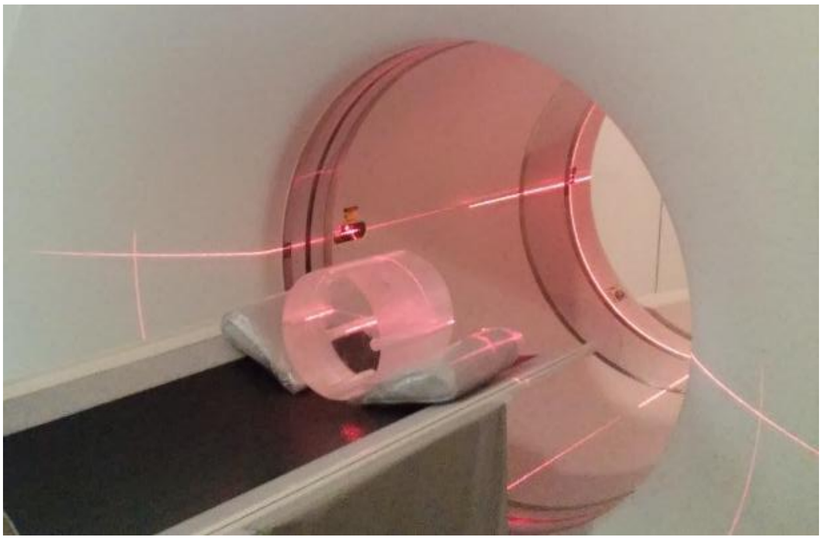

**Figure 1: Positioning of the phantom at the CT scanner.**

Using the optimized current and parameters: fixed the noise index in 10, slice thickness of 40mm, reconstruction of 5mm, tube rotation time of 0.8s, and pitch in 0.984. Irradiations were performed without the radiochromic films, with the objective of the analysis image noises, and the irradiations using the films positioned in the PMMA support, placed into the five openings of the head phantom. One film strip was used for the measurement of the background radiation. Radiations were performed for the voltages of 80, 100 and 120 kV with the scout. For comparison purpose, the irradiations with and without the film of the head protocol used in the hospital (non-optimized protocol) were performed with the parameters: AEC activated, fixed the noise index in 4.94, slice thickness of 20 mm, reconstruction of 1.25 mm, Tube rotation time of 0.7 s, and pitch in 0.969.

Film strips were scanned by the color image scanner in JPEG format, 300 ppi and reflection mode. The readings were performed through the ImageJ software [10], using the red channel, because the film has greater sensitivity in this region and selected an ROI of 10 cm long by 0.22 cm in height.

For the calibration of the radiochromic film was performed by measurements of kerma with the ionization chamber. The measurements with the ionization chamber were performed for the voltages of 80, 100 and 120 kV, fixed current at 200 mA and tube rotation time of 0.5 s, slice thickness of 10 mm, measurements were taken with the ionization chamber in all 5 phantom openings, which was positioned in the isocenter. These measures were then corrected for the optimized charge using equation (1). It is possible to used, because the Kerma is proportional a charge to low voltage [9].

$$K = K_c \frac{C_0}{C_c} \tag{1}$$

Since $K$ is the new value kerma (converted to the optimized charge range), $K_c$ is the kerma measured with the ionization chamber, $C_0$ is the optimized charge, $C_c$ is the charge used for measurements with the chamber.

The results of the films and the ionization chamber were related and then the calibration coefficient of the film was obtained, with this coefficient the data of the film in kerma were obtained and then the calculation of the $CTDI_{vol}$ and the MSAD.

## 2.2. **Image evaluation for optimized and non-optimized protocol**

The image evaluation was done through the RadiAnt DICOM View software [11], where it is possible to open DICOM format images. The images obtained from the optimized protocol were then analyzed through a ROI selection of the simulator central slice, from this region the standard deviation value and the mean of the Hounsfield scale value were taken for the calculation of the image noise, according to equation 2. This is used to calculate the noise of CT images, so the mean of the grays colors is increased by 1000.

$$R = \frac{\sigma}{M + 1000} \tag{2}$$

Since $R$ is the image noise, $\sigma$ is the standard deviation, and $M$ is the average intensity value in Hounsfield scale.

# 3. RESULTS AND DISCUSSION

In table 1 are presented the calibration coefficients of the film, $CTDI_{vol}$, and MSAD were calculated for the optimized and non-optimized protocols, using the simulator, ionization chamber and radiochromic film.

**Table 1: Results of calibration coefficients, MSAD and $CTDI_{vol}$ for the optimized and non-optimized adult head exam protocol**

| Protocol | Optimized | | | Not optimized |
|---|---|---|---|---|
| Voltage (kV) | 80 | 100 | 120 | 120 |
| Weighted calibration coefficient (mGy. Intensity$^{-1}$) | 0.353 | 0.394 | 0.390 | 0.781 |
| $CTDI_{vol}$ of the radiochromic film (mGy) | 8.303 | 8.906 | 9.022 | 67.867 |
| $CTDI_{vol}$ of the ionization chamber (mGy) | 8.140 | 8.596 | 8.581 | 67.098 |
| MSAD (mGy) | 8.016 | 8.459 | 8.458 | 64.43 |

Table 1 shows that the lowest $CTDI_{vol}$ value for the dosimeters used was the protocol whose voltage was 80 kV, but the values of 100 and 120 kV presented their values very close. Comparing 80 kV protocol with the one used in the hospital, it was possible to reduce the mean dose by approximately 87.5%.

Comparing the calculated MSADs for the optimized protocols presented lower doses than those suggested by the NRD for adult head examinations, and in the case of the non-optimized protocol it exceeded the recommended dose of 50 mGy.

The image noise value is presented in table 2. The standard deviation represents the uncertainty associated with the image and the average of the grays colors is the signal produced by the system, the calculated noise is the ratio between these quantities. It is observed that the noises for the optimized protocols are close and below 1%, since the protocol used by the hospital was below 0.5%.

**Table 2: Data noise for optimized and non-optimized protocol.**

| Protocol | Optimized | | | Not Optimized |
|---|---|---|---|---|
| Voltages (kV) | **80** | **100** | **120** | **120** |
| Standard deviation | 7.705 | 7.642 | 7.48 | 4.908 |
| Average Hounsfield value (intensity) | 87.06 | 103.34 | 112.55 | 110.75 |
| Noise (%) | 0.708 | 0.693 | 0.672 | 0.442 |

The protocols optimized and not optimized in its methodology used the AEC with the fixed noise index. Comparing table 1 with table 2, it is observed in the non-optimized protocol that it has a high dose and a low noise that in contrast in the optimized protocols there is a low dose and a noise considered medium, but this noise is acceptable for the image Diagnosis.

Figure 2, shows the relationship between dose (calculated from the radiochromic film) and noise. It is possible to observe which is the better protocol of acquisition to be chosen, through the protocol that presented less noise and lower dose for the patient, without interfering in the image quality.

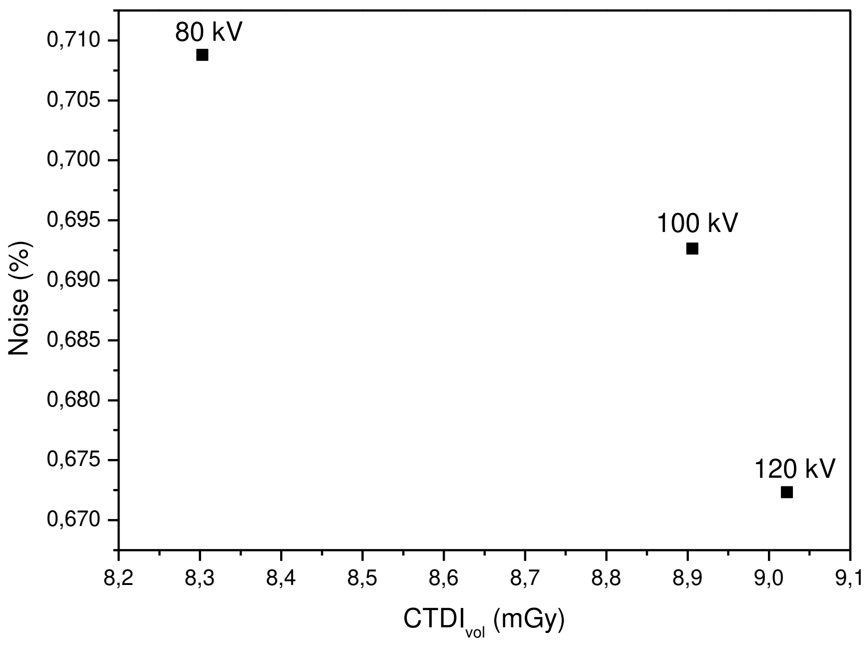


**Figure 2: Graph of the CTDI$_{vol}$ versus noise for optimized 80, 100 and 120 kV protocols.**

Note that the protocol that has the best dose-noise ratio is the 80 kV protocol, because its noise is close to 100 and 120 kV protocols, presenting a noise value of 0.051% higher, and has the lowest dose between them. Comparing the optimized 80 kV protocol with the non-optimized protocol, this optimized protocol has a noise value of 0.62% higher than in the non-optimized.

The kerma profiles of the optimized and non-optimized protocols for the five regions of the simulator are shown in figures 3, 4, 5 and 6, and it is possible to note that, the kerma is higher in position 12 than positions 6 and central position. The central position is lower due to attenuation in the peripheries of the simulator and in region 6 is due to attenuation of the CT table.

Figures 4 and 5 show the kerma profiles proximity for all regions of the simulator, since the beam is more penetrating and contributes to the kerma increase in the region 6 and central position, and consequently there is a kerma decrease in the positions 3, 9 and 12.

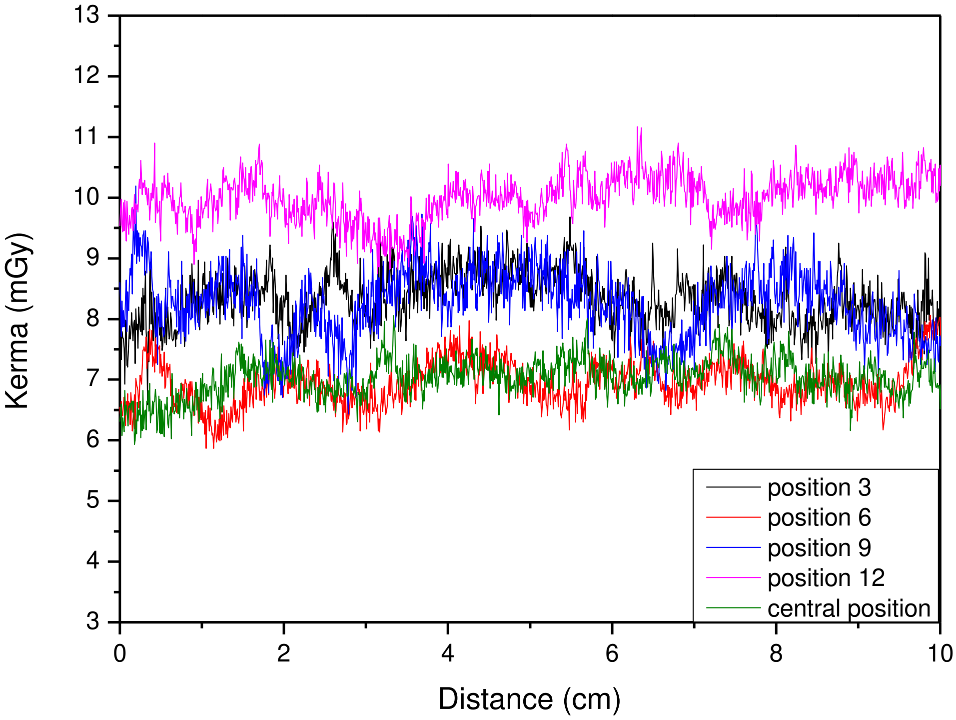


**Figure 3: Kerma profile for optimized protocol of 80 kV.**

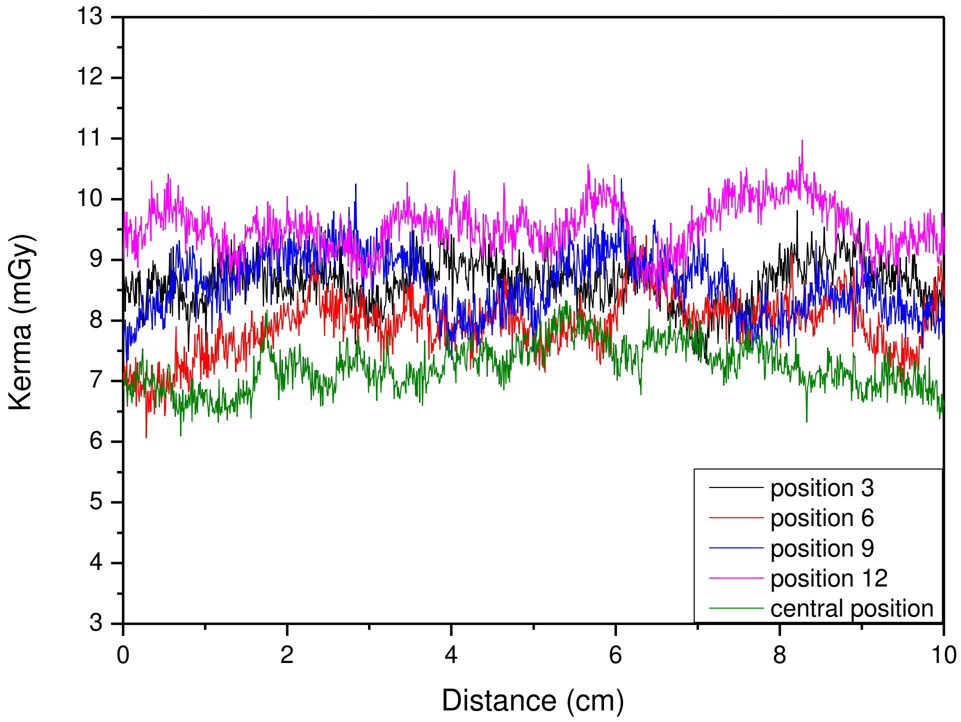


**Figure 4: Kerma profile for optimized protocol of 100 kV.**

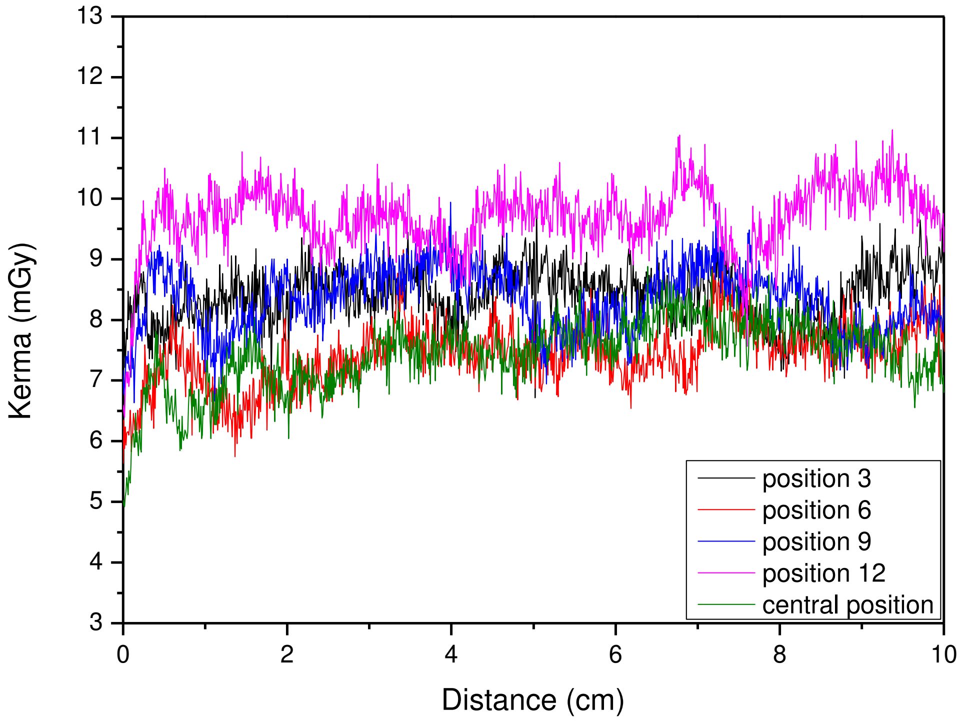


**Figure 5: Kerma profile for optimized protocol of 120 kV.**

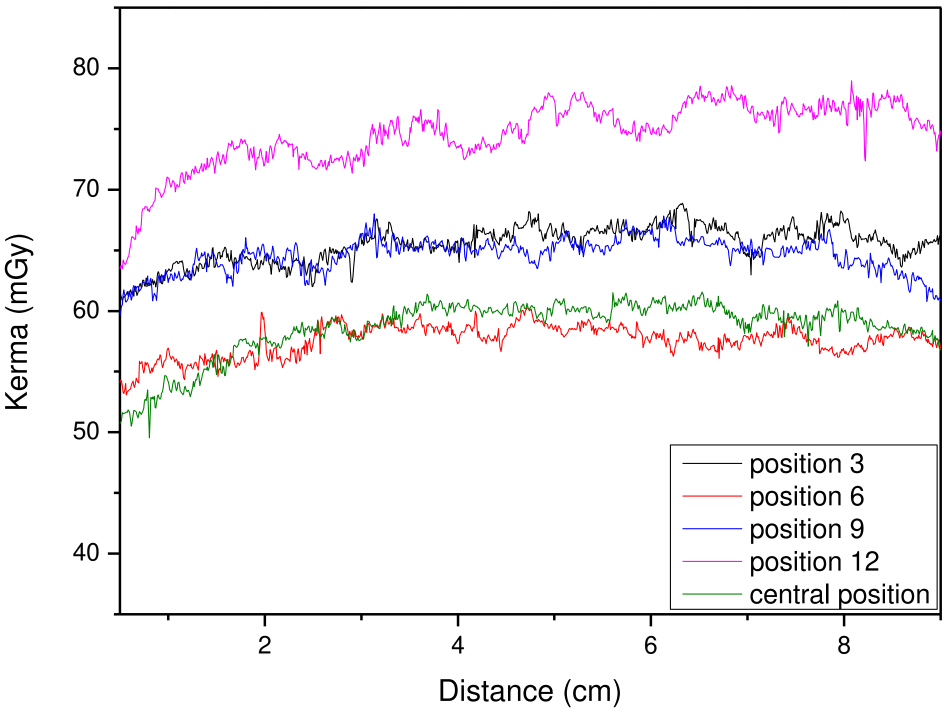


**Figure 6: Kerma profile for the non-optimized protocol.**

## 3. CONCLUSIONS

The advantages of using the radiochromic film in the service protocols optimization are: the time reduction to the acquisition of the dosimetric data compared to the use of the ionization chamber, can provide information when the kerma profile for later analyzes and easy handling.

The use of the AEC contributed to a quick and efficient choice of the best current to be used. In the case of the optimized protocols and the one used by the service, both were acquired with different methodologies, but in common they used the AEC and fixed the noise index. In the method used in the optimization of the service protocol the dose was reduced by up to 87.5% and a noise below 1% in homogeneous area, which is acceptable for the CT image. The high dose is due to the choice of the noise index fixation, which consequently interferes in the increase in the dose in the patient, so the analysis of the dose-noise ratio must be made to choose the best protocol to be used by the service.

The obtained MSAD results presented for the optimized protocols below the value of the NRD, being the protocol of 80kV the lowest value with 8.016mGy, and for the non-optimized protocol was 22.4% above the suggested value.

## ACKNOWLEDGMENTS

Thanks to CAPES, FAPEMIG and to Centro de Imagem Molecular (CIMol) of Faculdade de Medicina of UFMG.

## REFERENCES


1. B. B. Oliveira, A. P. Mourão, T. A. da Silva, "*Estimation of MSAD values in computed tomography scans using radiochromic films*", Radiol Bras, 2013 Mar/Apr, Vol. 46(2), pp.96–100.
2. T. S. Jornada, T. A. da Silva, *"Quantificação das grandezas dosimétricas em exames de tomografia computadorizada pediátricos do abdome".* Radiol Bras. 2014 Set/Oct, Vol. 47(5), pp.288–291.
3. J. Dalmazo, J. J. Elias, M. Brocchi, P. Costa, P. A. Marques. *"Otimização da dose em exames de rotina em tomografia computadorizada: estudo de viabilidade em um hospital universitário*". Radiol Bras, 2010, Vol. 43(4), pp.241–248.
4. A. C. SANTOS et al, *"Otimização dos Protocolos de Tomografia Computadorizada em Pacientes Pediátricos"*, Pleiade, 2016 Jul./Dec, Vol. 10(20), pp.94-101.
5. Ministério da Saúde. Secretaria de Vigilância Sanitária. Portaria nº 453, de 01 de junho de 1998, *"Diretrizes de proteção radiológica em radiodiagnóstico médico e odontológico",* Brasília, Diário Oficial da União, 02 de junho de 1998.
6. Committee 3 of the International Commission on Radiation Units and Measurements, "Diagnostic reference levels in medical imaging: review and additional advice", http://www.icrp.org/docs/DRL_for_web.pdf
7. American Association of Physicists in Medicine, "*The Measurement Reporting, and Management of Radiation Dose in CT"*, AAPM Report No. 96, College Park, MD, 2008.
8. International Atomic Energy Agency, *"Dosimetry in diagnostic radiology: an international code of practice"*, Technical Reports Series no. 457, Vienna, IAEA, 2007.
9. M. P. P. Albuquerque, "*Metodologia dosimétrica e sistema de referência para radiação X nível diagnóstico*", Instituto de Pesquisas Energéticas e Nucleares, Universidade de São Paulo, 1999.
10. Rasband, W.S., "*ImageJ*", U. S. National Institutes of Health, Bethesda, Maryland, USA, https://imagej.nih.gov/ij/, 1997-2016.
11. RadiAnt DICOM Viewer, https://www.radiantviewer.com/dicom-viewer-manual/.

*Original Article*

Dose-Response:
An International Journal
July-September 2022:1–6
© The Author(s) 2022
Article reuse guidelines:
sagepub.com/journals-permissions
DOI: 10.1177/15593258221119299
journals.sagepub.com/home/dos
SAGE

# Computed Dosimeter Dose Index on a 16-Slice Computed Tomography Scanner

**Tadelech S. Mekonin[1] and Tilahun T. Deressu[1]**

## Abstract

A computed tomography dose index can be used to quantify the radiation dose received during a CT scan and it is an indicator of the radiation dose to the polymetaylenmetaAcrylate (PMMA) standardized phantom. The objective of this study was 2-fold. The first was to measure the computed tomography (CT) radiation dose for the head and body polymetaylelenmetaAcrylate (PMMA) phantoms and to determine the accuracy of the CT radiation dose parameter displayed on the CT scanner console; these were measured in this investigation and compared with the dose displayed on the CT scanner console. The dose was calculated using the formalism described in the American Association of Physics in Medicine (AAPM) Report 96. The second was to compare the dosimetric results of the head and body polymetaylelenmetaAcrylate (PMMA) phantoms with dose reference levels published in international journals, as well as to measure the central cumulative dose ($DL^{'}$ (0)), as recommended by the American Association of Physics in Medicine (AAPM) report 111. This is a new, cutting-edge methodology for estimating the CT radiation dosage provided by the abdomen, thorax, and head of a PMMA phantom. We used a Philips Big Bore CT scanner with 16 slices. A CT dosimeter head phantom with a diameter of 16 cm, a CT dosimeter body phantom with a diameter of 32 cm, a 100 mm pencil chamber (PC), and a 20 mm short chamber (SC) were employed. These were coupled to an electrometer and a dosimetric readout device. The measured volume computed tomography dose index (CTDIvol) values were in good agreement with the CT radiation dose displayed on the corresponding CT scanner console. The percentage disagreement was less than 10%, with a maximal difference of 1.7% and 5.5% for the body and head phantom, respectively. The central cumulative dose (DL (0)) measurements (for $L^{'}$ = 100 mm) also matched nominal or the corresponding computed tomography dose index (CT) scanner console volume computed tomography dose index (CTDIvol) values. In this case, the agreement is always below 3% for abdomen scans and 1.0% for head examinations. This result implies that the radiation dose supplied by the 16-slice computed tomography (CT) system was in good agreement with the international dose reference level and we observed something different.

**Keywords**

radiation dose, computed tomography dose index, dosimetric reference levels, computed tomography scan

## Introduction

Computed tomography (CT) is a highly effective tool used by radiologists to detect illness in the human body. It was introduced in the early 1970s and was the first computer-based medical imaging modality.[1] The computed tomography dose index (CTDI) is used to calculate the radiation dosage during a CT scan.[2] The CTDI is measured in the radiation dose of the X-ray source using a pencil chamber (PC) with a length of L = 100 mm. It is defined as follows:

$$\mathrm{CTDI} = \frac{T}{L}\int_{\mathrm{L}}^{\mathrm{Z}} D(z)dz. \tag{1}$$

[1] Addis Ababa University, Addis Ababa, Ethiopia

Received 14 July 2022; accepted 24 July 2022

**Corresponding Author:**
Tadelech S. Mekonin, Department of Physics, Addis Ababa University, Addis Ababa 1176, Ethiopia.
Email: tadelech.sisay@aau.edu.et

Where,T is the total x-ray slice collimation.

The dose profile in the crania-caudal direction is denoted by −D (z).[1]

The general irradiation of a patient undergoing sequential computed tomography dose index (CT) examination to illustrate the CTDI approach in the patient dosimeter is shown in Figure 1,[3] where each circle represents a unitary dose expressed in arbitrary units. The dose absorbed in the patient slice of interest (highlighted in the figure) is given by the five central CT irradiations in the figure. The figure also shows that the first and final irradiations (placed at a distance from the slice of interest) do not contribute to the dose in this anatomical region. Consequently, the dose in the patient slice of interest is given by adding the contributions in the slice of interest (highlighted in the figure). It is equal to 10 in arbitrary units (Figure 1).

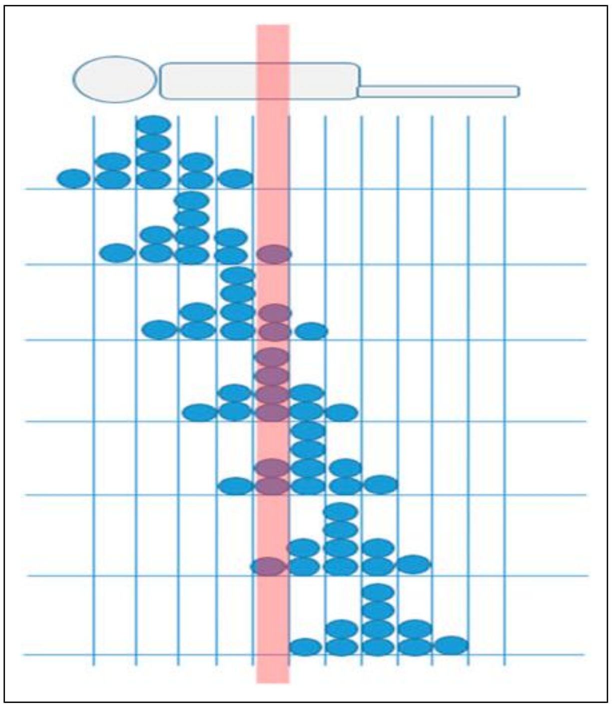

**Figure 1.** The typical dose profile in a sequential computed tomography (CT) examination is moving along the z-axis. The dose in the slice of interest is calculated by adding the contributions in the slice.[4]

The relationship between the CTDI and the dose in the patient slice is defined in equation (1). For simplicity, the patient slice was assumed to be 10 mm (x-ray) slice thickness (T = 10 mm). As shown in Figure 2, the pencil chamber (PC) averages Rx (X-ray) contributions to the dose over its length, L. As a result, in Figure 2, a final reading M = 1 in arbitrary units was obtained.

This reading M is also expressed by the relation $M = \frac{1}{L}\int_L^Z D(Z)dz$ allows rewriting equation (1) as follows:[1]

$$\mathrm{CTDI} = \frac{L}{T}M \tag{2}$$

Equation (2) yields a CTDI of 10 (au) for L = 100 mm and T = 10 mm. This is the same value of the dose absorbed in the patient slice obtained above by adding the dose contributions as shown in Figure 1. This numerical equivalence is crucial because it indicates that the CTDI value of a clinical CT scan is a dosimetric indicator estimating the dose in a patient slice. The weighted CTDI is the average dose over the central slice of a series of contiguous slices obtained during a head or body CT examination.[5,6] The CTDI measured using dosimetric phantoms is also referred to as the weighted computed tomography dose index (CTDIw). It is given by the following equation:

$$\mathrm{CTDI}_w = \frac{1}{3}\mathrm{CTDI}_C + \frac{2}{3}\mathrm{CTDI}_p, \tag{3}$$

where CTDIc = CTDI at the central position of the PMMA phantom[1] and CTDIp = the CTDI averaged over the four peripheral positions of the PMMA phantom.

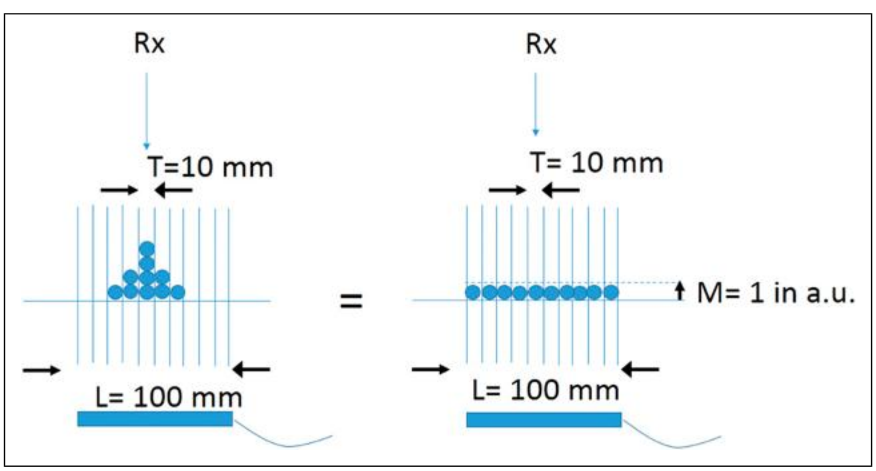


**Figure 2.** The pencil chamber (PC) reading averages the Rx (X-ray) contributions over its length, L.

**Figure 3.** Set-up for CTDI determination.

For helical CT examinations, the parameter estimating the dose in a patient slice is the CTDIvol.[7] It is defined as follows:

$$CTDI_{vol} = \frac{CTDIw}{p_f}, \qquad (4)$$

where $p_f$ is the pitch factor.[1,2]

The central cumulative dose DL′ (0) was introduced by the new modern American Association of Physics in Medicine (AAPM) to address the shortcomings of the conventional CTDI-based dosimetric approach.[8] This dosimetric indicator is defined as the dose in a patient slice caused by a CT examination with a scan length of L′. The method is highly practical because it allows for direct measurements of all clinical helical scans using short camber (SC) in the typical dosimetric head and body PMMA phantoms. DL′ (0) is the equilibrium dose (Deq) that is comparable to the CTDIvol for a scan length of L′ = 100 mm.[4,9] utilizing dose measurements obtained from the phantom's central hole (Deq, c) and those obtained from the phantom's peripheral hole (Deq, p)[1,10]

$$\frac{1}{3}DL'(0)c + \frac{2}{3}DL'(0)p \equiv CTDI_W = D(eq) \qquad (5)$$

where

DL′ (0) c=is refers to the DL′ (0) measured in the central position of the dosimetric phantom and DL′ (0)p = is the mean value of DL′ (0) measured in the peripheral locations of the same phantom.

Equation (5) explains one of the advantages of the American Association of Physics in Medicine (AAPM) dosimetric approach. It enables the assessment of (CTDIvol) by performing central cumulative dose (DL′ (0)) measurements for L′ = 100 mm on clinical scans.[10] The purpose of the present study was to estimate the CT dose index for head and body PMMA phantoms and to determine the accuracy of the CT radiation dose parameter displayed on the CT scanner console.[9] The CT dose index was estimated using the American Association of Physics in Medicine (AAPM) Report 96 formalism. The study was performed on a Philips 16-slice CT scanner with a 100 mm pencil ionization chamber. The measured body and head phantom doses were compared to selected international dose reference levels and varying deviations were observed. The role of the medical physicist in this study is to track and measure the dose to patients using appropriate indicators.[11,12]

## Materials and Methods

The measurements were performed on a Philips Big Bore 16-slice CT system installed at the Radiotherapy Department of the S. Chiara Hospital, Trento, Italy. The study involved the use of a standard CTDI head phantom, a standard CTDI body phantom, and a Radical 3CT pencil chamber (PC) with a length of 100 mm and a short 10 × 5 ionization chamber (SC) with a charge collection length of 20 mm. Both the chambers were coupled with a Radical 9010 electrometer (Figure 3).

The characterization of the computed tomography (CT) scanner involved preliminary measurements of the CTDI in free air, and the PC (pencil chamber) was placed at the CT center. The selected scan parameters of the series of single-rotation CT protocols were 90-120-140 kV, 100-200-400 mAs, and a slice thickness ranging from 3 mm to 24 mm.

The second series of measurements assessed the CTDIvol with head and body phantoms. These provided a direct comparison between measured CTDIvol values and the nominal value displayed on the CT scanner console and compared international dose reference levels.[4,13-15] The scan parameters for both types of phantom head and body were 120 kV, 100 mA, and a slice thickness of 24 mm.

The final dosimetric evaluations involved the measurement of the central cumulative dose DL′ (0) of the helical head, abdomen, and thorax scans with a scan length L′ of 100 mm and different scan parameters. In these conditions, we obtained DL (0) = CTDIvol. Therefore, we estimated equation (5). DL′ (0) was then compared with the corresponding nominal volume CTDIvol and to the CTDIvol international reference levels. The CT dosimetric values were estimated in

**Table 1.** Normalized Measured CTDI in free air for Different Voltages (kV), Tube Charges (mAs), and X-Ray Slice Collimations (mm).

| Voltage (kV) | Charge (mAs) | Rx (X-ray) slice thickness (mm) | PC Readings (mGy) | Normal. CTDI in free air (mGy) |
|---|---|---|---|---|
| 90 | 100 | 24 | 1.53 | 6.4 |
| 120 | 100 | 24 | 3.27 | 13.6 |
| 140 | 200 | 24 | 4.76 | 19.8 |
| 120 | 100 | 24 | 3.27 | 13.6 |
| 120 | 200 | 24 | 6.54 | 13.6 |
| 120 | 400 | 24 | 13 | 13.5 |
| 120 | 100 | 24 | 3.27 | 13.6 |
| 120 | 100 | 12 | 1.86 | 15.5 |
| 120 | 100 | 6 | 1.02 | 17.0 |
| 120 | 100 | 3 | .73 | 24.4 |

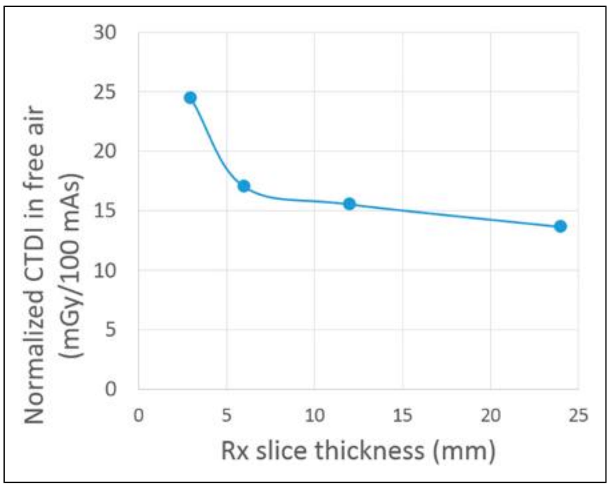


**Figure 4.** Normalized computed tomography dose index (CTDI) in free air (mGy) for different Rx (x-ray) slice thicknesses.

the American Association of Physics in Medicine (AAPM) report 96.[3]

## Results

The result of the (CTDI for free air measurements, in particular, the experimental data, verify that the CTDI calculated in accordance with equation (2) depends on the selected voltage, with higher values corresponding to a higher voltage in as shown in Table 1. The CTDI measurements in the present study, in accordance with data in the literature, showed a linear relationship between CTDI and mAs.[16] The experimental data also verified the relationship between X-ray slice thickness and CTDI in free air. In particular, narrow slices, for example, 3 mm, see Figure 1, emphasize the rule of over beaming.[1]

This result increased CTDI values and the Rx (X-ray) slice thickness will be decrease as shown in Figure 4.

The radiation dose delivered by the head and body PMMA phantom was in good agreement with the dose displayed on the corresponding computed tomography (CT) scanner console as shown in Table 2. According to various published data, the experimental CTDIvol values demonstrate significantly high agreement between the nominal (console) CTDI value and measured CTDI values.[2,14] On the other hand, as described in the earlier sections and in the literature.[1] As explained in the previous section, the CTDI-based approach shows certain limitations in dose assessment for helical scans. The present study provided certain central cumulative dose (DL′ (0)) measurements on helical CT scans to overcome this drawback.[17] These reveal, confirming a good agreement of the data with the corresponding CT scanner console volume CTDIvol and, subsequently, the robustness of the advanced AAPM approach. In addition, CTDIvol of 11.6 and 10.6 mGy obtained for abdomen and thorax scans match the prescriptions of international standards as seen in Table 3, which specify dose reference levels of 15 mGy for body examinations. A similar result was obtained for the head scan the measured and displayed on the corresponding CT scanner console CTDIvol values (<56 mGy) which were below the reference level of 60 mGy.[4]

The comparison of the dose delivered to head and body phantoms with international publication is shown in Table 4. The present study also shows that the dose delivered to patients by the 16-slice CT scanner is below the international dose reference levels for head and body phanton.[2,4,5,10,13-15,18]

## Discussion

The American Association of Physics in Medicine (AAPM) Report 96 formalism and the comprehensive methodology for the evaluation of radiation dose in the CT report of the American Association of Physics in Medicine (AAPM) task group 111 were used to evaluate CT radiation dose exposures.[3,8] The CTDI value was calculated in free air at tube potential (90.120, 140) kV, tube current (100, 200, and 400) mAs and X-ray slice thickness (3, 6, 12, and 24) mm were estimated in this study. The X-ray slice thickness increases the radiation dose for free air decrees and vice versa. The present study was to estimate the CTDI for head and body phantoms

**Table 2.** Percentage Disagreement Between CTDIvol Measurements And The Reported Result Of The Corresponding Dose Displayed on the console (Nominal CTDIvol on the CT Console).

| Body region | PC readings at different phantom locations (mGy) | | | | | CTDIvol (mGy) | | CTDI disagreement (%) |
|---|---|---|---|---|---|---|---|---|
| | Center | 3 | 6 | 9 | 12 | Calculated | Displayed | |
| Head | 2.29 | 2.48 | 2.31 | 2.46 | 2.60 | 10.0 | 10.2 | 1.7 |
| Body | .77 | 1.81 | 1.48 | 1.82 | 1.65 | 5.8 | 6.1 | 5.5 |

**Table 3.** Comparison of the Measured Central Cumulative Dose ($DL'(0)$) to the Dose Displayed on the Console.

| Exam | Charge (mAs/sl) | Pitch (unit less) | SC readings in different phantom locations (mGy) | | | | | Measured $DL'$ (0) (mGy) | Displayed CTDIvol (mGy) | $DL'$ (0)-CTDIvol Disag. (%) |
|---|---|---|---|---|---|---|---|---|---|---|
| | | | Center | 3 | 6 | 9 | 12 | | | |
| Abdomen | 220 | 1.188 | 6.92 | 13.85 | 13.92 | 14.49 | 15.3 | 11.9 | 11.6 | −2.5 |
| Thorax | 200 | 1.063 | 6.10 | 13.69 | 11.79 | 13.72 | 13.48 | 10.8 | 10.6 | −2.0 |
| Head | 550 | .313 | 52.28 | 57.2 | 53.16 | 57.44 | 61.28 | 55.6 | 55.9 | 0.5 |

**Table 4.** Comparison of the Dosimetric Results of the Head and Body Phantom with International Dose Reference Levels.

| Examination | CTDIvol (mGy) | | | | | |
|---|---|---|---|---|---|---|
| | This study | Europe (2004) | UK (2003) | ACR (2008) | Norway (2018) | Sweden (2019) |
| Body | 5.8 | 15 | 14 | 25 | 13 | 12 |
| Head | 10.0 | 60 | 65 | 75 | 60 | 60 |

and to determine the accuracy of the CT radiation dose parameter displayed on the CT scanner console using a 16-slice CT scanner, short ionization chamber, and pencil ionization chamber. The result of the CTDI in the present study was a good agreement for the corresponding CT scanner console value and also the selected international does reference level and varying deviations were observed. The measured CT radiation dose for head and body phantoms was less than the international dose reference level. We advised radiologists to utilize there must be carefully selection of technical parameter of CT scanner that control exposure of patient radiation dose and regular checking of scanner performance with measurement of the CT dose index parameter. The purpose of the present study was computed tomography. The CT dose measurement is a very important measurement in the acceptance of any CT scanner after installation. The CT radiation dose parameter is accepted.

## Conclusions

Computed tomography (CT) is a highly effective tool used by radiologists to detect illness inside the human body and deliver a high dose to patients compared with other imaging modalities. The CT radiation dose reported by the computed tomography console during a CT scan examination is based on the CTDI stated in reports by the American Association of Physics in Medicine (AAPM). The CTDI is a standardized measure of the dose output of the CT system. The present study showed a deviation of 1.7 % and 5.5 % using the American Association of Physics in Medicine's (AAPM) report 96 dose estimation formalism. The measured computed tomography (CT) radiation dose or dosimetric values of certain clinical CT scans are less than the international diagnostic reference levels (DRLs). In particular, this work is in agreement with other studies when it shows that a series of clinical CT scans match the prescriptions of international standards concerning patient exposure.[5] In general, the present study describes the most important examinations and activities of specialists in medical physics working on computed tomography (CT) radiation dose measurements.


### Acknowledgments

The author expresses gratitude to the International Center for Theoretical Physics (ICTP), Addis Ababa University's Physics Department, and Wachumo University for their assistance.

### Declaration Conflict of Interest

The author(s) declared no potential conflicts of interest with respect to the research, authorship, and/or publication of this article.

### Funding

The author(s) received no financial support for the research, authorship, and/or publication of this article.

## Ethical Approval

This article does not report any studies performed on animals.


## ORCID iD

Tadelech S. Mekonin https://orcid.org/0000-0001-9094-3931


## References


1. Bushberg Jerrold T, Seibert J. Anthony, Leidholdt JR Edwin M., Boone John M. *The essential physics of medical imaging*. 3rd ed.. Lippincott Williamas and Wilkins; 2011.
2. Hasford Francis, Bronwin Van Wyk, Thulani Mabhengu, Mboyo Di Tamba Vangu, Augustine Kwame Kyere, John Humphrey Amuasi et al. Determination of dose delivery accuracy in CT examinations. *Journal of Radiation Research and Applied Sciences* 2015;8(4):489-492. https://doi.org/10.1016/j.jrras.2015.05.006.
3. AAPM. The measurement, reporting, and management of radiation dose in CT AAPM Report No 96. *Report of AAPM Task Group 23 of the Diagnostic Imaging Council CT Committee College Park, MD*. (2008).
4. Bongartz G, Golding SJ, Golding AG, Leonardi M, Van Persijn Van Meerten E, Rodríguez R, Schneider K, Calzado A, Geleijns J, Jessen KA et al. European guidelines for multislice computed tomography. *European Commission* 2004;European Commission.
5. Perisinakis K. Determination of the weighted CT dose index in a modern multi-detector CT scanner. *Phys Med Biol*. (2007);52: 6485-6495
6. YuL Liu X, S Leng, JM Kofler, JC Ramirez-Giraldo, QuM Christner J, JC Fletcher, CH McCollough et al. Radiation dose reduction in computed tomography: techniques and future perspective. Imaging Med. *Imaging Med* 2009.
7. Penelope Allisy-Roberts, Jerry Williams. *Farr's Physics for Medical Imaging*. Second Edition. W.B. Saunders; 2008.
8. AAPM. Comprehensive methodology for the evaluation of radiation dose in X-ray computed tomography. In: *AAPM Report No. 111 the Report of AAPM Task Group 111*. College Park, MD: The Future of CT Dosimeter; (2010).
9. Sakhnin L. CT radiation dose optimization and reduction for routine head, chest and abdominal CT examination. *Radiol Diagn Imaging 2* 2017. doi:10.15761/RDI.1000120.
10. Trevisan D, Ravanelli D, Valentini A. Measurements of computed tomography dose index for clinical scans. *Radiat Prot Dosimetry*. (2014);158:389-398.
11. Hakan G. Radiation dose and image quality in diagnostic radiology optimization of the dose image quality relationship with clinical experience from scoliosis radiography, coronary intervention, and aat-panel digital detector. *Acta radiologica* 2002;43(427):1-43.
12. international2009iaea. Dose reduction in CT while maintaining diagnostic confidence feasibility/demonstration study. *INTERNATIONAL ATOMIC ENERGY AGENCY* 2009;(TECDOC Series):1621.
13. McCollough Cynthia, Branham Theresa, Herlihy Vince, Bhargavan Mythreyi, Robbins Lavonne, Bush Krista, McNitt-Gray Michael, Payne J Thomas, Ruckdeschel Tom, Pfeiffer Doug, Cody Dianna, Zeman Robert, ACR (American College of Radiology). Diagnostic Reference Levels From the ACR CT Accreditation Program. *Journal of the American College of Radiology* 2011;8:795-803.
14. European Commission and Directorate-General for Energy, W Jaschke, J Clark, M Hierath, J Damilakis, G Paulo, J Repussard, A Schegerer, G Frija, V Tsapaki, European Union. European study on clinical diagnostic reference levels for X-ray medical imaging: EUCLID. *Publications Office* 2021. doi: 10.2833/452154.
15. PC Shrimpton, Max Hillier, MA Lewis et al. *Doses from Computed Tomography (CT) Examinations in the UK-2003 Review*. Chilton Didcot, Oxon –UK: Chilton; 2005.
16. Douglas M, Barnes GT, Chakraborty DP. Semiempirical model for generating tungsten target x-ray spectra. *Med Phys*. (1991); 18:211-218,
17. Efstathopoulos EP, et al. Reduction of the estimated radiation dose and associated patient risk with prospective ECG-gated 256-slice CT coronary angiography. *Phis Med Biol*. (2009);54:5209-5222.
18. Al Ewaidat H, Zheng X, Khader Y, Abdelrahman M.K, Rawashdeh M.H, Mousa D.S.A, Alawneh K. Z. A et al. Assessment of radiation dose and image quality of multi-detector computed tomography. *Iranian Journal of Radiology* 2018;15. doi:10.5812/iranjradiol.59554.
19. Mkimel M, Mesradi M.R, El Baydaoui R, Toufique Y, Aitelcadi Z, El Kharrim A, Hilali A et al. *Assessment of computed tomography dose index (CTDI) using the platform GEANT4/GATE*. 12. Perspectives in Science; 2019.

Journal of Imaging

*Article*

# The Dose Optimization and Evaluation of Image Quality in the Adult Brain Protocols of Multi-Slice Computed Tomography: A Phantom Study

**Thawatchai Prabsattroo [1,*], Kanokpat Wachirasirikul [1], Prasit Tansangworn [1], Puengjai Punikhom [1] and Waraporn Sudchai [2]**

[1] Department of Radiology, Faculty of Medicine, Khon Kaen University, Khon Kaen 40002, Thailand; kanokpat.w@kkumail.com (K.W.); prasit_ta@kkumail.com (P.T.); pungjai4327@hotmail.com (P.P.)
[2] Nuclear Technology Service Center, Thailand Institute of Nuclear Technology, Nakhon Nayok 26120, Thailand; newsudchai18@gmail.com
* Correspondence: thawatp@kku.ac.th

**Abstract:** Computed tomography examinations have caused high radiation doses for patients, especially for CT scans of the brain. This study aimed to optimize the radiation dose and image quality in adult brain CT protocols. Images were acquired using a Catphan 700 phantom. Radiation doses were recorded as $CTDI_{vol}$ and dose length product (DLP). CT brain protocols were optimized by varying parameters such as kVp, mAs, signal-to-noise ratio (SNR) level, and Clearview iterative reconstruction (IR). The image quality was also evaluated using AutoQA Plus v.1.8.7.0 software. CT number accuracy and linearity had a robust positive correlation with the linear attenuation coefficient ($\mu$) and showed more inaccurate CT numbers when using 80 kVp. The modulation transfer function (MTF) showed a higher value in 100 and 120 kVp protocols ($p < 0.001$), while high-contrast spatial resolution showed a higher value in 80 and 100 kVp protocols ($p < 0.001$). Low-contrast detectability and the contrast-to-noise ratio (CNR) tended to increase when using high mAs, SNR, and the Clearview IR protocol. Noise decreased when using a high radiation dose and a high percentage of Clearview IR. $CTDI_{vol}$ and DLP were increased with increasing kVp, mAs, and SNR levels, while the increasing percentage of Clearview did not affect the radiation dose. Optimized protocols, including radiation dose and image quality, should be evaluated to preserve diagnostic capability. The recommended parameter settings include kVp set between 100 and 120 kVp, mAs ranging from 200 to 300 mAs, SNR level within the range of 0.7–1.0, and an iterative reconstruction value of 30% Clearview to 60% or higher.

**Keywords:** dose optimization; iterative reconstruction; image quality; radiation dose

check for updates

**Citation:** Prabsattroo, T.; Wachirasirikul, K.; Tansangworn, P.; Punikhom, P.; Sudchai, W. The Dose Optimization and Evaluation of Image Quality in the Adult Brain Protocols of Multi-Slice Computed Tomography: A Phantom Study. *J. Imaging* **2023**, *9*, 264. https://doi.org/10.3390/jimaging9120264

Academic Editor: Jussi Tohka

Received: 16 October 2023
Revised: 23 November 2023
Accepted: 24 November 2023
Published: 28 November 2023



## 1. Introduction

Computed tomography examinations have caused high radiation doses for patients, especially for CT scans of the brain [1]. Currently, CT machines use various technologies or innovations to reduce the radiation dose to patients or to ensure the most negligible radiation dose. In addition, there are also efforts to use low-radiation protocols and develop algorithms or image processing to improve image quality, resulting in better image quality [2–7]. Historically, CT protocols were established by the vendor and were not modified or optimized after being used for a long time. Image quality and radiation dose were not considered.

In radiation protection principles, optimization is considered an essential process to ensure that patients receive the appropriate amount of radiation for the examination and that image quality is sufficient for diagnosis [8–11]. Computed tomography (CT) is a diagnostic imaging modality that uses high radiation doses to create images and may expose the patient to radiation risk [12,13]. CT scans of the head expose sensitive tissue, especially the lenses of the eyes, which can be damaged and develop cataracts if the radiation dose exceeds a certain level [13–17].

According to a report by the United States and Canada, CT scan machines have been widely used in many countries and continued to increase among adults, but at a slower pace in more recent years from 2000 and 2016 [18]. The United Nations Scientific Committee on the Effects of Atomic Radiation (UNSCEAR) reported an average annual effective dose received in the United States. The significant increase in the use of ionizing radiation for medicinal reasons resulted in a total increase from 3.0 mSv in 1980 to 6.2 mSv in 2006. CT scan data showed 1.5 mSv of effective dose and contributed a radiation dose to patients of approximately 24.2% of the normal dose received in daily life [1,18]. Many parameters affect the patient's radiation exposure, such as kVp, mA, mAs, pitch, scan range, slice thickness, and the reconstruction algorithm. Acquisition parameters also affect image quality and the performance of images for diagnosis [15,19–22].

Several iterative reconstruction (IR) algorithms are currently available from various CT vendors. IR algorithms are designed to reduce image noise, improve low-contrast detail, reduce artifacts and radiation dose, and maintain high contract resolution. Iterative reconstruction (IR) algorithms are divided into two types: statistical IR algorithms or hybrid and model-based IR algorithms (MBIR) [23]. Statistical IR algorithms are performed using iterative filtration in projection and image space. ASIR, ASIR-V, AIDR3D, iDose, and SAFIRE are commercial statistical IR. MBIR algorithms which are performed using forward projection from the current image estimate in image space to projection space for simulating projection data. After comparing simulated and measured projection data, an image data update can be computed via the back projection of a correction term. The iterative cycle is repeated until a predefined stopping point is reached. VEO, IMR, ADMIRE, and FIRST were the MBIR algorithms [23,24]. ClearView IR operates iteratively in both projection space and image space. The noise that accompanies low-dose acquisitions can be removed while preserving all edges.

Objective and subjective evaluation methods can be used to analyze image quality in CT images [25–28]. In the objective evaluation method, images are evaluated quantitatively using the QA CT phantom. The subjective evaluation method involved the image quality being evaluated by radiologists or experts, who score the image quality. The typical quantitative parameters used to evaluate the image quality include CT number accuracy and linearity, high-contrast spatial resolution, modulation transfer function (MTF), low-contrast detectability and contrast-to-noise ratio (CNR), image noise, uniformity, and mean CT number [29,30].

Optimization protocols should balance radiation and image quality because acquisition parameter changes could affect the image quality. Therefore, the objectives of this study were to optimize the CT brain protocols by varying kVp, mAs, SNR, and the Clearview iterative reconstruction (IR) algorithm and to evaluate the image quality using the qualitative method, using Catphan700 phantom to obtain the image. Image quality evaluation can use AutoQA Plus software and demonstrate CT number accuracy and linearity, high-contrast spatial resolution, modulation transfer function (MTF), low-contrast detectability and contrast-to-noise ratio (CNR), image noise, uniformity, and mean CT number.

## 2. Materials and Methods

This study used a Catphan700 phantom to acquire images, and the CT scanner was Neusoft in a model of NeuViz 128 (Neusoft Medical Systems, Shenyang, China) with 128 slices. The optimized protocols were adjusted by varying kVp, mAs, SNR, and Clearview iterative reconstruction. After finishing the scanning, a radiation dose of CT was recorded as CTDIvol and DLP.

### *2.1. Image Acquisition Protocols*

The scan parameters are presented in Table 1. All CT scans were performed with the same scan parameters, and all data acquisitions were taken 3 consecutive times.

**Table 1.** Data acquisition protocols used for dose optimization in default clinical brain protocols of the Neusoft NeuViz 128 CT scanner.

| Parameters | Default (Optimized Protocol) |
|---|---|
| kVp | 120 (80, 100, 140) |
| mAs | 300 (100, 200, 400) |
| Rotation time | 1.0 s |
| Pitch | 0.5 |
| Slice thickness | 5 mm |
| SNR level | 1.0 (0.3, 0.7, 1.3, 1.7) |
| FOV | 250 mm |
| Kernel | F20 |
| IR | 50% (20%, 30%, 40%, 60%) Clearview |
| Matrix | 512 × 12 |

### 2.2. Data Acquisition and Image Quality Evaluation

The Catphan 700 phantom was used to acquire the image by scanning according to three clinical routine scans for the brain. The AutoQA Plus v.1.8.7.0 software (QA Benchmark, LLC, Ellicott City, MD, USA) was used to analyze image quality.

### 2.3. Catphan 700 Phantom

A Catphan 700 phantom (The Phantom Laboratory Incorporated, Salem, NY, USA) was used to evaluate all image quality [31,32]. The phantom has a cylindrical shape and contains 6 modules, including CTP682 (geometry sensitometry and point source module), CTP714 (30-line pair high-resolution module), CTP515 (subslice and supra-slice low contrast), CTP721 (wave insert), CTP723 (bead blocks), and CTP712 (uniformity section). CT scans of the Catphan phantom were obtained using Neusoft NeuViz 128 (Neusoft Medical Systems, Shenyang, China) [33]. Quality control (QC) testing was performed annually for all CT scanners and the CT number was also calibrated.

### 2.4. CT Number Accuracy and Linearity

The module CTP682, containing different sensitometry targets, was used to perform CT number accuracy and linearity [34–36]. This module has sensitometry targets made from Teflon®, Bone 50%, Delrin®, Bone 20%, acrylic, Polystyrene and low-density polyethylene (LDPE), polymethylpentene (PMP), Lung foam #7112, and air, including a water container. In the circular region of interest (ROI), approximately 80% of each target size was selected and the measured mean CT number was recorded for each target. The mean CT number of each target was compared to the range of actual CT numbers from the specifications of the phantom. The linearity was also tested using Pearson's correlation coefficient (r) between the measured CT number and each target's linear attenuation coefficients ($\mu$). The CT numbers' accuracy should not exceed the tolerance limit from the recommendation range of the Catphan 700 phantom.

### 2.5. The High-Contrast Spatial Resolution and Modulation Transfer Function (MTF)

High-contrast spatial resolution is the ability of a system to distinguish high-contrast objects from neighboring objects [37]. Two broad methods exist to analyze high-contrast spatial resolution by calculating the modulation transfer function (MTF) and objective analysis or resolution bar pattern assessment [37–39]. The spatial resolution is measured by calculating a small wire's point spread function (PSF) with 0.05 mm tungsten (module CTP682). PSF generates line spread functions (LSFs) in both vertical and horizontal directions. The MTF was calculated by taking the Fourier transform and shown in the value line pair/cm at 50%, 10%, and 2% of the MTF. The CTP714 high-resolution module with 1–30 line pair per cm gauges was used to evaluate high resolution. The tolerance levels of spatial resolution in the CT brain scan should exceed 5 lp/cm [36]. The expected values of MTF at 50%, 10%, and 2% exceeded 3, 5, and 7 cycles/cm, respectively [31,40,41].

### 2.6. Low-Contrast Detectability and Contrast-to-Noise Ratio (CNR)

Low-contrast resolution refers to the ability of a system to distinguish between low-contrast structures and their background [6,34,42,43]. Module CTP515 was used to determine CNR, which contains low-contrast supra-slice targets with diameters of 15, 9, 8, 7, 6, 5, 4, 3, and 2 mm, and contrast levels of 0.3%, 0.5%, and 1.0%. CNR measured the difference between target signals and background signals. Low-contrast detectability was also calculated and shown as the theoretical contrast–detail curve. The curve showed the minimum contrast level at the given diameter that should be visible. CNR performance should meet the standards at 1 for the adult head protocol [34].

### 2.7. Image Noise, Uniformity, and Mean CT Number

The CTP71 was used for the measurement of uniformity and image noise [31,34,36,44]. Image uniformity was measured by using the difference value of the maximum HU of the center and the 4 peripheral ROI at 3, 6, 9, and 12 o'clock locations. The noise level was defined as SD and measured at the center with a diameter of ROI 40% of the phantom. The mean CT number represents the center ROI mean for a phantom's 10% ROI size. The difference between the mean CT value of each peripheral ROI and the center ROI should not exceed 5 HU and the noise level should not exceed 5 [34]. The mean CT number should not exceed $12 \pm 10$ HU.

### 2.8. Radiation Dose

The CTDIvol and dose length product (DLP) were used as dose indices for the CT and collected from the dose report. The DLP was calculated by multiplying the CTDIvol by the scan length [21,45].

### 2.9. Statistical Analysis

Quantitative data from image quality evaluation and radiation dose were expressed as means. CT number linearity was tested by using Pearson's correlation. CT accuracy was compared with the tolerance values of recommendation. The parameters for the evaluation of image quality were analyzed using AutoQA Plus software and compared with the default protocol or the reference and tolerance values of the American College of Radiology (ACR) or the International Electrotechnical Commission (IEC). Radiation doses (CTDIvol, DLP) were compared with the default protocol and the percentage difference from the default protocol was also calculated. Statistical analysis was performed with one-way ANOVA followed by Tukey post hoc test for comparisons between groups.

## 3. Results

### 3.1. CT Number Accuracy

Table 2 shows that the correlation coefficient found was between 0.998 and 0.999. It indicates that CT numbers and linear attenuation coefficients have a very high positive relationship. For the default clinical brain protocols at 120 kVp, 300 mAs, SNR 1.0, and 50% Clearview IR algorithm, the CT numbers did not pass the evaluation criteria for Teflon and Delrin. When the kVp was changed to 80 kVp, Acrylic, Bone 50%, LDPE, Bone 20%, Polystyrene, and PMP did not pass the criteria, while Teflon and Delrin did not pass the criteria at 100 kVp. At 140 kVp, Bone 20% and Delrin did not pass the criteria. When the mAs were changed to 100, 200, and 400 mAs, with SNR levels of 0.3, 0.7, 1.3, and 1.7, and 20%, 30%, 40%, and 60% Clearview IR, Teflon and Delrin did not pass the criteria.

### 3.2. Modulation Transfer Function (MTF)

All optimized protocols demonstrated that the MTF passed the evaluation criteria for all percentages of MTF at 50%, 10%, and 2%, with tolerance levels of 3, 5, and 7 cycles/cm, respectively (Table 3). Varying kVp revealed that protocols at 100 and 120 kVp had an MTF value that was 50%, 10%, and 2% higher than protocols at 80 and 140 kVp ($p < 0.001$). When the mAs were optimized to 100, 200, 300, and 400 mAs, it was found that the MTF values at 50%, 10%, and 2% showed a higher MTF when the mAs were increased. When the SNR levels were varied to 0.3, 0.7, 1.0, 1.3, and 1.7, it was found that the MTF value increased as the SNR level increased. Finally, when the IR was at 20%, 30%, 40%, 50%, and 60% Clearview, it was discovered that the MTF value showed a similar value of MTF at 30%, 40%, 50%, and 60% Clearview, while a 20% MTF showed the worst MTF value.

**Table 2.** CT number accuracy in each optimized protocol and material, and correlation coefficient (r) showing the relationship between CT number and attenuation coefficient.

| **Materials** | **80 kVp 300 mAs** | **100 kVp 300 mAs** | **120 kVp 300 mAs (Default)** | **140 kVp 300 mAs** | **120 kVp 100 mAs** | **120 kVp 200 mAs** | **120 kVp 400 mAs** | |
|---|---|---|---|---|---|---|---|---|
| Air | −973.8 | −971.9 | −967.8 | −968 | −968 | −968 | −969.1 | |
| Lung | −806.5 | −805.1 | −798.5 | −800.3 | −798.4 | −800 | −800 | |
| PMP | −211.2 | −190.8 | −177.1 | −171.1 | −176.5 | −176.6 | −176.5 | |
| LDPE | −123.9 | −103.7 | −90 | −82.1 | −89.1 | −88.8 | −89 | |
| Polystyrene | −67.5 | −46.9 | −33.6 | −27.7 | −34.7 | −33.3 | −33.8 | |
| Water | −0.9 | 1.3 | 2.8 | 0.7 | 3.5 | 3.5 | 3.3 | |
| Acrylic | 98.5 | 112.6 | 122.6 | 127.1 | 123.5 | 124.6 | 123.3 | |
| Bone20 | 302 | 168.5 | 186.9 | 223.6 | 186.2 | 187.1 | 187.5 | |
| Delrin | 330.4 | 244.7 | 301.1 | 360.9 | 300.3 | 301.3 | 301.1 | |
| Bone50 | 908.3 | 643.1 | 629.9 | 636 | 628.2 | 631 | 629 | |
| Teflon | 969 | 813.5 | 882 | 931.1 | 882.4 | 882.1 | 883.1 | |
| *r* | 0.998 | 0.998 | 0.999 | 0.999 | 0.999 | 0.999 | 0.999 | |
| Materials | SNR 0.3 | SNR 0.7 | SNR 1.3 | SNR 1.7 | 20% Clearview | 30% Clearview | 40% Clearview | 60% Clearview |
| Air | −969.6 | −968.6 | −966.7 | −967.6 | −969.9 | −969.6 | −970.2 | −965.3 |
| Lung | −800.5 | −799.4 | −798.3 | −797.8 | −800.7 | −799.7 | −801.5 | −797.8 |
| PMP | −177.5 | −176.9 | −177.4 | −176.5 | −176.6 | −176.9 | −177.5 | −175.9 |
| LDPE | −90.8 | −89.3 | −88.8 | −89.2 | −89.3 | −89.9 | −89.7 | −89.6 |
| Polystyrene | −35.5 | −34.7 | −33.9 | −34.3 | −34.6 | −34.5 | −35 | −33.6 |
| Water | 2.2 | 2.5 | 1.8 | 2.6 | 2.7 | 3.7 | 1.4 | 3.2 |
| Acrylic | 122.6 | 124.1 | 123.3 | 123.8 | 123.6 | 123.2 | 123 | 123.3 |
| Bone20 | 188.8 | 186.4 | 187.7 | 188.3 | 188.8 | 189.1 | 187.8 | 184 |
| Delrin | 300.4 | 299.8 | 300.1 | 300 | 299.3 | 300.7 | 299.7 | 300.8 |
| Bone50 | 628.6 | 629.3 | 628.1 | 629.1 | 628.6 | 628.8 | 628.4 | 628.3 |
| Teflon | 881.6 | 881.7 | 879.7 | 880.4 | 882.4 | 881.1 | 879.9 | 882.7 |
| *r* | 0.999 | 0.999 | 0.999 | 0.999 | 0.999 | 0.999 | 0.999 | 0.999 |

**Table 3.** MTF at 50%, 10%, and 2% of optimized protocols.

| **MTF (%)** | **80 kVp 300 mAs** | **100 kVp 300 mAs** | **120 kVp 300 mAs (Default)** | **140 kVp 300 mAs** | **120 kVp 100 mAs** | **120 kVp 200 mAs** | **120 kVp 400 mAs** | |
|---|---|---|---|---|---|---|---|---|
| 50 | 3.74 | 4.37 | 4.18 | 3.86 | 4.03 | 4.28 | 4.5 | |
| 10 | 6.85 | 7.07 | 7.1 | 6.69 | 6.97 | 6.97 | 6.97 | |
| 2 | 8.33 | 8.34 | 8.82 | 8.41 | 8.09 | 8.09 | 8.31 | |
| MTF (%) | SNR 0.3 | SNR 0.7 | SNR 1.3 | SNR 1.7 | 20% Clearview | 30% Clearview | 40% Clearview | 60% Clearview |
| 50 | 4.41 | 4.41 | 4.41 | 4.41 | 3.95 | 4.12 | 4.12 | 4.29 |
| 10 | 6.87 | 6.93 | 6.94 | 7.02 | 6.83 | 6.95 | 7.12 | 7.12 |
| 2 | 8.45 | 8.5 | 8.52 | 8.62 | 8.54 | 8.55 | 8.59 | 8.59 |

### 3.3. High-Contrast Spatial Resolution

Figure 1 shows that the 80 kVp and 100 kVp protocols had higher high-contrast spatial resolution than the 120 kVp and 140 kVp protocols ($p < 0.001$). The mAs, SNR, and percentage Clearview IR algorithm did not affect the high-contrast spatial resolution.

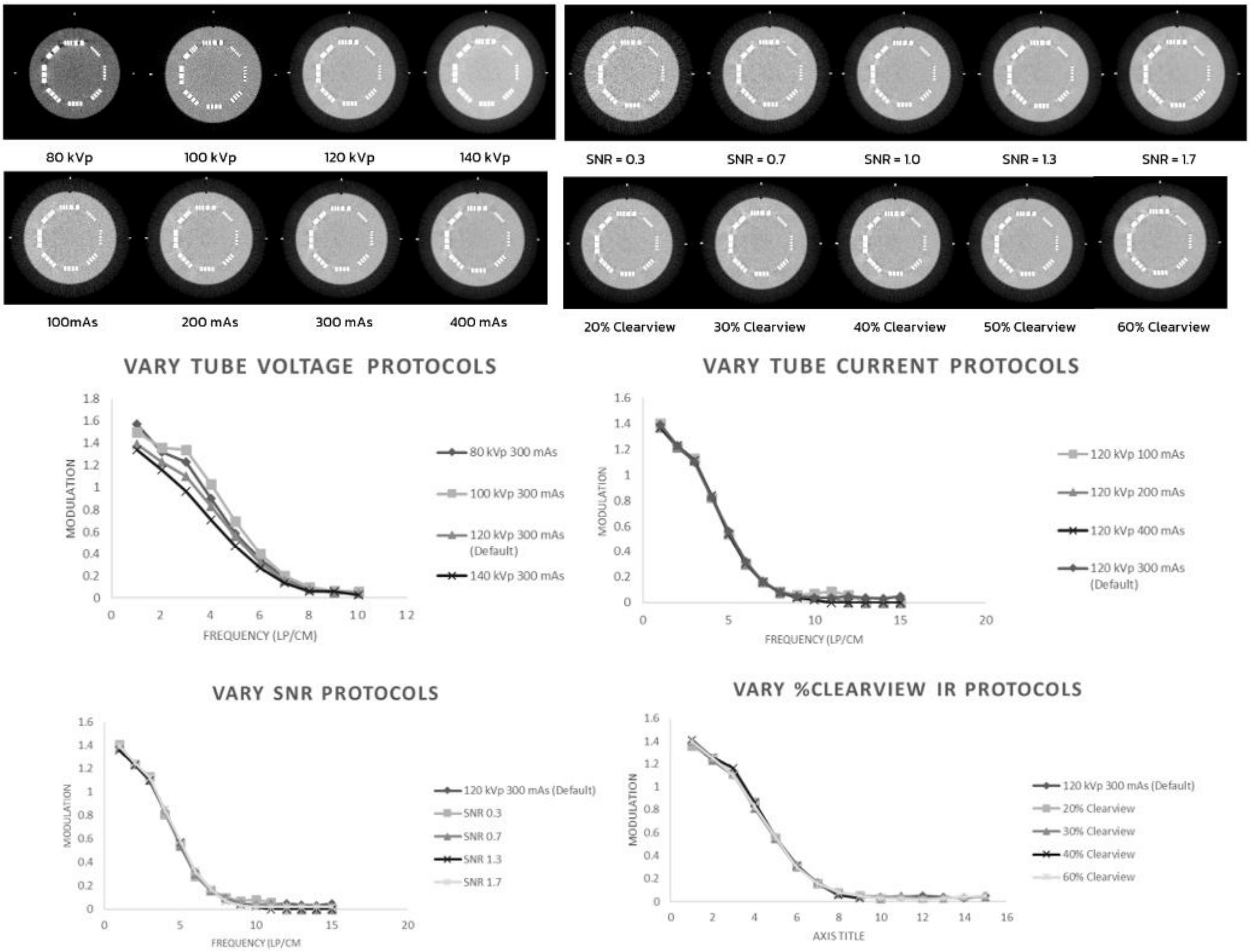


**Figure 1.** High-contrast spatial resolution of optimized protocols.

### 3.4. Low-Contrast Detectability

Figure 2 shows low-contrast detectability in the C-D model. It was found that increasing the kVp, mAs, SNR, and % Clearview IR caused an improvement in the low-contrast detectability in the low-contrast object and for objects with a small diameter. Conversely, decreasing the kVp, mAs, SNR, and % Clearview IR caused a decrease in low-contrast detectability.

### 3.5. Contrast-to-Noise Ratio (CNR)

Figures 3–5 show CNR at percentage contrast objects of 1%, 0.5%, and 0.3% with various object diameters. It was found that increasing the radiation dose by increasing kVp, mAs, and SNR produced a higher CNR, especially for protocols of SNR 1.7 and SNR 1.3. Increasing the % Clearview IR also caused a higher CNR. Conversely, decreasing radiation via decreased kVp, mAs, and SNR showed a decrease in low-contrast detectability. The higher % Clearview IR showed an improvement in CNR.

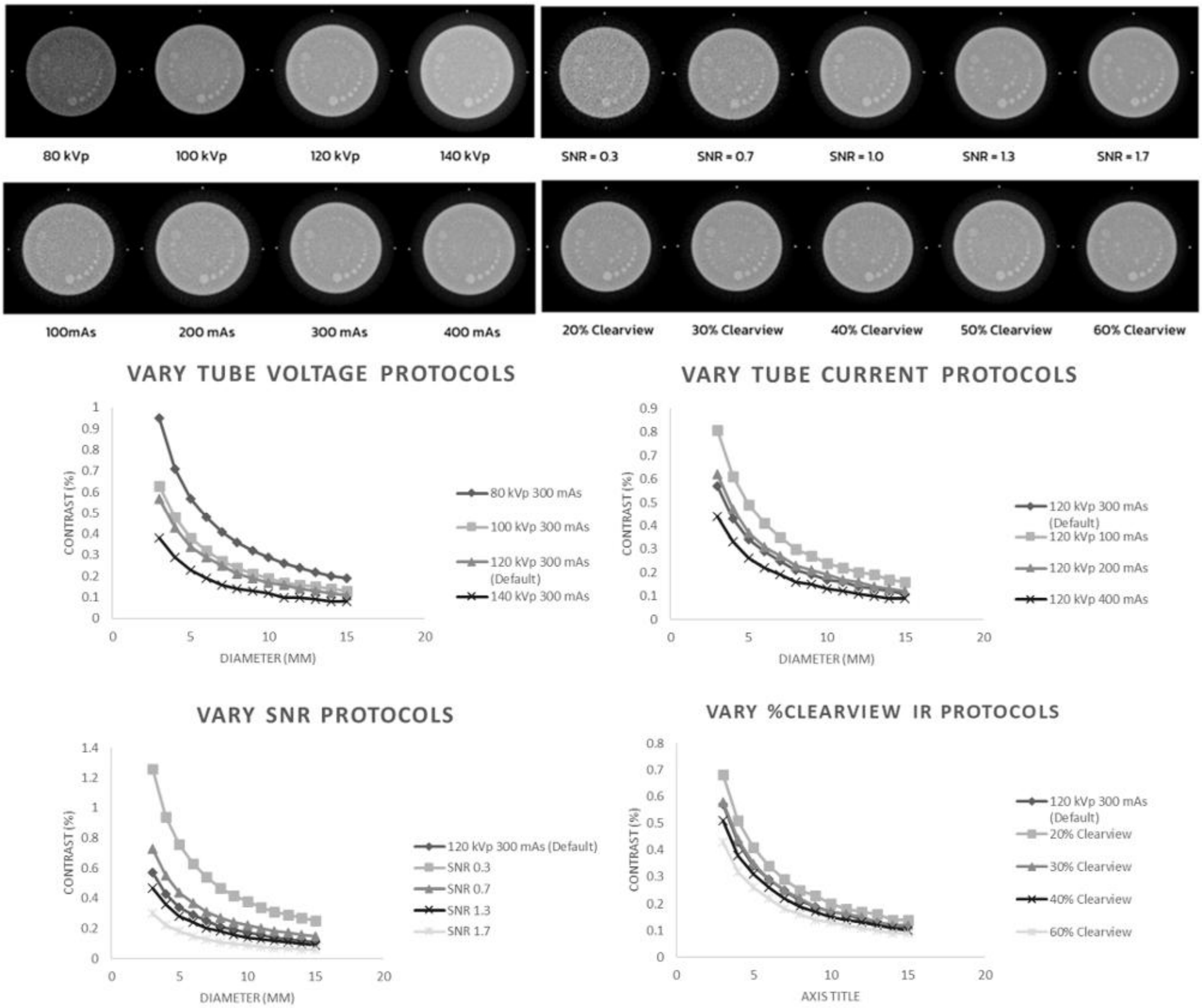


**Figure 2.** Low-contrast detectability of optimized protocols.

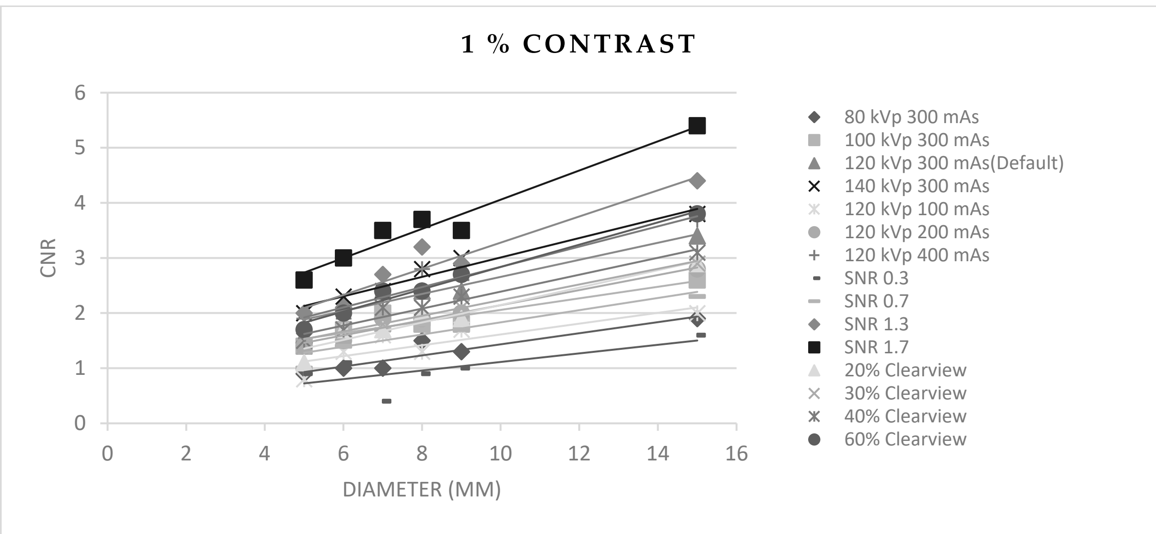


**Figure 3.** Contrast-to-noise ratio at 1% contrast with various diameters of optimized protocols.

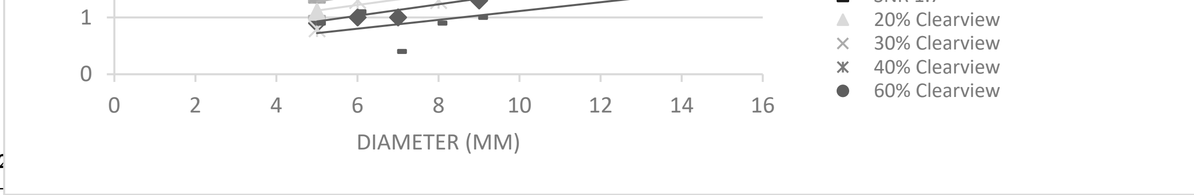


**Figure 4.** Contrast-to-noise ratio at 0.5% contrast with various diameters of optimized protocols.

**Figure 5.** Contrast-to-noise ratio at 0.3% contrast with various diameters of optimized protocols.

*3.6. Image Noise, Uniformity, and Mean CT Number*

Figure 6 shows the noise levels from various optimized protocols. Noise levels were found to be acceptable within a tolerance of 5 HU for protocols of 120 kVp, 140 kVp, 200 mAs, 400 mAs, SNR 0.7, SNR 1.3, SNR 1.7, and all percentages of the Clearview IR algorithm. Figure 7 shows that all protocols failed to meet the acceptable range of 4 HU. Figure 8 demonstrates that the mean CT number of all protocols was within the acceptable range of 12 $\pm$ 10 HU, except for protocol 80 kVp, which had a low mean CT number.

*3.7. Radiation Dose*

Figures 9 and 10 show the CTDIvol and DLP of the optimized protocols. The default clinical protocol of brain CT exhibited CTDIvol and DPL at 37.2 mGy and 827.4 mGy*cm, respectively. It was found that protocols of 80 kVp, 100 kVp, 100 mAs, 200 mAs, SNR 0.3, and SNR 0.7 had lower CTDIvol and DPL than the default clinical protocol ($p < 0.001$), while 140 kVp, 400 mAs, SNR 1.3, and SNR 1.7 showed higher CTDIvol and DLP than the default clinical protocol ($p < 0.001$). CTDIvol and DLP were not affected when the levels of the Clearview IR algorithm changed. Table 4 shows the percentage difference in CTDIvol and DLP compared to the default clinical protocol. The lower CTDIvol and DPL protocol could decrease CTDIvol to 33.3–80.1% mGy and DLP to 33.4–80.4% mGy*cm. A higher dose protocol could increase CTDIvol to 33.6–147.6% mGy and DLP to 30.3–141.8% mGy*cm.

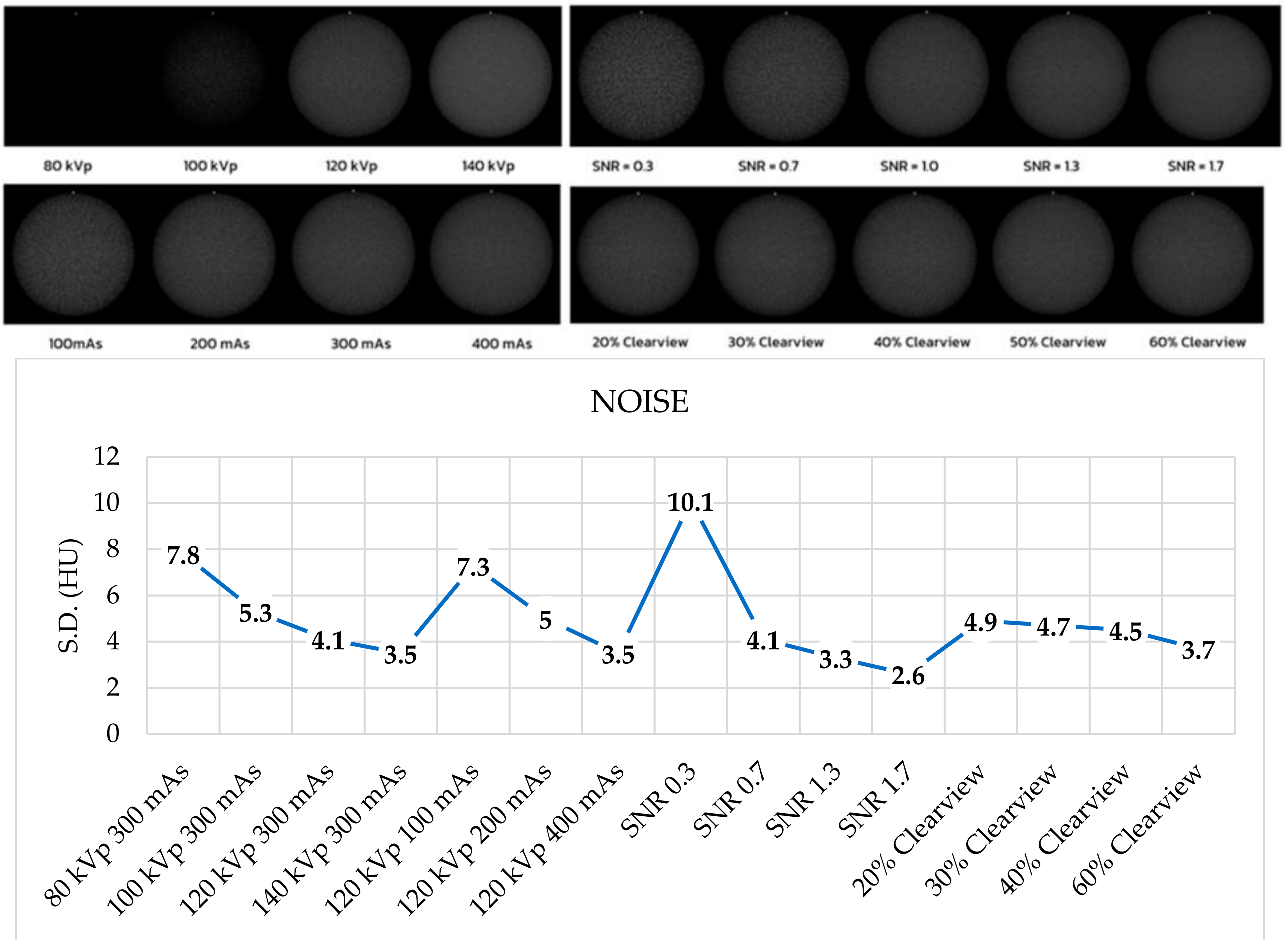


**Figure 6.** Noise level of optimized protocols.

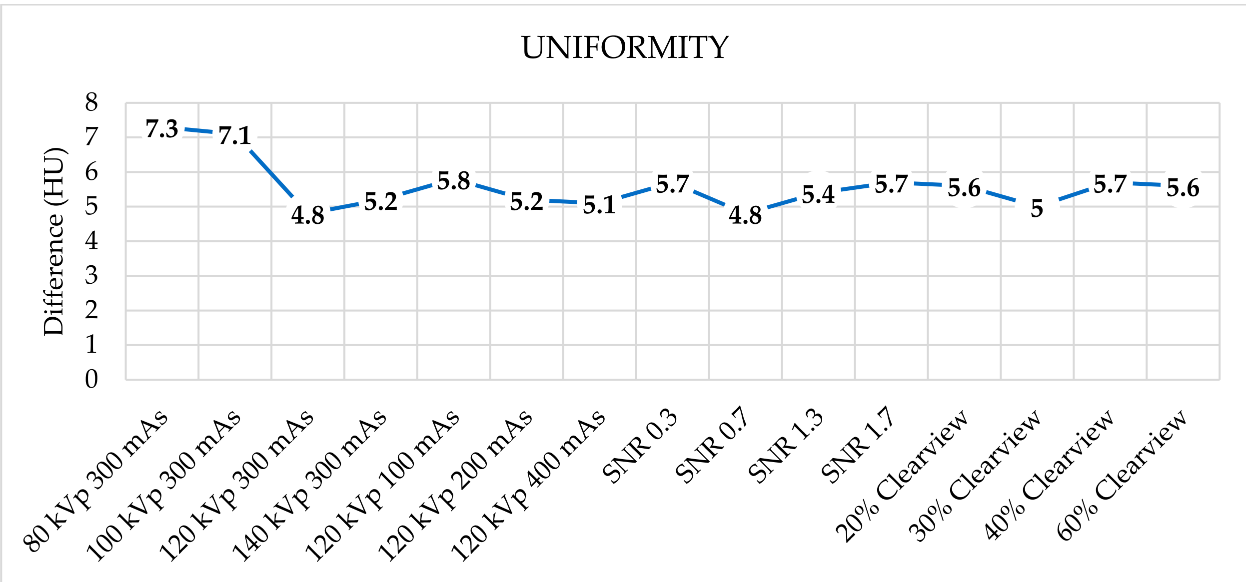


**Figure 7.** Uniformity of optimized protocols.

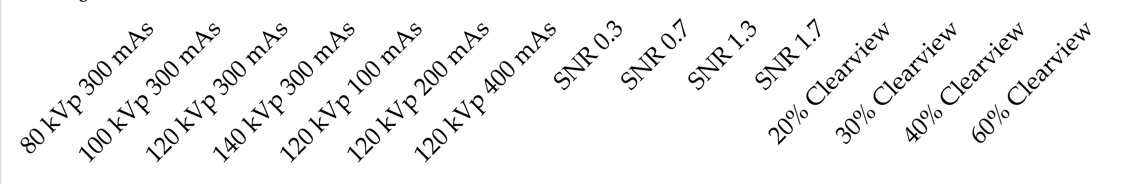


**Figure 8.** Mean CT number of optimized protocols.

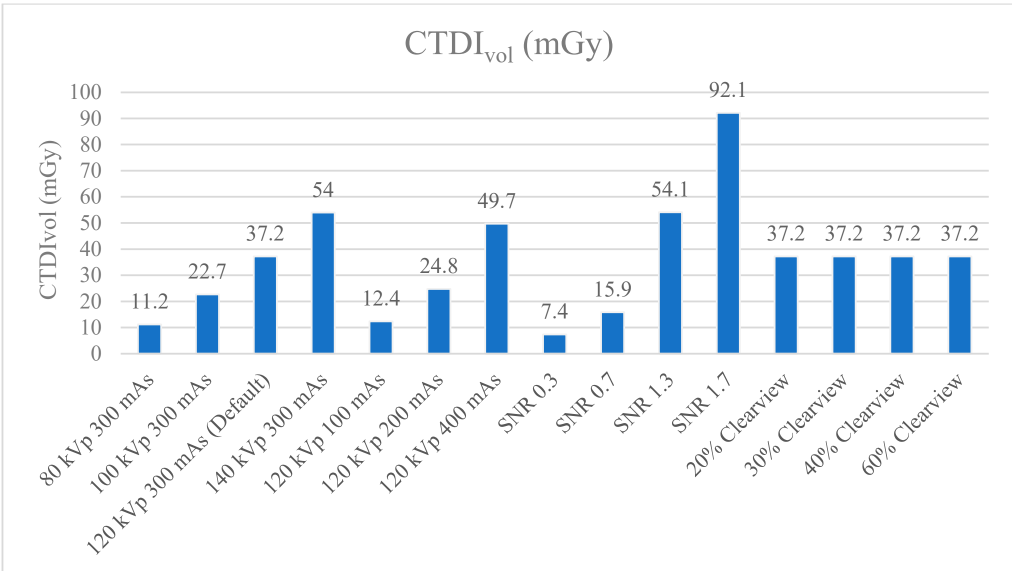


**Figure 9.** $CTDI_{vol}$ (mGy) of optimized protocols.

**Table 4.** Percentage difference in CTDIvol and DLP compared to default clinical protocols.

| | **80 kVp 300 mAs** | **100 kVp 300 mAs** | **120 kVp 300 mAs (Default)** | **140 kVp 300 mAs** | **120 kVp 100 mAs** | **120 kVp 200 mAs** | **120 kVp 400 mAs** | |
|---|---|---|---|---|---|---|---|---|
| % Diff of CTDIvol | −69.9 | −39.0 | 0.0 | 45.2 | −66.7 | −33.3 | 33.6 | |
| % Diff of DLP | −70.7 | −40.4 | 0.0 | 41.8 | −67.4 | −34.8 | 30.3 | |
| | SNR 0.3 | SNR 0.7 | SNR 1.3 | SNR 1.7 | 20% Clearview | 30% Clearview | 40% Clearview | 60% Clearview |
| % Diff of CTDIvol | −80.1 | −57.3 | 45.4 | 147.6 | 0.0 | 0.0 | 0.0 | 0.0 |
| % Diff of DLP | −80.4 | −58.3 | 45.3 | 141.8 | 0.0 | 0.0 | 0.0 | 0.0 |

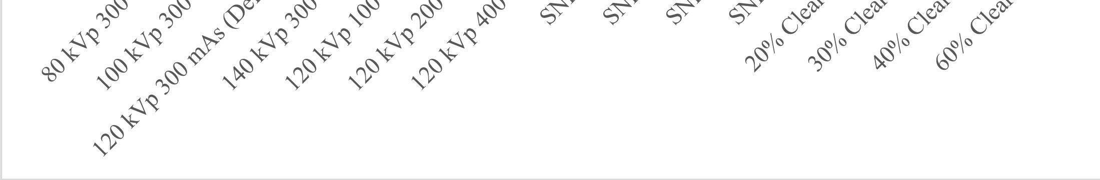

**Figure 10.** DLP (mGy*cm) of optimized protocols.

## 4. Discussion

Optimization is considered an essential process in the principles of radiation protection to ensure that patients receive the appropriate amount of radiation for the examination and that image quality is sufficient for diagnosis. Computed tomography (CT) is one of the diagnostic imaging modalities that uses high radiation doses to form images and may contribute to the radiation risk to the patient. CT scans of the head expose sensitive organs, particularly the lenses of the eyes, which may be damaged and develop cataracts if the radiation dose exceeds a certain threshold. This study aimed to optimize the protocol for CT brain scans, a routine protocol used in clinical practice. The protocol was adjusted with the following scanning parameters: kVp (80, 100, 120, 140), mAs (100, 200, 300, 400), SNR (0.3, 0.7, 1, 1.3, 1.7), and the Iterative Reconstruction algorithm (20%, 30%, 40%, 50%, 60% Clearview). Moreover, quantitative image quality was also evaluated using the Catphan700 phantom to acquire images and evaluate the CT number accuracy and linearity, MTF, high-contrast spatial resolution, low-contrast detectability, CNR, image noise and uniformity, and mean CT number. CTDIvol and DLP values were also recorded and evaluated in various adjusted brain protocols.

The results demonstrated that CT number accuracy was within the specified range for most materials and showed a linear relationship between each material's linear absorption coefficient (μ) and CT number. The correlation coefficient ($r$) was within the range of 0.998165 to 0.999701, showing a strong positive relationship. For the 80 kVp protocol adjustment, it was found that the CT number accuracy showed out-of-range CT numbers in many materials because the average energy was decreasing, affecting the absorption coefficient (μ) and resulting in the CT number increasing [35]. Usually, 120 kVp is used for CT scans; this machine has an effective energy of approximately 60 keV. Reducing the energy to 80 kVp will affect the average energy and CT number accuracy. In addition, the factors affecting the CT number accuracy depend on the filter and patient's slice thickness [46,47]. Therefore, the CT number measurement for diagnosis should be considered carefully because of the high error of CT number six. Some materials in another protocol also showed an error in CT number accuracy. It has been recommended that water calibration should be performed regularly to help maintain the accuracy of CT numbers, especially the CT number accuracy of the water material [36].

High-contrast spatial resolution is used to distinguish small objects with high contrast. It can be measured in two ways, using MTF and high-resolution bar patterns. MTF values of 50%, 10%, and 2% of all protocols were found to have passed the 3 lp/cm, 5 lp/cm, and 7 lp/cm benchmarks, respectively. The results demonstrated that the 80 and 140 kVp protocol showed lower MTF values than 100 and 120 kVp because of the increasing noise at 80 kVp and the scatter radiation at 140 kVp [48]. Increasing mAS and SNR could increase radiation, resulting in low noise levels. The 20% Clearview IR showed the worst MTF because the power of IR at 20% was not enough to improve the image quality. High-resolution assessments using bar patterns at 80 and 100 kVp protocols showed higher high-contrast spatial resolution because the lower kVp could increase the high-contrast resolution of the images. According to the previous study, the factors affecting MTF and spatial resolution were not only the reconstruction algorithms, but also the detector width, effective slice thickness, object-to-detector distance, X-ray tube focal spot size, and matrix size. These factors also affect MTF and spatial resolution [49,50]. Research by Yali Li et al. found that 10% of MTF was 6.98 $\pm$ 0.40 lp/cm, correlating with a subjective assessment showing 7 lp/cm. Moreover, Clearview is suitable for low-dose protocols because it reduces noise and artifacts [42]

Low-contrast detectability is the ability to separate low-contrast objects from the background. It was found that protocols that use low radiation doses tend to have decreased low-contrast resolution, such as the SNR 0.3 protocol, 80 kVp protocol, and 100 kVp protocol. The protocols with improved low-contrast resolution were the SNR 1.7 protocol, 140 kVp protocol, and 60% Clearview protocol. In addition, it was found that the CNR value decreased with the percentage contrast of the object decrease and the small diameter of the object. Studies by Manson EN et al. and Gulliksrud K et al. showed that noise was an essential factor that reduced low-contrast resolution and CNR [51,52]. Moreover, higher radiation dose protocols and a higher percentage of reconstruction algorithms could improve the low-contrast resolution and CNR [51].

The evaluation of image uniformity was undertaken to measure the stability of the CT number by comparing the CT number values in the center of the phantom with the peripheral edges of the phantom. It was found that the uniformity of the images was not within the criteria specified in every protocol, with values exceeding $\pm$4 HU. Noise is the average of the standard deviation (SD) measured at the center of the phantom. Protocols that use high radiation doses, such as high mAs, high kVp, and high IR % Clearview, tend to decrease noise. Research by Yali Li et al. found that the protocol that increased the radiation dose and iterative reconstruction algorithm reduced noise and improved the image quality [42].

CTDIvol and DLP were used to evaluate the radiation dose and to act as a dose index in the CT. Annual quality controls are conducted in CT to measure the CTDIvol, and the value shown in the CT display was not different from the acceptable threshold of $\pm$20%. The DLP value obtained from CTDIvol multiplied by scan length according to the clinical default protocol of CT brain showed 37.2 mGy of CTDIvol. Increasing mAs, kVp, and SNR showed a higher CTDIvol, while increasing the percentage of the Clearview IR algorithm did not affect CTDIvol, but did affect image quality [43,53]. Research by Ozdil Baskan et al. [2] demonstrated that many parameters reduced the radiation dose to some extent, such as kVp, mAs, automated tube current modulation, adaptive dose collimation, and appropriate noise-reduction reconstruction algorithms. Adjusting such parameters will affect the image quality; therefore, adjusting the parameters should be considered. The data demonstrate that a higher % Clearview IR could enhance the MTF, CNR, and low-contrast detectability, and suppress the noise level. In other words, when decreasing the radiation dose or using low protocol, IR can improve and maintain image quality in the acceptable range [54,55].

Because this study was carried out on a Catphan phantom, CT images of patients should also be analyzed. Furthermore, optimization was performed in one CT machine from a specific manufacturer; the optimization parameter, algorithm, and image quality result could differ if another manufacturer were used. We propose that this research be conducted in the CT brain's low-dose protocol to evaluate the performance of the Clearview

IR algorithm for noise reduction. Other parameters that affect radiation dose and image quality could be investigated, and radiologists' subjective evaluations should be included for the overall image quality evaluation. Moreover, the proper training of radiologist and technologist staff is very important to select the most appropriate CT image acquisition and reconstruction parameters to improve image quality and optimize patient radiation exposure. It was found that staff training on radiation dose and dose optimization applied in pediatric CT scans showed efficacy for dose reduction and increasing dose awareness in patients [56,57].

## 5. Conclusions

The default clinical brain protocol should be optimized for image quality and radiation dose balance. kVp should be set between 100 and 120 kVp because adjusting the kVp below 100 kVp results in a large discrepancy in the CT number. The mAs should be in the range of 200–300 mAs, because adjusting the mAs value to 200 will reduce the radiation dose, but the image quality in CNR and low-contrast detectability will be similar to the default brain protocol. The SNR level should be in the range of 0.7–1.0, because adjusting the SNR level to 0.7 will reduce the radiation dose but result in a CNR, low-contrast detectability, and noise within an acceptable range. However, the value of uniformity will increase. Iterative reconstruction should be adjusted to a value between 30% Clearview and 60% Clearview or more. Adjusting Clearview to 30% or more will result in CNR, low-contrast detectability, and noise reduction without affecting radiation dose. However, the noise and non-uniformity of CT images increased when using low-dose protocols.

**Author Contributions:** Conceptualization, P.T.; methodology, P.T., K.W. and T.P.; software, P.T. and W.S.; validation, P.T.; formal analysis, P.T., K.W. and T.P.; investigation, P.T., K.W. and T.P.; resources, P.P.; data curation, P.T. and W.S.; writing—original draft preparation, P.T., K.W. and T.P.; writing—review and editing, P.T.; visualization, P.T., K.W. and T.P.; supervision, P.T.; project administration, P.T. All authors have read and agreed to the published version of the manuscript.

**Funding:** This research received no external funding.

**Institutional Review Board Statement:** Not applicable.

**Informed Consent Statement:** Not applicable.

**Data Availability Statement:** Data are contained within the article.

**Conflicts of Interest:** The authors declare no conflict of interest.

## Abbreviations

CNR, contrast-to-noise ratio; CT, computed tomography; HU, Hounsfield units; keV, kiloelectronvolt; kVp, kilovolt peak; DLP, dose length product; SNR, signal-to-noise ratio; IR, iterative reconstruction; MTF, modulation transfer function.

## References

1. Baselet, B.; Rombouts, C.; Benotmane, A.M.; Baatout, S.; Aerts, A. Cardiovascular diseases related to ionizing radiation: The risk of low-dose exposure. *Int. J. Mol. Med.* **2016**, *38*, 1623–1641. [CrossRef] [PubMed]
2. Baskan, O.; Erol, C.; Ozbek, H.; Paksoy, Y. Effect of radiation dose reduction on image quality in adult head CT with noise-suppressing reconstruction system with a 256 slice MDCT. *J. Appl. Clin. Med. Phys.* **2015**, *16*, 285–296. [CrossRef] [PubMed]
3. Wang, R.; Schoepf, U.J.; Wu, R.; Reddy, R.P.; Zhang, C.; Yu, W.; Liu, Y.; Zhang, Z. Image quality and radiation dose of low dose coronary CT angiography in obese patients: Sinogram affirmed iterative reconstruction versus filtered back projection. *Eur. J. Radiol.* **2012**, *81*, 3141–3145. [CrossRef]
4. Wichmann, J.L.; Hardie, A.D.; Schoepf, U.J.; Felmly, L.M.; Perry, J.D.; Varga-Szemes, A.; Mangold, S.; Caruso, D.; Canstein, C.; Vogl, T.J.; et al. Single-and dual-energy CT of the abdomen: Comparison of radiation dose and image quality of 2nd and 3rd generation dual-source CT. *Eur. Radiol.* **2017**, *27*, 642–650. [CrossRef] [PubMed]

5. Schuhbaeck, A.; Achenbach, S.; Layritz, C.; Eisentopf, J.; Hecker, F.; Pflederer, T.; Gauss, S.; Rixe, J.; Kalender, W.; Daniel, W.G.; et al. Image quality of ultra-low radiation exposure coronary CT angiography with an effective dose< 0.1 mSv using high-pitch spiral acquisition and raw data-based iterative reconstruction. *Eur. Radiol.* **2013**, *23*, 597–606.
6. Nakaura, T.; Kidoh, M.; Sakaino, N.; Utsunomiya, D.; Oda, S.; Kawahara, T.; Harada, K.; Yamashita, Y. Low contrast-and low radiation dose protocol for cardiac CT of thin adults at 256-row CT: Usefulness of low tube voltage scans and the hybrid iterative reconstruction algorithm. *Int. J. Cardiovasc. Imaging* **2013**, *29*, 913–923. [CrossRef] [PubMed]
7. Nagayama, Y.; Iwashita, K.; Maruyama, N.; Uetani, H.; Goto, M.; Sakabe, D.; Emoto, T.; Nakato, K.; Shigematsu, S.; Kato, Y.; et al. Deep learning-based reconstruction can improve the image quality of low radiation dose head CT. *Eur. Radiol.* **2023**, *33*, 3253–3265. [CrossRef] [PubMed]
8. Vassileva, J.; Rehani, M. Diagnostic reference levels. *AJR Am. J. Roentgenol.* **2015**, *204*, W1–W3. [CrossRef] [PubMed]
9. Vañó, E.; Miller, D.; Martin, C.; Rehani, M.; Kang, K.; Rosenstein, M.; Ortiz-López, P.; Mattsson, S.; Padovani, R.; Rogers, A. ICRP publication 135: Diagnostic reference levels in medical imaging. *Ann. ICRP* **2017**, *46*, 1–144. [CrossRef]
10. Seibert, J.A. Tradeoffs between image quality and dose. *Pediatr. Radiol.* **2004**, *34*, S183–S195. [CrossRef]
11. Strauss, K.J.; Goske, M.J.; Kaste, S.C.; Bulas, D.; Frush, D.P.; Butler, P.F.; Morrison, G.; Callahan, M.J.; Applegate, K.E. Image gently: Ten steps you can take to optimize image quality and lower CT dose for pediatric patients. *Am. J. Roentgenol.* **2010**, *194*, 868–873. [CrossRef] [PubMed]
12. Power, S.P.; Moloney, F.; Twomey, M.; James, K.; O'Connor, O.J.; Maher, M.M. Computed tomography and patient risk: Facts, perceptions and uncertainties. *World J. Radiol.* **2016**, *8*, 902. [CrossRef]
13. Brody, A.S.; Frush, D.P.; Huda, W.; Brent, R.L.; Section on Radiology. Radiation risk to children from computed tomography. *Pediatrics* **2007**, *120*, 677–682. [CrossRef] [PubMed]
14. Omer, H.; Alameen, S.; Mahmoud, W.E.; Sulieman, A.; Nasir, O.; Abolaban, F. Eye lens and thyroid gland radiation exposure for patients undergoing brain computed tomography examination. *Saudi J. Biol. Sci.* **2021**, *28*, 342–346. [CrossRef] [PubMed]
15. Tarkiainen, J.; Nadhum, M.; Heikkilä, A.; Rinta-Kiikka, I.; Joutsen, A. Radiation dose of the eye lens in CT examinations of the brain in clinical practice—The effect of radiographer training to optimise gantry tilt and scan length. *Radiat. Prot. Dosim.* **2023**, *199*, 391–398. [CrossRef]
16. Tien, H.C.; Tremblay, L.N.; Rizoli, S.B.; Gelberg, J.B.; Spencer, F.; Caldwell, C.; Brenneman, F.D. Radiation exposure from diagnostic imaging in severely injured trauma patients. *J. Trauma Acute Care Surg.* **2007**, *62*, 151–156. [CrossRef] [PubMed]
17. Lin, E.C. Radiation risk from medical imaging. In *Mayo Clinic Proceedings*; Elsevier: Amsterdam, The Netherlands, 2010; pp. 1142–1146.
18. Smith-Bindman, R.; Kwan, M.L.; Marlow, E.C.; Theis, M.K.; Bolch, W.; Cheng, S.Y.; Bowles, E.J.A.; Duncan, J.R.; Greenlee, R.T.; Kushi, L.H.; et al. Trends in use of medical imaging in US health care systems and in Ontario, Canada, 2000–2016. *JAMA* **2019**, *322*, 843–856. [CrossRef]
19. Geise, R.A. Computed tomography: Physical principles, clinical applications, and quality control. *Radiology* **1995**, *194*, 782. [CrossRef]
20. Mayo-Smith, W.W.; Hara, A.K.; Mahesh, M.; Sahani, D.V.; Pavlicek, W. How I do it: Managing radiation dose in CT. *Radiology* **2014**, *273*, 657–672. [CrossRef]
21. McNitt-Gray, M.F. AAPM/RSNA physics tutorial for residents: Topics in CT: Radiation dose in CT. *Radiographics* **2002**, *22*, 1541–1553. [CrossRef]
22. Raman, S.P.; Mahesh, M.; Blasko, R.V.; Fishman, E.K. CT scan parameters and radiation dose: Practical advice for radiologists. *J. Am. Coll. Radiol.* **2013**, *10*, 840–846. [CrossRef] [PubMed]
23. Stiller, W. Basics of iterative reconstruction methods in computed tomography: A vendor-independent overview. *Eur. J. Radiol.* **2018**, *109*, 147–154. [CrossRef] [PubMed]
24. Geyer, L.L.; Schoepf, U.J.; Meinel, F.G.; Nance, J.W., Jr.; Bastarrika, G.; Leipsic, J.A.; Paul, N.S.; Rengo, M.; Laghi, A.; De Cecco, C.N. State of the art: Iterative CT reconstruction techniques. *Radiology* **2015**, *276*, 339–357. [CrossRef] [PubMed]
25. Kim, J.H.; Yoon, H.J.; Lee, E.; Kim, I.; Cha, Y.K.; Bak, S.H. Validation of deep-learning image reconstruction for low-dose chest computed tomography scan: Emphasis on image quality and noise. *Korean J. Radiol.* **2021**, *22*, 131. [CrossRef]
26. Padole, A.M.; Sagar, P.; Westra, S.J.; Lim, R.; Nimkin, K.; Kalra, M.K.; Gee, M.S.; Rehani, M.M. Development and validation of image quality scoring criteria (IQSC) for pediatric CT: A preliminary study. *Insights Imaging* **2019**, *10*, 1–11. [CrossRef]
27. Scholtz, J.-E.; Kaup, M.; Kraft, J.; Nöske, E.-M.; Scheerer, F.; Schulz, B.; Burck, I.; Wagenblast, J.; Kerl, J.M.; Bauer, R.W.; et al. Objective and subjective image quality of primary and recurrent squamous cell carcinoma on head and neck low-tube-voltage 80-kVp computed tomography. *Neuroradiology* **2015**, *57*, 645–651. [CrossRef]
28. Tamura, A.; Mukaida, E.; Ota, Y.; Kamata, M.; Abe, S.; Yoshioka, K. Superior objective and subjective image quality of deep learning reconstruction for low-dose abdominal CT imaging in comparison with model-based iterative reconstruction and filtered back projection. *Br. J. Radiol.* **2021**, *94*, 20201357. [CrossRef]
29. Pahn, G.; Skornitzke, S.; Schlemmer, H.P.; Kauczor, H.U.; Stiller, W. Toward standardized quantitative image quality (IQ) assessment in computed tomography (CT): A comprehensive framework for automated and comparative IQ analysis based on ICRU Report 87. *Phys. Med.* **2016**, *32*, 104–115. [CrossRef]

30. Hussain, F.A.; Mail, N.; Shamy, A.M.; Alghamdi, S.; Saoudi, A. A qualitative and quantitative analysis of radiation dose and image quality of computed tomography images using adaptive statistical iterative reconstruction. *J. Appl. Clin. Med. Phys.* **2016**, *17*, 419–432. [CrossRef]
31. Mail, T.B. Catphan® 700 Manual. 2013. Available online: https://static1.squarespace.com/static/5367b059e4b05a1adcd295c2/t/58b5c5ff2994ca89008893d9/1488307742189/Catphan700Manual.pdf (accessed on 1 August 2023).
32. Goodenough, D.; Levy, J.; Kristinsson, S.; Fredriksson, J.; Olafsdottir, H.; Healy, A. Method and phantom to study combined effects of in-plane (x, y) and z-axis resolution for 3D CT imaging. *J. Appl. Clin. Med. Phys.* **2016**, *17*, 440–452. [CrossRef]
33. Neusoft Medical Systems Co., Ltd. Nuesoft NeuViz 128 Computed Tomography [Internet]. 2016. Available online: https://intermed1.com/wp-content/uploads/2019/03/NeuViz128_brochure_0716.pdf (accessed on 15 September 2023).
34. Dillon, C.; Davidson, C.; Hernandez, D. 2017 Computed Tomography Quality Control Manual. American College of Radiology. 2017, pp. 73–74. Available online: https://www.acr.org/-/media/ACR/Files/Clinical-Resources/QC-Manuals/CT_QCManual.pdf (accessed on 15 September 2023).
35. Anam, C.; Amilia, R.; Naufal, A.; Budi, W.S.; Maya, A.T.; Dougherty, G. The automated measurement of CT number linearity using an ACR accreditation phantom. *Biomed. Phys. Eng. Express* **2022**, *9*, 017002. [CrossRef] [PubMed]
36. McCollough, C.H.; Bruesewitz, M.R.; McNitt-Gray, M.F.; Bush, K.; Ruckdeschel, T.; Payne, J.T.; Brink, J.A.; Zeman, R.K. The phantom portion of the American College of Radiology (ACR) Computed Tomography (CT) accreditation program: Practical tips, artifact examples, and pitfalls to avoid. *Med. Phys.* **2004**, *31*, 2423–2442. [CrossRef] [PubMed]
37. Friedman, S.N.; Fung, G.S.; Siewerdsen, J.H.; Tsui, B.M. A simple approach to measure computed tomography (CT) modulation transfer function (MTF) and noise-power spectrum (NPS) using the American College of Radiology (ACR) accreditation phantom. *Med. Phys.* **2013**, *40*, 051907. [CrossRef] [PubMed]
38. Takenaga, T.; Katsuragawa, S.; Goto, M.; Hatemura, M.; Uchiyama, Y.; Shiraishi, J. Modulation transfer function measurement of CT images by use of a circular edge method with a logistic curve-fitting technique. *Radiol. Phys. Technol.* **2015**, *8*, 53–59. [CrossRef] [PubMed]
39. Judy, P.F. The line spread function and modulation transfer function of a computed tomographic scanner. *Med. Phys.* **1976**, *3*, 233–236. [CrossRef] [PubMed]
40. Bissonnette, J.P.; Moseley, D.J.; Jaffray, D.A. A quality assurance program for image quality of cone-beam CT guidance in radiation therapy. *Med. Phys.* **2008**, *35*, 1807–1815. [CrossRef]
41. STRÅLSKYDDSFRÅGOR NRO. A Quality Control Programme for Radiodiagnostic Equipment: Acceptance Tests. 1999. Available online: https://citeseerx.ist.psu.edu/document?repid=rep1&type=pdf&doi=bf7cceea8dabd373fd33df43393d1c569f70be03 (accessed on 15 September 2023).
42. Li, Y.; Jiang, Y.; Liu, H.; Yu, X.; Chen, S.; Ma, D.; Gao, J.; Wu, Y. A phantom study comparing low-dose CT physical image quality from five different CT scanners. *Quant. Imaging Med. Surg.* **2022**, *12*, 766. [CrossRef]
43. Bellesi, L.; Wyttenbach, R.; Gaudino, D.; Colleoni, P.; Pupillo, F.; Carrara, M.; Braghetti, A.; Puligheddu, C.; Presilla, S. A simple method for low-contrast detectability, image quality and dose optimisation with CT iterative reconstruction algorithms and model observers. *Eur. Radiol. Exp.* **2017**, *1*, 1–10. [CrossRef]
44. Anam, C.; Amilia, R.; Naufal, A.; Sutanto, H.; Dwihapsari, Y.; Fujibuchi, T.; Dougherty, G. Impact of Noise Level on the Accuracy of Automated Measurement of CT Number Linearity on ACR CT and Computational Phantoms. *J. Biomed. Phys. Eng.* **2023**, *13*, 353.
45. Romans, L.E. *Computed Tomography for Technologist, A Comprehensive Text*; Wolter Kluwer Health; Lippincott Williams and Wilkins: Philadelphia, PA, USA, 2011.
46. Baxter, B.S.; Sorenson, J.A. Factors affecting the measurement of size and CT number in computed tomography. *Investig. Radiol.* **1981**, *16*, 337–341. [CrossRef]
47. Cann, C.E. Quantitative CT for determination of bone mineral density: A review. *Radiology* **1988**, *166*, 509–522. [CrossRef]
48. Rueckel, J.; Stockmar, M.; Pfeiffer, F.; Herzen, J. Spatial resolution characterization of a X-ray microCT system. *Appl. Radiat. Isot.* **2014**, *94*, 230–234. [CrossRef] [PubMed]
49. Grimmer, R.; Krause, J.; Karolczak, M.; Lapp, R.; Kachelriess, M. Assessment of spatial resolution in CT. In *2008 IEEE Nuclear Science Symposium Conference Record*; IEEE: New York, NY, USA, 2008; pp. 5562–5566.
50. Roa, A.M.A.; Andersen, H.K.; Martinsen, A.C.T. CT image quality over time: Comparison of image quality for six different CT scanners over a six-year period. *J. Appl. Clin. Med. Phys.* **2015**, *16*, 350–365. [CrossRef] [PubMed]
51. Gulliksrud, K.; Stokke, C.; Martinsen, A.C.T. How to measure CT image quality: Variations in CT-numbers, uniformity and low contrast resolution for a CT quality assurance phantom. *Phys. Medica* **2014**, *30*, 521–526. [CrossRef] [PubMed]
52. Manson, E.N.; Fletcher, J.J.; Della Atuwo-Ampoh, V.; Addison, E.K.; Schandorf, C.; Bambara, L. Assessment of some image quality tests on a 128 slice computed tomography scanner using a Catphan700 phantom. *J. Med. Phys./Assoc. Med. Phys. India* **2016**, *41*, 153. [CrossRef] [PubMed]
53. Ghetti, C.; Ortenzia, O.; Serreli, G. CT iterative reconstruction in image space: A phantom study. *Phys. Medica* **2012**, *28*, 161–165. [CrossRef] [PubMed]
54. Löve, A.; Siemund, R.; Höglund, P.; Van Westen, D.; Stenberg, L.; Petersen, C.; Björkman-Burtscher, I.M. Hybrid iterative reconstruction algorithm in brain CT: A radiation dose reduction and image quality assessment study. *Acta Radiol.* **2014**, *55*, 208–217. [CrossRef] [PubMed]

55. Xu, Y.; He, W.; Chen, H.; Hu, Z.; Li, J.; Zhang, T. Impact of the adaptive statistical iterative reconstruction technique on image quality in ultra-low-dose CT. *Clin. Radiol.* **2013**, *68*, 902–908. [CrossRef]
56. Hojreh, A.; Weber, M.; Homolka, P. Effect of staff training on radiation dose in pediatric CT. *Eur. J. Radiol.* **2015**, *84*, 1574–1578. [CrossRef]
57. Trattner, S.; Pearson, G.D.; Chin, C.; Cody, D.D.; Gupta, R.; Hess, C.P.; Kalra, M.K.; Kofler, J.M.; Krishnam, M.S.; Einstein, A.J. Standardization and optimization of CT protocols to achieve low dose. *J. Am. Coll. Radiol.* **2014**, *11*, 271–278. [CrossRef]

International Journal of Scientific Research in Science and Technology
Print ISSN: 2395-6011 | Online ISSN: 2395-602X (www.ijsrst.com)
doi : https://doi.org/10.32628/IJSRST52310237

# Implementation of Standard Deviation Map (SDM) for an Automation of Spatial Resolution Measurements on Computed Tomography Images of ACR CT Accreditation Phantom

**Didik Rahmadi [1] , Choirul Anam [1,*] , Eko Hidayanyo [1] , Ariij Naufal [1]**

[1]Department of Physics, Faculty of Sciences and Mathematics, Diponegoro University, Jl. Prof Soedarto SH, Tembalang, Semarang, Central Java, Indonesia

* Corresponding author: anam@fisika.fsm.undip.ac.id

**ARTICLEINFO**

**Article History:**

Accepted: 05 March 2023
Published: 22 March 2023

**Publication Issue**
Volume 10, Issue 2
March-April-2023

**Page Number**
256-262

**ABSTRACT**

This study is to develop an automated method to determine the spatial resolution of computed tomography (CT) images on line-pair objects of the American College of Radiology (ACR) CT accreditation phantom. The ACR phantom was scanned using a GE Healthcare 128-slice CT scanner with seven different reconstruction filters of E1, E2, E3, LU, S1, S2, S3. The automated method involved building a standard deviation map (SDM), segmenting the line-pair objects within SDM images, determining the region of interest (ROI) within line pair object, and determining a resolvable line-pair object with dynamic threshold which is dependent on image noise. The scanning parameters were fixed at 120 kVp and 160 mAs. The results of automated method were compared with those from manual measurements performed by five human observers. The automatic method produced spatial resolution results of 0.7, 0.7, 0.7, 0.7, 0.6, 0.6, and 0.6 lp/mm for filters E1, E2, E3, LU, S1, S2, and S3, respectively, while the manual measurements yielded results of 0.6, 0.6, 0.6, 0.7, 0.6, 0.5, and 0.5 lp/mm. The differences between the manual and automatic measurement results were small, with a maximum difference of 0.1 lp/mm. Hence, the automatic measurement of spatial resolution on line-pair objects of the ACR CT accreditation phantom is a feasible and reliable method.

**Keywords:** CT scanner, ACR CT accreditation phantom, reconstruction filter, automatic, spatial resolution

## I. INTRODUCTION

Computed tomography (CT) is an imaging modality commonly and widely used clinically (Chokami et al., 2020). In CT practice, acceptable image quality of CT should be achieved with low radiation dose (Sanders et al., 2016). Therefore, many advanced techniques to obtain good quality images have developed, such as iterative reconstruction (IR) technique, tube current modulation (TCM) technique, and so on (Solomon et al., 2020, Christianson et.al, 2015). Good image quality is characterized by several parameters, one of which is spatial resolution (Goldman et al., 2007, Love et al., 2013, Anam et al., 2018).

Spatial resolution refers to ability of an imaging system to distinguish small objects that are close together (Brüllmann and Schulze, 2015; Bushberg et al, 2020). Every object in the image is blurred so that if there are two small objects that are close together at a very close distance, then they may appear as one object because the two objects are overlapping each other. Practically, spatial resolution of the image can be identified from the last resolvable number of line-pair objects separated at a certain distance in centimeters or millimeters. The last line-pair object is observed by visual observation of white lines (line-pairs) on a black background (Bushong, 2020; Seeram, 2016; Staude et al., 2011). It is important to note that visual observation on the last resolvable line-pairs object is observer-dependent (Gopal, 2009).

Droege and Morin have developed a method of measuring spatial resolution numerically by making region of interest (ROI) on line-pair objects to get the response and reconstructed a curve of modulation transfer function (MTF) from them (Droege and Morin, 1982). It is noted that MTF curve is an acceptable comprehensive representation of spatial resolution of an image. MTF is usually obtained from point spread function (PSF), line-spread function (LSF), or edge-spread function (ESF), and not from line-pairs object. Therefore, the work of Droege and Morin is important contribution for providing an alternative approach to obtain MTF curve. However, the proposed method by Droege and Morin is still carried out manually so it may not impractical in routine quality assurance (QA) procedures, especially in busy medical centers. Hence, we developed a new alternative algorithm for automated method for measuring spatial resolution on line-pair object to overcome weaknesses of manual method. In this regard, we employed recent technique in CT image processing, i.e. standard deviation map (SDM) described in AAPM TG 233 (AAPM). Therefore, the purpose of this study is to automatically measure the spatial resolution of CT images on line-pair objects of ACR CT accreditation phantom using the SDM.

## II. METHODS AND MATERIAL

### A. Phantom images

We used spatial resolution module of the ACR CT accreditation phantom. This module consists of eight line-pair objects with sizes of 0.4, 0.5, 0.6, 0.7, 0.8, 0.9, 1.0 and 1.2 lp/mm. Image samples of the module are shown in Figure 1. Window-width (WW) and window-level (WL) at 100 and 1100 Hounsfield unit (HU) are recommended for visual observation of line pairs [15,16] (Figure 1b). We scanned the phantom with a GE Revolution EVO 128-slice CT scanner with input parameters shown in Table 1. The images were stored in Digital Imaging and Communications in Medicine (DICOM) format. Image samples with various reconstruction filters are shown in Figure 2.

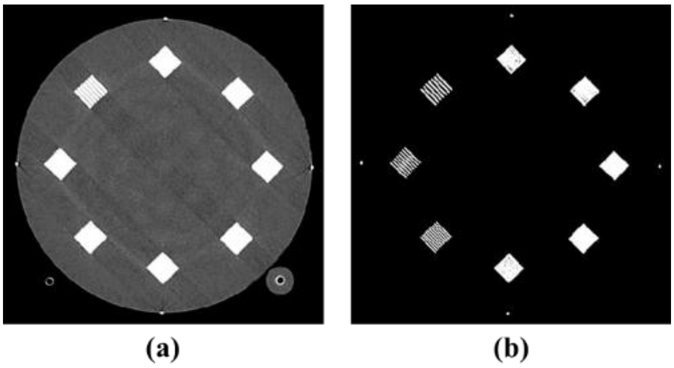


Figure 1. Image sample of ACR CT Accreditation phantom displayed with two different windows: (a) with soft tissue window, and (b) with window-width (WW) of 100 HU and window-level (WL) of 1100 HU.

Table 1. CT input parameters in this study

| Parameters | Value |
|---|---|
| Scan type | Helical |
| Convolution kernels | Standard |
| Revolution time | 0.8 seconds |
| Tube current | 160 mA |
| Tube voltage | 120 kV |
| Slice thickness | 1.25 mm |
| Field of view | 211 mm |
| Pitch | 0.531 |
| Reconstruction filter | E1, E2, E3, LU, S1, S2, S3 |

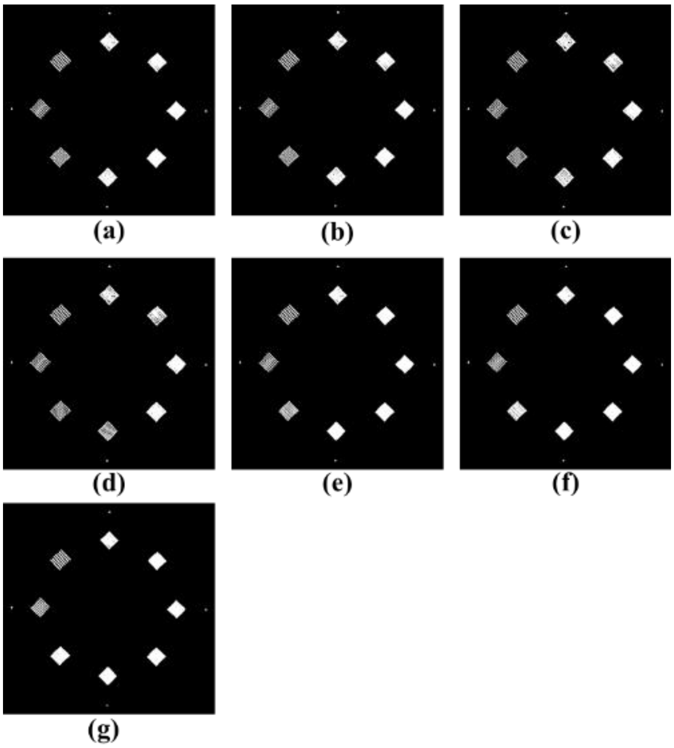

Figure 2. Image samples of ACR CT Accreditation phantom reconstructed with various reconstruction filters: (a) E1, (b) E2, (c) E3, (d) LU, (e) S1, (f) S2, and (g) S3.

B. Automatic Spatial Resolution Measurement

We proposed a new algorithm for automatic spatial resolution measurement on the line-pair object of ACT CT accreditation phantom. The automatic measurement for spatial resolution in this study was integrated to the software IndoQCT [17]. The graphical user interface (GUI) for automatic measurement of spatial resolution is shown in Figure 3.

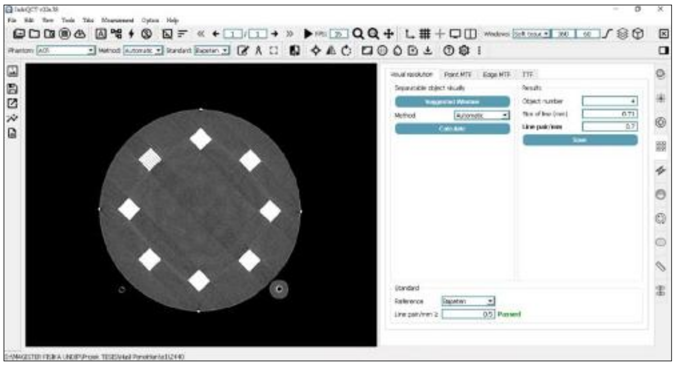

Figure 3. Graphical user interface (GUI) automatic measurement of spatial resolution

The main idea for automatic spatial resolution measurement on the line-pair objects is by using a SDM. This method was started with opening the original image (Fig. 4a). The original image was then converted to SDM [18]. The conversion is carried out with a 3 × 3 pixels of sliding window to calculate the SD at each pixel location within the image. This process changed the image in HU to an SDM displayed with a hot colormap (Fig. 4b). In this SDN, the pixels that appear brighter indicate a higher SD. After that, detection of the line-pair object was performed by segmentation on the SDM with a threshold of 20 HU (Fig. 4c) and erosion on the binary image with the purpose of eliminating small objects. This process produced a binary image that contains line-pair objects and free of artifacts (Fig. 4d). To detect all line–pair objects and avoid hollows in line-pair objects, the holes in the line-pairs objects were filled (Fig. 4e). Centroids of each line-pair object were then determined with equation (1).

$$x_{cen}, y_{cen}) = \frac{1}{N}\sum_{i=1}^{N}(x_i, y_i) \qquad (1)$$

Circle ROIs with adjusted radius were then placed on the SDM based on each centroid coordinate of line pairs (Fig. 4f). The average values of SD were taken from inside the ROI.

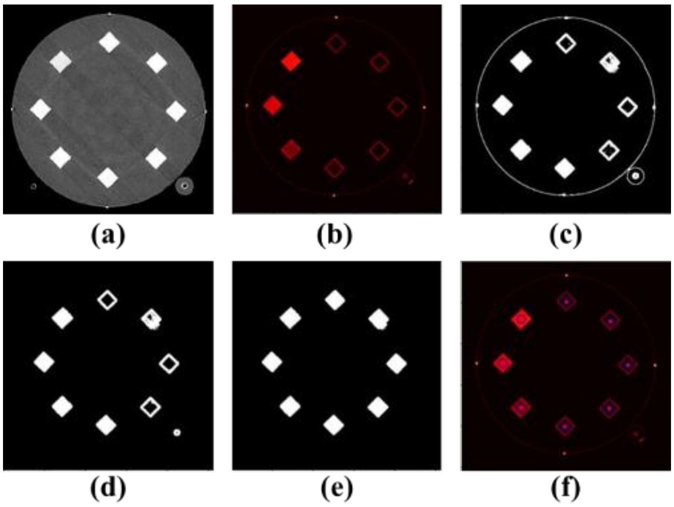


Figure 4. Steps of automatic spatial resolution measurement on line-pair object: (a) original image, (b) standard deviation map (SDM) with hot colormap, (c) binary image obtained with threshold of 20 HU, (d) eroded binary image, (e) hollow line-pair objects is filled, (f) circular region of interests (ROIs) placed on each line-pair object of SDM.

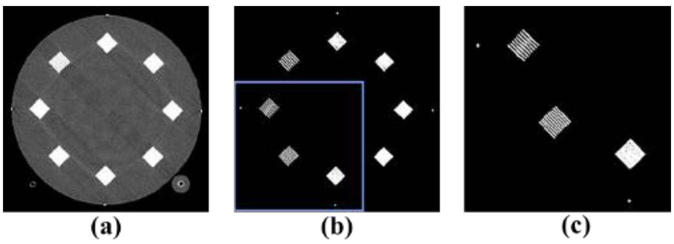


Figure 5. Images for manual observation: (a) Image with soft tissue window, (b) image with window-width (WW) of 100 HU and window-level (WL) of 1100 HU, and (c) zoomed-in image.

The last resolvable line-pair object was calculated with a certain dynamic threshold depending on the image noise, as shown in Equation (2).

$$threshold = \frac{(25 \times SD_{max})}{300} \tag{2}$$

This threshold corresponds to the last resolvable line-pair object that can still be distinguished by human observation.

### C. Human observer

The manual measurement was determined by five human observers. This method was carried out on images with recommended window settings to increase line-pair visibility (Fig. 5b). Furthermore, the image was zoomed-in to make the line-pair object to be clearer for observers (Fig. 5c). The observers selected the last resolvable line-pair object based on their subjectivities. The method was applied to all reconstruction filters (i.e. E1, E2, E3, LU, S1, S2, and S3). Results from five human observers were averaged to obtain one value of spatial resolution.

## III. RESULTS AND DISCUSSION

Figure 6 shows six SDMs of the spatial resolution module of the ACR CT accreditation phantom and ROIs located within the lair-pair objects. It is seen that our software accurately locates the ROIs automatically for all reconstruction filters of E1, E2, E3, LU, S1, S2, and S3. The results of the automatic and manual measurements of spatial resolution are tabulated in Table 2. It appears that all spatial resolution values are greater than 0.5 lp/mm, which is fairly good for image with matrix size of 512 × 512. It is found that automatic method tends to produce greater spatial resolution than from manual observation, with maximum difference between both is 0.1 lp/mm.

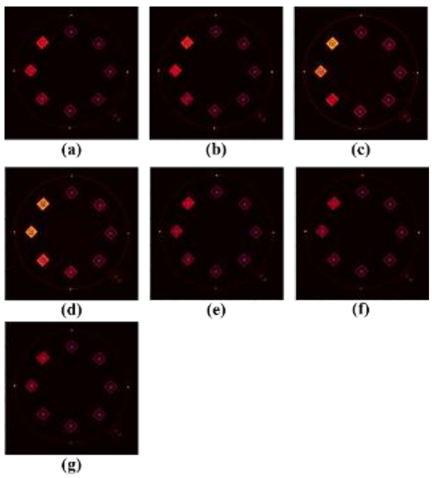


Figure 6. SDMs of the spatial resolution module of the ACR CT accreditation phantom and locations of ROIs within the lair-pair objects for various reconstruction filters: (a) E1, (b) E2, (c) E3, (d) LU, (e) S1, (f) S2, and (g) S3.

Table 2. Comparison of the results of spatial resolution measurements between automatic and manual measurements on the ACR CT accreditation phantom.

| Reconstruction filter | Noise (HU) | Measurements of spatial resolution (lp/mm) | | Difference (lp/mm) |
|---|---|---|---|---|
| | | Automatic | Manual | |
| | Mean ± SD | Mean ± SD | Mean ± SD | |
| E1 | 9.1 ± 0.3 | 0.7 ± 0.0 | 0.6 ± 0.0 | 0.1 |
| E2 | 9.7 ± 0.4 | 0.7 ± 0.0 | 0.6 ± 0.0 | 0.1 |
| E3 | 14.6 ± 0.6 | 0.7 ± 0.0 | 0.6 ± 0.0 | 0.1 |
| LU | 15.3 ± 0.6 | 0.7 ± 0.0 | 0.7 ± 0.0 | 0.0 |
| S1 | 7.3 ± 0.3 | 0.6 ± 0.0 | 0.6 ± 0.0 | 0.0 |
| S2 | 6.8 ± 0.3 | 0.6 ± 0.0 | 0.5 ± 0.0 | 0.1 |
| S3 | 6.4 ± 0.2 | 0.6 ± 0.0 | 0.5 ± 0.0 | 0.1 |

This study aimed at development of an automated method for measuring spatial resolution using line-pair object of the American College of Radiology (ACR) CT accreditation phantom and to evaluate its performance on various reconstruction filters. The reconstruction filters used in this study were categorized into three groups: edge filters (E1, E2, E3), lung filters (LU), and smoothing filters (S1, S2, S3).

The results of this study showed that results of the automated measurements are comparable to those from human observations. The maximum discrepancy between both is only 0.1 lp/mm, with results of automatic method tends to be greater than those from manual observations. This indicates that the manual measurement of the last resolvable line-pair object is perceived similarly to the human eye. Although individual observations may produce slightly different results, the average calculated spatial resolution is expected to be close to the automatic measurement.

Our method relies on the standard deviation map (SDM) which is influenced by image noise. Therefore, testing the method on various types of reconstruction filters is essential. Reconstruction filters have their own unique characteristics noise level, noise texture, spatial resolution. In addition, the reconstruction can cause some artifacts and impact the resulted images. However, morphological operations such as erosion and dilation can be used to overcome these artifacts that may disturb an automatic spatial resolution measurement. Additionally, some filters can shift the CT number of the line pair forming material, resulting in variations in the SDM and incorrect counting of line pair objects. An adaptive dynamic threshold to image noise is a promising approach to address this problem. Nonetheless, the effect of artifacts other than those in the images used in this study is still unknown. Therefore, it is recommended to measure a spatial resolution from images with minimal artifacts.
The results demonstrated that edge and lung filters produced the highest spatial resolution value of 0.7 lp/mm, while the smoothing filter had the lowest spatial resolution value of 0.6 lp/mm. This indicates that reconstruction filters of edge and lung filters have a greater spatial resolution than smooth filters [19,20]. Table 2 shows the spatial resolutions for each reconstruction filter, providing useful information for researchers and practitioners in selecting an appropriate filter for their specific needs.

The developed automatic method provides a reliable and efficient method for measuring the spatial resolution of CT images using the line-pair object of the ACR phantom. However, testing the developed method on other parameters, such as various tube current, tube voltage, pitch, slice thickness, does not carry out yet. In addition, the method has been tested on images from one CT scanner. Therefore, comprehensive evaluations of the method should be carried out in the next studies.

## IV. CONCLUSION

In conclusion, an automated method for measuring spatial resolution in CT images using the line-pair objects of the ACR phantom has been successfully developed. The automatic method runs well for various reconstruction filters. Results of the automatic measurements are comparable to the manual measurements, with only small difference of 0.1 lp/mm. We also observed that the software is robust against artifacts in images produced by different reconstruction filters.

## V. ACKNOWLEDGMENTS

This work was funded by the World Class Research University (WCRU), Diponegoro University, No. 118-08/UN7.6.1/PP/2021.

## VI. REFERENCES

[1]. Chokami HK, Hosseini SA, Ghorbanzadeh M, Mohammadi M. QCT: A measuring tool dedicated to the estimation of image parameters for quality assurance/quality control programs of CT scanners. 2020 IEEE International Symposium on Medical Measurements and Applications (MeMeA). 2020; 1-6.

[2]. Sanders J, Hurwitz L, Samei E. Patient-specific quantification of image quality: An automated method for measuring spatial resolution in clinical CT images. Medical Physics. 2016; 43(10): 5330-5338.

[3]. Solomon J, Lyu P, Marin D, Samei E. Noise and spatial resolution properties of a commercially available deep learning-based CT reconstruction algorithm. Medical Physics. 2020; 47(9): 3961-3971.

[4]. Christianson O, Winslow J, Frush DP, Samei E. Automated technique to measure noise in clinical CT examinations. American Journal of Roentgenology. 2015; 205(1): W93–W99.

[5]. Goldman LW. Principles of CT: radiation dose and image quality. Journal of Nuclear Medicine Technology. 2007 Dec;35(4): 213-25.

[6]. Love A, Olsson ML, Siemund R, et al. Six iterative reconstruction algorithms in brain CT: a phantom study on image quality at different radiation dose levels. British Journal of Radiology. 2013;86: 20130388.

[7]. Anam C, Fujibuchi T, Budi WS, Haryanto F, Dougherty G. An algorithm for automated modulation transfer function measurement using an edge of a PMMA phantom: Impact of field of view on spatial resolution of CT images. Journal of Applied Clinical. Medical Physics. 2018; 19(6): 244–252.

[8]. Brüllmann D, Schulze RK. Spatial resolution in CBCT machines for dental/maxillofacial applications-what do we know today?. Dentomaxillofacial Radiology. 2015;44(1): 20140204.

[9]. Mahesh M. The Essential Physics of Medical Imaging, Third Edition. Medical Physics. 2013 Jul;40(7) :28524933.

[10]. Bushong, Stewart C. Radiologic science for technologists e-book: physics, biology, and protection. Elsevier Health Sciences, 2020.

[11]. Seeram, Euclid. Computed Tomography-E-Book: Physical Principles, Clinical Applications, and Quality Control. Elsevier Health Sciences, 2015.

[12]. Staude A, Goebbels J. Determining the spatial resolution in computed tomography comparison

of MTF and line-pair structures. International Symposium on Digital Industrial Radiology and Computed Tomography. 2011; 16(11).

[13]. Gopal A, Samant SS. Use of a line-pair resolution phantom for comprehensive quality assurance of electronic portal imaging devices based on fundamental imaging metrics. Medical Physics. 2009;36(6): 2006-2015.

[14]. Droege RT, Morin RL. A practical method to measure the MTF of CT scanners. Medical Physics. 1982;9(5): 758–60.

[15]. McCollough CH, Bruesewitz MR, McNitt-Gray MF, et al. American College of Radiology. The phantom portion of the American College of Radiology (ACR) computed tomography (CT) accreditation program: practical tips, artifact examples, and pitfalls to avoid. Medical Physics. 2004 Sep;31(9): 2423-42.

[16]. Cropp RJ, Seslija P, Tso D, Thakur Y. Scanner and kVp dependence of measured CT numbers in the ACR CT phantom. Journal of Applied Clinical Medical Physics. 2013; 14 (6): 338-349.

[17]. Anam C, Naufal A, Fujibuchi T, Matsubara K, Dougherty G. Automated development of the contrast-detail curve based on statistical low-contrast detectability in CT images. Journal of Applied Clinical Medical Physics. 2022;23(9): e13719.

[18]. Anam C, Arif I, Haryanto F. An improved method of automated noise measurement system in CT images. Journal of Biomedical Physics and Engineering. 2021;11(2): 163-174.

[19]. Seung-Wan Lee, Chang-Lae Lee, Hyo-Min Cho, Hye-Suk Park, Dae-Hong Kim, Yu-Na Choi and Hee-Joung Kim. Effects of reconstruction parameters on image noise and spatial resolution in cone-beam computed tomography. Journal of the Korean Physical Society. 2011; 59 (4): 2825-2832.

[20]. Rueckel J, Stockmar M, Pfeiffer F & Herzen J. Spatial resolution characterization of an X-ray microCT system. Applied Radiation and Isotopes. 2014;94, 230-234.

**Cite this article as :**

Didik Rahmadi, Choirul Anam, Eko Hidayanyo, Ariij Naufal, "Implementation of Standard Deviation Map (SDM) for an Automation of Spatial Resolution Measurements on Computed Tomography Images of ACR CT Accreditation Phantom", International Journal of Scientific Research in Science and Technology (IJSRST), Online ISSN : 2395-602X, Print ISSN : 2395-6011, Volume 10 Issue 2, pp. 256-262, March-April 2023. Available at doi : https://doi.org/10.32628/IJSRST52310237

Journal URL : https://ijsrst.com/IJSRST52310237

Radiation Physics and Chemistry 140 (2017) 260–265

Contents lists available at ScienceDirect

Radiation Physics and Chemistry

journal homepage: www.elsevier.com/locate/radphyschem

# Optimization of dose and image quality in adult and pediatric computed tomography scans

Kwo-Ping Chang[a,*], Tzu-Kun Hsu[b], Wei-Ting Lin[c], Wen-Lin Hsu[d]

[a] Department of Medical Imaging and Radiological Sciences & Institute of Radiological Sciences, Tzu Chi University of Science and Technology, Hualien, Taiwan

[b] Department of Radiology, Taitung Hospital, Tainting Hospital Ministry of Health and Welfare, Taitung, Taiwan

[c] Department of Radiology, Buddhist Tzu Chi General Hospital, Hualien, Taiwan

[d] Department of Radiation Oncology, Buddhist Tzu Chi General Hospital, Hualien, Taiwan

ARTICLE INFO

*Keywords:*
CT image quality
CNR
CT dose index ($CTDI_{vol}$)
Figure-of-merit (FOM)
Iteration reconstruction (IR)

ABSTRACT

Exploration to maximize CT image and reduce radiation dose was conducted while controlling for multiple factors. The kVp, mAs, and iteration reconstruction (IR), affect the CT image quality and radiation dose absorbed. The optimal protocols (kVp, mAs, IR) are derived by figure of merit (FOM) based on CT image quality (CNR) and CT dose index ($CTDI_{vol}$). CT image quality metrics such as CT number accuracy, SNR, low contrast materials' CNR and line pair resolution were also analyzed as auxiliary assessments. CT protocols were carried out with an ACR accreditation phantom and a five-year-old pediatric head phantom. The threshold values of the adult CT scan parameters, 100 kVp and 150 mAs, were determined from the CT number test and line pairs in ACR phantom module 1and module 4 respectively. The findings of this study suggest that the optimal scanning parameters for adults be set at 100 kVp and 150–250 mAs. However, for improved low- contrast resolution, 120 kVp and 150–250 mAs are optimal. Optimal settings for pediatric head CT scan were 80 kVp/50 mAs, for maxillary sinus and brain stem, while 80 kVp /300 mAs for temporal bone. SNR is not reliable as the independent image parameter nor the metric for determining optimal CT scan parameters. The iteration reconstruction (IR) approach is strongly recommended for both adult and pediatric CT scanning as it markedly improves image quality without affecting radiation dose.

## 1. Introduction

Due to the rapid growth in scanning technology and computer calculation speed, there has been an increase in the use of Computed Tomography (CT) examination. According to the NCRP No. 160, the largest increase in population radiation dose was found in patient exposure to medical procedures (National Council on Radiation Protection and Measurements, 2009). Radiation dose increases with higher CT image quality due to the use of higher voltage and/or electric current. Explicit consideration of the relationship of CT image quality to applied dose is crucial in CT radiation protection. Ensuring high CT image quality with reduced radiation exposure is invariably an issue for radiologists and researchers. Of the CT procedures, pediatric CT scans account for nearly 5–11% of all procedures. (Miglioretti et al., 2013). This patient population remains vulnerable and requires specific examination of the effects of CT and methods to reduce radiation dose.

The metrics for image quality assessment for CT scanners and radiation dose were proposed in the ICRU Report 87 and remains an international standard (ICRU Report No. 87, 2012). Pahn's study, based on ICRU No. 87 examined metrics such as noise magnitude, CT numbers, and uniformity, which were assessed on large samples of ROIs and low-contrast resolution (CNR, SNR). These were then quantitatively evaluated as a function of lesion contrast (Pahn et al., 2016). Brunner measured the dose and evaluated image quality using a phantom under clinical scan conditions to perform an objective image analysis using metrics such as high-contrast resolution, noise, and high/low contrast CNR (Brunner et al., 2013). Yang proposed the low-dose pediatric PET-CT protocols to optimize CT and reduce radiation dose (Yang et al., 2014). Several studies have investigated the effect of iterative reconstruction (IR) algorithm on the CT image quality and reducing the radiation dose. Choi's study validated the IR algorithm for use in reducing image noise while maintaining image quality (Choi et al., 2013). Brady demonstrated that a maximum dose reduction of 82% is possible using IR approach while producing diagnostically accurate pediatric CT scans (Brady et al., 2012).

The current literature focusing on CT image quality and radiation

* Corresponding author.
*E-mail addresses:* chang.kwoping@gmail.com, kpchang@ems.tcust.edu.tw (K.-P. Chang).

http://dx.doi.org/10.1016/j.radphyschem.2017.02.006
Received 30 June 2016; Received in revised form 27 January 2017; Accepted 1 February 2017
Available online 03 February 2017

dose, generally focuses on only one or a few metrics to explore adjustments in the parameters of interest effects on the image quality versus dose independently. The effect of adjustments of the known parameters (kVp, mAs, IR, metric of interest: CNR, CT number, SNR, etc.) are complex and may be interrelated, which may alter the CT image quality and radiation dose. This study aims to determine the optimal CT scanning protocols based on all possible metrics, while conducting an overall evaluation of the effects of the scan parameters on CT image quality and radiation dose.

The optimal protocols (kVp, mAs, IR) are derived by figure of merit (FOM) based on CT image quality (CNR) and CT dose index ($CTDI_{vol}$). CT image quality metrics such as CT number accuracy, SNR, low contrast materials' CNR and line pair resolution were also analyzed as auxiliary assessments. The effects of the iterative reconstruction (IR) algorithm on image quality have been explored to further optimize the CT scan parameters. All tests were carried out with an ACR accreditation phantom. Due to the increased risks for children of radiation exposure, the optimal conditions of the pediatric CT examination were also investigated on a five-year-old pediatric phantom.

## 2. Materials and methods

The 128-row multiple slice CT scanner (Brilliance iCT, Philips Medical Systems) was used to perform the CT investigation on the standard phantom (ACR phantom) to simulate the adult CT scan and the CIRS five- year- old pediatric head phantom. Multiple parameters were employed for CT scan as follows: Tube voltage, kVp: 80,100, 120. Tube current-time, mAs: 50, 100,150, 200, 250, 300, 350, and 400. Axial Head 2D mode, thickness =2 mm. Each parameter was tested with and without the iterative reconstruction (IR) algorithm (Reconstruction mode iDose$^4$, level 3) in order to assess the effect of IR on image quality.

### *2.1. CT examination on phantoms and CT image quality analyses*

Two phantoms were used for CT testing to investigate multiple protocols and their effects on the image quality and radiation dose. The image quality was evaluated using (1) the accuracy of the CT number (HU) compared to the standard values of the standard phantoms. (2) The contrast-to-noise ratio (CNR), (3) the signal-to-noise ratio (SNR), (4) low contrast materials' CNR, (5) line-pair resolution.

The definition of CNR and SNR are as follows:

$$\mathrm{CNR}=\frac{|CT\#_{ROI} - CT\#_{bg}|}{SD_{bg}} \tag{1}$$

$$\mathrm{SNR}=\frac{CT\#_{ROI}}{SD_{ROI}} \tag{2}$$

where $CT\#_{ROI}$ and $CT\#_{bg}$ are CT number of ROI and background respectively; $SD_{ROI}$ and $SD_{bg}$ are standard deviation of ROI and background respectively. CNR used absolute values as $CT\#_{ROI}$ in specific tissues may be less than $CT\#_{bg}$. (if the average physical density of the ROI selected is less than that of the surrounding region).

The ACR accreditation phantom is equipped with four modules and only modules 1, 2 and 4 were used in this study (Fig. 1(a)). Module 1 was used to assess CT number accuracy. The cylinders houses five different materials. The standard CT numbers are: polyethylene: −95 (−87 to −107), bone: 995 (850–975), acrylic: 120 (110–135), and air: −1000 (−970 to −1005). The background material is water- equivalent (CT number: 0 (−5 to +5)). The materials in module 1 were also used for CNR, SNR and FOM assessments. The region of background was set at 3–6 mm away from the circumference of the ROI. Module 2 was used to assess low contrast resolution. A 25 mm cylinder is used to verify the cylinder-to-background contrast level (Fig. 1(b)). CNR, SNR and FOM were assessed using the same method as applied in Module 1. Module 4 was used to assess the high contrast(spatial) resolution. The line pair numbers/cm were similarly analyzed using multiple protocols. CT image analyses for the specific materials (e.g. polyethylene) were performed at the same slice of the CT images using multiple protocols (kVp, mAs, with/without IR).

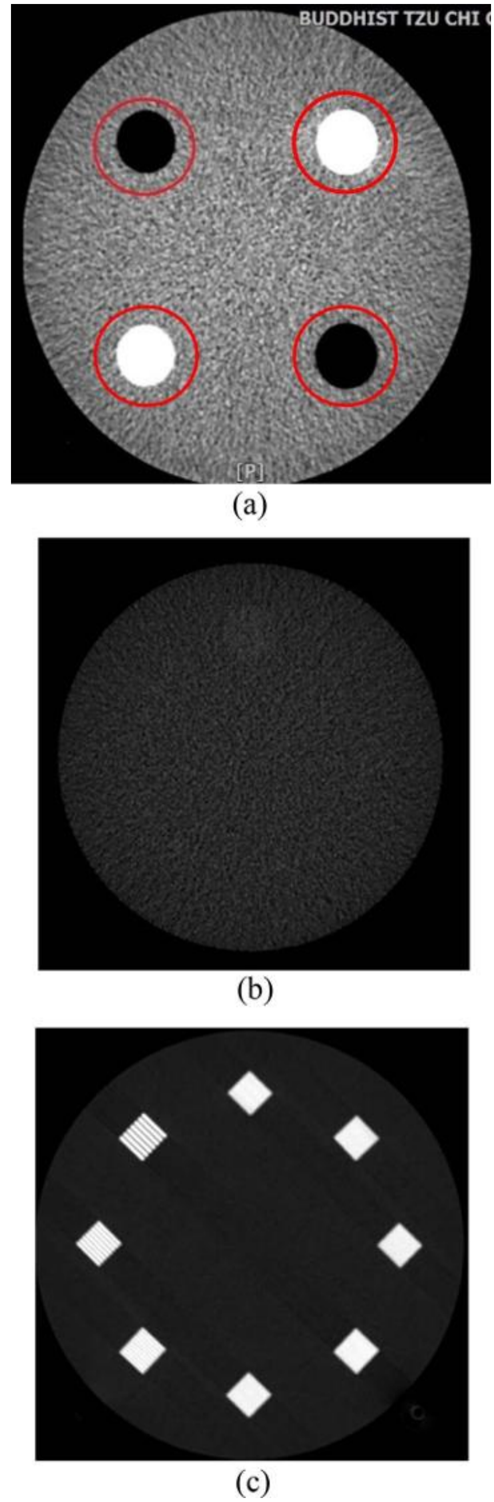


**Fig. 1.** (a) The ROIs selected in the ACR phantom. Top (left) polyethylene; Top (right) bone; Bottom (left) acrylic; Bottom (right) air. (b) ACR phantom module 2 (low contrast). (c) Module 4 in ACR phantom (line pair).

The pediatric phantom (ATOM, CIRS; 5-year-old pediatric phantom) was used to analyze the CNR and FOM in the cranial region (Fig. 2). The head phantom was of particular interest as cranial scanning is very common in pediatric CT scans. All parameters (kVp,

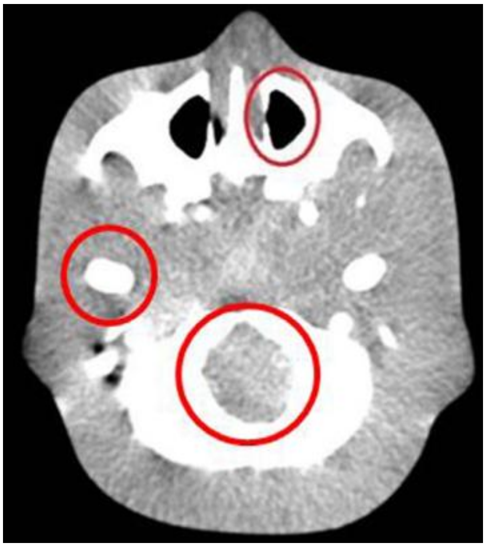

**Fig. 2.** The ROIs selected in the ATOM CIRS pediatric phantom. Top: maxillary sinus; Middle: temporal bone-mastoid process; Bottom: brain stem).

mAs, IR) and the metrics(CNR, SNR and FOM) for optimization were similarly investigated in the ACR phantom.

### 2.2. Radiation dose assessments

Radiation dose was assessed by $CTDI_{vol}$ which allows for evaluation of the entire radiation dose at the ROI. It is an useful index when comparing protocols and technical parameters (AAPM Report No 204, 2011). The $CTDI_{vol}$(mGy) values were calculated by the CT scanner and displayed on the CT scanner consoles.

### 2.3. Overall evaluations on image and radiation dose

To assess the overall effects and a possible trade-off between image quality and radiation dose, FOM, was used and defined as:

$$FOM=\frac{CNR^2}{CTDI_{vol}} \tag{3}$$

The FOMs of all regions of interest in the phantoms were examined. CT image quality metrics (e.g. CT number accuracy, SNR) were also analyzed as auxiliary assessments.

**Table 2**
CT image of bone of ACR phantom with the current 200 mAs.

| | kVp | | | | | |
|---|---|---|---|---|---|---|
| | **80** | **80+**[a] | **100** | **100+**[a] | **120** | **120+**[a] |
| **CT(ROI)** | 1206.2 | 1205.9 | 956.6 | 958.8 | 826.5 | 825.5 |
| **S.D(ROI)** | 15.3 | 15.1 | 9.7 | 8.2 | 7.3 | 7.2 |
| **CT(bg)** | 3.8 | 15.6 | 1.3 | 1.9 | −1.3 | −4.6 |
| **S.D(bg)** | 11.6 | 11.5 | 10.5 | 8.9 | 6.6 | 5.9 |
| **Noise** | 15.3 | 15.1 | 9.7 | 8.2 | 7.3 | 7.2 |
| **CNR** | 45.7 | 53.8 | 51.1 | 58.1 | 51.4 | 64.2 |
| **CTDI** | 8.3 | 8.3 | 16.9 | 16.9 | 27.6 | 27.6 |
| **SNR** | 79.1 | 79.6 | 98.2 | 117.5 | 114.0 | 114.2 |
| **FOM** | 251.6 | 348.3 | 154.7 | 199.9 | 95.9 | 149.4 |
| **CT number**[b] **test** | X | X | □√ | □√ | Δ | Δ |

[a] : + means plus the IDOS (Iteration reconstruction algorithm in Philips CT scanner software)
[b] : the standard value of bone CT values are **850–975**. All CT(ROI) in this case are within this range

## 3. Results

### 3.1. CT number, CNR, SNR, $CTDI_{vol}$ and FOM evaluation of ACR module 1

As shown in Table 1, an example of the CT image analysis of the ROI(bone) in Module 1 of the ACR phantom below100 kVp remains within the standard value range. As shown in Table 2, some CT numbers under same protocols but with 80 kVp were at the extreme of deviation or out of the standard range completely. This may be attributed to the low energy photons (80 kVp) being insufficient for penetration of the ACR phantom (16 cm length ×20 cm diameter).

The CNR values with iDose[4] (Iterative statistical algorithm, IR) were consistently higher than those without IR (as shown in Table 1, Table 2 and Figs. 3(a)–(b)). The CNR increases from 10% to 40% at the ROIs in the ACR phantom. CNR clearly increases with kVp and mAs (Figs. 3(a) and (b) respectively).

As the $CTDI_{vol}$ is independent of the IR method, the FOM improves with IR for all protocols (as shown in Table 1). Therefore, the FOM comparisons amongst protocols (mAs, kVp, ROIs) have been evaluated only with IR (iDose[4], level 3). As previously described, 80 kVp results in CT number errors and thus was excluded from the FOM for the comparative analysis. The FOM results for specific materials in the ACR phantom are shown in Table 2 and Fig. 3(c). The optimal protocol was 100 kVp (marginally better than 120 kVp). The tube current times' (mAs) effect on FOM of bone is shown in Fig. 3(d). FOM is inversely proportional to mAs in bone. It was determined that 50–250 mAs with IR is the optimal range. In summary, 100 kVp/50–250 mAs are the preferred protocols when CT scanning on the bone. The results of SNR

**Table 1**
CT results for the bone in ACR phantom with voltage 100 kVp.

| | mAs | | | | | | | | | | | | | | | |
|---|---|---|---|---|---|---|---|---|---|---|---|---|---|---|---|---|
| | **50** | **50+** | **100** | **100+** | **150** | **150+** | **200** | **200+** | **250** | **250+** | **300** | **300+** | **350** | **350+** | **400** | **400+** |
| **CT (ROI)** | 956 | 957 | 958 | 958 | 958 | 957 | 957 | 958 | 957 | 959 | 959 | 958 | 956 | 957 | 957 | 957 |
| **S.D. (ROI)** | 22.5 | 16.2 | 14.0 | 13.2 | 10.9 | 10.3 | 9.7 | 8.2 | 10.7 | 8.1 | 8.6 | 7.5 | 7.7 | 6.5 | 7.9 | 6.5 |
| **CT (b.g.)** | 11.6 | 7.4 | 4.2 | 6.9 | 7.0 | 6.4 | 7.1 | 7.1 | 7.8 | 7.4 | 5.6 | 7.3 | 6.7 | 7.5 | 6.1 | 6.9 |
| **S.D.(b.g.)** | 30.8 | 25.7 | 23.5 | 22.3 | 20.7 | 16.0 | 18.6 | 16.4 | 17.8 | 13.2 | 15.8 | 13.4 | 14.8 | 13.2 | 14.6 | 12.9 |
| **Noise** | 22.5 | 16.2 | 14.0 | 13.2 | 10.9 | 10.3 | 9.7 | 8.2 | 10.7 | 8.1 | 8.6 | 7.5 | 7.7 | 6.5 | 7.9 | 6.5 |
| **CNR** | 30.6 | 37.0 | 40.6 | 42.6 | 46.0 | 59.4 | 51.1 | 58.1 | 53.3 | 71.9 | 60.2 | 71.2 | 64.2 | 72.1 | 64.9 | 73.8 |
| **CTDIvol** | 4.2 | 4.2 | 8.4 | 8.4 | 12.6 | 12.6 | 16.9 | 16.9 | 21.1 | 21.1 | 25.3 | 25.3 | 29.5 | 29.5 | 33.7 | 33.7 |
| **SNR** | 42.4 | 59.2 | 68.5 | 72.8 | 88.0 | 93.3 | 98.2 | 118 | 89.1 | 119 | 112 | 128 | 124 | 148 | 122 | 148 |
| **FOM** | 224 | 326 | 196 | 216 | 168 | 280 | 155 | 200 | 135 | 245 | 144 | 201 | 140 | 176 | 125 | 162 |
| **CT number**[a] | √ | √ | √ | √ | √ | √ | √ | √ | √ | √ | √ | √ | √ | √ | √ | √ |

*: + means plus the IDOS (Iterative reconstruction algorithm in Philips CT scanner software)
[a] : the standard value of bone CT values are **850–975**. All CT(ROI) in this case are within this range

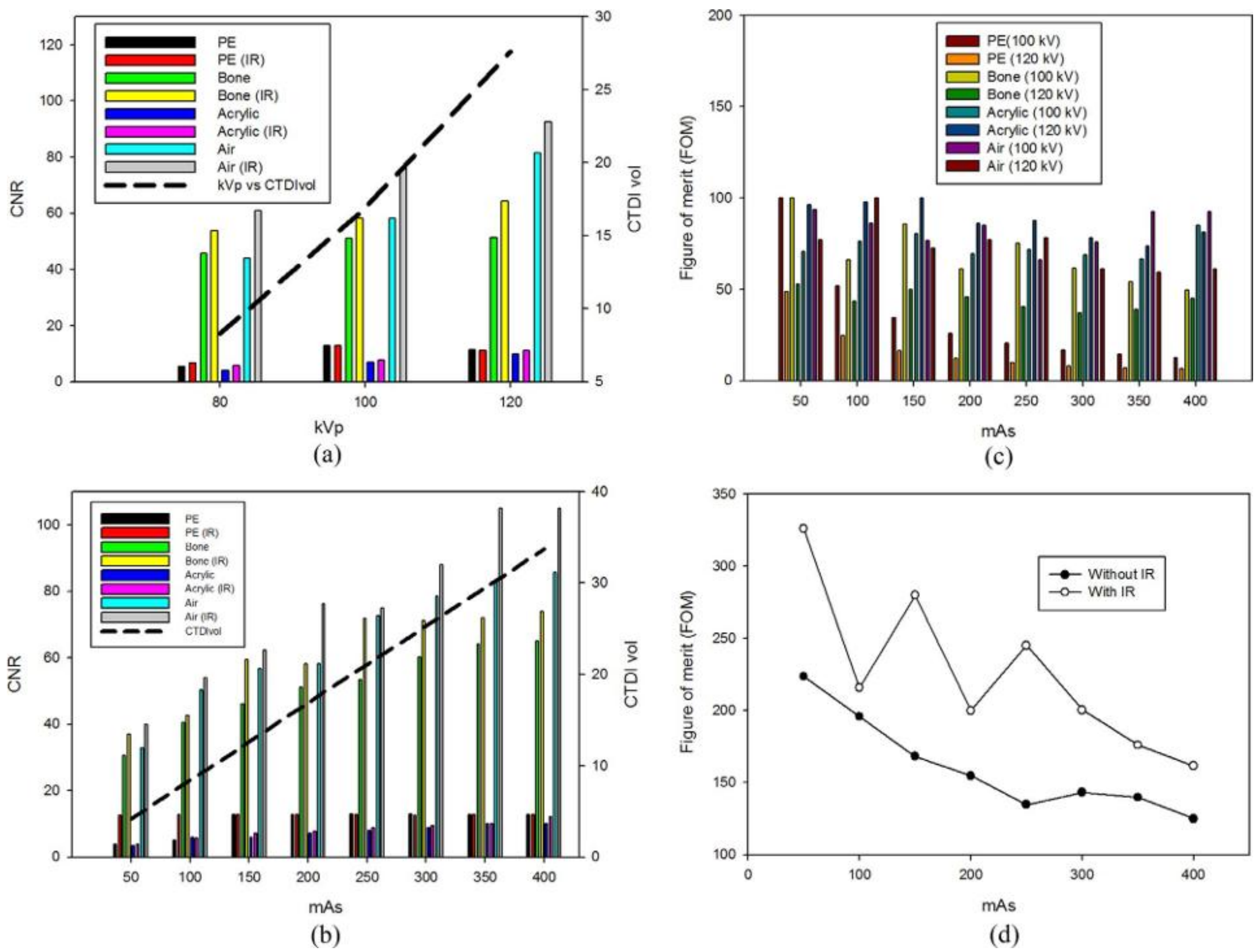


**Fig. 3.** (a) Effect of kVp on CNR and $CTDI_{vol}$ of selected ROIs under 200 mAs in module 1 of the ACR phantom, under 100 kVp. (b) Effect of mAs on CNR, $CTDI_{vol}$ of ROIs in module 1 of the ACR phantom, under 100 kVp. (c) FOMs of ROIs (polyethylene, bone, acrylic and air) of ACR phantom with IR. (d) Effects of mAs and IR on FOM of bone in ACR phantom under 100 kVp.

were similar to those of CNR for most protocols (Table 1). However, in the range of 100–120 kVp (Table 2), SNR is in poor agreement with CNR, which will be addressed in the discussion section.

### 3.2. ACR Module 2 evaluation (low contrast)

The effect of kVp on low contrast was illustrated in Table 3. Results show that the CNR increases with kVp and mAs (Fig. 4(a)). The optimal parameters of low contrast material in ACR phantom module 2 are 120 kVp/150–250 mAs (Fig. 4(b)).

**Table 3**
CT image of ACR phantom module 2 (low contrast region) with the current 200 mAs and IR.

| | kVp | | |
|---|---|---|---|
| | **80** | **100** | **120** |
| **CT(ROI)** | 78.3 | 91.1 | 99.0 |
| **S.D(ROI)** | 10.1 | 6.4 | 5.9 |
| **CT(bg)** | 71.9 | 85.0 | 91.8 |
| **S.D(bg)** | 22.2 | 15.4 | 9.6 |
| **CT(ROI)-CT(bg)** | 6.4 | 6.1 | 7.1 |
| **CNR** | 0.3 | 0.4 | 0.7 |
| **CTDI** | 8.3 | 16.9 | 27.6 |
| **SNR** | 7.8 | 14.2 | 16.8 |
| **FOM ($10^{-3}$)** | 10.1 | 9.2 | 19.9 |

### 3.3. ACR module 4 evaluation (line pair)

The line pairs resulted in similar sharpness for all kVps (6 lp/cm). When using tube current-time less than 150 mAs, the pair was less than 6 lp/cm. Therefore, the line pair resolution is independent of kVp and minimum 150 mAs is recommended for CT scanning.

### 3.4. Pediatric phantom evaluation

The iteration reconstruction (IR) increases the FOM markedly for most ROIs as shown in Table 4. The optimal protocol for scanning maxillary sinus is 80 kVp/50 mAs, temporal bone is 80 kVp/300 mAs and brain stem is 80 kVp/50 mAs in the pediatric phantom(Fig. 5(a)). CNR tends to increase with kVp (Fig. 5(b)), however, high voltage (120 kVp) resulted in worse FOMs (Fig. 5(b)). The optimal CNR protocol incorporated 100 kVp for the temporal bone. To summarize, 80 kVp is preferable for pediatric CT scans. When consideration is only CNR for image quality, the 100 kVp is preferable for the temporal bone. IR is strongly recommended for pediatric CT scanning.

## 4. Discussion

Whether or not the radiation dose of diagnostic exposure levels is harmful to human biology, remains a controversy (e.g. radiation hormesis (Baldwin and Grantham, 2015). From this perspective, the well-accepted image quality parameter, CNR, may be considered the dominant factor for optimization of CT scans. However, the optimal

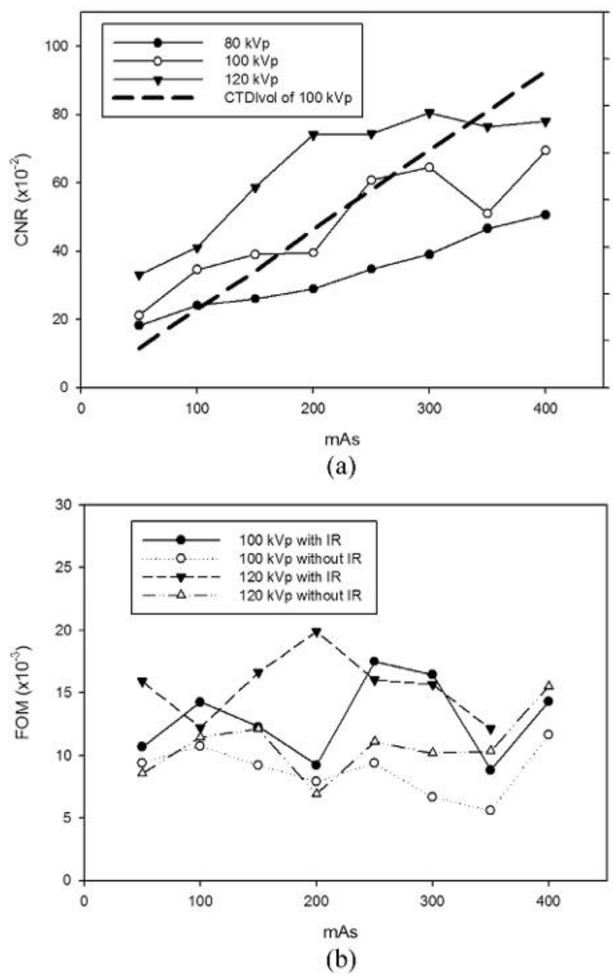


**Fig. 4.** (a) CNR and $CTDI_{vol}$ of low contrast material in ACR phantom module 2. (b) FOM of low contrast material in ACR phantom Module 2 under 100 kVp.

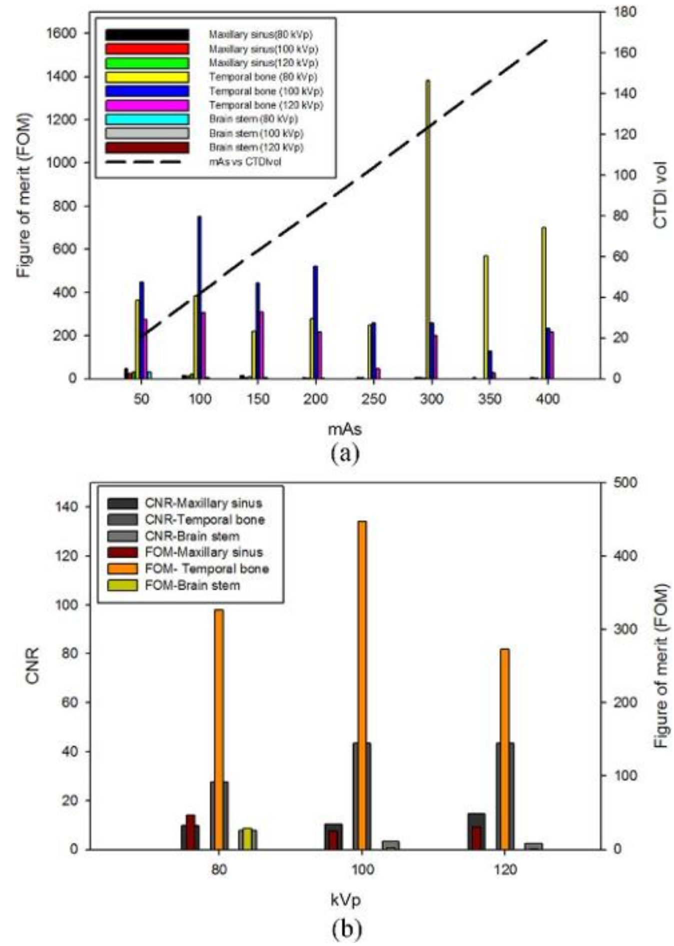


**Fig. 5.** (a) FOM and $CTDI_{vol}$ of ROIs (maxillary sinus, temporal bone and brain stem) in the pediatric phantom. (b) The kVp effect on CNR and FOM of the ROIs (maxillary sinus, temporal bone and brain stem) under 50 mAs with IR.

protocols for scanning adults or children are not readily determined by CNR alone(or any other metrics, i.e. SNR, CT number, noise). Also, the image oriented parameters are dependent on exposure oriented parameters, such as kVp, mAs, IR, as well as tissues under investigation (Rampado et al., 2012). How these factors may yet interact remains unclear and needs to be further explored, which is the purpose of the current study.

When scanning bone, using 80 kVp in the ACR phantom results in low CT numbers outside the standard range. This may be due to low peak voltage (80 kVp) which provides insufficient penetration of bone. The CT number range, as the basic requirement for CT scanning is not appropriate for adult CT scanning. The high peak voltage (120 kVp) would result in the CT number within the margin of the standard range.

When kVp increases in ACR module 1, all of the $CT_{ROI}$, $SD_{ROI}$, $CT_{bg}$ and $SD_{bg}$ decrease, while the difference of $CT_{ROI}$ and $CT_{bg}$ increases as shown in Table 1. Therefore, CNR increases with kVp. In addition, CNR will also increase with mAs. It is inferred that high peak voltage provides sufficient penetration of photons. High current will give more photons which will reduce the noise (or standard deviation as shown in Table 1and Table 2). However, higher photon energy and current time will result in greater radiation dose in the ROI, as previously stated (also shown in Tables 1, 2 and Figs. 3(a) and (b)).

Some studies utilized the SNR as the one of the parameters to

**Table 4**
The results of CT image of the temporal bone of the pediatric phantom with the voltage 80 kVp.

| | mAs | | | | | | | | | | | | | | |
|---|---|---|---|---|---|---|---|---|---|---|---|---|---|---|---|
| | 50 | 50+[a] | 100 | 100+ | 150 | 150+ | 200 | 200+ | 250 | 250+ | 300 | 300+ | 350 | 350+ | 400 |
| **CT(ROI)** | 958.7 | 967.4 | 958.4 | 963.0 | 953.5 | 962.7 | 960.2 | 962.0 | 960.2 | 965.4 | 969.8 | 963.6 | 965.7 | 961.3 | 957.9 |
| **S.D(ROI)** | 58.5 | 35.8 | 47.2 | 41.5 | 42.7 | 39.0 | 37.6 | 31.7 | 46.4 | 25.7 | 23.2 | 36.2 | 24.3 | 41.2 | 50.8 |
| **CT(bg)** | 18.5 | 29.8 | 15.9 | 25.0 | 8.5 | 26.3 | 8.5 | 17.2 | 22.8 | 16.2 | 28.9 | 11.8 | 21.1 | 18.2 | 24.3 |
| **S.D(bg)** | 38.8 | 34.0 | 27.6 | 23.4 | 20.1 | 25.1 | 20.2 | 19.7 | 26.9 | 18.7 | 29.3 | 7.2 | 20.9 | 10.4 | 22.6 |
| **Noise** | 58.5 | 35.8 | 47.2 | 41.5 | 42.7 | 39.0 | 37.6 | 31.7 | 46.4 | 25.7 | 23.2 | 36.2 | 24.3 | 41.2 | 50.8 |
| **CNR** | 24.2 | 27.6 | 34.1 | 40.0 | 47.1 | 37.3 | 47.0 | 47.9 | 34.8 | 50.9 | 32.1 | 131.4 | 45.1 | 91.1 | 41.3 |
| **CTDI** | 2.1 | 2.1 | 4.2 | 4.2 | 6.3 | 6.3 | 8.3 | 8.3 | 10.4 | 10.4 | 12.5 | 12.5 | 14.6 | 14.6 | 16.7 |
| **SNR** | 16.4 | 27.0 | 20.3 | 23.2 | 22.3 | 24.7 | 25.5 | 30.3 | 20.7 | 37.5 | 41.7 | 26.7 | 39.8 | 23.3 | 18.9 |
| **FOM** | 279.4 | 362.5 | 277.1 | 381.3 | 351.9 | 220.6 | 266.2 | 276.5 | 116.5 | 248.8 | 82.2 | 1381.5 | 139.3 | 568.5 | 102.2 |

[a] : + means plus the IDOS (Iteration reconstruction algorithm in Philips CT scanner software), where 400 mAs only without IDOS due to the automatic setting of IDOS setting

assess the CT image quality (Choi et al., 2013; Linsen et al., 2016). The present study, incorporates both $CT_{ROI}$ and $SD_{ROI}$ which is inversely correlated with kVp (Tables 1 and 2). The effect of kVp on SNR remains unclear (from Eq. (2)), which is apparent as SNR varies inconsistently with kVp in the range of 100–120 kVp (Table 2). It could be concluded that SNR may not be used as the independent image standard nor the metric for determining optimal protocols.

As radiation dose ($CTDI_{vol}$) increases with kVp and mAs, a trade-off exists between CNR and $CTDI_{vol}$ for determining the FOM, as is exemplified in other research (Yang et al., 2014; Goldman, 2007; McNitt-Gray, 2002). In this study, the optimal settings for the parameters of kVp and mAs for scanning adult bone (Tables 1 and 2, Fig. 3(c)–(d)) were 100 kVp/50–250 mAs.

For the line-pair test in Module 4 of ACR phantom, the threshold current- time is 150 mAs, below which the contrast would be outside the standard. Therefore, the best parameters for adult CT scanning are 100 kVp/150–250 mAs. For the low contrast region (Module 2 in ACR phantom), the $SD_{bg}$ is significantly decreased with increasing kVp as shown in Table 3; therefore FOM of the low contrast region will be proportional to kVp. There is an distinct trade-off between spatial resolution and low contrast resolution in CT imaging (Bissonnette et al., 2012). The optimal parameters of FOM for low contrast region are 120 kVp/150–250 mAs as shown in Fig. 4(b). In summary, the FOM parameters remain dependent on the ROI in adult CT scanning. Iteration regression (IR) is strongly recommended for adult CT scanning. The use of IR reduces noise (standard deviation of ROI's and back-ground's CT number) (as shown in Table 1 and Figs. 3(a), 3(b), 4(d)) without affecting the $CTDI_{vol}$, while increasing the CNR and FOM, which is in agreement with other studies (Choi et al., 2013; Andersen et al., 2014).

In summary: For adult CT scanning, high tube voltage and tube current-time results in better quality for CNR and consequently increased radiation dose. From FOM comparisons, it is recommended that the scanning parameters for adults are set at 100 kVp and 150–250 mAs. The optimal protocol for better low contrast resolution is 120 kVp and 150–250 mAs. IR is advised as it further increases the CNR by up to 40% without increasing the radiation dose.

In pediatric brain phantom CT scanning, IR approach can increase the CNR and FOM for all ROIs. Regarding adult CT scans, IR is also recommended in pediatric CT scan. From the FOM comparison, 80 kVp /300 mAs and 80 kVp/50 mAs are optimal for temporal bone and other ROIs respectively. This is reasonable as low kVp is preferable due to limited thickness of the pediatric head phantom. Higher mAs for temporal bone will decrease significantly the $SD_{bg}$(Table 4), thus increasing the CNR and FOM. However, as good image quality is most relevant for patient scanning, the 100 kVp with lower mAs and IR are determined as the optimal protocol for pediatric CT scanning.

## 5. Conclusions

The threshold values of adult CT scan parameters, 100 kVp and 150 mAs, were derived from the CT number test and line pairs in ACR phantom module 1and module 4 respectively. It is recommended that the scanning parameters for adults be set at 100 kVp and 150–250 mAs. However, for better low- contrast resolution, 120 kVp and 150–250 mAs are suggested settings. For pediatric head CT scan, 80 kVp/50 mAs were found to be optimal for maxillary sinus and brain stem, while 80 kVp /300 mAs is appropriate for temporal bone. SNR is not sufficient as the independent image parameter nor the metric for deriving the optimal CT scan settings. The iteration IR approach is strongly recommended for both adult and pediatric CT scanning as it further increases the CNR by up to 40% without increasing the radiation dose.

## Acknowledgments

We would like to thank Ms. Natasha Tomicic for trouble shooting the manuscript and also express our gratitude to Miss Fang Ying Rou for helping on the CT scans analyses.

## References

AAPM Report No. 204, 2011. Size-specific dose estimates (SSDE) in pediatric and adult body CT examinations. Am. Assoc. Phys. Med..

Andersen, H.K., Jensen, K., Berstad, A.E., Aalokken, T.M., Kristiansen, J., von Gohren Edwin, B., Hagen, G., Martinsen, A.C., 2014. Choosing the best reconstruction technique in abdominal computed tomography: a systematic approach. J. Comput. Assist. Tomogr. 38, 853–858.

Baldwin, J., Grantham, V., 2015. Radiation hormesis: historical and current perspectives. J. Nucl. Med. Technol. 43, 242–246.

Bissonnette, J.P., Balter, P.A., Dong, L., Langen, K.M., Lovelock, D.M., Miften, M., Moseley, D.J., Pouliot, J., Sonke, J.J., Yoo, S., 2012. Quality assurance for image-guide radiation therapy utilizing CT-based technologies: a report of the AAPM TG-179. Med. Phys. 39, 1946–1963.

Brady, S.L., Yee, B.S., Kaufman, R.A., 2012. Characterization of adaptive statistical iterative reconstruction algorithm for dose reduction in CT: a pediatric oncology perspective. Med. Phys. 39, 5520–5531.

Brunner, C.C., Stern, S.H., Minniti, R., Parry, M.I., Skopec, M., Chakrabarti, K., 2013. CT head-scan dosimetry in an anthropomorphic phantom and associated measurement of ACR accreditation-phantom imaging metrics under clinically representative scan conditions. Med. Phys. 40, 081917.

Choi, J.W., Lee, J.M., Yoon, J.H., Baek, J.H., Han, J.K., Choi, B.I., 2013. Iterative reconstruction algorithms of computed tomography for the assessment of small pancreatic lesions: phantom study. J. Comput. Assist. Tomogr. 37, 911–923.

Goldman, L.W., 2007. Principles of CT: radiation dose and image quality. J. Nucl. Med. Technol. 35, 213–215.

ICRU Report No. 87, 2012. : radiation dose and image-quality assessment in computed tomography. J. ICRU 12, 1–149.

Linsen, P.V., Coenen, A., Lubbers, M.M., Dijkshoorn, M.L., Ouhlous, M., Nieman, K., 2016. Computed tomography angiography with a 192-slice dual-source computed tomography system: improvements in image quality and radiation dose. J. Clin. Imaging Sci. 6, 44–50.

McNitt-Gray, M.F., 2002. AAPM/RSNA physics tutorial for residents: topics in CT. Radiation dose in CT. Radiographics 22, 1541–1553.

Miglioretti, D.L., Johnson, E., Williams, A., Greenlee, R.T., Weinmann, S., Solberg, L.I., Feigelson, H.S., Roblin, D., Flynn, M.J., Vanneman, N., Smit.h-Bindman, R., 2013. The use of computed tomography in pediatrics and the associated radiation exposure and estimated cancer risk. JAMA Pediatr. 167, 700–707.

National Council on Radiation Protection and Measurements, 2009. Ionizing Radiation Exposure of the Population of the United States (NCRP Report No 160). National Council on Radiation Protection and Measurements, Bethesda, Md.

Pahn, G., Skornitzke, S., Schlemmer, H.P., Kauczor, H.U., Stiller, W., 2016. Toward standardized quantitative image quality (IQ) assessment in computed tomography (CT): a comprehensive framework for automated and comparative IQ analysis based on ICRU Report 87. Phys. Med. 32, 104–115.

Rampado, O., Bossi, L., Garabello, D., Davini, O., Ropolo, R., 2012. Characterization of a computed tomography iterative reconstruction algorithm by image quality evaluation with an anthropomorphic phantom. Eur. J. Radio. 81, 3172–3177.

Yang, C.C., Liu, S.H., Mok, G.S., Wu, T.H., 2014. Evaluation of radiation dose and image quality of CT scan for whole-body pediatric PET/CT: a phantom studyMed. Phys. 41, 092505.

# Iterative Reconstruction in Head CT: Image Quality of Routine and Low-Dose Protocols in Comparison with Standard Filtered Back-Projection

**PATIENT SAFETY**

A. Korn
M. Fenchel
B. Bender
S. Danz
T.K. Hauser
D. Ketelsen
T. Flohr
C.D. Claussen
M. Heuschmid
U. Ernemann
H. Brodoefel

**BACKGROUND AND PURPOSE:** IR has recently demonstrated its capacity to reduce noise and permit dose reduction in abdominal and thoracic CT applications. The purpose of our study was to assess the potential benefit of IR in head CT by comparing objective and subjective image quality with standard FBP at various dose levels.

**MATERIALS AND METHODS:** Ninety consecutive patients were randomly assigned to undergo nonenhanced and contrast-enhanced head CT at a standard dose (320 mAs; CTDI, 60.1) or 15% (275 mAs; CTDI, 51.8) and 30% (225 mAs; CTDI, 42.3) dose reduction. All acquisitions were reconstructed with IR in image space, and FBP and images were assessed in terms of quantitative and qualitative IQ.

**RESULTS:** Compared with FBP, IR resulted in lower image noise ($P \leq .02$), higher CNR ($P \leq .03$), and improved subjective image quality ($P \leq .002$) at all dose levels. While degradation of objective and subjective IQ at 15% dose reduction was fully compensated by IR (CNR, 1.98 ± 0.4 at 320 mAs with FBP versus 2.05 ± 0.4 at 275 mAs with IR; IQ, 1.8 versus 1.7), IQ was considerably poorer at 70% standard dose despite using the iterative approach (CNR, 1.98 ± 0.3 at 320 mAs with FBP versus 1.85 ± 0.4 at 225 mAs with IR, $P = .18$; IQ, 1.8 versus 2.2, $P = .03$). Linear regression analysis of CNR against tube current suggests that standard CNR may be obtained until approximately 20.4% dose reduction when IR is used.

**CONCLUSIONS:** Compared with conventional FBP, IR of head CT is associated with significant improvement of objective and subjective IQ and may allow dose reductions in the range of 20% without compromising standard image quality.

**ABBREVIATIONS:** CNR = contrast-to-noise ratio; CTDI = CT dose index; $CTDI_{vol}$ = volume CT dose index; DLP = dose-length product; FBP = filtered back-projection; GM = gray matter; IQ = image quality; IR = iterative reconstruction; IRIS = iterative reconstruction in image space; MDCT = multidetector row CT

The technical evolution of MDCT has not only revolutionized image quality and scanning speed but has also dramatically increased the number of CT examinations in the industrialized world. As a result, there is a growing concern regarding the associated radiation dose.[1] Today, >70 million annual CT scans are obtained in the United States and may be responsible for about 2% of all incident cancer cases.[1,2] As head CT has evolved as the technique of choice to assess traumatic and nontraumatic neurologic conditions, its use has become particularly frequent in both the adult and pediatric populations.[3]

In the past decade, various dose-reduction strategies, such as automated tube current modulation, low voltage scanning, and noise-reduction filters, have been explored but could not prevent a steady increase of average effective dose with advanced scanner technology.[4-9] Unfortunately, the most straightforward technique in lowering dose, notably the reduction of tube current, is associated with unacceptable increase of image noise. This effect is partly due to limitations in the current standard reconstruction method of FBP. With FBP, increased spatial resolution is directly correlated with increased image noise and is traded against noise by application of different reconstruction kernels.

Only recently, an alternative mathematic algorithm, IR, was introduced to CT. To a certain extent, IR allows decoupling of spatial resolution and image noise and may thus be used to lower noise at standard or improved resolution of images.[10,11] In IR, a correction loop is introduced in the image reconstruction process. Once an image has been reconstructed from the measured projection data, a ray-tracing in the image is performed to calculate new projections that exactly represent the reconstructed image, as if the reconstructed image had been the measurement object of a CT scan. This step, called forward projection, simulates the CT measurement. If the image reconstruction were perfect, no deviation between measured and calculated projections would be observed. In reality, due to the approximate nature of FBP reconstruction typically used for image reconstruction, there is a deviation between measured and calculated projections. This is used to derive correction projections, reconstruct a correction image, and update the original image. This loop is continued until the deviation between measured and calculated projections is

Received April 11, 2011; accepted after revision May 13.

From the Departments of Diagnostic und Interventional Neuroradiology (A.K., M.F., B.B., S.D., T.K.H., U.E.) and Diagnostic and Interventional Radiology (D.K., C.D.C., M.H., H.B.), Eberhard-Karls-University, Tübingen, Germany; and Computed Tomography Division (T.F.), Siemens HealthCare, Forchheim, Germany.

Please address correspondence to Harald Brodoefel, MD, Department of Diagnostic Radiology, Eberhard-Karls-University, Hoppe-Seyler-Str. 3, 72076 Tübingen, Germany; e-mail: h.brodoefel@t-online.de

http://dx.doi.org/10.3174/ajnr.A2749

smaller than a predefined limit. Each time the original image is updated, nonlinear image processing algorithms, so called "regularizations," are used to stabilize the resolution. While the repeated calculation of correction projections removes artifacts introduced by the approximate nature of FBP, it is this regularization procedure that is essential for the noise-reduction properties of an IR.[12] With proper regularization, image noise can be lowered without loss of detail resolution, which—as a consequence—allows reduction of radiation exposure to the patient.

IRIS is 1 variant of IR that applies the regularization procedure to the image data in an iterative loop without forward projection and calculation of correction projections.[12] As a consequence, IRIS aims at reduction of image noise and not at reduction of potential image artifacts, such as conebeam artifacts, which are not a severe problem anyway in CT systems with relatively small detector width in the z-direction. In the IRIS approach, an iterative series of 3D nonlinear image-filtering steps, corresponding to the regularization in a standard IR, is performed after reconstruction of an initial high-resolution image by means of the FBP technique. This high-resolution image contains all measured information that is otherwise partially suppressed in a standard CT reconstruction to obtain acceptable image-noise levels. Depending on the clinical task, 3–5 iterations of regularizations are performed. They aim at maintaining or even enhancing spatial resolution, while reducing image noise without degrading the image texture.

The primary asset to all forms of IR is that they are consistently associated with significant reduction of image noise and may thus be used to perform CT examinations at lower dose, yet robust, image quality. Until now, this concept has been demonstrated for thoracic, abdominal, and cardiac CT examinations.[13-19]

The aim of our study was to systematically assess IR at various tube currents in head CT and thereby determine the practicability of reducing dose without compromising standard image quality.

## Materials and Methods

### *Patient Groups*

The study was approved by the local institutional review board. Because unpublished customer and vendor experience suggests preservation of diagnostic image quality at all dose levels used in our study, informed consent of patients was waived and all examinations were performed as standard of care.

The participants were 90 consecutive patients who were scheduled for both nonenhanced and contrast-enhanced head CT and who were randomly assigned to 1 standard and 2 low-dose CT protocols. Reasons to perform the examination were manifold and included tumor staging, exclusion of septic emboli, and ischemia.

### *Data Acquisition and Reconstruction*

All CT examinations were performed by using a 128-section dual-source CT scanner (Somatom Definition Flash; Siemens, Forchheim, Germany). Image-acquisition parameters of the standard protocol included a collimation of $40 \times 0.6$ mm, pitch of 0.55, rotation time of 1.0 second, tube voltage of 120 kV, and tube current of 320 mAs. Scan parameters for low-dose studies were identical except for tube current, which was reduced to 275 or 225 mAs, respectively. Contrast-enhanced examinations were performed 180 seconds postadministration of 65 mL of iodinated contrast medium (Imeron 400 [iomeprol], 400 mg I/mL; Bracco Altana Pharma, Konstanz, Germany).

Raw data of all CT examinations were reconstructed by using both mathematic algorithms, FBP and IR. Reconstruction parameters included an H30s+ medium smooth convolution kernel for FBP and the equivalent J30 medium smooth kernel for IR, a section-thickness of 4.5 mm with a 4.5-mm increment, and an FOV appropriate to head size. The time for reconstruction was recorded in 10 patients.

For a subset analysis of image sharpness, additional reconstructions were performed in 15 patients with bone window kernels, notably the H70 for FBP and the equivalent J70 for IR. Section-thickness and increment in these reconstructions were 2 mm.

### *Dose Measurements*

The $CTDI_{vol}$ and DLP were recorded for every CT examination. Effective dose (millisievert) was estimated by multiplying DLP with a constant region-specific conversion coefficient of 0.0023 mSv/(mGy × cm).[20]

### *Quantitative Image Analysis*

Assessment of quantitative image parameters was done by a board-certified, not subspecialty-certified, reader with 1 year of training in neuroradiology (H.B.). For each pair of FBP and IR reconstructions, 4 $mm^2$ regions of interest were placed in identical infra- and supratentorial WM and GM locations, the ventricle, and air, 5 mm outside the skull at its widest circumference. Measurements from infra- and supratentorial WM and GM regions were averaged for further analysis. Signal intensity was defined as CT attenuation in Hounsfield units; image noise, as the SD of attenuation within a region of interest. SNRs and CNRs were calculated by using the following standard equations:

$$\text{SNR} = \text{Mean HU of Tissue in Region of Interest} / \text{SD of HU in Region of Interest}$$

$$\text{CNR} = (\text{Mean GM HU} - \text{Mean WM HU}) / [(\text{SD GM HU})^2 + (\text{SD WM HU})^2]^{1/2}.$$

For a subset analysis of image sharpness, FBP and IR bone window reconstructions of 15 patients were assessed by a Matlab tool (MathWorks, Natick, Massachusetts) on a separate workstation. The program measures CT attenuation values in Hounsfield units across pixels that are lined perpendicular to the skull circumference. Sharpness is quantified as maximal slope (Change in HU/Pixel).

### *Qualitative Image Analysis*

Qualitative analysis of images was independently performed by 2 board-certified, subspecialty-certified readers (A.K.) and (M.F.) with 3 and 4 years of training in neuroradiology. Before the grading of study images, the reading radiologists were trained for consensus regarding our image-quality scoring system on 20 routine head CT examinations. For randomized and anonymous analysis of study patients, subjects were randomly selected by 1 of our authors (B.B.) and FBP and IR reconstructions of nonenhanced and contrast-enhanced scans were simultaneously displayed to the readers, by using two $325 \times 433$ mm screen-size monitors with a $160 \times 372$ mm image size per individual series. The order of display for FBP and IR series was changed in a random fashion, and information on the type of reconstruction or dose level was masked. All images were reviewed at a PACS workstation (Centricity; GE Healthcare, Milwaukee, Wiscon-

Table 1: Patient characteristics and radiation dose in CT protocols with various tube currents

| Characteristic | 320 mAs | 275 mAs | 225 mAs | $P$ |
|---|---|---|---|---|
| Age | 63 ± 14 | 67 ± 13 | 66 ± 12 | .54 |
| Sex (male/female) | 12/18 | 14/16 | 19/11 | .17 |
| $CTDI_{vol}$ (mGy) | 60.1 | 51.8 | 42.3 | — |
| DLP (mGy.cm) | 1043 ± 53 | 890 ± 34 | 733 ± 52 | <.0001 |
| Effective dose (mSv) | 2.2 ± 0.1 | 1.8 ± 0.07 | 1.5 ± 1.0 | <.0001 |

sin) with use of standard display settings (window level, 36; width, 80).

Subjective image quality was assessed in terms of noise, GM-WM differentiation, sharpness of subarachnoid space margins, distinctness of posterior fossa contents, and overall diagnostic acceptability. Noise was graded as the following: 1, very low; 2, low; 3, considerable with preserved diagnostic image quality; 4, high, causing nondiagnostic image quality. All other parameters were scored as the following: 1, excellent; 2, good; 3, suboptimal, but still diagnostic; and 4, unacceptable and nondiagnostic. Grades for image quality were averaged across both readers for further analysis.

### *Statistical Analysis*

Statistical analysis was performed with software (JMP, Version 6, SAS Institute, Cary, North Carolina; Prism, Version 4.00, GraphPad Software, San Diego, California). A $P$ value $< .05$ indicated statistical significance. An unpaired $t$ test and $\chi^2$ test were used to compare continuous and proportional patient characteristics between subgroups. Regarding objective imaging parameters, intraprotocol comparisons between FBP and IR were done by paired $t$ tests. For comparisons between various tube currents or CT protocols, an unpaired $t$ test or 1-way analysis of variance with a subsequent Tukey multiple comparison test was used.

The Wilcoxon signed rank test, Mann-Whitney $U$ test, or Kruskal-Wallis with the Dunn multiple comparison test was used for analysis of subjective image-quality scores. Inter-rater agreement in the assessment of image quality was quantified by weighted $\kappa$ statistics.

## Results

Noncontrast and contrast-enhanced imaging was performed in 90 patients; the characteristics of subjects within the distinct study groups are shown in Table 1. Median time for reconstruction was substantially longer with use of the iterative algorithm, notably 68 seconds (range, 61–74 seconds) versus 25 seconds (range 22–27 seconds).

### *Radiation Dose*

Dose-related parameters are summarized in Table 1. While the $CTDI_{vol}$ was 60.1 mGy in the 320-mAs reference group, it was reduced to 85.5% in the low-dose group 1 (275 mAs) or 70.3% in low-dose group 2 (225 mAs). Accordingly, compared with 1043 mGy.cm and 2.2 mSv in standard head CT, DLP and effective dose were cut down to 85.3% with use of 275 mAs and 70.2% when applying 225 mAs.

### *Quantitative Analysis*

A 15-patient subset analysis of image sharpness at bone window kernels demonstrated an insignificant 3% decrease with the use of IR (396.9 ± 111.3 versus 386.3 ± 117 change in HU/Pixel; $P = .55$).

By contrast, analysis of attenuation values did not reveal any difference between tube currents and reconstruction algorithms used. Accordingly, the reduction of noise in WM and GM, liquor, and background for all of the 3 CT protocols resulted in significant enhancement of SNR (Table 2) and CNR (Fig 1) with IR postprocessing. The average improvement of CNR by using IR versus FBP was 13% (1.82 ± 0.4 versus 2.06 ± 0.4; $P < .0001$).

Conversely, in both IR and FBP reconstruction, reduction of tube current was associated with a significant increase of image noise or degradation of SNR (Table 2) and CNR (Fig 1). In detail, with FBP, the decrease of CNR was 10% (1.98 ± 0.4 versus 1.78 ± 0.4; $P = .016$) in a 275-mAs and 17% (1.98 ± 0.4 versus 1.65 ± 0.4; $P = .0008$) in a 225-mAs low-dose protocol.

Hence, compared with the standard 320-mAs CT with FBP, quantitative degradation of image quality by lowering the tube current to 275 mAs was fully compensated when applying IR (1.98 ± 0.4 versus 2.05 ± 0.4, Fig 1). CNR in 225-mAs datasets with IR was approximately 7% below the average of a standard 320-mAs FBP protocol (1.98 ± 0.3 versus 1.85 ± 0.4; $P = .18$, Fig 1).

Linear regression analysis of CNR against tube current suggests that standard CNR may be obtained until about 20.4% dose reduction (255 mAs) when IR is used (Fig 2).

### *Qualitative Analysis*

With all tube currents, use of an iterative algorithm was associated with significant improvement of scores for noise, GM-WM differentiation, sharpness of subarachnoid space, and overall diagnostic acceptability (Table 3 and Fig 3). The benefit of IR was less consistent with regard to the visualization of posterior fossa contents.

When compared with the 320-mAs FBP standard protocol, lowering the tube current to 225 mAs resulted in considerable deterioration of overall diagnostic acceptability with both reconstruction algorithms (1.8 versus 2.7 for FBP, $P < .0001$; 1.8 versus 2.2 for IR, $P = .03$). No difference was observed between 320 mAs with FBP and 275 mAs with IR reconstruction (1.8 versus 1.7, $P = .63$; Fig 4).

The interobserver agreement in the assessment of various image-quality parameters was good (weighted $\kappa$, 0.68).

## Discussion

The increasing use of MDCT has fueled a heightened concern regarding potential hazards and has evoked an extensive interest in minimizing radiation exposure. Unfortunately, many traditional dose-reduction strategies (eg, low tube current and voltage scanning or specific noise reduction kernels) come at the price of degraded image quality. While for many applications of conventional body CT, a mild increase of noise may not limit diagnostic accuracy, classic neuroradiologic issues such as detection of acute ischemia, edema, or hemorrhage require exceptional image quality and leave little room for compromise. The reason lies with minute attenuation differences between WM and GM, the shielding of tissue by the skull, and the inherently unfavorable SNR.

IR has long been discussed as a highly promising reconstruction concept to achieve considerable dose reduction without losing image quality. Unlike traditional FBP, the method is based on a correction loop within the image-generation process, which leads to significant reduction of noise

| Table 2: Mean and SD of SNR in various CT protocols with either IR or FBP[a] | | | | | | |
|---|---|---|---|---|---|---|
| | Tube Current 320 mAs | | Tube Current 275 mAs | | Tube Current 225 mAs | |
| | IR | FBP | IR | FBP | IR | FBP |
| Non-Enhanced | | | | | | |
| WM | 8.8 ± 2.1 | 7.9 ± 1, $P = 0.01$ | 8.0 ± 1.7 | 7.0 ± 1.3, $P < .0001$ | 7.6 ± 1.5 | 6.7 ± 1.4, $P = .006$ |
| GM | 10.9 ± 2 | 9.4 ± 1.4, $P < .0001$ | 9.8 ± 1.4 | 8.3 ± 1.3, $P < .0001$ | 9.7 ± 1.8 | 8.4 ± 1.6, $P < .0001$ |
| LQ | 1.4 ± 0.5 | 1.2 ± 0.4, $P < .0001$ | 1.3 ± 0.4 | 1.0 ± 0.3, $P < .0001$ | 1.2 ± 0.3 | 1.0 ± 0.3, $P < .0006$ |
| BG | −448 | −302, $P < .0001$ | −385 | −210, $P < .0001$ | −295 | −244, $P < .0001$ |
| Contrast-Enhanced | | | | | | |
| WM | 8.9 ± 1.8 | 7.6 ± 1.4, $P < .0001$ | 7.9 ± 1.5 | 6.8 ± 1.1, $P < .0001$ | 7.8 ± 1.4 | 6.5 ± 1.0, $P < .0001$ |
| GM | 11.2 ± 1.7 | 10.2 ± 1.6, $P = .001$ | 10.2 ± 1.7 | 9.0 ± 1.4, $P = .0008$ | 9.4 ± 2.1 | 8.6 ± 1.7, $P = .02$ |
| LQ | 1.3 ± 0.6 | 1.0 ± 0.4, $P < .0001$ | 1.2 ± 0.5 | 1.0 ± 0.4, $P = 0.004$ | 1.1 ± 0.3 | 0.9 ± 0.4, $P < .001$ |
| BG | −385 | −328, $P < .0001$ | −222 | −192, $P < .008$ | −221 | −191, $P < .0001$ |

**Note:**—LQ indicates liquor; BG, background.
[a] Data are shown for WM, GM, LQ, and BG measurements in air outside the skull. *P* values refer to differences between IR and FBP.

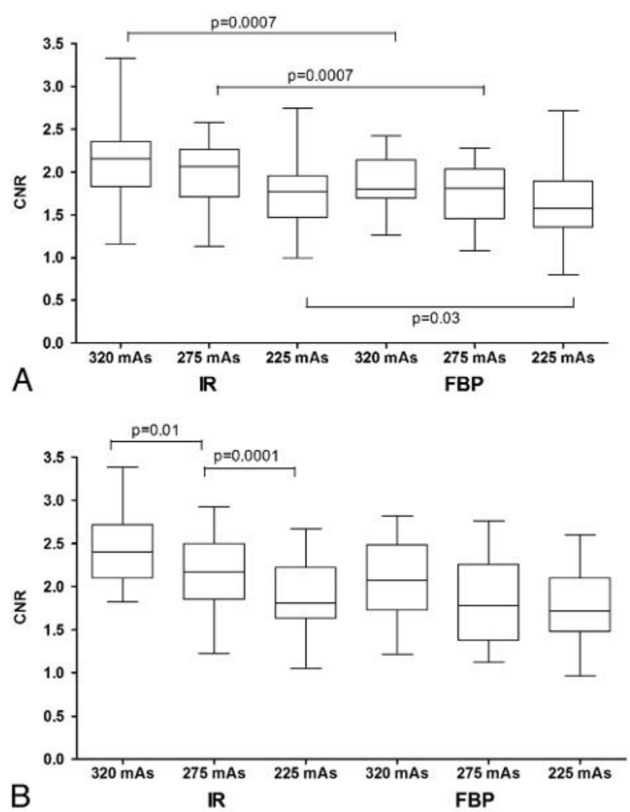


**Fig 1.** CNR in nonenhanced (*A*) and contrast-enhanced (*B*) head CT with the use of various tube currents and reconstruction of data by FBP or IR. In the boxplot diagrams, the line across the middle of the box identifies the median sample value; boxes extend from the 25th to the 75th quartile, and whiskers, down to the lowest and highest values.

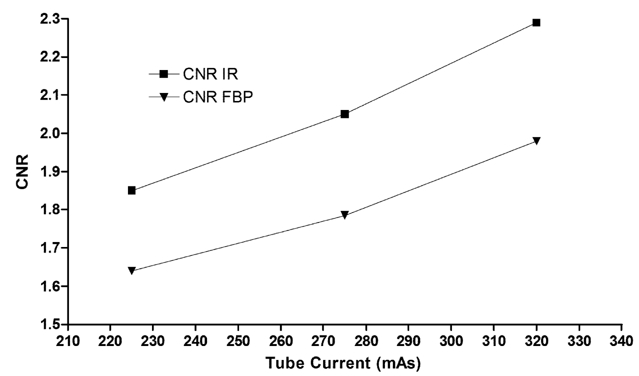


**Fig 2.** Regression plot of CNR against tube current with IR and FBP. According to linear regression equation, the x-intercept is at a tube current of 255 mAs when y is at a standard 1.98 CNR (320-mAs FBP).

with maintenance of image resolution.[11] However, for a long time, the required computational power for everyday use has not been available and variations of the algorithm have only recently been introduced into clinical routine. At this stage, several studies have confirmed the capability of IR to achieve robust image quality in low-dose abdominal, thoracic, and cardiovascular CT examinations.[13-19,21]

Our study is the first to assess the iterative approach in head CT. We find that IR achieves a significant reduction of image noise, which is robust among various dose protocols and nonenhanced and contrast-enhanced studies. Image sharpness is decreased by approximately 3%, yet this difference proved insignificant in a smaller subset analysis and does not translate into deterioration of subjective image quality. In fact, the latter is improved by lower noise levels that correlate with increased SNR and CNR due to the preservation of attenuation values. While IR achieves robust objective and subjective image quality in an 85% low-dose protocol, a 30% dose reduction is associated with noticeable degradation of quality. In terms of quantitative imaging parameters, a linear regression equation suggests that standard quality may be preserved until approximately 20% dose reduction whenever IR is used.

Due to the computational complexity, time for reconstruction was substantially increased with use of the iterative algorithm. However, with a median reconstruction interval of 68 seconds, clinical efficiency was not affected. Also, as both the method and computational power continue to evolve, a further decrease of processing time is expected in the near future.

When compared with dose savings of 33%–50% or 36%–75% in abdominal and thoracic applications, our findings for head CT may appear somewhat modest.[15-17,19,21] Apart from conceivable variations in different vendors or products, the most likely explanation for such discrepancies is the critical CNR in the GM-WM differentiation and a more marked increase of noise with the reduction of tube current in head CT. Nonetheless, maintaining standard image quality at dose savings in the range of 20% still represents a considerable step in terms of patient dose reduction and may particularly benefit the large number of patients with serial follow-up examinations.

In this context, the standards for image quality in our study were derived from a relatively high-dose protocol, designed for applications that require an exceptional CNR. Accord-

**Table 3: Mean and median of qualitative image scores in various CT protocols with either IR or FBP[a]**

| | Tube Current 320 mAs | | Tube Current 275 mAs | | Tube Current 225 mAs | |
|---|---|---|---|---|---|---|
| | IR | FBP | IR | FBP | IR | FBP |
| Non-Enhanced | | | | | | |
| Noise | 1.2 (1) | 1.6 (1.5), $P = .003$ | 1.6 (2) | 1.9 (1.75), $P = .001$ | 2.0 (2) | 2.5 (2.5), $P < .0001$ |
| GM/WM | 1.4 (1) | 1.8 (2), $P = .002$ | 1.6 (1.5) | 2.2 (2.25), $P = .009$ | 2.2 (2) | 2.9 (3.0), $P < .0001$ |
| SS | 1.4 (1) | 1.7 (2), $P = .007$ | 1.6 (2) | 2.0 (2), $P = .01$ | 2.1 (2) | 2.7 (3), $P = .0006$ |
| PF | 1.6 (2) | 2.0 (2), $P = .1$ | 2.0 (2) | 2.7 (2.5), $P = .001$ | 2.8 (3) | 3.4 (3), $P = .0002$ |
| DA | 1.3 (1) | 1.7 (2), $P = .002$ | 1.7 (2) | 2.2 (2), $P = .0005$ | 2.2 (2) | 2.8 (2.5), $P < .0001$ |
| Contrast-Enhanced | | | | | | |
| Noise | 1.2 (1) | 1.4 (1.5), $P = .02$ | 1.4 (1) | 1.8 (1.75), $P = .003$ | 2.1 (2) | 2.5 (2.5), $P = .0002$ |
| GM/WM | 1.3 (1) | 1.6 (2), $P = .002$ | 1.6 (1.5) | 2.1 (2), $P = .001$ | 2.1 (2) | 2.7 (3), $P = .0004$ |
| SS | 1.3 (1) | 1.6 (2), $P = .004$ | 1.5 (1.75) | 1.9 (2), $P = .008$ | 2.0 (2) | 2.6 (3), $P < .0001$ |
| PF | 1.6 (2) | 2.0 (2), $P = .01$ | 2.2 (2) | 2.5 (2.5), $P = .09$ | 2.8 (3) | 3.0 (3), $P = .2$ |
| DA | 1.2 (1) | 1.8 (2), $P = .007$ | 1.6 (2) | 2.0 (2), $P = .008$ | 2.1 (2) | 2.6 (2.5), $P = .0003$ |

**Note:**—SS indicates subarachnoid space margins; PF, distinctness of posterior fossa contents; DA, overall diagnostic acceptability.
[a]Image-quality grading is provided for noise, GM-WM matter differentiation, sharpness of SS, PF, and overall DA. Median is in parentheses.

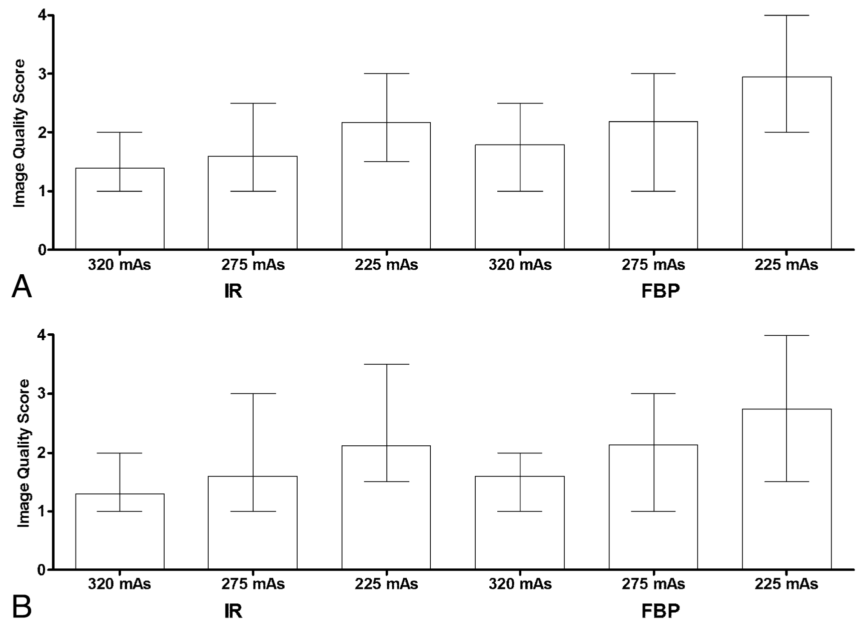


**Fig 3.** Subjective grading of WM-GM differentiation in nonenhanced (*A*) and contrast-enhanced (*B*) head CT with use of various tube currents and reconstruction of data by FBP or IR. Data are presented as means and ranges.

ingly, automatic tube current modulation was not applied and the collimation was set to 40 × 0.6 mm. The resultant $CTDI_{vol}$ and DLP of our routine protocol are in line with the European diagnostic reference levels.[22] Whether the associated level of image quality always translates into a heightened accuracy or better diagnosis is debatable; however, this problem is beyond the scope of our current study. Notably, other institutions have different standards for diagnostic confidence, and systematic analyses of routine protocols have shown a considerable variability of radiation dose and image quality between institutions or scanners.[23,24] Undoubtedly, many everyday applications such as follow-up examinations of hematoma, tumors, or the evaluation of ventricular shunts carry the potential for significant reduction of routine dose, which—independent of individual standards for diagnostic confidence—may be even more substantial when IR is used. Finally, because iterative processing is still a very young approach, it is likely that more advanced and powerful variations of the technique will emerge in the near future and, thereby, enable additional dose savings.

The first limitation of our study is the small sample size per group, requiring confirmation of our findings in a larger patient series. Different tube currents were applied to different patient cohorts so that a more accurate—yet practically almost impossible—intrapatient comparison of protocols could not be performed. As indicated above, the focus of our study was on subjective and objective image quality; we did not assess the diagnostic accuracy of IR low-dose acquisitions in comparison with standard protocols.

## Conclusions

Our data support the use of IR in head CT as a valuable tool for significant dose reduction. The algorithm is robust in lowering image noise and improves quantitative and qualitative imaging parameters in both nonenhanced and contrast-enhanced scans at variable radiation doses. The potential of IR to maintain standard image quality at ≤20% dose reduction justifies larger clinical studies with a focus on diagnostic accuracy.

Disclosures: Thomas Flohr, *Unrelated*: employment Siemens.

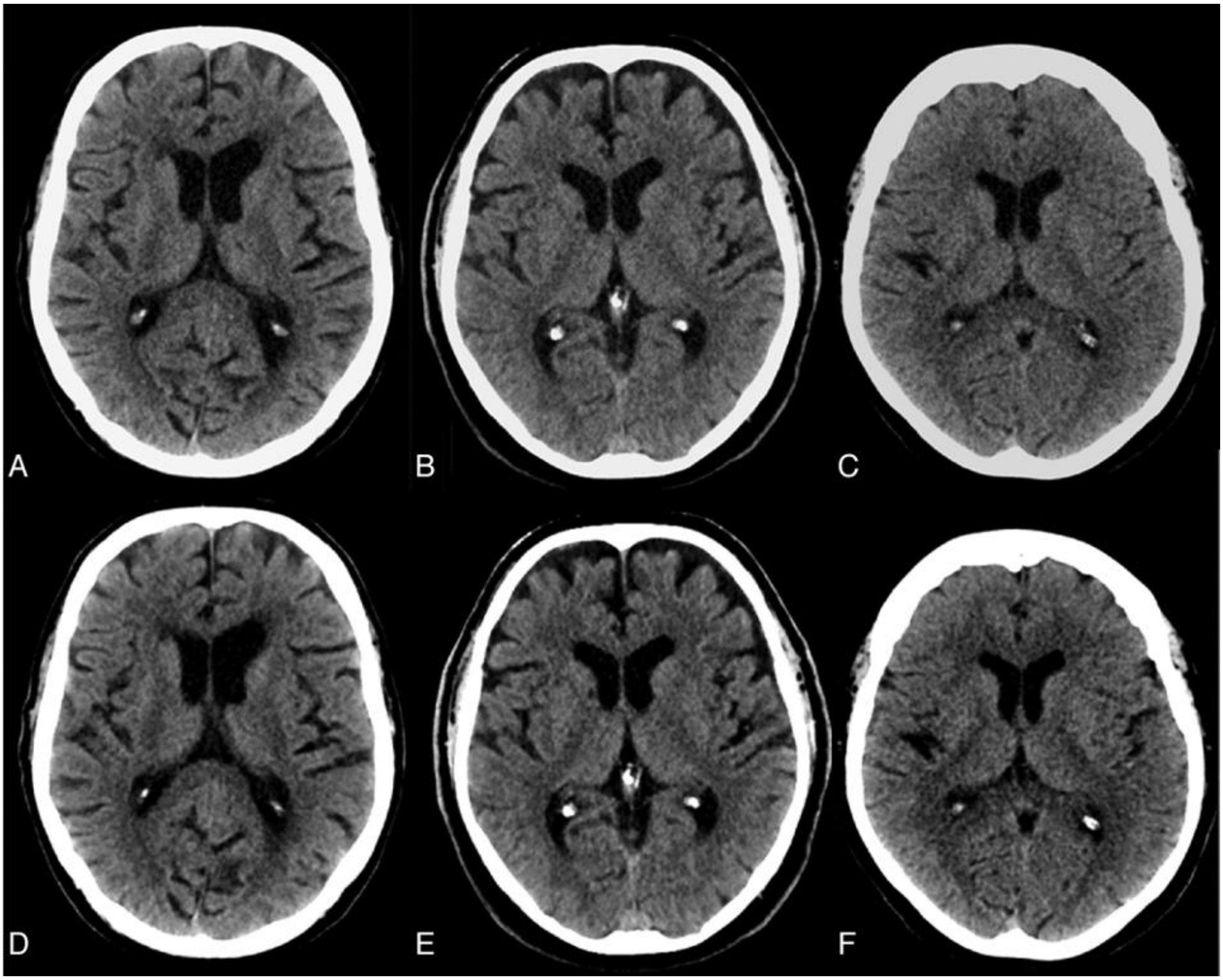


**Fig 4.** Example of image quality at 320 (*A* and *D*), 275 (*B* and *E*), and 225 (*C* and *F*) mAs. At all dose levels, use of IR (*D*–*F*) is associated with a considerable reduction of noise and enhancement of image quality. As demonstrated in our study, this is achieved without significant loss of image sharpness. While image quality at 85% dose and IR (*E*) is similar to the standard of reference (*A*), a 30% dose reduction results in substantial increase of noise despite using IR (*F*).

## References


1. Brenner DJ, Hall EJ. **Computed tomography: an increasing source of radiation exposure.** *N Engl J Med* 2007;357:2277–84
2. Brenner DJ. **Slowing the increase in the population dose resulting from CT scans.** *Radiat Res* 2010;174:809–15
3. Mahesh M. **NCRP report number 160: its significance to medical imaging.** *J Am Coll Radiol* 2009;6:890–92
4. Kalra MK, Maher MM, Blake MA, et al. **Detection and characterization of lesions on low-radiation-dose abdominal CT images postprocessed with noise reduction filters.** *Radiology* 2004;232:791–97
5. Kalra MK, Maher MM, Toth TL, et al. **Techniques and applications of automatic tube current modulation for CT.** *Radiology* 2004;233:649–57
6. Mettler FA Jr, Wiest PW, Locken JA, et al. **CT scanning: patterns of use and dose.** *J Radiol Prot* 2000;20:353–59
7. Mullins ME, Lev MH, Bove P, et al. **Comparison of image quality between conventional and low-dose nonenhanced head CT.** *AJNR Am J Neuroradiol* 2004;25:533–38
8. Udayasankar UK, Braithwaite K, Arvaniti M, et al. **Low-dose nonenhanced head CT protocol for follow-up evaluation of children with ventriculoperitoneal shunt: reduction of radiation and effect on image quality.** *AJNR Am J Neuroradiol* 2008;29:802–06
9. Vock P. **CT dose reduction in children.** *Eur Radiol* 2005;15:2330–40
10. Nuyts J, De Man B, Dupont P, et al. **Iterative reconstruction for helical CT: a simulation study.** *Phys Med Biol* 1998;43:729–37
11. Thibault JB, Sauer KD, Bouman CA, et al. **A three-dimensional statistical approach to improved image quality for multislice helical CT**. *Med Phys* 2007;34:4526–44
12. Bruder H RR, Sunnegardh J, Stiersturter K, et al. **Translation of statistical iterative reconstruction into non-linear image processing**. In: *Proceedings of the Annual Meeting of the Radiological Society of North America*, Chicago, Illinois. November 28-December 3, 2010
13. Bittencourt MS, Schmidt B, Seltmann M, et al. **Iterative reconstruction in image space (IRIS) in cardiac computed tomography: initial experience**. *Int J Cardiovasc Imaging* 2010;27:1081–87
14. Gosling O, Loader R, Venables P, et al. **A comparison of radiation doses between state-of-the-art multislice CT coronary angiography with iterative reconstruction, multislice CT coronary angiography with standard filtered back-projection and invasive diagnostic coronary angiography**. *Heart* 2010;96:922–26
15. Leipsic J, Nguyen G, Brown J, et al. **A prospective evaluation of dose reduction and image quality in chest CT using adaptive statistical iterative reconstruction.** *AJR Am J Roentgenol* 2010;195:1095–99
16. Pontana F, Duhamel A, Pagniez J, et al. **Chest computed tomography using iterative reconstruction vs filtered back projection. Part 2. Image quality of low-dose CT examinations in 80 patients**. *Eur Radiol* 1011;21:636–43. Epub 2010 Nov 16
17. Sagara Y, Hara AK, Pavlicek W, et al. **Abdominal CT: comparison of low-dose CT with adaptive statistical iterative reconstruction and routine-dose CT with filtered back projection in 53 patients**. *AJR Am J Roentgenol* 2010;195:713–19
18. Silva AC, Lawder HJ, Hara A, et al. **Innovations in CT dose reduction strategy: application of the adaptive statistical iterative reconstruction algorithm.** *AJR Am J Roentgenol* 2010;194:191–99
19. Singh S, Kalra MK, Hsieh J, et al. **Abdominal CT: comparison of adaptive statistical iterative and filtered back projection reconstruction techniques**. *Radiology* 2010;257:373–83. Epub 2010 Sep 9
20. Shrimpton PC, Hillier MC, Lewis MA, et al. **National survey of doses from CT in the UK: 2003.** *Br J Radiol* 2006;79:968–80

21. Singh S, Kalra MK, Gilman MD, et al. **Adaptive statistical iterative reconstruction technique for radiation dose reduction in chest CT: a pilot study**. *Radiology* 2011;259:565–73. Epub 2011 Mar 8
22. Bogartz G, Golding SJ, Jurik AG, et al, for the European Study Group of Radiologists and Physicists. **European Guidelines on Quality Criteria for Computed Tomography.** 1999. http://www.drs.dk/guidelines/ct/quality. Accessed May 15, 2011
23. Jaffe TA, Hoang JK, Yoshizumi TT, et al. **Radiation dose for routine clinical adult brain CT: variability on different scanners at one institution**. *AJR Am J Roentgenol* 2010;195:433–38
24. Tsapaki V, Aldrich JE, Sharma R, et al. **Dose reduction in CT while maintaining diagnostic confidence: diagnostic reference levels at routine head, chest, and abdominal CT: IAEA-coordinated research project.** *Radiology* 2006;240:828–34. Epub 2006 Jul 12

PATIENT SAFETY

# Cranial CT with Adaptive Statistical Iterative Reconstruction: Improved Image Quality with Concomitant Radiation Dose Reduction

O. Rapalino
Shervin Kamalian
Shahmir Kamalian
S. Payabvash
L.C.S. Souza
D. Zhang
J. Mukta
D.V. Sahani
M.H. Lev
S.R. Pomerantz

FELLOWS' JOURNAL CLUB

**BACKGROUND AND PURPOSE:** To safeguard patient health, there is great interest in CT radiation-dose reduction. The purpose of this study was to evaluate the impact of an iterative-reconstruction algorithm, ASIR, on image-quality measures in reduced-dose head CT scans for adult patients.

**MATERIALS AND METHODS:** Using a 64-section scanner, we analyzed 100 reduced-dose adult head CT scans at 6 predefined levels of ASIR blended with FBP reconstruction. These scans were compared with 50 CT scans previously obtained at a higher routine dose without ASIR reconstruction. SNR and CNR were computed from Hounsfield unit measurements of normal GM and WM of brain parenchyma. A blinded qualitative analysis was performed in 10 lower-dose CT datasets compared with higher-dose ones without ASIR. Phantom data analysis was also performed.

**RESULTS:** Lower-dose scans without ASIR had significantly lower mean GM and WM SNR ($P = .003$) and similar GM-WM CNR values compared with higher routine-dose scans. However, at ASIR levels of 20%–40%, there was no statistically significant difference in SNR, and at ASIR levels of ≥60%, the SNR values of the reduced-dose scans were significantly higher ($P < .01$). CNR values were also significantly higher at ASIR levels of ≥40% ($P < .01$). Blinded qualitative review demonstrated significant improvements in perceived image noise, artifacts, and GM-WM differentiation at ASIR levels ≥60% ($P < .01$).

**CONCLUSIONS:** These results demonstrate that the use of ASIR in adult head CT scans reduces image noise and increases low-contrast resolution, while allowing lower radiation doses without affecting spatial resolution.

**ABBREVIATIONS:** ACR = American College of Radiology; ASIR = Adaptive Statistical Iterative Reconstruction; CNR = contrast-to-noise ratio; $CTDI_{vol}$ = volume CT dose index; DLP = dose-length product; ED = effective dose; FBP = filtered back-projection; GM = gray matter; HU = Hounsfield unit; lp = line pair



The use of CT is increasing rapidly at a rate of approximately 10% per year, and >68 million CT studies were performed in the United States during 2008.[1-3] The foremost concern with the increasing use of CT technology is the associated dose of ionizing radiation and the potential risk of cancer development later in life.[1] The situation is even more worrisome in the pediatric population, which is at greater risk than adults from a given dose of radiation.[1] However, dose reduction in CT is hindered by the increased image noise in lower radiation-dose protocols by using the current FBP reconstructions.

CT imaging demands the development of more efficient reconstruction techniques to diminish radiation dose. Iterative reconstruction techniques promise to drastically reduce image noise and artifacts, thereby allowing significant dose reduction. Most of these techniques are computationally intensive and require long reconstruction times. The most comprehensive iterative-reconstruction algorithm models the system optics by taking into account the finite size of the pixel and the focal spot as well as the shape and size of the detector-cell spacing. In addition, it also models the photon statistics in x-ray attenuation. ASIR (GE Healthcare, Chalfont St. Giles, UK) is a modified iterative-reconstruction technique that is time-efficient and already clinically available. It models the photon statistics in x-ray attenuation but does not model the system optics. Thus, it is more computationally complex than FBP but considerably less computationally complex than more comprehensive iterative-reconstruction methods.[3] This technique produces significant noise reduction that potentially improves image quality and allows reduction in radiation dose. High levels of ASIR processing create image texture (smooth appearance) and noise characteristics unfamiliar to radiologists.[3,4] In clinical practice, one can use variably blended images created with FBP and ASIR techniques to produce different levels of ASIR.

The purpose of this study was to evaluate the impact of ASIR on both qualitative and quantitative measures of image quality in reduced-dose head CT scans for adult patients. Our hypothesis was that the use of ASIR decreases CT image noise resulting in increased SNR and CNR ratios as well as improved qualitative scores of contrast resolution without compromising spatial resolution. We evaluated its effect on quantitative and qualitative measures of brain image quality in adult reduced-dose head CT scans at multiple ASIR levels in comparison with regular-dose CT studies.

Received May 9, 2011; accepted after revision June 29.

From the Department of Radiology (O.R., Shervin K., Shahmir K., S.P., L.C.S.S., D.Z., D.V.S., M.H.L., S.R.P.), Massachusetts General Hospital, Boston, Massachusetts; and GE Healthcare (J.M.), CT Research, Boston, Massachusetts.

Otto Rapalino and Shervin Kamalian contributed equally to this work.

Please address correspondence to Otto Rapalino, MD, Massachusetts General Hospital, Department of Radiology-GRB 273, Boston, MA, 02114-9657; e-mail: orapalino@partners.org

http://dx.doi.org/10.3174/ajnr.A2826

## Materials and Methods

### *Patient Selection*

Institutional review board approval was obtained for this retrospective analysis of CT datasets, and Health Insurance Portability and Accountability Act–compliant practices were used during this study. We selected 100 consecutive non-contrast reduced-dose adult head CT studies performed during April and May 2009 for all indications by using a 64-section Discovery CT750HD CT scanner (GE Healthcare) with ASIR reconstruction capability. These were compared with 50 consecutive regular-dose adult head CT scans obtained on the same scanner during March 2009 before the availability of ASIR. A total of 150 CT scans were obtained from 140 patients. Ten patients had scans with reduced- and regular-dose techniques.

### *Image Acquisition*

One hundred scans obtained on the ASIR-capable scanner were acquired by using a reduced-dose protocol. Imaging parameters for these studies were as follows: 120 kV, fixed tube current of 200 mA (140 mAs), pitch of 0.531:1, table speed of 10.62, gantry rotation speed of 0.7 seconds, $CTDI_{vol}$ of 49.7 mGy (reported on the scanner console), FOV of 22 cm, and matrix of 512 × 512. The scanning raw data were used for FBP (standard kernel) reconstruction, which was blended with varying degrees of the ASIR algorithm (0%, 20%, 40%, 60%, 80%, and 100%). This blending is a linear combination of FBP and ASIR images, depending on the percentage of ASIR chosen (eg, 30% ASIR would be a blend of 30% ASIR and 70% FBP images). The 50 head CTs performed on the same scanner before ASIR availability were performed at a relatively higher radiation dose in keeping with our routine clinical protocols with imaging parameters as follows: 120 kV, fixed tube current of 250 mA (175 mAs), pitch of 0.531:1, table speed of 10.62, gantry rotation speed of 0. 7 seconds, $CTDI_{vol}$ of 66.51 mGy, FOV of 22 cm, and matrix of 512 × 512 with a standard FBP kernel. Images were reconstructed as 5-mm-thick contiguous sections.

### *CT Radiation-Dose Calculation*

The $CTDI_{vol}$ of a single CT section of both protocols (low and higher routine doses) was reported on the basis of scanner output (dose report), which is a fixed number when a fixed tube current is used in the protocol. The average DLP, calculated as the $CTDI_{vol}$ multiplied by the scan length (section thickness × number of sections) in centimeters was also reported. The ED DLP can be estimated from the DLP, which is reported on most CT systems: ED (mSv) = k × DLP. The conversion factor (k) for adult head is 0.0021.[5]

### *Phantom Study*

A phantom study was performed independently from the assessment of clinical CT scans. The effect of ASIR on image noise, low contrast resolution, and high contrast resolution was evaluated by using an ACR CT phantom following recommended guidelines.[6,7] Phantom raw data were acquired by using FBP reconstruction (with a standard kernel) blended with varying degrees of ASIR algorithm (0%–100%, 10 blending levels) by using reduced-dose and higher routine radiation dose CT protocols. CNR was assessed quantitatively following ACR guidelines.[6,7] CNR measurements were compared between the reduced-dose and routine higher-dose protocols and among different ASIR levels. We also qualitatively assessed high contrast resolution comparing the identification of high-resolution bar patterns between the reduced-dose and routine higher radiation dose groups and with different levels of ASIR. This blinded assessment was performed by 2 experienced neuroradiologists (M.H.L. and S.R.P.).

**Table 1: Evaluation parameters and 5-point grading system**

<table>
<tr><th>Score</th><th>Image Noise</th><th>Scatter-Related Artifacts</th><th>GM-WM Differentiation</th><th>Visibility of Small Structures</th><th>Image Sharpness</th></tr>
<tr><td>1</td><td colspan="2">Unacceptable</td><td colspan="3">Very poor</td></tr>
<tr><td>2</td><td colspan="2">Above average</td><td colspan="3">Suboptimal</td></tr>
<tr><td>3</td><td colspan="2">Average</td><td colspan="3">Acceptable</td></tr>
<tr><td>4</td><td colspan="2">Less than average</td><td colspan="3">Above average</td></tr>
<tr><td>5</td><td colspan="2">Minimal</td><td colspan="3">Excellent</td></tr>
</table>

### *Clinical CT Dataset Analysis*

CT attenuation measurements were acquired by using circular ROIs placed in normal deep GM (lentiform nucleus) and adjacent normal WM structures (internal capsule) by using soft-tissue algorithm brain images. ROIs were slightly adjusted to fit the measured anatomic structure to avoid volume-averaging artifacts. SNR, defined as mean attenuation (in Hounsfield units) divided by the SD[8] was calculated for each ROI. We calculated CNR, defined as the difference in mean attenuation for 2 regions divided by the square root of the sum of their variance,[8] comparing GM with adjacent WM (GM-WM CNR). The ratio of the intensity of a signal to the intensity of the noise (SNR) indicates the quality of the signal intensity within an anatomic region, and CNR indicates the capability of differentiating tissues of different electron attenuation in relation to the background noise.

The qualitative analysis was performed in 10 cases that had head CT studies by using both reduced- and regular-dose techniques.

Anonymized image datasets were created at 0%, 30%, 60%, and 100% ASIR levels. The blinded qualitative visual analysis of these datasets was performed by 2 experienced board-certified neuroradiologists (O.R. and S.R.P). The reviewers were blinded to the radiation dose and reconstruction algorithm. Evaluation parameters and the 5-point grading system are summarized in Table 1.

### *Statistical Analysis*

ANOVA was used to determine statistical significance among the reduced-dose subgroups at each ASIR level and for determination of the statistical significance of differences in SNR and CNR measurements between the routine higher-dose non-ASIR datasets and the reduced-dose datasets at each ASIR level. A nonparametric Kruskal-Wallis test was used to determine statistical significance for the qualitative analysis data (Table 2).

All values were expressed as means ± standard error of the mean. STATA software Version 10.0 (StataCorp, College Station, Texas) was used for statistical analysis.

## Results

### *Patient Demographics*

A total of 150 adult patients were included; 100 were scanned by using a reduced-dose head CT protocol (mean age, 64 ± 1.69 years; range, 21–93 years; 39 men, 61 women), and 50

**Table 2: Summary of image-reconstruction subgroups and statistical analysis**

| Clinical CT Datasets | | Statistical Analysis for GM-SNR, WM-SNR, and GM-WM CNR | |
|---|---|---|---|
| Protocol | Image Reconstruction | | |
| Routine dose ($n = 50$) | 100% FBP | Control group | |
| Reduced dose ($n = 100$) | 100% FBP<br>80% FBP + 20% ASIR<br>60% FBP + 40% ASIR<br>40% FBP + 60% ASIR<br>20% FBP + 80% ASIR<br>100% ASIR | Repeated-measures ANOVA | Dunnett multiple comparison test |

**Table 3: Acquisition parameters of routine and lower-dose CT groups**

| Radiation Dose | Reconstruction Technique | $CTDI_{vol}$ (mGy)[a] | DLP (mGy.cm) | Effective Dose (mSv) |
|---|---|---|---|---|
| Regular dose (175 mAs) | 100% FBP | 66.51 | 1270.34 ± 24.46 | 2.66 ± 0.05 |
| Lower dose (140 mAs) | 100% FBP<br>20% ASIR + 80% FBP<br>40% ASIR + 60% FBP<br>60% ASIR + 40% FBP<br>80% ASIR + 20% FBP<br>100% ASIR | 49.7 | 932.25 ± 11.46 | 1.95 ± 0.02 |

[a] Clinical scans were below the recommended ACR levels ($CTDI_{vol}$) of 75 mGy.[20]

**Table 4: Statistical differences (*P* values) between the regular- and lower-dose CT groups**

| | | Quantitative Measurements (*P* values) | | |
|---|---|---|---|---|
| Radiation Dose | Reconstruction Technique | GM-SNR | WM-SNR | GM-WM CNR |
| Regular (175 mAs) | 100% FBP | | Control group | |
| Lower-Dose (140 mAs) | 100% FBP | .003[a] | .003[a] | .4 |
| | 20% ASIR + 80% FBP | .649 | .541 | 1 |
| | 40% ASIR + 60% FBP | .302 | .668 | .03[a] |
| | 60% ASIR + 40% FBP | <.0001[a] | <.0001[a] | <.0001[a] |
| | 80% ASIR + 20% FBP | <.0001[a] | <.0001[a] | <.0001[a] |
| | 100% ASIR | <.0001[a] | <.0001[a] | <.0001[a] |

[a] Statistical significance between the lower-dose (with different ASIR/FBP levels) and regular-dose groups.

patients underwent routine higher-dose head CT scans as a part of their clinical evaluation (mean age, 65 ± 2.49 years; range, 23–89 years; 21 men, 29 women).

There was no significant difference in mean age (unpaired *t* test, $P = .35$) between the groups.

### *CT Radiation Dose*

The $CTDI_{vol}$ of a single CT section at 140 mAs (reduced-dose group: fixed tube current of 200 mA at 0.7 s/rotation) and 175 mAs (routine higher-dose group: fixed tube current of 250 mA at 0.7 s/rotation) was 49.07 and 66.51 mGy, respectively. The average DLP and the ED at 140 mAs (reduced-dose protocol) were 932.25 ± 11.46 mGy.cm and 1.95 ± 0.02 mSv; the same values at 175 mAs (routine higher-dose protocol) were 1270.34 ± 24.46 mGy.cm and 2.66 ± 0.05 mSv, respectively (Tables 3 and 4). The total dose in the reduced-dose group was approximately 26.2% lower compared with the routine higher-dose protocol (based on $CTDI_{vol}$).

### *Phantom Results*

Noise measurements showed a gradual decrease in image noise with higher ASIR levels with both protocols (reduced-dose and higher routine radiation dose protocols) (Fig 1*A*). Noise measurements at a 30%–40% ASIR level with the reduced-dose technique were comparable with the higher routine radiation dose protocol without ASIR (Fig 1*A*). CNR progressively increased with higher ASIR levels in both the reduced-dose and higher routine-dose groups. CNR values were comparable between reduced-dose scans at 20%–30% ASIR and routine higher-dose scans without ASIR. Reduced-dose scans with >30% ASIR levels resulted in higher CNR in comparison with routine higher-dose scans without ASIR (Fig 1*B*). For the assessment of high-contrast resolution, ≤7 lp/cm bar patterns were resolved (higher than the required 5 lp/cm bar pattern based on ACR CT phantom guidelines). There were no differences in the identification of these high-contrast-resolution bar patterns between the reduced-dose (with different levels of ASIR blending) and higher routine-dose groups (Fig 2).

### *Clinical CT Dataset Analysis*

**Quantitative Assessment.** The mean ROI area for GM and WM was 38.85 ± 1.25 $mm^2$. The mean GM and WM attenuation values for the reduced-dose group (140 mAs) were 34.5 and 24.2 HU, respectively, and for the routine higher-dose group (175 mAs), they were 35.5 and 25.6 HU, respectively.

There was a significant increase in GM and WM SNR with increasing ASIR levels in the reduced-dose subgroups ($P <$ .01, repeated-measures ANOVA) (Fig 3). GM-SNR and WM-SNR increased from 6.61 ± 0.11 and 5.06 ± 0.11, respectively, in the reduced-dose without ASIR subgroup to 16.87 ± 0.52 and 11.81 ± 0.39 in the reduced-dose with 100% ASIR sub-

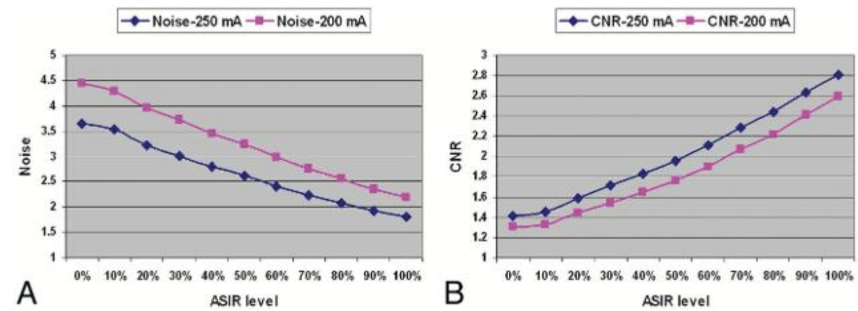


**Fig 1.** ACR phantom quantitative study.[7] *A*, Noise-level comparison between lower-dose and routine higher-dose protocols at different ASIR levels. Lower dose (200 mA) images at an ASIR level of 30% have image noise comparable with that of routine higher-dose (250 mA) scans without ASIR. *B*, CNR analysis. Lower-dose scans at an ASIR level of 20% have CNR comparable with that of routine higher-dose scans without ASIR.

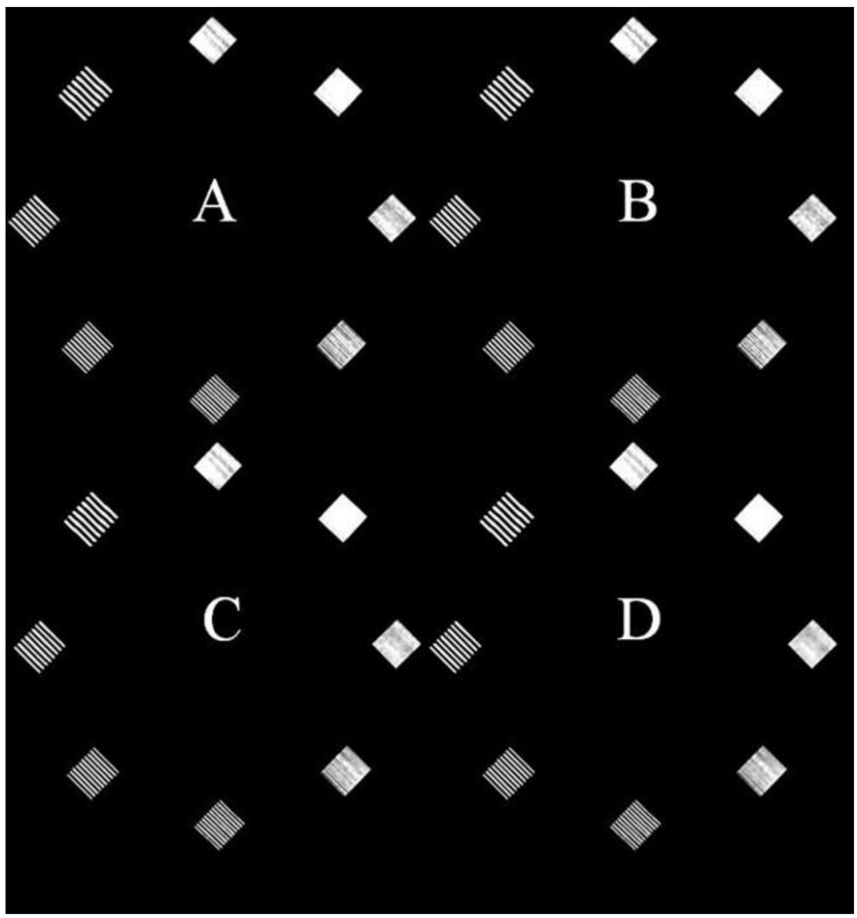


**Fig 2.** High-contrast-resolution assessment by using the ACR phantom.[7] CT images obtained at a regular dose without ASIR (*A*), at a lower dose without ASIR (*B*), and at a lower dose with 60% (*C*) and 100% (*D*) of ASIR blending demonstrate the effect of different ASIR levels and the lower-dose technique in comparison with the regular-dose technique on high-contrast-resolution bar patterns. There are no apparent differences in the ability to discriminate individual bar patterns between these techniques.

group ($P < .0001$) (Fig 3). Mean GM-SNR and WM-SNR in adult head CTs at 175 mAs (higher-dose) were $7.94 \pm 0.20$ and $6.22 \pm 0.14$, respectively, which were not significantly different from the mean GM-SNR and WM-SNR of scans acquired at 140 mAs (reduced-dose) with ASIR level of 20% and 40% (ANOVA, Dunnett multiple comparison test). The SNR values in the routine higher-dose group were significantly lower compared with reduced-dose scans with ≥60% ASIR blending (all $P < .0001$) and significantly higher when ASIR was not applied in the reduced-dose group (all $P = .003$) (Tables 3 and 4).

There was a progressive increase in GM-WM CNR with increasing ASIR levels in lower-dose subgroups ($P < .0001$, repeated measures ANOVA). GM-WM CNR increased from $1.48 \pm 0.04$ in the reduced-dose subgroup with 0% ASIR to $3.42 \pm 0.10$ at 100% ASIR. Mean CNR between GM and WM for routine higher-dose head CT studies was $1.61 \pm 0.05$, which was not significantly different from the values in the reduced-dose CT subgroups with ASIR levels of 0% and 20%, but it was significantly lower in comparison with the reduced-dose subgroups with ASIR levels of ≥40% (all $P < .0001$) (Fig 3).

**Qualitative Assessment.** There was a significant decrease in image noise and scatter-related artifacts when applying 60%

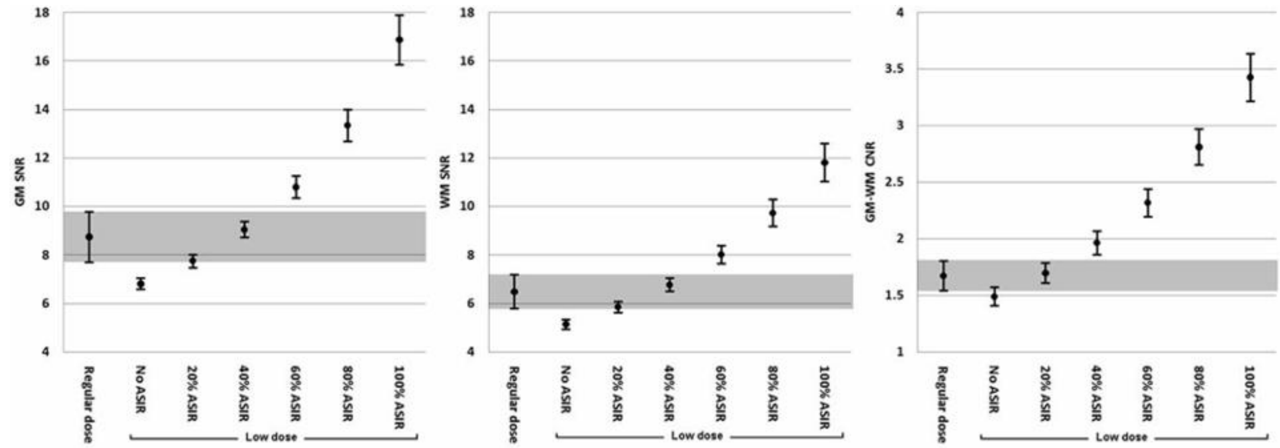


**Fig 3.** Comparison of average SNR and CNR values between regular- and lower-dose (with variable ASIR) groups. GM-SNR (left), WM-SNR (middle), and GM-WM CNR (right) measurements are plotted in the y-axis. The x-axis depicts the regular-dose group (without ASIR) and different lower-dose subgroups with increasing ASIR levels (0%–100%). Shaded areas demonstrate equivalent average SNR and CNR values between the regular- and lower-dose groups.

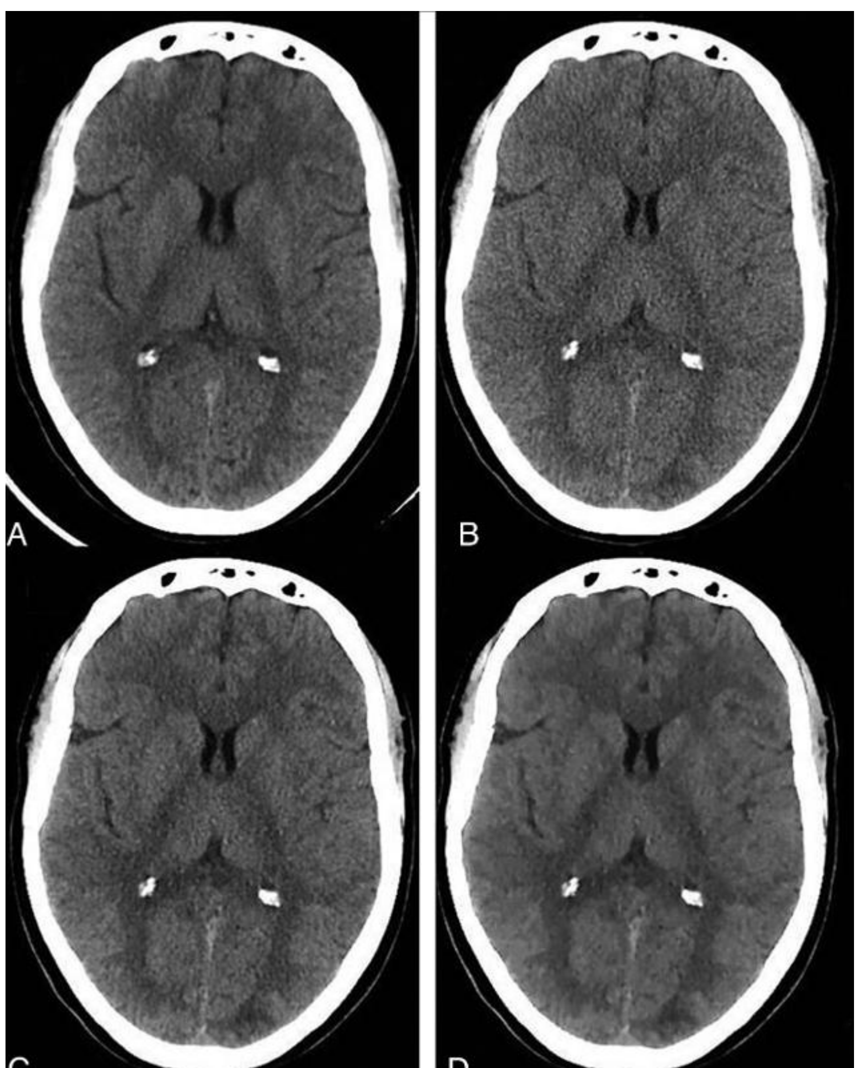


**Fig 4.** Examples of nonenhanced head CT images of an adult patient obtained at a regular dose without ASIR (*A*), a lower dose without ASIR (*B*), and a lower dose with 60% (*C*) and 100% (*D*) of ASIR.

**Table 5: Qualitative assessment of regular-dose and reduced-dose clinical CT datasets with variable ASIR blending using the 5-point grading system**

| Radiation Dose | Reconstruction Technique | Noise | Scatter-Related Artifacts | GM-WM Differentiation | Visibility of Small Structures | Image Sharpness |
|---|---|---|---|---|---|---|
| Regular dose (175 mAs) | 100% FBP | 2.80 ± 0.09 | 2.70 ± 0.10 | 2.82 ± 0.12[a] | 2.85 ± 0.08 | 3.00 ± 0.26 |
| Lower dose (140 mAs) | 100% FBP | 2.10 ± 0.06[a] | 2.85 ± 0.10 | 2.09 ± 0.11 | 2.82 ± 0.09 | 3.09 ± 0.25 |
| | 30% ASIR + 70% FBP | 2.90 ± 0.10 | 3.00 ± 0.07 | 2.90 ± 0.11 | 3.00 ± 0.00 | 3.19 ± 0.24 |
| | 60% ASIR + 40% FBP | 3.70 ± 0.12[a] | 3.55 ± 0.11[a] | 3.61 ± 0.12[a] | 3.05 ± 0.05 | 3.28 ± 0.30 |
| | 100% ASIR | 4.25 ± 0.12[a] | 3.70 ± 0.14[a] | 4.00 ± 0.15[a] | 3.00 ± 0.12 | 3.00 ± 0.39 |

[a] Qualitative assessment: mean scores ± standard error.

and 100% ASIR in the lower-dose group in comparison with the regular- and lower-dose groups without ASIR ($P < .0001$). A statistically significant increase in GM-WM differentiation was noted when using ASIR levels of 60% and 100% in the lower-dose group in comparison with the regular dose and lower-dose groups without ASIR ($P < .0001$) (Fig 4). The image-quality indices in the routine higher-dose group (175 mAs) were not significantly different from similar indices from scans acquired at 140 mAs (reduced-dose group) with an ASIR level of 30%.

Regarding the visibility of small anatomic structures and image sharpness, there was no statistically significant difference between the lower- (independent of ASIR level) and regular-dose groups (Table 5).

## Discussion

Iterative methods for reconstruction of CT data are not new, and algebraic iterative-reconstruction algorithms were actually used in the first CT scanners.[3,9,10] Mainly due to high computational requirements (approximately 100-1000 times in comparison with FBP algorithms),[3] the iterative-reconstruction algorithms were displaced after a few years by the now widely available FBP methods. However, iterative-reconstruction algorithms are very accurate and perform better than the FBP methods in many cases,[11-14] particularly when dealing with a small number of projections or noisy datasets.[12,15] Iterative reconstruction algorithms have been used more commonly in SPECT and PET imaging.[3]

Recently, iterative-reconstruction algorithms have become increasingly used in CT imaging due to continuous improvements in computer hardware and software. The use of iterative-reconstruction methods appears to result in significant improvements in overall image quality and noise reduction.[4,9,12-19] Our results demonstrate that the use of ASIR improves measurements of SNR and CNR of GM and WM brain structures in reduced-dose head CT scans for adult patients. This effect appears to be related to the noise reduction produced by this type of iterative-reconstruction algorithm.[9,12-19] These results were obtained with a commercially available CT scanner with acquisition and postprocessing times similar to those of routine FBP reconstructions on comparable multisection scanners.

The progressive decrease of quantum noise with CT images acquired at progressively higher levels of ASIR blends results in a more uniform appearance.[12,15] Consequently, radiologists may perceive these images as overly smooth or "painted," with concern that critical findings or fine anatomic features may be obscured.[4] These perceptions make the switch from FBP to ASIR processing more difficult to accept. Based on our study of adult clinical CT and phantom datasets, there was no apparent compromise of high- and low-contrast resolution with increasing ASIR levels by using a lower-dose technique in comparison with regular-dose datasets (Fig 2).

Additional studies will be helpful for evaluation of the potential effect of this type of iterative-reconstruction algorithm on diagnostic performance, particularly at very high ASIR levels, and for definition of an "optimal" level of ASIR effect, particularly with different section thicknesses. Our findings demonstrate that the use of ASIR levels of 20%–40% on reduced-dose scans (26.2% of dose reduction) by using 5-mm thick images results in quantitative and qualitative indices of image quality comparable with regular-dose scans, and ASIR levels of >40% on reduced-dose scans with similar section thickness result in significant improvement of image-quality indices and noise reduction in comparison with regular-dose scans reconstructed with FBP algorithms.[9,12-19] CT images with moderate ASIR levels (eg, 60%) will show the expected benefits of decreased image noise and increased contrast resolution while allowing a lower radiation dose without experiencing the more pronounced smoothing effect seen with higher ASIR levels. Recent studies by using iterative-reconstruction methods (including ASIR) in different anatomic locations have shown similar results with noise reduction and improved image quality at lower radiation levels without compromising diagnostic accuracy.[3,9,12-19]

One of the limitations of this study is that the reduced-dose and higher routine-dose clinical CT scans were not obtained at the same scanning session due to the fact that these studies were for diagnostic purposes. However, the scans were acquired by using very similar techniques (with the exception of the radiation dose). Another limitation was evident during the qualitative assessment: The readers reviewing the imaging datasets were blinded to the radiation dose and degree of ASIR blending of the CT datasets. However, high ASIR levels have an expected smoothing effect on the appearance of CT images, limiting the blinded status of the readers.

## Conclusions

ASIR can produce significant improvements in different qualitative and quantitative aspects of image quality in adult head CT studies, while, at the same time, allowing a significant reduction in radiation exposure.

Disclosures: Joshi Mukta—*UNRELATED*: *Employment*: GE Healthcare. Dushyant Sahani—*RELATED*: *Grant*: GE Healthcare;* *UNRELATED*: *Payment for Manuscript Preparation*: Bracco Diagnostics; *Royalties*: Elsevier. Michael Lev—*RELATED*: GE Healthcare,* Comments: research support (software, hardware), Research Assistant support; *Consulting Fee or Honorarium*: GE Healthcare, Millennium Pharmaceuticals, CoAxia, Comments: consultant.

Stuart Pomerantz—*RELATED*: *Grant:* GE Healthcare,* Comments: for research assistant support. **Money paid to institution.*

## References


1. Brenner DJ, Hall EJ. **Computed tomography: an increasing source of radiation exposure.** *N Engl J Med* 2007;357:2277–84
2. Boland GW, Guimaraes AS, Mueller PR. **The radiologist's conundrum: benefits and costs of increasing CT capacity and utilization.** *Eur Radiol* 2009;19:9–11, discussion 12
3. Xu J, Mahesh M, Tsui BM. **Is iterative reconstruction ready for MDCT?** *J Am Coll Radiol* 2009;6:274–76
4. Silva AC, Lawder HJ, Hara A, et al. **Innovations in CT dose reduction strategy: application of the adaptive statistical iterative reconstruction algorithm.** *AJR Am J Roentgenol* 2010;194:191–99
5. McCollough C, Cody D, Edyvean S, et al. *The Measurement, Reporting, and Management of Radiation Dose in CT: AAPM Report No. 96.* College Park, Maryland: American Association of Physicists in Medicine; 2008
6. McCollough CH, Bruesewitz MR, McNitt-Gray MF, et al. **The phantom portion of the American College of Radiology (ACR) computed tomography (CT) accreditation program: practical tips, artifact examples, and pitfalls to avoid.** *Med Phys* 2004;31:2423–42
7. ACR. CT Accreditation Phantom Instruction. 2011. http://www.acr.org/accreditation/computed/qc_forms/Phantom_Testing_Instruction_Final.aspx. 10-10-11 version. Accessed 10 October 2011
8. Mullins ME, Lev MH, Bove P, et al. **Comparison of image quality between conventional and low-dose nonenhanced head CT.** *AJNR Am J Neuroradiol* 2004;25:533–38
9. Wang G, Yu H, De Man B. **An outlook on x-ray CT research and development.** *Med Phys* 2008;35:1051–64
10. Gordon R, Bender R, Herman GT. **Algebraic reconstruction techniques (ART) for three-dimensional electron microscopy and x-ray photography.** *J Theor Biol* 1970;29:471–81
11. Rogalla P, Kloeters C, Hein PA. **CT technology overview: 64-slice and beyond.** *Radiol Clin North Am* 2009;47:1–11
12. Wang G, Snyder DL, O'Sullivan JA, et al. **Iterative deblurring for CT metal artifact reduction.** *IEEE Trans Med Imaging* 1996;15:657–64
13. Nuyts J, De Man B, Dupont P, et al. **Iterative reconstruction for helical CT: a simulation study.** *Phys Med Biol* 1998;43:729–37
14. Ziegler A, Kohler T, Proksa R. **Noise and resolution in images reconstructed with FBP and OSC algorithms for CT.** *Med Phys* 2007;34:585–98
15. McCollough CH, Primak AN, Braun N, et al. **Strategies for reducing radiation dose in CT.** *Radiol Clin North Am* 2009;47:27–40
16. Prakash P, Kalra MK, Kambadakone AK, et al. **Reducing abdominal CT radiation dose with adaptive statistical iterative reconstruction technique.** *Invest Radiol* 2010;45:202–10
17. Prakash P, Kalra MK, Digumarthy SR, et al. **Radiation dose reduction with chest computed tomography using adaptive statistical iterative reconstruction technique: initial experience.** *J Comput Assist Tomogr* 2010;34:40–45
18. Marin D, Nelson RC, Schindera ST, et al. **Low-tube-voltage, high-tube-current multidetector abdominal CT: improved image quality and decreased radiation dose with adaptive statistical iterative reconstruction algorithm—initial clinical experience.** *Radiology* 2010;254:145–53
19. Singh S, Kalra MK, Gilman MD, et al. **Adaptive statistical iterative reconstruction technique for radiation dose reduction in chest CT: a pilot study.** *Radiology* 2010;259:565–73
20. ACR. ACR Practice Guideline For Diagnostic Reference Levels in Medical X-Ray Imaging. 2008. http://www.acr.org/SecondaryMainMenuCategories/quality_safety/RadSafety/RadiationSafety/guideline-diagnostic-reference.aspx. Accessed October 1, 2008

JOURNAL OF APPLIED CLINICAL MEDICAL PHYSICS, VOLUME 16, NUMBER 3, 2015

# Effect of radiation dose reduction on image quality in adult head CT with noise-suppressing reconstruction system with a 256 slice MDCT

Ozdil Baskan,[1a] Cengiz Erol,[1] Hanefi Ozbek,[2] Yahya Paksoy[1]
*Department of Radiology,[1] Istanbul Medipol University School of Medicine, Istanbul, Turkey; Istanbul Medipol University School of Medicine,[2] Istanbul, Turkey*
*ozdil.baskan@yahoo.com*

Received 26 September, 2014; accepted 21 January, 2015

The purpose of our study was to investigate the effect of iterative reconstruction (IR) as a dose reduction system on the image quality (IQ) of the adult head computed tomography (CT) at various low-dose levels, and to identify ways of setting the amount of dose reduction. We performed two noncontrast low-dose (LD) adult head CT protocols modified by lowering the tube current with IR which were decided in the light of a group of phantom studies. Two groups of patients, each 100 underwent noncontrast head CT with LD-I and LD-II, respectively. These groups were compared with 100 consecutive standard dose (STD) adult head CT protocol in terms of quantitative and qualitative IQ. The signal-to-noise ratio (SNR) of the white matter (WM) and gray matter (GM) and contrast-to-noise ratio (CNR) values in the LD groups were higher than the STD group. The differences were statistically significant. When the STD and the LD groups were compared qualitatively, no significant differences were found in overall quality. By selecting the appropriate level of IR 34%, radiation dose reduction in adult head CT can be achieved without compromising IQ.

PACS number: 87.57.-s

Key words: image quality, dose reduction, reconstruction methods, phantom studies, MDCT

## I. INTRODUCTION

Following its introduction by Godfrey Hounsfield in 1972,(1,2) CT has become an important method in medical diagnosis.(3) The development of spiral CT — and thereafter multidetector CT (MDCT) — in the past few years has allowed a shorter examination time and thinner sections. CT use for diagnostic evaluation has increased dramatically all over the world.(4-7) The total number of CT examinations performed annually in the US has risen from 3.3 million in 1980–82 to 68.7 million in 2007.(4,8) As head CT has evolved as the technique of choice to assess traumatic and nontraumatic neurological conditions, its use has become particularly frequent.(9) In the US, 19 million head CTs were performed (i.e., 28.4% of all CT procedures) in 2007.(4)

The most important problem with the increasing use of CT is the associated dose of ionizing radiation and the potential risk of cancer development later in life.(7,10-13) To date, attention has focused on risks from pediatric CT scans. However, Berrington de González et al.(13) estimate that, in terms of absolute numbers, the potential public health impact of current use patterns is highest for adults aged 35 to 54 years because of the high frequency of use. It is important

[a] Corresponding author: Ozdil Baskan, Istanbul Medipol University School of Medicine, TEM Goztepe Cikisi No: 1 Bagcılar 34214, Istanbul, Turkey; phone: (+90) 212 460 7070; fax: (+90) 212 460 7777; email: ozdil.baskan@yahoo.com

for the radiologist to be sure that CT examination is required for the patient and that all efforts are made for reducing the radiation dose. Radiologists should have a control mechanism while reducing the dose in order not to sacrifice the image quality (IQ).

For that reason, many dose methods to reduce radiation exposure during CT examinations have been developed.[14-16] Radiation dose reduction can be obtained by reducing tube potential (kVp) or current (mAs), resulting in increased image noise and decreased IQ.[14,17] With increasing computational power, a reconstruction method, statistical iterative reconstruction (IR), has become an alternative in overcoming these concerns while reducing radiation exposure.[18] iDose$^4$ (Phillips Healthcare, Best, the Netherlands) is one of the IR techniques can be used effectively, that was investigated in previous papers.[19,20]

In this article, we study the effect of the radiation dose reduction on IQ in adult head CT with IR technique (iDose$^4$) using a 256 slice MDCT. Because IQ decreases with the radiation dose, careful choice of the appropriate IR level is necessary. We try to describe a roadmap, while reducing the radiation dose, in order to achieve an optimal balance between image noise and quality, and compared our findings with the previous studies.

## II. MATERIALS AND METHODS

When we decided on the application of the IR in our department, we performed two noncontrast low-dose (LD) adult head CT protocols with IR which were constituted in the light of a group of phantom studies. The local institutional review board approved this study. Because vendor experience and our prior phantom studies suggest preservation of diagnostic image quality at all dose levels used in our study, informed consent of patients was waived and all examinations were performed as standard of care.

All phantom and patient CT examinations were performed by using a 256 slice MDCT scanner (Brilliance iCT, Phillips Healthcare).

### A. Phantom studies

A female adult anthropomorphic phantom (model 702-D; CIRS, Norfolk, VA), which contains tissue-equivalent epoxy resins in all aspects of the phantom (the manufacturer supplied information, model 702-D; CIRS) was used.

The STD head CT protocol that is recommended by the vendor was the beginning point. The scan parameters are shown in Table 1. Subsequently, phantom scanning was repeated by reducing the mAs by 30 mAs, while all other scan parameters remained constant (300, 270, 240, 210, 180, 150). Each scan was reconstructed by the filtered backprojection (FBP) algorithm and five levels of the IR technique (iDose$^4$ 1–5) that were predefined by the vendor. A total of 36 scans were analyzed. The noise (in SD) of each study was evaluated while 1 cm$^2$ region of interest (ROI) was drawn in the same place (Fig. 1). According to our experience, multiple ROI measurements will lead to the more accurate conclusion. In this study, all (phantom and patient) ROI measurements were done in three consecutive slices and their average value was used. Additionally, we repeated the same protocol and method with 100 kV and 140 kV in order to check the reliability.

Table 1. The STD head CT protocol's scan parameters recommended by the vendor.

| | |
|---|---|
| tube voltage | 120-kVp |
| tube current | 300 mAs |
| pitch | 0.391 |
| Gantry rotation time | 0.5 s |
| slice thickness and reconstruction interval | 5 mm |
| detector collimation | 64×0.625 |
| field-of-view | 25 cm |

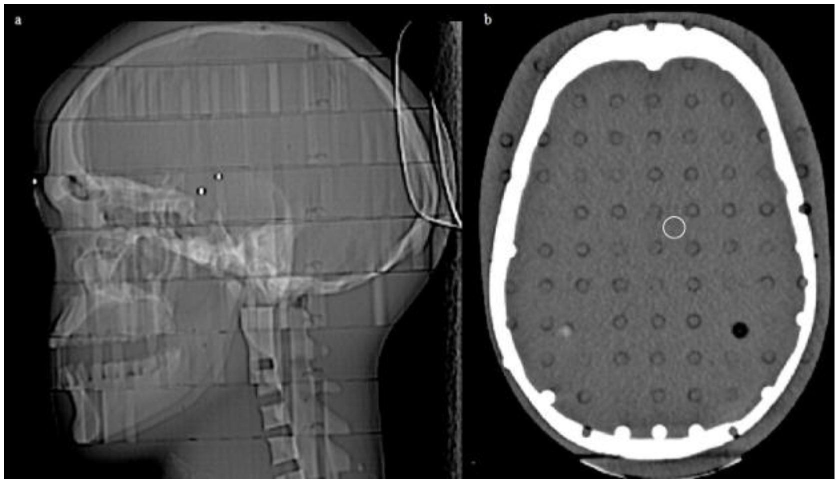


Fig. 1. CIRS phantom: (a) lateral scout; (b) the axial slice scanned at 300 mAs, demonstrating region-of-interest placement.

As a result of the noise information acquired through the anthropomorphic phantom measurements, Catphan 504 phantom (Phantom Laboratory, Salem, NY) was scanned with a STD and two LD head CT protocols. CT parameters were: STD protocol (as defined before) with mAs 300 and FBP reconstruction, LD-I head CT protocol 250 mAs with iDose$^4$2, LD-II head CT protocol 200 mAs with iDose$^4$3. All scanning parameters were identical, except mAs. These protocols were compared by using the four modules of the Catphan phantom for objective IQ before the patient applications.

The effect of dose and IR (iDose$^4$) on image noise, SNR, CNR, uniformity, low-contrast resolution, and high-contrast resolution were evaluated. The methods and formulas were based on the literature[21-23] and the information supplied by the manufacturer (Catphan 504 Manual, The Phantom Laboratory).

To measure the image noise, SNR and CNR linearity module (CTP 404) was used. Image noise was defined as SD of the 10 mm diameter ROI located in background at the center of the module.

SNR was determined by dividing the mean Hounsfield units (HU) value by the SD of the same ROIs.

$$SNR = Mean\ HU\ of\ the\ ROI/SD\ of\ the\ ROI \tag{1}$$

CNR was determined by dividing the difference between the mean value obtained from the ROI in one of the round objects (acrylic) within the phantom and the mean value of the background by the SD of the background.

$$CNR = Mean\ HU\ of\ the\ acrylic\text{-}Mean\ HU\ of\ background/(SD\ of\ the\ background) \tag{2}$$

The CT number ($CT_n$) uniformity according to the location, edge, and center, was determined by using the image uniformity module (CTP 486). We measured the $CT_n$ (in HU) from the center of the module and at 3, 6, 9 and 12 o'clock locations of the module. All $CT_n$ for all five ROIs must be within ± 5 HU of the center ROI mean value.

The low-contrast module (CTP 515) was used for contrast detail evaluation. This module is made of several sets of cylindrical low contrast objects. We chose the 1.0% contrast level to determine whether the contrast detail changed visually and numerically. We evaluated the number and the diameter of the objects that are visible.

For the assessment of high-contrast resolution, the high resolution module (CTP 528) was used.[19] The high-resolution bar patterns and the corresponding line pairs/cm (lp/cm$^{-1}$) were evaluated and the scans were compared.

## B. Patient groups

The first 100 patients underwent noncontrast LD-I head CT protocol and the second 100 patients underwent LD-II head CT protocol between October and December 2013. These groups were compared with 100 consecutive STD head CT protocol that we used before the application of the IR in our department during August to September 2013. No limitations were used for the indications. The CT scans (totally 18) with motion artifacts were excluded from the study.

## C. Radiation dose

The $CTDI_{vol}$ and DLP were obtained at the end of each scan from the dose information page of the scanner. ED in mSv was calculated by multiplying DLP (mGy*cm) with a constant adult head specific conversion factor (κ) 0.0021 mSv/ (mGy*cm).[24]

## D. CT data analysis

Head measurements were done for every patient from the CT images. We looked for the homogeneity between the patient groups. Anatomic landmarks were chosen. The distance between glabella and opisthocranion (GOD) and biparietal diameter (BPD) was measured.

## E. Quantitative image analysis

One radiologist who was not involved in the qualitative IQ analysis made quantitative measurements on CT images.

Image noise measurement was made by recording the SD of the circular ROI in the air, cerebrospinal fluid (CSF), bone, WM, and GM. SD and $CT_n$ were obtained for all series in all groups. The size, shape, and position of the ROIs were kept constant among the image sets for comparison by applying a copy and paste function at the workstation (Brilliance Workspace, Philips Healthcare). The ROIs of 1 cm$^2$ in-air were placed at the level of frontal sinus 1 cm away from the bone. The ROIs (15–20 mm$^2$) of CSF were drawn in the lateral ventricle corpus or the frontal horn. The ROIs (50–60 mm$^2$) for WM were placed in the frontal lobe and GM was placed in the thalamus. The ROIs (25–30 mm$^2$) for bone were placed in the clivus.

The SNR of the images were calculated for the WM and GM which were drawn in the frontal lobe and thalamus, respectively. SNR: $CT_n$/SD.

In order to calculate the CNR, four ROIs with 4 mm$^2$ measurements in the GM and WM at the level of centrum semiovale of three consecutive slices were detected and get the averages of the $CT_n$ and SD values. The calculations were made by the following equation, as defined in the literature previously.[25-27]

$$CNR: (mean\ GM\ HU\text{-}mean\ WM\ HU)/\ [(SD\ GM)^2 + (SD\ WM)^2]^{1/2} \tag{3}$$

## F. Qualitative image analysis

All datasets were randomized and reviewed on the workstation (Brilliance Workspace, Philips Healthcare) for assessment of qualitative analysis. Two radiologists with more than 10 years of experience assessed all image datasets independently. They were blinded to the whole scan parameters. Images were graded for subjective noise, artifacts, and descriptiveness of the posterior fossa contents, GM–WM differentiation, and overall image quality on a five-point Likert scale (1 worst to 5 best). For grading the descriptiveness of posterior fossa contents: visualization of the brain stem structures, contours of the basal cisterns and ventricular system, and cerebellar folia were evaluated. WM and GM differentiation: visualization and differentiation of the basal ganglia and the cortex were graded. We thought that these parameters reflect the lesion detectability of the images. Grades for image quality were averaged across both readers for further analysis.

### G. Statistical analysis

For the statistical analysis of the quantitative imaging parameters, one-way ANOVA was used. A $p < 0.05$ indicated statistical significance. The homogeneity of the variance of the study groups were analyzed by the Levene test. The groups that have $p > 0.05$ were considered homogenous. Tukey's HSD test for homogenous groups and Tamhane's T2 test for nonhomogenous groups were used for post hoc analysis. The chi-square test was used for gender comparison.

A nonparametric Kruskal-Wallis variance analyze test and the Mann-Whitney U test was used to determine statistical significance for the qualitative image analysis. Interobserver agreement in the assessment of image quality was quantified by weighted statistics (kappa statistics). Kappa value is a statistical measure of interobserver agreement for qualitative measurements. The κ value can be interpreted as 0.21–0.40 fair, 0.41–0.60 moderate, and 0.61–0.80 good.

## III. RESULTS

### A. Phantom study

CIRS phantom studies demonstrated noise reduction when the same tube current was reconstructed with increasing levels of iDose$^4$ (Table 2). The noise levels at 20% and 30% decreased mAs reconstructed by iDose$^4$2 and iDose$^4$3, respectively, were almost equal to the STD with FBP algorithm. For that reason these iDose$^4$ and mAs reduction levels were chosen for further study. The results were the same for the different tube voltages (100, 120, 140 kV, Table 2).

Table 2. The noise data (in SD) scanning of the CIRS head phantom at intervals of decreasing mAs and increasing iDose$^4$ levels relative to STD head CT protocol using 120 kVp. The same protocol and method with 100 kVp and 140 kVp. mAs = tube current; FBP = filtered backprojection; $CTDI_{vol}$ = volume CT dose index; kVp = tube voltage; LD = low dose; STD = standard dose.

| | | | | *120 kVp* | | | |
|---|---|---|---|---|---|---|---|
| *mAs* | *FBP* | *iDose$^4$1* | *iDose$^4$2* | *iDose$^4$3* | *iDose$^4$4* | *iDose$^4$5* | *$CTDI_{vol}$* |
| 300 | 3.3 | 2.9 | 2.8 | 2.6 | 2.3 | 2.1 | 41.24 |
| 270 | 3.7 | 3.3 | 3.2 | 2.9 | 2.7 | 2.5 | 37.1 |
| 240 | 3.8 | 3.5 | 3.2 | 2.9 | 2.7 | 2.4 | 32.96 |
| 210 | 4 | 3.6 | 3,4 | 3.2 | 2.9 | 2.6 | 28.99 |
| 180 | 4.4 | 3.9 | 3.6 | 3.4 | 3.1 | 2.8 | 24.67 |
| 150 | 4.5 | 4 | 3.7 | 3.4 | 3.2 | 2.9 | 20.53 |
| | | | | *100 kVp* | | | |
| 300 | 4.4 | 3.9 | 3.6 | 3.4 | 3.1 | 2.7 | 25.18 |
| 270 | 5.1 | 4.5 | 4.3 | 3.9 | 3.6 | 3.2 | 22.65 |
| 240 | 5.5 | 4.8 | 4.5 | 4.2 | 3.8 | 3.4 | 20.12 |
| 210 | 5.5 | 4.9 | 4.6 | 4.4 | 3.9 | 3.4 | 17.59 |
| 180 | 6.1 | 5.5 | 5.2 | 4.8 | 4.5 | 4.1 | 15.07 |
| 150 | 6.9 | 6.1 | 5.7 | 5.3 | 4.8 | 4.4 | 12.54 |
| | | | | *140 kVp* | | | |
| 300 | 2.6 | 2.5 | 2.2 | 2.1 | 1.9 | 1.7 | 60.17 |
| 270 | 2.9 | 2.6 | 2.4 | 2.2 | 2 | 1.8 | 54.13 |
| 240 | 3.1 | 2.8 | 2.6 | 2.4 | 2.2 | 2 | 48.09 |
| 210 | 3.5 | 3.2 | 3 | 2.7 | 2.5 | 2.3 | 42.3 |
| 180 | 3.8 | 3.4 | 3.2 | 3 | 2.7 | 2.5 | 36 |
| 150 | 4.1 | 3.7 | 3.4 | 3.2 | 2.9 | 2.6 | 29.96 |

When the STD, LD-I and LD-II protocols were compared by using the Catphan phantom, the background noise levels were lower, and the SNR and the CNR values were higher in LD protocols than the STD protocol (Table 3).

Field uniformity measurements were preserved, and the difference of the values according to the locations and the protocols were within the limitations, as described in the Materials & Methods section (Table 4). Comparison of low-contrast images showed comparable appearances of the 4 mm objects at 1% in all of the protocols similar to data published in the literature (Fig. 2). There were no differences in the identification of these high-contrast resolution bar patterns between the groups (5 lp/cm based on phantom guidelines) (Fig. 3). The low-dose application with iDose$^4$ did not decrease the high-contrast resolution.

Table 3. The background noise levels, the SNR, and the CNR values of the STD, LD-I and LD-II protocols were compared by using the Catphan phantom, module 404. LD = low dose; STD = standard dose; CNR = contrast-to-noise ratio; SNR = signal-to-noise ratio.

| | *STD* | *LD-I* | *LD-II* |
|---|---|---|---|
| background noise | 3.9 | 3.5 | 3.7 |
| background SNR | 26.3 | 29 | 27.2 |
| CNR | 5.9 | 6.4 | 6.2 |

Table 4. Field uniformity measurements of Catphan phantom using CTP 486 module. $CT_n$ given in HU. LD = low dose; STD = standard dose; $CT_n$ = CT number; HU = Hounsfield units.

| | *STD* | *LD-I* | *LD-II* |
|---|---|---|---|
| Center | 17.2 | 17.56 | 17.56 |
| 3 o'clock | 15.66 | 15.8 | 16.06 |
| 6 o'clock | 16.03 | 15.6 | 15.56 |
| 9 o'clock | 14.86 | 14.83 | 15.1 |
| 12 o'clock | 15.83 | 15.76 | 15.7 |

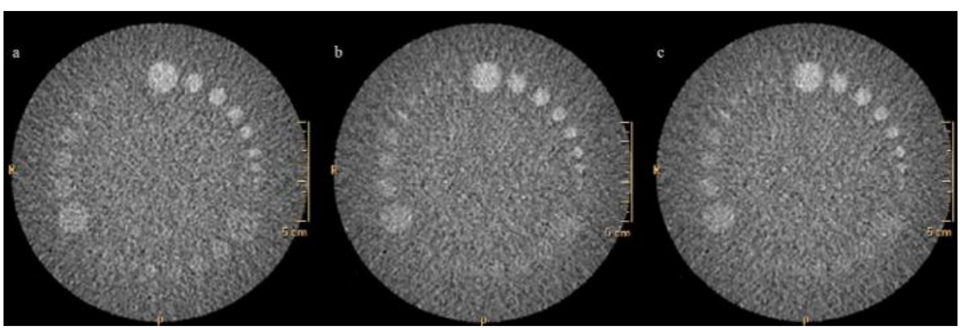


Fig. 2. Catphan low-contrast phantom module (CTP 515) is made of several sets of cylindrical low-contrast objects: (a) STD protocol (300 mAs, with FBP reconstruction); (b) LD-I (250 mAs, with iDose$^4$2); (c) LD-II (200 mAs, iDose$^4$3). Comparison of low-contrast images showed comparable visualization of the 7 disc objects, up to 4 mm diameter, at 1% in all of the protocols similar to data published in the literature. FBP = filtered backprojection; LD = low dose; STD = standard dose.

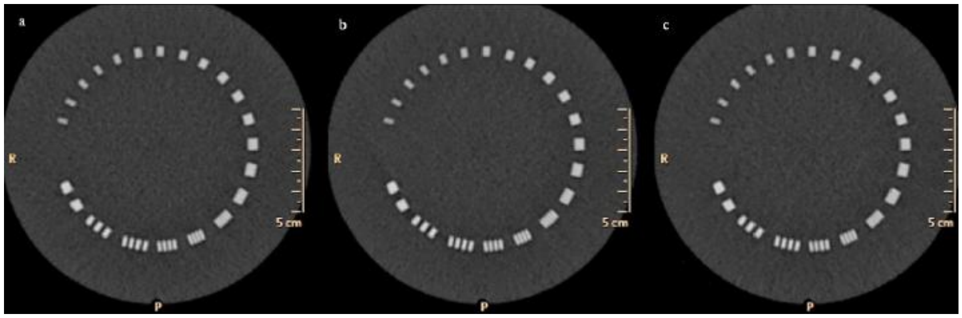


Fig. 3. Catphan high-resolution phantom module (CTP 528) with high-resolution bar patterns: (a) STD protocol (300 mAs, with FBP reconstruction); (b) LD-I (250 mAs, with iDose[4]2); (c) LD-II (200 mAs, iDose[4]3). There were no differences in the identification of these high-contrast resolution bar patterns between the groups. LD = low dose; FBP = filtered backprojection; STD = standard dose.

## B. Patient demographics

There were no significant differences in the age and sex distribution between the groups ($p > 0.05$) (Table 5). The BPD and GOD were similar in the groups ($p > 0.05$) (Table 5). We achieved a significant dose reduction of 16.73% in $CTDI_{vol}$ and 16.06% in the DLP in LD-I and 33.49% in the $CTDI_{vol}$ and 34.46% in the DLP in LD-II group ($p < 0.0001$) (Table 5). The ED (mSv) was significantly lower in both LD groups compared with the STD group.

Table 5. Patient characteristics and dose parameters of the three groups. LD = low dose; STD = standard dose; M = male; F = female; BPD = biparietal diameter; GOD = glabella and opisthocranion; $CTDI_{vol}$ = volume CT dose index; DLP = dose-length product; ED = effective dose.

| | *STD* | *LD-I* | *LD-II* | *p* |
|---|---|---|---|---|
| Age | 46.6±19.4 | 45.2±20.3 | 44.4±17.46 | 0.7 |
| Gender (M/F) | 57/43 | 57/43 | 48/52 | 0.33 |
| BPD | 146.2±6.4 | 146.6±6.9 | 145.3±6.2 | 0.48 |
| GOD | 175±8.8 | 174.8±7.3 | 175.2±8.5 | 0.92 |
| CTDIvol (mGy) | 41.24 | 34.34 | 27.43 | <0.0001 |
| DLP (mGy.cm) | 770±52 | 646±41 | 504±30 | <0.0001 |
| ED (mSv) | 1.6±0.1 | 1.3±0.08 | 1.05±0.06 | <0.0001 |

## C. Quantitative analysis

The noise levels of the CSF (STD-LD-I $p = 0.001$, STD-LD-II $p < 0.0001$), WM (STD-LD-I $p < 0.0001$, STD-LD-II $p < 0.0001$), and GM (STD-LD-I $p < 0.0001$, STD-LD-II $p < 0.0001$) in the low-dose groups were significantly less than the STD group. The noise levels of the bone in the low-dose groups were less than the STD group. The difference between the STD and LD-II group was significant ($p = 0.032$) and insignificant between STD-LD-I ($p = 0.603$). The average noise value for air was high in LD-II than the STD ($p = 0.030$) and no difference is detected between STD and LD-I groups ($p = 0.829$) (Table 6).

The SNR of the WM (STD- LD-I $p < 0.0001$, STD-LDII $p = 0.033$) and GM (STD- LD-I $p < 0.0001$, STD-LDII $p < 0.0001$) values and the CNR (STD- LD-I $p < 0.0008$, STD-LDII $p < 0.0001$) levels in the LD groups were higher than the STD group. The differences were statistically significant (Table 6). We did not observe any artifacts in either group that made interpretation impossible.

Table 6. Mean and SD of noise, SNR and CNR in various CT protocols. (p-values are mentioned in the main text). LD = low dose; STD = standard dose; CSF = cerebrospinal fluid; WM = white matter; GM = gray matter; SD = standard deviation.

| | *STD* | *LD-I* | *LD-II* |
|---|---|---|---|
| NOISE | | | |
| Air | 2.64±0.42 | 2.60±0.33 | 2.77±0.31 |
| CSF | 3.30±0.41 | 3.09±0.42 | 2.79±0.41 |
| WM | 2.94±0.38 | 2.71±0.32 | 2.75±0.34 |
| GM | 3.45±0.34 | 3.11±0.37 | 3.10±0.31 |
| Bone | 48.58±12.69 | 46.73±14.57 | 43.70±13.55 |
| SNR WM | 9.46±1.46 | 10.47±1.63 | 10.00±1.49 |
| SNR GM | 9.68±1.24 | 10.75±1.96 | 10.69±1.58 |
| CNR | 3.17±0.73 | 3.54±1.09 | 3.82±0.65 |

## D. Qualitative analysis

When the STD and the LD-I groups were compared, no significant differences were found in descriptiveness of the posterior fossa contents ($p = 0.225$) and overall quality ($p = 0.083$) (Fig. 4). The subjective noise ($p = 0.003$), artifact ($p = 0.038$), and GM–WM differentiation ($p = 0.045$) scores were better in LD-I group than the STD group. There were no significant difference in subjective noise ($p = 0.456$), artifacts ($p = 0.697$), and overall quality ($p = 0.306$) between the STD group and LD-II group. Scores for descriptiveness of the posterior fossa contents ($p = 0.027$) and GM–WM differentiation ($p = 0.011$) were better in the STD group than LD-II group (Table 7).

For the subjective analysis, the kappa values for interobserver agreement in evaluating various image quality parameters were moderate (weighted $\kappa = 0.56$-$0.61$).

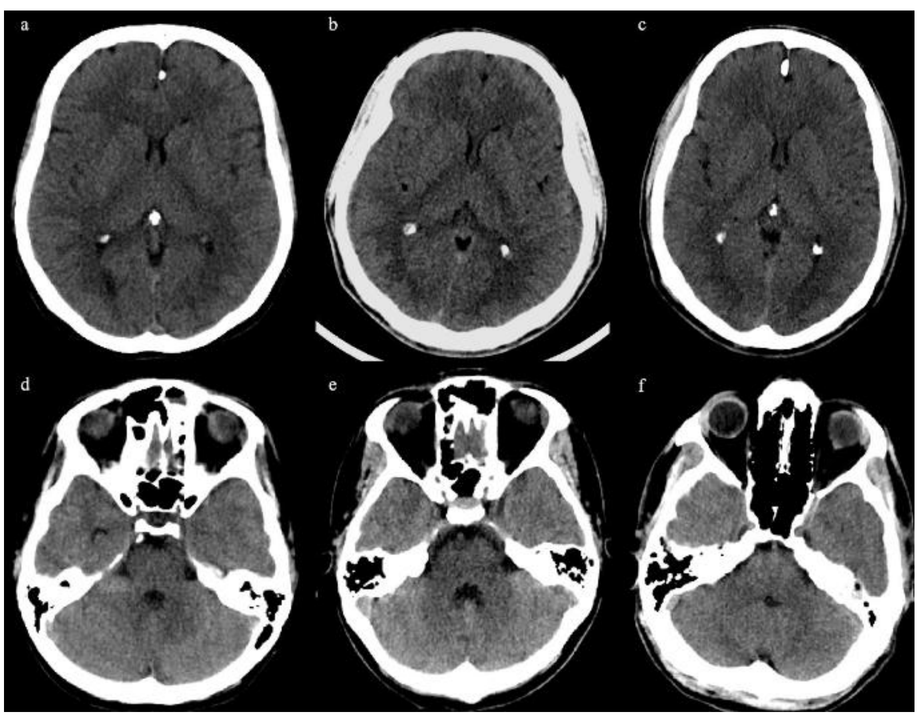


Fig. 4. CT axial images of various protocols: (a) and (d) STD protocol (300 mAs, with FBP reconstruction); (b) and (e) LD-I (250 mAs, with iDose[4]2); (c) and (f) LD-II (200 mAs, iDose[4]3). The overall IQ is similar. FBP = filtered backprojection; IQ = image quality; LD = low dose; STD = standard dose.

TABLE 7. Mean and SD, median of qualitative image scores in various CT protocols (p-values are mentioned in the main text). LD = low dose; STD = standard dose; SD = standard deviation.

| | *STD* | *LD-I* | *LD-II* |
|---|---|---|---|
| Subjective noise | 4.28±0.57(4) | 4.45±0.55(4) | 4.32±0.58(4) |
| Artifact | 4.1±0.44(4) | 4.19±0.42(4) | 4.08±0.48(4) |
| Descriptiveness of posterior fossa | 4.52±0.54(5) | 4.59±0.51(5) | 4.41±0.54(4) |
| GM–WM differentiation | 4.22±0.62(4) | 4.34±0.63(4) | 4.07±0.6(4) |
| Overall image quality | 4.19±0.46(4) | 4.28±0.46(4) | 4.14±0.47(4) |

## IV. DISCUSSION

Due to the widespread use, MDCT has become the major source of radiation related to diagnostic imaging and this has raised concerns about radiation exposure in the general population. The risk of cancer from diagnostic X-rays reported from 0.6% to 3.0% in developed countries.(28)

Radiation dose is proportional to the total number of the photons and the photon energy within the X-ray beam.(29) Many strategies have been introduced to reduce the radiation dose including optimizing the kVp and the mAs, automated tube current modulation, adaptive dose collimation, and noise-reduction reconstruction algorithms.(16,27,29) Unfortunately the basic methods, such as lowering the kVp or mAs, sacrifice the IQ.

Image noise and resolution are the major determinants of IQ. Reconstructed image noise is affected mostly by radiation dose and image-processing methods.(18) IR has focused on noise suppression and artifact reduction associated with lowering the radiation dose.(29)

In our study, a reduction of $CTDI_{vol}$ by 16.73% in LD-I and by 33.49% in LD-II protocols were achieved with no significant change in the overall image quality compared with the STD protocol. Similar findings were reported more recently. The application of various IR methods has been described to lower the radiation dose in head CT — in studies by Kilic et al.(30) a 31% decrease in DLP, by Rapalino et al.(31) a reduction of 26% in $CTDI_{vol}$, by Alper et al.(32) a reduction of 38% in DLP achieved without affecting diagnostic acceptability. Another study published by Korn et al.(33) compared their original nonenhanced and enhanced head CT FBP protocol with two LD IR protocols. The authors found that a 15% dose reduction did not contribute with IQ, but a 30% dose reduction resulted in degradation of IQ when reconstructed with IR (IRIS).

WM, GM, and CSF demonstrated significantly decreased noise levels in our LD protocols relative to the STD protocol. The CSF was the most prominent region. This is similar to the findings of the other studies which they attributed to the propensity of IR to reduce noise in smoother areas more prominently.(30,34,35) Bone demonstrated significantly low noise in LD protocols which is not statistically significant in LD-I. In previous studies no significant difference had been shown between the noise levels in WM and bone, which is not consistent with our study.(30,34) Additionally, we studied the GM noise and found lower levels in LD groups. Air noise measurements demonstrated no significant difference between the STD and LD-I groups and was higher in LD-II than the STD group. We think that this might be because of the small FOV in front of the frontal bone. We could not change the FOV in order to compare the LD and the STD groups.

The SNR of WM and GM and CNR in both LD groups were significantly higher than the STD group. Kilic et al.(30) had demonstrated higher CNR in their LD and IR protocol; however, unlike our study, WM measurements (noise and SNR) and subjective scores of noise were better in the STD group. Rapalino et al.(31) demonstrated that the use of IR (ASIR) improves measurements of SNR and CNR of GM and WM brain structures in reduced-dose head CT scans for adult patients similar to our results.

The subjective imaging quality is dependent on the amount of noise and the effect of blurring while using IR with low radiation doses. The level of noise is inversely related to the tube potential,[36] and the blurring effect is proportional to the level of IR used. They must be in equilibrium. If the level of IR is high, the images become blurred; if the level of IR is low, images will be noisy. Unlike other IR algorithms, (e.g., ASIR; GE Healthcare, Waukesha, WI), the exact percentage of IR in different levels of iDose$^4$ is not clearly demonstrated in the CT protocol. In order to avoid excessively noisy or smooth image reconstructions,[31,35] the recommended levels by the vendor might be followed.

In our study, we tried to find out the optimum IR level by performing a group of phantom studies before the patient applications which is described in the literature.[34,37] We evaluate the low-contrast and high-resolution quality of the protocols which are especially important for head and neck protocols.[19] There were no differences between the protocols. The SNR and CNR became higher by the iDose$^4$ levels in lower doses.

We achieved subjective differences in sharpness by evaluating the GM–WM differentiation and the posterior fossa descriptiveness. They were found to be better in the STD group than the LD-II in qualitative evaluation, while the SNR and CNR were better in quantitative and phantom evaluations. Kilic et al.[30] observed better image sharpness scores in the STD group than in the LD group. The authors attributed this to the oversmoothing effect of IR (ASIR) as well as to the noise. Wu et al.[38] has mentioned that the blurring of imaging texture became evident in the infratentorial region. When the IR is increased unproportionately, a noiseless appearance occurs in the images, and radiologists may evaluate these images as oversmoothed or artificial, neither of which are desired.[31] Changing the algorithm of the routine procedures from FBP to IR might be difficult. Perhaps for that reason, while the phantom and quantitative evaluation of the LD-II protocol CNR and SNR values were better and comparable with the STD protocol, the scores of the qualitative evaluation were lower. The interobserver agreement for qualitative measurements (kappa values) was lower in LD-II scores, too.

Differences in image sharpness might also depend on physical features of the patient. Variations in cranial thickness and amount of subcutaneous tissue surrounding the calvarium may contribute to subjective image sharpness.[32] For that reason we measured the BPD and GOD and compared them as variables. Wu et al.[38] had found that the head diameter was the only significant factor inversely correlated with infratentorial imaging quality. Head diameter cranial bone structures and thickness of the scalp might be investigated as variables while making the dose regulations and deciding on the amount of the radiation dosage. One of the limitations of our study is that we measured the diameters between the outer tabulas and didn't consider the amount of subcutaneous tissue in the calvarium. The thickness of the supratentorial and infratentorial diploe might be measured separately and compared among the groups as variables. This can be studied and compared, and some standardization might be found such as body mass index.

The posterior fossa was the part most affected by the lowering of the dose. We evaluated the posterior fossa qualitatively, but did not evaluate it quantitatively. This is the one of the limitations of our study. Artifacts, such as the operation materials, might be studied more specifically. We did not evaluate the special pathologies and the diagnostic accuracy of the protocols, which is another limitation of our study.

We additionally repeated the same procedure with 100 kVp and 140 kVp instead of the 120 kVp of our STD protocol. Our phantom data suggest that additional radiation dose reduction may be feasible with similar image noise, if the studies are reconstructed with a higher level of IR (e.g., 120 kV 180 mAs iDose$^4$4) or by changing kV (e.g., 100 kV 300 mAs iDose$^4$3, 140 kV 150 mAs iDose$^4$2). These protocols can be used in future studies. We used only the noise level, but the CNR can be added too.

## V. CONCLUSIONS

Radiologists and physicists should be familiar with such dose-reduction techniques and should optimize the imaging protocols to achieve the best images with a lower radiation dose. For analyzing various protocols, the vendor's phantoms might be used. The phantom studies can be used as a preview before trying a new dose-reducing method. Our study showed that, by selecting the appropriate level of IR, radiation dose reduction up to 34% can be achieved in adult head CT examinations without compromising the overall IQ.

## REFERENCES


1. Hounsfield GH. Computerized transverse axial Scanning (tomography). I. Description of system. Br J Radiol. 1973;46(552):1016–22.
2. Ambrose J. Computerized transverse axial scanning (tomography): Part 2. Clinical application. Br J Radiol. 1973;46(552):1023–46.
3. Weber AL. History of head and neck radiology: past, present, and future. Radiology. 2001;218(1):15–24.
4. Mettler FA Jr, Bhargavan M, Faulkner K, et al. Radiologic and nuclear medicine studies in the United States and worldwide: frequency, radiation dose, and comparison with other radiation sources--1950-2007. Radiology. 2009;253(2):520–31.
5. van der Molen AJ, Schilham A, Stoop P, Prokop M, Geleijns J. A national survey on radiation dose in CT in The Netherlands. Insights Imaging. 2013;4(3):383–90.
6. Goo HW. CT radiation dose optimization and estimation: an update for radiologists. Korean J Radiol. 2012;13(1):1–11.
7. Hall EJ and Brenner DJ. Cancer risks from diagnostic radiology: the impact of new epidemiological data. Br J Radiol. 2012;85(1020):e1316–e1317.
8. IMV Medical Information Division. Benchmark Report: MRI 2007. Des Plaines, IL: IMV; 2007.
9. Mahesh M. NCRP Report Number 160: its significance to medical imaging. J Am Coll Radiol. 2009;6(12):890–92.
10. Brenner DJ and Hall EJ. Computed tomography: an increasing source of radiation exposure. N Engl J Med. 2007;357(22):2277–84.
11. Hall EJ and Brenner DJ. Cancer risks from diagnostic radiology. Br J Radiol. 2008;81(965):362–78.
12. Smith-Bindman R, Lipson J, Marcus R, et al. Radiation dose associated with common computed tomography examinations and the associated lifetime attributable risk of cancer. Arch Intern Med. 2009;14;169(22):2078–86.
13. Berrington de González A, Mahesh M, Kim KP, et al. Projected cancer risks from computed tomographic scans performed in the United States in 2007. Arch Intern Med. 2009;169(22):2071–77.
14. Kalra MK, Maher MM, Toth TL, et al. Strategies for CT radiation dose optimization. Radiology. 2004;230(3):619–28.
15. Kalra MK. MDCT radiation dose: recent advances. In: Kalra MK, Saini S, Rubin GD, editors. MDCT: from protocols to practice. Berlin Heidelberg: Springer-Verlag; 2008. p.31–41.
16. Smith AB, Dillon WP, Gould R, Wintemark M. Radiation dose-reduction strategies for neuroradiology CT protocols. AJNR Am J Neuroradiol. 2007;28(9):1628–32.
17. Gramer BM, Muenzel D, Leber V, et al. Impact of iterative reconstruction on CNR and SNR in dynamic myocardial perfusion imaging in an animal model. Eur Radiol. 2012;22(12):2654–61.
18. Xu J, Mahesh M, Tsui BM. Is iterative reconstruction ready for MDCT? J Am Coll Radiol. 2009;6(4):274–76.
19. Noël PB, Fingerle AA, Renger B, Munzel D, Rummeny EJ, Dobritz M. Initial performance characterization of a clinical noise-suppressing reconstruction algorithm for MDCT. AJR Am J Roentgenol. 2011;197(6):1404–09.
20. Hou Y, Liu X, Xv S, Guo W, Guo Q. Comparisons of image quality and radiation dose between iterative reconstruction and filtered back projection reconstruction algorithms in 256-MDCT coronary angiography. AJR Am J Roentgenol. 2012;199(3):588–94.
21. Funama Y, Awai K, Nakayama Y, et al. Radiation dose reduction without degradation of low-contrast detectability at abdominal multisection CT with a low-tube voltage technique: phantom study. Radiology. 2005;237(3):905–10.
22. Verdun FR, Denys A, Valley JF, Schnyder P, Meuli RA. Detection of low-contrast objects: experimental comparison of single- and multi-detector row CT with a phantom. Radiology. 2002;223(2):426–31.
23. Smyth J, Sutton D, Houston J. Evaluation of the quality of CT-like images obtained using a commercial flat panel detector system. Biomed Imaging Interv J. 2006;2(4):e48.
24. American Association of Physicists in Medicine. The measurement, reporting, and management of radiation dose in CT. AAPM Report No. 96. Report of AAPM Task Group 23 of the Diagnostic Imaging Council CT Committee. 2007. Available at: http://www.aapm.org/pubs/reports/rpt_96.pdf
25. Lev MH, Kulke SF, Sorensen AG, et al. Contrast-to-noise ratio in functional MRI of relative cerebral blood volume with sprodiamide injection. J Magn Reson Imaging. 1997;7(3):523–27.
26. Mullins ME, Lev MH, Bove P, et al. Comparison of image quality between conventional and low-dose nonenhanced head CT. AJNR Am J Neuroradiol. 2004;25(4):533–38.
27. Udayasankar UK, Braithwaite K, Arvaniti M, et al. Low-dose nonenhanced head CT protocol for follow-up evaluation of children with ventriculoperitoneal shunt: reduction of radiation and effect on image quality. AJNR Am J Neuroradiol. 2008;29(4):802–06.

28. Berrington de Gonzalez A, Darby S. Risk of cancer from diagnostic x-rays: estimates for the UK and 14 other countries. Lancet. 2004;363(9406):345–51.
29. Ibrahim M, Parmar H, Christodoulou E, Mukherji S. Raise the bar and lower the dose: current and future strategies for radiation dose reduction in head and neck imaging. AJNR Am J Neuroradiol. 2014;35(4):619–24.
30. Kilic K, Erbas G, Guryildirim M, Arac M, Ilgit E, Coskun B. Lowering the dose in head CT using adaptive statistical iterative reconstruction. AJNR Am J Neuroradiol. 2011;32(9):1578–82.
31. Rapalino O, Kamalian S, Kamalian S, et al. Cranial CT with adaptive statistical iterative reconstruction: improved image quality with concomitant radiation dose reduction. AJNR Am J Neuroradiol. 2012;33(4):609–15.
32. Alper S, Mohan P, Chaves I, Kane R, Calandra J. Image quality and radiation dose comparison between filtered back projection and adaptive statistical iterative reconstruction in non-contrast head CT studies. OMICS J Radiology. 2013;2:147.
33. Korn A, Fenchel M, Bender B, et al. Iterative reconstruction in head CT: image quality of routine and low-dose protocols in comparison with standard filtered back-projection. AJNR Am J Neuroradiol. 2012;33(2):218–24.
34. Vorona GA, Zuccoli G, Sutcavage T, Clayton BL, Ceschin RC, Panigrahy A. The use of adaptive statistical iterative reconstruction in pediatric head CT: a feasibility study. AJNR Am J Neuroradiol. 2013;34(1):205–11.
35. Marin D, Nelson RC, Schindera ST, et al. Low-tube-voltage, high-tube-current multidetector abdominal CT: improved image quality and decreased radiation dose with adaptive statistical iterative reconstruction algorithm—initial clinical experience. Radiology. 2010;254(1):145–53.
36. Gervaise A, Osemont B, Lecocq S, et al. CT image quality improvement using adaptive iterative dose reduction with wide volume acquisition on 320-detector CT. Eur Radiol. 2012;22(2):295–301.
37. Hara AK, Paden RG, Silva AC, Kujak JL, Lawder HJ, Pavlicek W. Iterative reconstruction technique for reducing body radiation dose at CT: feasibility study. AJNR Am J Roentgenol. 2009;193(3):764–71.
38. Wu TH, Hung SC, Sun JY, et al. How far can the radiation dose be lowered in head CT with iterative reconstruction? Analysis of imaging quality and diagnostic accuracy. Eur Radiol. 2013;23(9):2612–21.

Radiation Physics and Chemistry 205 (2023) 110735

Contents lists available at ScienceDirect

Radiation Physics and Chemistry

journal homepage: www.elsevier.com/locate/radphyschem

# Dose optimization of adult head computed tomography examination in an academic hospital in Ghana

Samuel Anim-Sampong [a], Benard Ohene-Botwe [a,b,*], Esther Boatemaa Adom [a], Samuel Nii Adu Tagoe [a]

[a] Dept. of Radiography, School of Biomedical & Allied Health Sciences, University of Ghana, P.O Box KB 14, Korle Bu Campus, Accra, Ghana

[b] Department of Midwifery and Radiography, School of Health & Psychological Sciences, City, University of London, Northampton Square, London, EC1V 0HB, UK

ARTICLE INFO

Handling Editor: Chris Chantler

*Keywords:*
Patients
Computed tomography
Dose optimization
Image quality

ABSTRACT

The study investigated radiation doses and image quality of adult head CT and optimization options using an anthropomorphic RANDO phantom on the only available AquilionONE CT scanner in Ghana. Dose length product (DLP) and volume-weighted CT dose index ($CTDI_{vol}$) dose descriptors were retrospectively obtained from 402 adult head CT examinations performed (from 2020 to 2021) at a Ghanaian hospital, while the effective dose ($D_{eff}$) was estimated from the product of the DLP and a convention coefficient ($k = 0.0023$). Using the same routine head CT protocol, the anthropomorphic RANDO phantom was scanned with the hospital's 640-slice Toshiba AquilionONE CT scanner. Subsequently, exposure factors were varied to study their effects on the dose and image quality. The adult head and phantom images were obtained in Digital Imaging and Communications in Medicine (DICOM) format, and their signal-to-noise (SNR) ratios were analyzed with ImageJ software. The facility's mean $CTDI_{vol}$, DLP, and effective dose ($D_{eff}$) were 86.00 ± 0.00 mGy, 1559.68 ± 197.18 mGy cm, and 3.57 ± 0.46 mSv respectively (SNR = 7.04). For a fixed tube potential, $CTDI_{vol}$, DLP, and $D_{eff}$ of 51.30 mGy, 1013.80 mGy cm, and 2.33 mSv were respectively achieved (SNR = 5.49) after optimization. Using automatic exposure control (AEC) in the optimization process, the respective $CTDI_{vol}$, DLP and $D_{eff}$ values were 59.50 mGy, 1176.00 mGy cm and 2.70 mSv (SNR = 5.62). We conclude that substantial $D_{eff}$ reductions of 40.4% and 31.0% using a fixed tube potential, and AEC while maintaining diagnostic image quality were respectively achieved. The protocols associated with these dose-reductions are, therefore, recommended as optimization measures for head CT on the AquilionONE scanner in Ghana.

## 1. Introduction

Computed tomography (CT) is a non-invasive medical imaging modality that utilizes ionizing radiation to produce cross-sectional and detailed images of parts of the body, as defined by the World Health Organization (2021). Advances in CT imaging technology and its extensive use in clinical practice have resulted in increased CT examinations and reduced the need for emergency surgery from 13% to 5%, eliminating many exploratory surgical procedures (Power et al., 2016). In Ghana, Botwe et al. (2020) estimated that 204,760 patients undergo CT examinations yearly. High radiation doses delivered to patients undergoing CT examinations are a major global concern due to the associated biological effects and inherent risks compared to other radiological examinations (Anim-Sampong et al., 2016; Sackey, 2015).

Although CT procedures deliver organ doses in the range of 10 mGy–100 mGy which are generally below levels required to induce deterministic effects, according to the linear non-threshold theory, patient risk of stochastic effects is correlated with radiation dose at any level (Alm-Carlsson et al., 2007; Shrimpton et al., 2016). It is thus, essential to reduce patient dose while maintaining diagnostic image quality, and consequently minimize the associated health effects.

Several CT dose-reduction approaches including the alteration of exposure factors (lowering tube current and peak tube voltage), use of automated exposure control (AEC), monitoring, and integration of different iterative reconstruction software have been provided by various manufacturers. These approaches, however, have different effects on the image quality needed for a specific diagnosis or task (Demb et al., 2017). Hence, appropriate dose optimization measures are

* Corresponding author. Department of Midwifery and Radiography, School of Health & Psychological Sciences, City, University of London, Northampton Square, London, EC1V 0HB, UK.

*E-mail address:* sirbenard13@gmail.com (B. Ohene-Botwe).

https://doi.org/10.1016/j.radphyschem.2022.110735
Received 6 October 2022; Received in revised form 24 November 2022; Accepted 18 December 2022
Available online 21 December 2022

required to ensure that patients presenting for a particular CT imaging including head scans receive optimized radiation doses to reduce the inherent risk but maintain diagnostic image quality (Smith-Bindman et al., 2019).

According to Bauhs et al. (2008), the CT dose index (CTDI) is the integral of the single scan radiation dose profile along the z-axis, normalized to the thickness of the imaged section and expressed differently for single-slice computed tomography (SSCT) and multi-slice computed tomography (MSCT) as:

$$CTDI_{SSCT} = \frac{1}{T}\int_{-\infty}^{+\infty} D(z)dz \tag{1}$$

$$CTDI_{MSCT} = \frac{1}{NT}\int_{-L/2}^{+L/2} D(z)dz \tag{2}$$

where $T$ is the detector width or minimal beam collimation thickness, $D$ is the dose profile, and $N$ is the number of detectors. The volume-weighted CTDI ($CTDI_{vol}$) is the pitch-corrected weighted CTDI ($CTDI_w$) and is expressed as

$$CTDI_{vol} = \frac{CTDI_w}{p} = \frac{1}{p}\left[\frac{1}{3}CTDI_{100,centre} + \frac{2}{3}CTDI_{100,periphery}\right] \tag{3}$$

where $p$ is the scan pitch. According to Smith-Bindman et al. (2011), the $CTDI_{vol}$ and dose length product (DLP) are important CT dose descriptors for estimating the average absorbed dose for a series of irradiated tissue sections. The DLP reflects the potential biologic effect as it represents the total energy produced by a given protocol in a complete scan acquisition and varies directly with the total scanned radiation dose (Kisembo et al., 2015; Strauss, 2014). It is calculated as the product of the intensity ($CTDI_{vol}$) and the length of the scanned tissue (Nagel, 2007) via Eqn (4) as

$$DLP = CTDI_{vol} x L = \frac{L}{p} CTDI_w \tag{4}$$

where $L$ is the scan length for the examinations determined via

$$L = \frac{DLP}{CTDI_{vol}} \tag{5}$$

The effective dose ($D_{eff}$) is an inference of an individual's whole-body dose resulting from radiation exposures and relates to the risk resulting from the exposure to the individual organ and tissue contributions of the absorbed doses. It is determined to assess incidence rates for biological responses such as the stochastic effects. According to Semelka et al. (2007), $D_{eff}$ is the product of an organ's equivalent dose ($H_T$) and radiosensitivity which offers a whole-body dose with the same risk as a partial dose provided by a localized radiologic procedure. It is dependent on patient size, imaging parameters and scanner technology, and is often clinically estimated from measured DLPs, as reported in the literature (Sodickson et al., 2009).

Quantitatively, $D_{eff}$ for a patient can be calculated from the product of DLP and a conversion factor coefficient ($k$) for the specific body region (Brady et al., 2015; Postorino et al., 2021) as

$$D_{eff} = \sum W_t H_t \tag{6}$$

and

$$D_{eff} = kDLP = k[CTDI_{vol}] = \frac{kL}{p} CTDI_w \tag{7}$$

where $W_t$ is the tissue-specified weighting factor for tissue or organ ($t$) under examination, and $k = 0.0023$ for head CT scan according to the European guidelines on quality criteria for CT (Bongartz et al., 2000).

The signal-to-noise ratio (SNR) is a measure of image quality and is defined as the ratio of the mean to the standard deviations of the pixel value of regions of interest (ROIs) (Chang et al., 2017).

One of the central goals of medical radiation protection is to minimize the risks of stochastic effects of radiation to levels considered as low as reasonably achievable (ALARA), while dose optimization ensures that minimum patient doses are administered to achieve the desired purpose and image quality. This study, therefore, investigated a method of optimizing the dose received by adult patients undergoing CT head examinations while maintaining the quality of the diagnostic image. This is important to minimize head CT doses and biological effects associated with high radiation exposures, provide new protocols for adult head CT examinations, create awareness and education of radiographers in optimizing head CT doses, and thereby enhance patient radiation protection per the ALARA principle.

## 2. Materials and methods

A retrospective and quasi-experimental design which allowed for alteration of the scan parameters for head CT examinations and non-probability purposive sampling were used in this study which was conducted at the CT unit of the radiology department of a hospital in Ghana. According to Anim-Sampong et al. (2016), adult patients are more commonly referred for CT examinations of the head and other parts of the body than pediatric patients. Therefore, this study consisted of 402 adult patients who presented for head CT examinations at the hospital from January 2020–January 2021.

Constant values of tube voltage, tube current, rotation time, and pitch were used for routine head CT examinations, while scan lengths depending on the coverage area planned on the scanogram and limited to head CT examination with a major focus on the brain varied. These and other head CT scan parametric (slice number, slice thickness, $CTDI_{vol,}$ and DLP) data, as well as patient demographics, were retrospectively retrieved from the Picture Archiving and Communication System (PACS) workstation of the hospital's 640 multi-slice Toshiba Aquilon ONE TSX-301A CT scanner (Table 1) and recorded on the self-designed data collection sheet. The technical specifications of the Toshiba Aquilon ONE TSX-301A CT scanner are presented in Table 2. Quality control (QC) tests to validate the efficiency of the CT scanner have been reported in the literature (Botwe et al., 2021).

The $D_{eff}$ for each patient was subsequently calculated from the product of DLP and a conversion coefficient for the specific body region

**Table 1**
Patient characteristics, exposure factors, and scanning parameters.

| Age (yrs) | Male | | Female | | Total | |
|---|---|---|---|---|---|---|
| | Number | Percent, % | Number | Percent, % | Number | Percent, % |
| 18–27 | 27 | 6.5 | 21 | 5.2 | 48 | 11.7 |
| 28–27 | 16 | 4.0 | 33 | 8.2 | 49 | 12.2 |
| 38–47 | 37 | 9.2 | 26 | 6.5 | 63 | 15.7 |
| 48–57 | 32 | 8.0 | 43 | 10.7 | 75 | 18.7 |
| 58–67 | 44 | 11.0 | 41 | 10.2 | 85 | 21.1 |
| 68–77 | 28 | 7.0 | 31 | 7.7 | 59 | 14.7 |
| 78–87 | 7 | 1.7 | 12 | 3.0 | 19 | 4.7 |
| 88–97 | 1 | 0.2 | 3 | 0.7 | 4 | 0.9 |
| Total | 192 | 47.8 | 210 | 52.2 | 402 | 100.0 |
| Mean | 51.83 ± 17.54 | | | | | |

| Exposure factors and scanning parameters | Value |
|---|---|
| Tube voltage ($kV_p$) | 120.00 |
| Tube current (mA) | 300.00 |
| Rotation time (sec) | 0.75 |
| Pitch | 0.66 |
| Scan length (cm) | 18.14 ± 2.29 |
| Slice thickness (mm) | 5.00 |
| Sequence(s) | 1.00 |

**Table 2**
Technical specifications of Toshiba Aquilon CT scanner.

| Design parameter | Value (quantity, volume, etc) |
|---|---|
| CT scanner mode: Multislice | Multislice |
| Slices per rotation | 16-cm volume (320 × 0.5 mm) |
| Other rotation speed options (sec) | 0.35, 0.375, 0.4, 0.45, 0.5, 0.6, 0.75, 1, 1.5 |
| Minimum rotation speed | 350msec |
| Gantry diameter | 72 cm |
| Minimum temporal resolution (msec) | 16 cm full volume 350 msec |
| Maximum beam width | 16 cm |
| Minimum room size (length x width x height) | Site dependent |
| Table weight limit | 660 lb |
| Table movement range | 33–98.8 vertical/20–195 cm longitudinal |
| X-ray generator kV range | 80-135 $kV_p$ |
| Maximum scan range | 200 cm |
| X-ray tube heat capacity | 7.5 MHU |
| Power requirement | 480 VAC, 135 kVA |

(0.0023) proposed by the European Commission (Brady et al., 2015). Subsequently, the mean $D_{eff}$ was calculated for all 402 patients.

With knowledge of the average dose output ($CTDI_{vol}$ and DLP) used for performing routine diagnostic head CT examinations at the study site, an optimization study was then conducted. The RANDO anthropomorphic phantom was used for the optimization study by scanning it with the routine head scan protocols used at the facility and subsequently varying the exposure factors to study their effects on the dose and image quality.

Image quality analyses were performed on the phantom images obtained in DICOM format to identify the best modified protocol(s) that resulted in radiation dose-reduction while maintaining acceptable image quality for the intended purpose. Both objective and subjective image quality analyses were conducted. Objectively, four square ROIs of the same dimensions (10 mm × 10mm) were drawn on the homogeneous 5 mm cut brain tissue at the same slice number for each image, located about midway between the total number of slices for each image. The signal-to-noise ratio (SNR) values were estimated using ImageJ software version 1.53 (Wayne Rasband and Contributors, National Institutes of Health, USA) to assess the objective image quality. Fig. 1 shows how the signal and the noise information were obtained quantitatively using ImageJ software version 1.53. Subjectively, image quality can be assessed via radiologists' reviews of images. In this regard, radiologists at the hospital reviewed and approved the images as fit for diagnostic purposes for routine head CT examinations. The subjective assessment provided information on whether the images were diagnostically acceptable (good) or not (bad) for the intended clinical task.

The ethical clearance for this study was reviewed and approved by the Ethics and Protocol Review Committee of the School of Biomedical and Allied Health Sciences of the University of Ghana (Reference: SBAHS/AA/RAD/10680009/2020–2021).

## 3. Results

The highest and least number of referrals for head CT procedures were recorded among patients aged 58–67 years (21.1%), and 88–97 years (0.9%). More females (52.2%) presented for head CT scans than males (47.8%).

### 3.1. Dosimetry

The mean $CTDI_{vol}$ and DLP values were 86.00 mGy and 1559.70 mGy cm respectively, with associated 75th percentiles of 86.00 mGy and 1613.60 mGy cm. The measured values at the CT unit exceeded values recommended by the ICRP 73, American College of Radiology (ACR) and other literature reports (ACR, 2008; Shrimpton et al., 2016). The mean $D_{eff}$ (of all 402 patients) obtained for the images of the adult head CT patients was 3.57 ± 0.46 mSv.

### 3.2. Dose optimization of routine protocol for head scans

Eight phantom head CT images were assessed to determine the image quality and mean dose descriptor values were obtained for different exposure parameters (Table 4). Image A was obtained using the mean routine adult CT head parameters with a DLP of 1699.60 mGy cm. A DLP of 1037.30 mGy cm was obtained from scanning Image B with the same tube potential (120.00 kV) and pitch (0.66) but with a reduced tube current of 200.00 mA. Images C and D were acquired with the same tube current and pitch as Image A, but with reduced tube potentials of 100.00 kV and 80.00 kV respectively, resulting in DPL of 1013.80 mGy cm (Image C) and 553.80 mGy cm (Image D). Image E was acquired with the same scan parameters utilized in the study except that a higher pitch of 0.84 was used, yielding a DLP of 792.90 mGy cm. Other phantom Images F, G and H were obtained using different tube potentials of

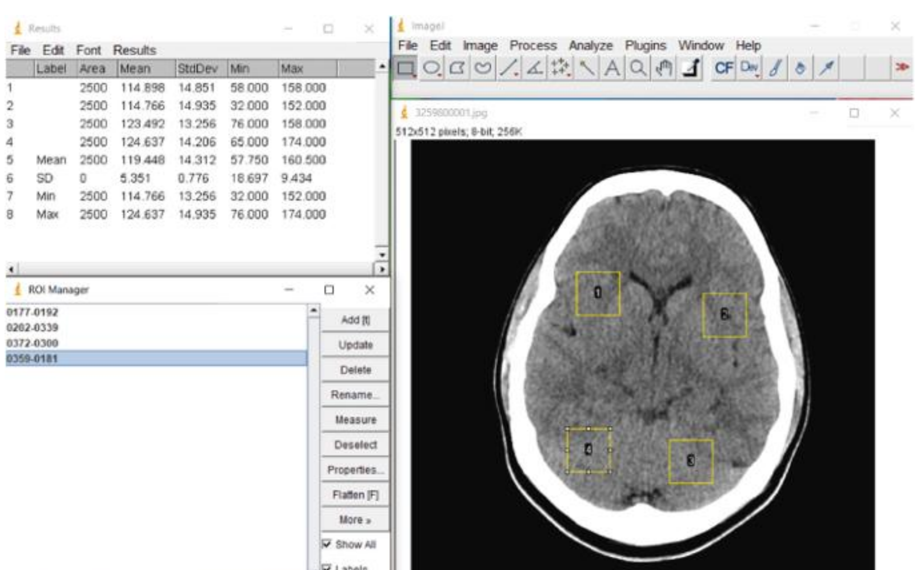


**Fig. 1.** Analysis of image quality using ImageJ software.

120.00 kV, 100.00 kV and 80.00 kV respectively with the AEC standard (Sure Exp. 3D) switched on. The resulting DLP values were 1227.70 mGy cm, 1176.00 mGy cm and 778.80 mGy cm, respectively.

In accordance with the Rose model criteria (Burgess, 1999; Hsieh et al., 2022), a signal must be five standard deviations from the above background to be detectable. This means that diagnostic images with SNR >5 are adjudged as having acceptable image quality. In this study, the calculated SNRs for all the phantom images at the different parameters exceeded 5 except for Images D, E and H. The highest SNR of 6.88 was found for Image A, which was acquired with the routine scan protocol for adult head CT. A reduced tube current of 200.00 mA for Image B resulted in reduced SNR of 5.25. Also, using reduced tube potentials of 100.00 kV and 80.00 kV for Images C and D resulted in reduced SNR values of 5.49 and 3.50 respectively. Accordingly, Image D was declared unfit for diagnostic purposes. An increased pitch factor of 0.84 for image E resulted in an SNR of 4.9 and hence was also regarded as unfit for diagnostic purposes. Images F, G, and H were obtained with the AEC switched on which yielded SNRs of 6.11, 5.62, and 4.63 respectively.

A comparison of DLP and SNR as well as the $D_{eff}$ and SNR of the various studied protocols for head CT imaging are presented in Figs. 2 and 3 and showed that 5 out of 8 phantom images (Images A, B, C, F, and H) satisfied the Rose model's acceptance criteria for good image quality.

The lowest DLP (1013.80 mGy cm) and $D_{eff}$ (2.33 mSv) were estimated for Image C which was subsequently, selected as the best option among the optimized images. This was achieved by reducing the tube potential from 120.00 kV to 100.00 kV while keeping other parameters unchanged. This resulted in a 40.4% reduction in $D_{eff}$ through the optimization process without deteriorating image quality.

## 4. Discussions

### 4.1. Patient characteristics

According to the age distribution (age range: 18–94 years; mean age: 51.83 ± 17.54 years), the majority of patients were younger and middle-aged (58.2%) compared to older adults (41.8%). However, the largest referrals for head CT examinations were recorded among patients aged 58–67 years (21.2%), of whom the majority were males (11.0%). This finding may be associated with a higher incidence of dementia as well as Parkinson's disease with old age as suggested by Orozco-Arroyave et al. (2014) for which head CT examination may be the first line for diagnosis. Hernández et al. (2015) observed that the proportion of individuals that undergo medical imaging procedures increased with age.

More female patients (52.2%) presented for head CT examinations.

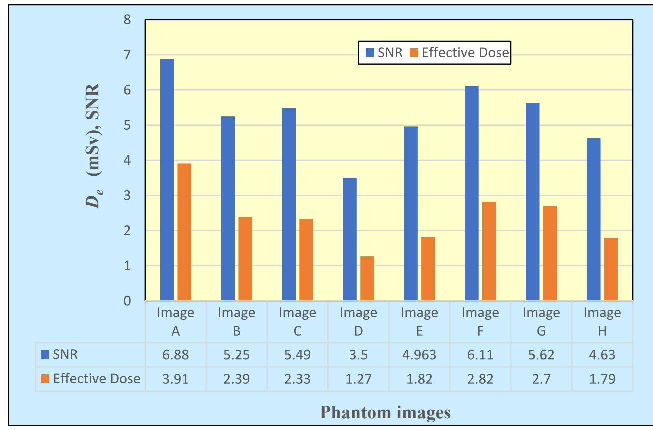


**Fig. 3.** Comparison of $D_{eff}$ and SNR values associated with the studied protocols.

Consistent with the literature, Akyea-Larbi (2015) reported that more females (67.6%) than males (32.4%) presented for CT procedures in a Ghanaian health facility, while Shrimpton et al. (2016) indicated that more females (60.0%) presented for head CT examinations than males (40.0%). In the context of cumulative radiation exposures, the findings of this study suggest that females are more liable to medical radiation exposures and associated risks from CT examinations, and are thus, more likely to develop radiation-induced stochastic and non-stochastic damages as well as diseases such as cancer (Smith-Bindman et al., 2011).

### 4.2. Dosimetry

Constant values of $CTDI_{vol}$ for adult head CT were recorded at the CT unit irrespective of patient age or gender. This may be attributed to the use of fixed exposure factors and pitch. The mean value of the $CTDI_{vol}$ was 86.00 ± 0.00 mGy. The DLP values however varied depending on the area of coverage selected by the radiographer, with corresponding recorded mean and 75th percentile values of 1559.68 ± 197.18 mGy cm and 1613.60 mGy cm respectively. This yielded a substantially high mean $D_{eff}$ of 3.57 ± 0.46 mSv compared with the ICRP international standards.

The measured $CTDI_{vol}$ and DLP values obtained in this study were comparatively higher than reported elsewhere in the literature (Table 3), necessitating actions to reduce the radiation doses. In a Kenyan study conducted on 50% of CT facilities in that setting, Korir

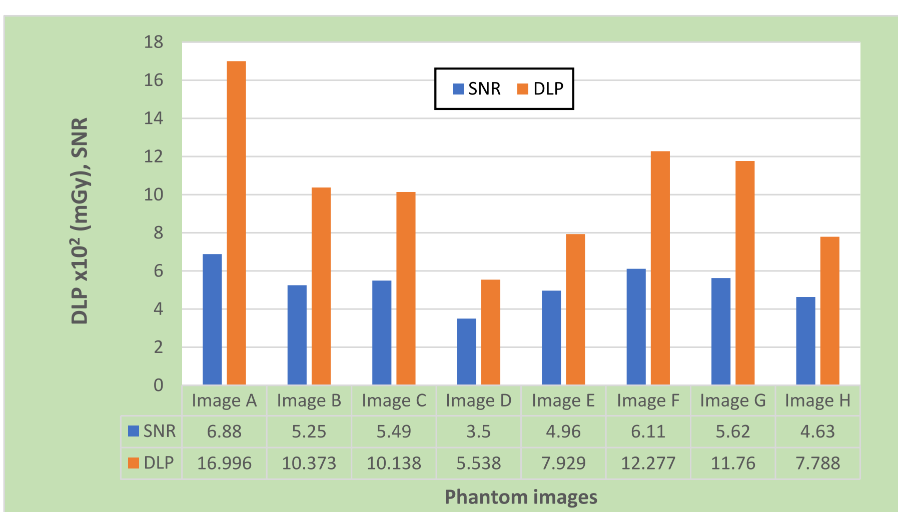


**Fig. 2.** Comparison of DLP and SNR values associated with the studied protocols.

**Table 3**
Exposure parameters and dosimetry.

| Reported studies | Mean values | | 75th percentile |
|---|---|---|---|
| | $CTDI_{vol}$ (mGy) | DLP (mGy.cm) | DLP (mGy.cm) |
| This study | **86.00** | **1559.68** | **1613.60** |
| Shrimpton et al [7] | – | – | 787.00 |
| Bongartz et al [22] | – | – | 1050.00 |
| ACR [24] | – | – | – |
| Korir et al [29] | 55.00 | 1274.00 | 1612.00 |
| Salama et al [30] | 28.80 | 1000.50 | 1358.60 |
| Tsapaki et al [31] | 39.00 | 527.00 | 544.00 |
| Sakhnini [32] | 43.80 | 760.00 | – |
| Gharbi et al [33] | 46.79 | 837.25 | – |
| Toori et al [34] | – | – | 750.00 |
| Moifo et al [35] | – | – | 1151.00 |
| Najafi et al [36] | – | – | 700.00 |
| Brix et al [42] | 60.60 | 1016.00 | – |
| ICRP 73 [43] | – | – | 1050.00 |

- = No available data given in the publication.

et al. (2016) reported optimized mean $CTDI_{vol}$ and DLP doses of 55.00 mGy and 1274.00 mGy cm respectively. Although a lower average $CTDI_{vol}$ value of 28.80 mGy was reported in an Egyptian study conducted on a cohort of 900 patients undergoing head CT examination, Salama et al. (2017) concluded that further actions were needed to reduce the DLP of 1000.50 mGy cm. Tsapaki et al. (2006) also reported mean $CTDI_{vol}$ and DLP values of 39 mGy and 527 mGy cm in a dose-reduction head CT scans study. Substantial dose-reductions in CT examinations are achievable through dose optimization strategies. In particular, Sakhnini (2017) recorded a 44.3% reduction in $CTDI_{vol}$ and a 37.6% reduction in DLP after optimization. In a dose optimization study employing the use of tube current modulation (AEC), Gharbi and Labidi (2017) also stated a 20.1% reduction in average $D_{eff}$ without loss of image quality.

From Table 3, the 75th percentile values for the CT dose descriptors were also higher than the ICRP 73 recommendations of 60.0 mGy for $CTDI_{vol}$ and 1050.00 mGy cm for the DLP. Toori et al. (2015) reported large scales of CT dose for the same examination among 7 different Iranian hospitals and, therefore, established optimized $CTDI_{vol}$ and DLP doses of 59.5 mGy and 750 mGy cm respectively, which were relatively lower compared to the ICRP 73 reference doses. Other studies (Bongartz et al., 2000; Shrimpton et al., 2016) have demonstrated similar and lower findings concerning dose-reductions. The difference between reported values in this study and the literature is explained by the use of higher exposure parameters at the study site, which required dose-reduction strategies to keep the patient dose ALARA.

### 4.3. Dose optimization for adult head CT examination

According to Power et al. (2016), several dose optimization strategies are available. Optimization methods for Images C and G were considered suitable and acceptable for this study site, subsequent to a 16.7% reduction in tube potential (Image C) with a slight increase in noise (20.20%) as shown in the SNR value. However, this increase did not sufficiently degrade the image quality for the intended clinical purpose since the subjective assessment or radiologists reported the images as good for the task (as shown in Table 4). Therefore, the associated exposure parameters (Table 4) are recommended for head CT examinations using the only AquilionOne 640-slice scanner currently in use in Ghana. Meanwhile, it was also found that AEC may be used in circumstances where image quality may have considerably deteriorated while employing fixed tube potential. This will also result in a significant dose-reduction, as predicted by Zarb et al. (2011) and confirmed with a 31.0% $D_{eff}$ reduction (Image G) with a good radiologist comment. The results of this study are further supported by Khan et al. (2013) who indicated that a reduction in tube voltage from 120.0 kVp to 100.0 kVp reduces radiation dose by 33.0%. Smith-Bindman et al. (2019) also suggested that a 50.0% dose-reduction is achievable without reducing its diagnostic purpose.

Vetter (2008) reported that dose-reduction strategies using AEC systems significantly reduced radiation dose in CT imaging. However, Greess et al. (2000) emphasized that the use of AEC as a dose-reduction approach was dependent on the scanned body region and certain circumstances. According to Singh et al. (2011), the use of AEC may not be recommended in CT head scans due to the fact that the variations of patients' brain sizes and shapes are expected to be small. Also, relatively different lesser attenuations in the head compared to other regions may attribute to the poor recommendation of AEC in head CT scans. Generally, AEC systems reduce patient dose; therefore in cases where image quality may be significantly deteriorated using fixed tube current and tube potential, AEC may be incorporated (Greess et al., 2000). If the use of AEC is prevalent, then the optimization method adopted for image G in this study will be deemed suitable for diagnostic purposes, even though it is expected that the dose-reductions by using AEC would be small for these patients.

## 5. Conclusion

The measured $CTDI_{vol}$ and DLP values were higher than the ICRP 73 recommended values and other published studies. The consideration of tube potential alteration and utilization of AEC as dose optimization protocols for adult head CT examinations resulted in reductions in the DLP and $D_{eff}$ without affecting image quality sustancially for diagnostic purposes. Therefore the study recommends optimization methods C and the associated exposure parameters (Table 4) for scanning CT head when using the only AquilionOne-640 slice scanner currently in Ghana. However, due to the small variations in patients' head sizes and shapes, the AEC approach is not strongly recommended and may be utilized when fixed tube potential significantly deteriorates image quality.

## Funding

This research did not receive any specific grant from funding agencies in the public, commercial, or not-for-profit sectors.

**Table 4**
Mean phantom dose descriptor values, SNR and subjective assessment of images obtained with different exposure parameters.

| Image ID | SL (cm) | Tube voltage (kV) | Tube current mA | Pitch | $CTDI_{vol}$ (mGy) | DLP (mGy. cm) | $D_{eff}$ (mSv) | AEC | SNR | Radiologist quality assessment comment |
|---|---|---|---|---|---|---|---|---|---|---|
| A | 18.00 | 120.00 | 300.00 | 0.66 | 86.00 | 1699.60 | 3.91 | No | 6.88 | Good |
| B | 18.00 | 120.00 | 200.00 | 0.66 | 52.50 | 1037.30 | 2.39 | No | 5.25 | Good |
| C | 18.00 | 100.00 | 300.00 | 0.66 | 51.30 | 1013.80 | 2.33 | No | 5.49 | Good |
| D | 18.00 | 80.00 | 300.00 | 0.66 | 28.00 | 553.80 | 1.27 | No | 3.50 | Bad |
| E | 18.00 | 100.00 | 300.00 | 0.84 | 39.90 | 792.90 | 1.82 | No | 4.96 | Bad |
| F | 18.00 | 120.00 | 124.00 | 0.66 | 62.10 | 1227.70 | 2.82 | Yes | 6.11 | Good |
| G | 18.00 | 100.00 | 191.00 | 0.66 | 59.50 | 1176.00 | 2.70 | Yes | 5.62 | Good |
| H | 18.00 | 80.00 | 315.00 | 0.66 | 39.40 | 778.80 | 1.79 | Yes | 4.63 | Bad |

## Author statement

All authors disclose that there have no financial or personal relationships that may be perceived as influencing their work. The corresponding author of this manuscript certifies that the contributors' and conflicts of interest statements included in this paper are correct and have been approved by all co-authors.

## Declaration of competing interest

The authors declare that they have no known competing financial interests or personal relationships that could have appeared to influence the work reported in this paper.

## Data availability

Data will be made available on request.

## Acknowledgement

The support of the radiology department of the hospital is duly acknowledged.

## References

ACR, 2008. ACR Practice Guideline for Diagnostic Reference Levels in Medical X-Ray Imaging, vols. 1–6. Continuing Medical Education.
Akyea-Larbi, K.O., 2015. Effective Dose Estimation and Cancer Risk Assessment Due to Some Selected CT Examinations at Sweden Ghana Medical Centre. M.Phil. Thesis. University of Ghana.
Alm-Carlsson, G., Dance, D.R., DeWerd, L., Kramer, H.-M., Ng, K.-H., Pernicka, F., Ortiz-Lopez, P., 2007. Dosimetry in Diagnostic Radiology: an International Code of Practice IAEA Technical Reports Series No. 457. International Atomic Energy Agency), Vienna.
Anim-Sampong, S., Antwi, W.K., Ohene-Botwe, B., Boateng, R.S., 2016. Comparison of 640-slice Aquilon ONE CT scanner's measured dosimetric parameters with ICRP dose reference levels for head, chest, and abdominal CT examinations. Saf. Health 2 (1), 1–8.
Bauhs, J.A., Vrieze, T.J., Primak, A.N., Bruesewitz, M.R., McCollough, C.H., 2008. CT dosimetry: comparison of measurement techniques and devices. Radiographics : a review publication of the Radiological Society of North America. Inc 28 (1), 245–253. https://doi.org/10.1148/rg.281075024.
Bongartz, G., Golding, S.J., Jurik, A.G., Leonardi, M., Meerten, Geleijns, J., Jessen, K.A., Panzer, W., Shrimpton, P.C., Tosi, G., 2000. European Guidelines on Quality Criteria for Computed Tomography. - Publications Office of the EU, European Commission.
Botwe, B.O., Schandorf, C., Inkoom, S., Faanu, A., Rolstadaas, L., Goa, P.E., 2021. National indication-based diagnostic reference level values in computed tomography: preliminary results from Ghana. Phys. Med. 84 (March), 274–284.
Botwe, B., Schandorf, C., Inkoom, S., Faanu, A., 2020. An investigation into the infrastructure and management of computerized tomography units in Ghana. J. Med. Imag. Radiat. Sci. 51 (1), 165–172.
Brady, S.L., Mirro, A.E., Moore, B.M., Kaufman, R.A., 2015. How to appropriately calculate effective dose for CT using either size-specific dose estimates or dose-length product. Am. J. Roentgenol. 204 (5), 953–958.
Burgess, A.E., 1999. The Rose model, revisited. J. Opt. Soc. Am. A 16 (3), 633–646.
Chang, K.-P., Hsu, T.-K., Lin, W.-T., Hsu, W.-H., 2017. Optimization of dose and image quality in adult and pediatric computed tomography scans. Radiat. Phys. Chem. 140, 260–265. https://doi.org/10.1016/j.radphyschem.2017.02.006.
Demb, J., Chu, P., Nelson, T., Hall, D., Seibert, A., Lamba, R., Boone, J., Krishnam, M., Cagnon, C., Bostani, M., Gould, R., Miglioretti, D., Smith-Bindman, R., 2017. Optimizing radiation doses for computed tomography across institutions: dose auditing and best practices. JAMA Intern. Med. 177 (6), 810–817.
Gharbi, S., Labidi, S., 2017. Radiation dose optimization in computed tomography with current modulation and Iterative Reconstruction. In: 2016 7th International Conference on Sciences of Electronics, Technologies of Information and Telecommunications, (SETIT), pp. 220–223, 2016.
Greess, H., Wolf, H., Baum, U., Lell, M., Pirkl, M., Kalender, W., Bautz, W.A., 2000. Dose reduction in computed tomography by attenuation-based on-line modulation of tube current: evaluation of six anatomical regions. Eur. Radiol. 10 (2), 391–394. https://doi.org/10.1007/s003300050062.
Hernández, L., Terradas, M., Camps, J., Martín, M., Tusell, L., Genescà, A., 2015. Aging and radiation: bad companions. Aging Cell 14 (2), 153–161.
Hsieh, S.S., Leng, S., Yu, L., Huber, N.R., McCollough, C.H., 2022. A minimum SNR criterion for computed tomography object detection in the projection domain. Med. Phys. 49, 4988–4998.
Khan, A.N., Khosa, F., Shuaib, W., Nasir, K., Blankstein, R., Clouse, M., 2013. Effect of tube voltage (100 kVp vs. 120 kVp) on radiation dose and image quality using prospective gating 320-row multi-detector computed tomography angiography. J. Clin. Imaging Sci. 3, 62.
Kisembo, N.H., Kisembo, H., Samson, S., Kavuma, A., Nakatudde, R., Bugeza, S., 2015. A survey of pediatric CT radiation doses in two selected hospitals in Kampala, Uganda: a radiation safety survey of paediatric CT radiation doses in two selected hospitals in Kampala, Uganda: a radiation safety concern. Int. J. Cancer Ther. Oncol. 3 (3), 13–17.
Korir, G.K., Wambani, J.S., Korir, I.K., Tries, M.A., Boen, P.K., 2016. National diagnostic reference level initiative for computed tomography examinations in Kenya. Radiat. Protect. Dosim. 168 (2), 242–252. https://doi.org/10.1093/rpd/ncv020.
Nagel, H.D., 2007. CT parameters that influence the radiation dose. In: Tack, D., Gevenois, P.A. (Eds.), Radiation Dose from Adult and Pediatric Multidetector Computed Tomography. Medical Radiology. Springer, Berlin, Heidelberg, pp. 51–79. https://doi.org/10.1007/978-3-540-68575-3_4.
Orozco-Arroyave, J.R., Arias-Londõ No, J.D., Vargas-Bonilla, J.F., González-Rátiva, M.C., Nöth, E., 2014. New Spanish speech corpus database for the analysis of people suffering from Parkinson's disease. In: Proceedings of the Ninth International Conference on Language Resources and Evaluation (LREC'14), 342–347, Reykjavik, Iceland. European Language Resources Association (ELRA).
Postorino, M., Lizio, D., De Mauri, A., Marino, C., Tripepi, G.L., Zoccali, C., Brambilla, M., Balestra, E., Bellino, D., Benevento, R., Bregant, C., Bregant, P., Cannillo, B., Casto, G., Chiarinotti, D., Cimolai, S., Colussi, G., De Agostini, A., Declich, F., et al., 2021. Radiation dose from medical imaging in end-stage renal disease patients: a Nationwide Italian Survey. J. Nephrol. 1–9.
Power, S.P., Moloney, F., Twomey, M., James, K., O'Connor, O.J., Maher, M.M., 2016. Computed tomography and patient risk: facts, perceptions and uncertainties. World J. Radiol. 8 (12), 902.
Sackey, T.A., 2015. Cancer Risk Assessment of Patients Undergoing Computed Tomography Examination at the Korle Bu Teaching Hospital (KBTH). University of Ghana. http://ugspace.ug.edu.gh.
Sakhnini, L., 2017. CT radiation dose optimization and reduction for routine head, chest and abdominal CT examination. Radiol. Diagn. Imaging 2 (1), 1–4. https://doi.org/10.15761/RDI.1000120.
Salama, D.H., Vassileva, J., Mahdaly, G., Shawki, M., Salama, A., Gilley, D., Rehani, M. M., 2017. Establishing national diagnostic reference levels (DRLs) for computed tomography in Egypt. Phys. Med. 39, 16–24.
Semelka, R.C., Armao, D.M., Elias, J., Huda, W., 2007. Imaging strategies to reduce the risk of radiation in CT studies, including selective substitution with MRI. J. Magn. Reson. Imag. 25 (5), 900–909.
Shrimpton, P.C., Jansen, J.T., Harrison, J.D., 2016. Updated estimates of typical effective doses for common CT examinations in the UK following the 2011 national review. Br. J. Radiol. 89 (1057), 20150346.
Singh, S., Kalra, M.K., Thrall, J.H., Mahesh, M., 2011. Pointers for optimizing radiation dose in head CT protocols. J. Am. Coll. Radiol. 8 (8), 591–593. https://doi.org/10.1016/j.jacr.2011.05.001.
Smith-Bindman, R., Miglioretti, D.L., McCollough, C.H., Leng, S., Yu, L., Cody, D.D., Boone, J.M., McNitt-Gray, M.F., 2011. CTDI $_{vol}$, DLP, and effective dose are excellent measures for use in CT quality improvement. Radiology 261 (3), 999.
Smith-Bindman, R., Wang, Y., Chu, P., Chung, R., Einstein, A.J., Balcombe, J., Cocker, M., Das, M., Delman, B.N., Flynn, M., Gould, R., Lee, R.K., Yellen-Nelson, T., Schindera, S., Seibert, A., Starkey, J., Suntharalingam, S., Wetter, A., Wildberger, J. E., Miglioretti, D.L., 2019. International variation in radiation dose for computed tomography examinations: prospective cohort study. BMJ 364, 1–12.
Sodickson, A., Baeyens, P.F., Andriole, K.P., Prevedello, L.M., Nawfel, R.D., Hanson, R., Khorasani, R., 2009. Recurrent CT, cumulative radiation exposure, and associated radiation-induced cancer risks from CT of adults. Radiology 251 (1), 175–184.
Strauss, K.J., 2014. Developing patient-specific dose protocols for a CT scanner and exam using diagnostic reference levels. Pediatr. Radiol. 44 (3), 479–488.
Toori, J.A., Shabestani-Monfared, A., Deevband, M.R., Nabahati, M., 2015. Dose assessment in computed tomography examination and establishment of local diagnostic reference levels in Mazandaran, Iran. J. Biomed. Phys. Eng. 5 (4), 177–184.
Tsapaki, V., Aldrich, J.E., Sharma, R., Staniszewska, M.A., Krisanachinda, A., Rehani, M., Hufton, A., Triantopoulou, C., Maniatis, P.N., Papailiou, J., Prokop, M., 2006. Dose reduction in CT while maintaining diagnostic confidence: Diagnostic Reference Levels at routine head, chest, and abdominal CT-IAEA-Coordinated Research Project 1. Radiology 240 (3).
Vetter, R.J., 2008. ICRP publication 103, the recommendations of the international Commission on radiological protection. Health Phys. 95 (4), 445–446.
WHO, 2021. World Health Organization Imaging Modalities. https://www.who.int/diagnostic_imaging/imaging_modalities/dim_comptomography/en/.
Zarb, F., Rainford, L., McEntee, M.F., 2011. Developing optimized CT scan protocols: phantom measurements of image quality. Radiography 17 (2), 109–114.

Journal of Radiation Research and Applied Sciences 18 (2025) 101771

Contents lists available at ScienceDirect

Journal of Radiation Research and Applied Sciences

journal homepage: www.journals.elsevier.com/journal-of-radiation-research-and-applied-sciences

# On cranial CT imaging: The role of low-dose protocols in enhancing patient safety and reducing radiation exposure

Duygu Tunçman Kayaokay [a], Fahrettin Fatih Kesmezacar [b], Osman Günay [c], Songül Çavdar Karaçam [d], Ali Demirci [e], Mustafa Demir [f], Ghada ALMisned [g], Huseyin Ozan Tekin [h,i,*]

[a] Istanbul University-Cerrahpasa, Vocational School of Health Services, Radiotherapy Program, Istanbul, Turkey
[b] Istanbul University-Cerrahpasa, Vocational School of Health Services, Medical Imaging Techniques Program, Istanbul, Turkey
[c] Yıldız Technical University, Faculty of Electrical & Electronics, Biomedical Engineering, Istanbul, Turkey
[d] Istanbul University – Cerrahpasa, Vocational School of Health Services, Radiotherapy Program, Istanbul, Turkey
[e] Istinye University, Faculty of Medicine, Radiology Department, Istanbul, Turkey
[f] Istanbul University – Cerrahpasa, Cerrahpasa Faculty of Medicine, Department of Internal Medicine Department of Nuclear Medicine, Istanbul, Turkey
[g] Department of Physics, College of Science, Princess Nourah Bint Abdulrahman University, P.O. Box 84428, Riyadh 11671, Saudi Arabia
[h] Department of Medical Diagnostic Imaging, College, of Health Sciences, University of Sharjah, Sharjah, United Arab Emirates
[i] Computer Engineering Department, Faculty of Engineering and Natural Sciences, Istinye University, Istanbul, Turkey

ARTICLE INFO

*Keywords:*
Computed tomography (CT)
Radiation dose reduction
Low-dose protocols
Organ doses
ALARA principle
Cranial imaging

ABSTRACT

This study evaluates the impact of low-dose protocols on radiation dose reduction for critical organs during cranial CT imaging, adhering to the ALARA (As Low As Reasonably Achievable) principle. Using the Alderson Rando Phantom and MTS-100 thermoluminescent dosimeters, absorbed doses in radiosensitive organs, such as the thyroid, eye lenses, and salivary glands, were quantified under low-dose (350 mAs) and high-dose (671 mAs) imaging protocols. The Siemens Somatom Definition AS + CT scanner facilitated protocol optimization through adjustable tube current and pitch parameters. Low-dose protocols significantly reduced absorbed doses across critical organs. The thyroid exhibited a reduction exceeding 64 %, while eye lens doses decreased by over 50 %. Salivary glands and brain tissues demonstrated reductions ranging from 30 % to 46 %. Statistical analyses, including paired t-tests and Mann-Whitney U tests, confirmed the significance of these findings ($p < 0.05$). Despite reduced radiation exposure, diagnostic image quality was preserved. This research highlights the efficacy of protocol optimization in mitigating radiation risks, particularly for radiosensitive organs and frequent imaging scenarios. It can be concluded that adhering to international dose guidelines and emphasizing the implementation of low-dose protocols are essential for ensuring patient safety and maintaining diagnostic accuracy in clinical practice.

## 1. Introduction

Computed Tomography (CT) technology has become an indispensable tool for detailed anatomical imaging of the head and neck region, significantly contributing to medical diagnosis and treatment planning. However, the ionizing radiation used during CT scans, particularly in repeated scans or when high-dose protocols are employed, raises concerns regarding the radiation dose absorbed by patients (Sodickson et al., 2009). This is especially important for critical organs in the head and neck region, such as the eye lenses, thyroid gland, and brain tissue, which are highly sensitive to ionizing radiation (Perisinakis et al., 2005). Among these, the eye lenses are particularly susceptible to cataract formation, the thyroid gland is vulnerable to long-term radiation-induced effects, and the brainstem, although generally receiving lower doses, requires precise dose measurements. Similarly, salivary glands are associated with side effects such as xerostomia (dry mouth) (Jensen et al., 2019). The protocol parameters used in CT imaging such as tube current, tube voltage, slice thickness, and scan interval play a critical

* Corresponding author. Department of Medical Diagnostic Imaging, College, of Health Sciences, University of Sharjah, Sharjah, United Arab Emirates.
*E-mail addresses:* duygu.tuncman@iuc.edu.tr (D. Tunçman Kayaokay), f.kesmezacar@iuc.edu.tr (F.F. Kesmezacar), ogunay@yildiz.edu.tr (O. Günay), songul.karacam@iuc.edu.tr (S. Çavdar Karaçam), ali.demirci1@istinye.edu.tr (A. Demirci), mustafa.demir@iuc.edu.tr (M. Demir), gaalmisned@pnu.edu.sa (G. ALMisned), htekin@sharjah.ac.ae, tekin765@gmail.com (H.O. Tekin).

https://doi.org/10.1016/j.jrras.2025.101771
Received 23 January 2025; Received in revised form 26 June 2025; Accepted 6 July 2025
Available online 12 July 2025
1687-8507/

role in determining both the radiation dose and the image quality (Günay et al., 2020). Additionally, parameters like the Computed Tomography Dose Index (CTDI) and Dose-Length Product (DLP) provide key insights into the local and overall radiation burden. CTDI represents the radiation dose for a single CT slice, measured in milligray (mGy), while DLP combines CTDI with the scan length to estimate the total radiation dose in milligray-centimeters (mGy·cm) (Mohd, 2024). Optimizing these parameters can reduce patient dose without compromising diagnostic image quality. In recent years, there has been a growing emphasis on developing and implementing low-dose protocols to enhance patient safety and reduce radiation risks (Anim-Sampong et al., 2023). These protocols focus on reducing parameters such as tube current (mA) and pitch while maintaining diagnostic image quality through advanced reconstruction techniques. Studies have shown that low-dose protocols can reduce radiation dose to critical organs by 30–60 %, underscoring the need for optimal parameter settings (Santos et al., 2019). While high-dose protocols offer superior image quality, they may expose critical organs to unnecessary radiation, emphasizing the importance of dose optimization strategies (Toori et al., 2015). Meanwhile, phantom-based dosimetry studies play a crucial role in evaluating the effects of low-dose protocols, providing reliable and reproducible data on critical organ doses. These studies enable comparisons between low-dose and high-dose protocols, aiding in the identification of the most appropriate parameters to ensure patient safety (Husseiny Salama et al., 2017). This study aims to compare the absorbed doses in critical organs during low- and high-dose cranial CT scans using the Alderson Rando Phantom® model. By analyzing organ-specific absorbed doses in conjunction with CTDI and DLP values, the effectiveness of low-dose protocols in mitigating radiation risks is assessed. The findings are crucial for revising scanning protocols and adhering to the "As Low As Reasonably Achievable" (ALARA) principle to enhance patient safety (Alashban & Alghamdi, 2025). Ionizing radiation is a well-documented risk factor for inducing stochastic effects, including cancer, particularly in radiosensitive tissues like the thyroid and lens of the eyes. In children and patients requiring frequent imaging, these risks are further magnified (Kleinerman, 2006; International Atomic Energy Agency (IAEA), 2013). This study provides a quantitative assessment of absorbed doses in critical organs, demonstrating how low-dose protocols can effectively reduce radiation exposure without compromising diagnostic image quality. The research utilized the Alderson Rando Phantom, a widely recognized model designed to simulate human anatomy and tissue responses to radiation with high fidelity. Measurement points corresponding to critical organs were equipped with thermoluminescent dosimeters (TLDs) to accurately quantify radiation doses. The study employed a Siemens Somatom Definition AS + CT scanner, a multi-slice system with advanced imaging capabilities, including customizable parameters such as tube voltage, current, and pitch, which were adjusted for both low- and high-dose protocols. These parameters were carefully selected to analyze their impact on dose distributions to critical organs like the eye lenses, thyroid, and salivary glands. By integrating phantom-based dosimetry with precise imaging equipment, this research effectively evaluates dose optimization strategies and their implications for patient safety in routine clinical settings.

## 2. Materials and methods

### 2.1. Phantom and experimental setup

This study employed the Alderson Rando Phantom to simulate human anatomy and tissue interactions with ionizing radiation (see Fig. 1). The phantom is composed of tissue-equivalent materials with a density of 0.985 g/cm$^3$, providing realistic dosimetric results comparable to actual patient scenarios (Rodrigues et al., 2023). The skeleton of the phantom is constructed using natural human bone powder, and the model represents a female body with a height of 155 cm and a weight of 50 kg. It consists of 32 horizontal cross-sectional slices, each 2.5 cm thick, which can be separated to allow precise placement of dosimeters in cavities corresponding to critical organs (Jeong et al., 2012). For dose measurements, MTS-100 thermoluminescent dosimeters (TLDs) were utilized. These dosimeters are made of lithium fluoride doped with magnesium and titanium (LiF:Mg,Ti), which provides a stable response across a broad energy spectrum ranging from 10 keV to 3 MeV. This characteristic ensures accurate measurements of various radiation types, making MTS-100 TLDs a reliable tool for evaluating organ-specific doses. The TLDs were strategically placed in the phantom slices corresponding to critical organs to measure absorbed radiation doses. Table 1

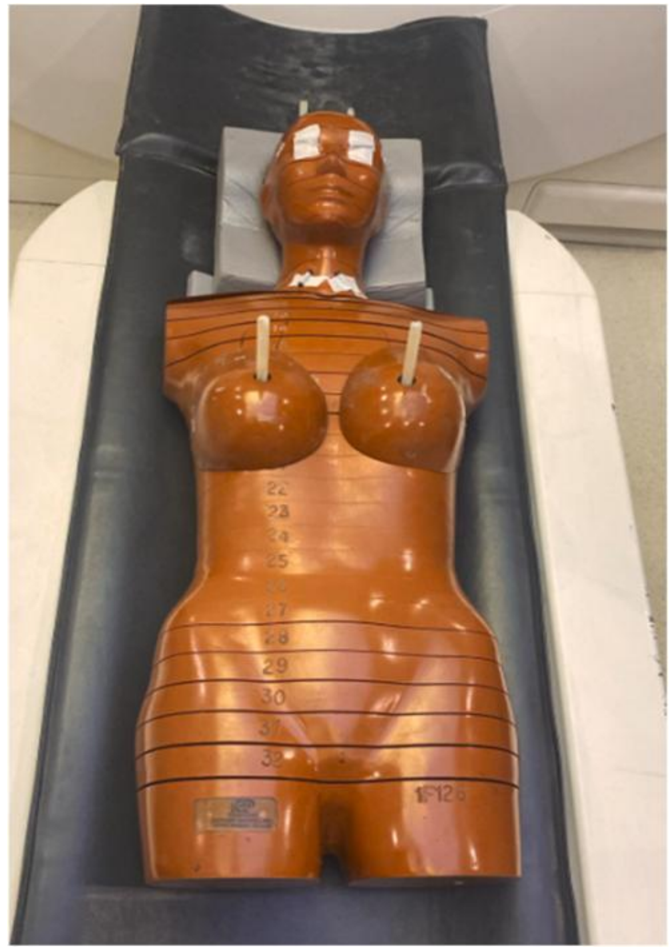

**Fig. 1.** Physical appearance of utilized Alderson Rando Phantom.

**Table 1**
Placement of TLDs in slices within the Alderson Rando Phantom.

| Phantom Slice | Organ | TLD ID |
|---|---|---|
| 10 | Right Thyroid | 1–2 |
| 10 | Left Thyroid | 3–4 |
| 7 | Sublingual Gland | 5–6 |
| 6 | Spinal Cord (C1-C2) | 7–8 |
| 6 | Left Parotid Gland | 9–10 |
| 6 | Right Parotid Gland | 11–12 |
| 6 | Right Mandibular Gland | 13–14 |
| 6 | Left Mandibular Gland | 15–16 |
| 3 | Left Temporal Squamous | 17–18 |
| 3 | Right Temporal Squamous | 19–20 |
| 3 | Pituitary Gland | 21–22 |
| 3 | Ethmoid Bone | 23–24 |
| 3 | Right Lens | 25–26 |
| 3 | Left Lens | 27–28 |
| 10 | Left Thyroid Surface | 29–30 |
| 10 | Right Thyroid Surface | 31–32 |

provides the detailed mapping of the TLD placement, including the phantom slice number, associated organ, and TLD identification numbers.

### 2.2. TLD calibration process

The TLDs were calibrated at the Radkor Dosimetry Laboratory to ensure measurement accuracy. During calibration, the dosimeters were exposed to a known radiation dose (10.03 mSv, equivalent to 10.03 mGy with 3.2 mm Al filtration) and their light outputs were measured. Element Correction Coefficients (ECC) were applied to account for individual dosimeter variability and align their responses with the population mean. A total of 70 TLDs were initially zeroed and irradiated under controlled conditions at the Secondary Standards Dosimetry Laboratory (SSDL), with dosimeters showing ECC values within ±15 % considered acceptable. From this pool, the 20 best-performing TLDs with responses within ±1 % were selected for the study. These TLDs were further irradiated with doses ranging from 0.1 mSv to 200 mSv, and their calibration factors were determined to construct a calibration curve. This curve was subsequently used for dose calculations during the experimental measurements.

### 2.3. Device calibration process

The study was conducted using a Siemens Somatom Definition AS Plus single-source, multi-slice Computed Tomography (CT) scanner to evaluate critical organ doses and radiation dose optimization for cranial CT imaging. The CT system underwent thorough calibration and quality control assessments prior to its use in the study. The calibration was performed following internationally recognized standards, including the ACR CT QC Manual, EC Radiation Protection 162, IAEA HHS-19, IPEM 91, and TS EN 61223-3-5 guidelines (Edyvean, 2013; IPEM, 2002; McCollough et al., 2004; Sohrabi et al., 2018; Özden et al., 2014) The calibration and quality control tests involved the use of RaySafe CT Detectors in conjunction with standardized CTDI body and head phantoms to assess the accuracy of dose delivery. The technical parameters during calibration were set as follows: the tube voltage was 120 kVp, the current values were 200 mA for the body phantom and 250 mA for the head phantom, with a slice thickness of 1 × 10 mm and a tube rotation time of 1 s (see Tables 2 and 3). Measurements were conducted at both central and peripheral positions (North, East, South, and West) to evaluate dose distribution consistency. To ensure data reliability, calibration was performed under controlled environmental conditions: the ambient temperature was 22.5 °C, the atmospheric pressure was 1017 hPa, and the relative humidity was 45.1 %. The entire procedure was conducted by a qualified quality control expert and compliance with the specified standards was confirmed. The CT system, after successful calibration, was used to perform cranial CT imaging on the Alderson Rando phantom.

### 2.4. CT imaging protocol

The technical specifications of the CT scanner are detailed in Table 4. The scanner operates in multislice mode with options for 64, 128, or higher slices per rotation, providing high-resolution imaging essential for detailed cranial assessments. The scanner operates in multislice mode with 128 slices per rotation, providing high-resolution imaging essential for detailed cranial assessments. Gantry diameter is 78 cm, which accommodates the phantom while allowing for proper positioning and stability during scans. The scanner's table weight limit of 227 kg (500 lbs.) ensures robust support for various phantom and patient configurations. Additional technical features include a maximum scan range of 190 cm, enabling extensive coverage for full cranial or extended anatomical imaging. Although the scanner offers kVp options of 80, 100, 120, and 140, a fixed voltage of 100 kVp was used in both protocols, as shown in Table 5. The system supports flexible rotation speeds of 0.3, 0.5, 0.6, and 1.0 s per rotation, which facilitate protocol optimization for either rapid or detailed imaging needs. The x-ray tube heat capacity, ranging between 2.0 and 3.5 Mega Heat Units (MHU), ensures consistent performance during prolonged scans, particularly under high-dose protocols. The power requirement for the system is 0–400 kV-amperes (kVa), highlighting its operational efficiency and versatility for varying clinical conditions. These technical specifications allowed the implementation of both high-dose and low-dose protocols during imaging sessions. The flexibility in tube voltage, tube current, and rotation speed enabled precise adjustments for dose optimization while maintaining the image quality required for evaluating critical organ doses.

### 2.5. High-dose and low-dose imaging parameters

To evaluate the effects of low-dose and high-dose protocols on absorbed radiation doses in critical organs, two distinct imaging protocols were implemented using the Siemens Somatom Definition AS + CT scanner. The parameters were carefully chosen to reflect variations in tube current while maintaining other scanning conditions constant to ensure consistency and comparability. In both protocols, the tube voltage was set to 100 kVp, and the rotation time was fixed at 1 s per rotation. The slice thickness was kept at 1 mm, and the Field of View (FOV) remained constant at 241 mm for both settings. However, key variations were introduced in tube current and pitch, which directly influenced the dose metrics. In low-dose protocol, tube current was set to 350 mA with a pitch value of 0.65, optimizing the balance between radiation exposure and image quality. On the other hand, tube current was increased to 671 mA while reducing the pitch to 0.45 in high-dose protocol, leading to higher exposure for improved image resolution. The effects of these adjustments were reflected in the Computed Tomography Dose Index (CTDIvol) and Dose Length Product (DLP) values.

### 2.6. Image quality evaluation methods

The acquired volumetric data were exported in DICOM format for use in quantitative image analysis tools. Phantom image samples were analysed using Lite-IQ. Quantitative image quality was assessed using signal data obtained from regions of interest (ROIs) drawn over cortical bone and soft tissue (cerebrum) of equal size on the same axial slice in both Low Dose and High Dose acquisitions. Image quality evaluation was performed using the signal-to-noise ratio (SNR) and contrast-to-noise ratio (CNR) parameters, calculated according to Equations (1) and (2).

$$\mathrm{SNR} = \frac{\mathrm{HU(bone)}}{\mathrm{SD\ (soft\ tissue)}} \tag{1}$$

**Table 2**
Results of CT dose index (CTDI) measurements using a body phantom at different positions.

| Measure Position | Dose (mGy) | Dose (mGy) | Dose (mGy) | $CTDI_{100}$ | $CTDI_{vol}$ | Measured $CTDI_w$ | Observed $CTDI_w$ | Deviation |
|---|---|---|---|---|---|---|---|---|
| Center | 0.776 | 0.778 | 0.775 | 7.760 | 12.03 | 12.03 | 11.86 | 1.44 % |
| North | 1.551 | 1.553 | 1.554 | 15.53 | | | | |
| East | 1.402 | 1.405 | 1.404 | 14.04 | | | | |
| South | 1.289 | 1.290 | 1.291 | 12.90 | | | | |
| West | 1.418 | 1.419 | 1.421 | 14.19 | | | | |

**Table 3**
CT Dose Index (CTDI) measurements using a head phantom at various positions.

| Measure Position | Dose (mGy) | Dose (mGy) | Dose (mGy) | $CTDI_{100}$ | $CTDI_{vol}$ | Measured $CTDI_w$ | Observed $CTDI_w$ | Deviation |
|---|---|---|---|---|---|---|---|---|
| Center | 3.008 | 3.015 | 3.012 | 30.12 | 30.27 | 30.27 | 31.65 | −4.35 % |
| North | 3.181 | 3.175 | 3.179 | 31.78 | | | | |
| East | 3.044 | 3.045 | 3.041 | 30.43 | | | | |
| South | 2.888 | 2.890 | 2.895 | 29.91 | | | | |
| West | 3.026 | 3.027 | 3.031 | 30.28 | | | | |

**Table 4**
Siemens Somatom Definition AS + CT scanner technical specifications.

| Parameters | Values |
|---|---|
| CT scanner mode | Multislice (64, 128 or above) |
| Slices per rotation | 64 or 128 |
| Other rotation speed options (sec) | 0.3, 0.5, 0.6 & 1.0 |
| Minimum rotation speed | 0.3 |
| Gantry diameter | 78 cm |
| Table weight limit | 227 kg (500 lbs). |
| X-ray generator kV range | 80, 100, 120 and 140 |
| Maximum scan range | 190 cm |
| X-ray tube heat capacity | 2.0 to 3.5 MHU (Mega Heat Units) |
| Power requirement | 00 to 400 kVA |

**Table 5**
Exposure factors and scanning parameters.

| Scaning parameters | Low dose | High dose |
|---|---|---|
| Tube voltage (kVp) | 100 | 100 |
| Tube current (mA) | 350 | 671 |
| Rotation time (sec) | 1 s. | 1 s. |
| Pitch | 0.65 | 0.45 |
| Slice thickness (mm) | 1 | 1 |
| Field of View (FOV) | 241 | 241 |
| CTDI (mGy) | 30.50 | 58.74 |
| DLP (mGy.cm) | 518.5 | 998.58 |

$$\mathrm{CNR} = \frac{\mathrm{HU(bone)} - \mathrm{HU\ (soft\ tissue)}}{\mathrm{SD\ (soft\ tissue)}} \tag{2}$$

Here HU: Hounsfield Unit, SD: Standard deviation.

### 2.7. Data collection and analysis

Following irradiation, the dosimeters were retrieved and analysed to determine the absorbed doses for each organ. Dose measurements were expressed in milligrays (mGy) and were statistically analysed to compare differences between low- and high-dose protocols. The results were evaluated in conjunction with CTDI and DLP values to assess the efficiency and safety of dose optimization strategies.

### 2.8. Statistical analysis

To evaluate the significance of dose differences between high-dose and low-dose protocols, statistical tests were conducted for the critical organs. A paired *t*-test was performed to compare the absorbed doses under high-dose (671 mAs) and low-dose (350 mAs) protocols. The analysis yielded a t-value of 4.57 and a p-value of 0.00017. Since the p-value is well below the significance level of 0.05, the results confirm that the differences in absorbed doses between the two protocols are statistically significant. These findings reinforce the effectiveness of low-dose protocols in reducing organ-specific radiation exposure. The significant results highlight that reductions in radiation dose are not due to random variations but are directly attributable to protocol optimization. To further validate the findings, a non-parametric Mann-Whitney *U* test was conducted. The analysis resulted in a U-value of 238 and a p-value of 0.000036. The extremely low p-value confirms that the differences between high-dose and low-dose protocols are statistically significant across all measured critical organs. Both the paired *t*-test and Mann-Whitney *U* test consistently demonstrated significant dose reductions across critical organs when shifting from high-dose to low-dose protocols.

## 3. Results

### 3.1. Device calibration results

The calibration and quality control measurements for the Siemens Definition AS Plus CT scanner confirmed its compliance with dose accuracy requirements. Results obtained for the CTDI body and head phantoms demonstrated that the measured values were within acceptable limits, as defined by TS EN 61223-3-5 standards (see Tables 2 and 3). For the CTDI body phantom, the central dose value was measured as 7.76 mGy, while the peripheral dose values ranged between 12.03 mGy (East) and 14.19 mGy (West). The calculated CTDIvol for the body phantom was 12.03 mGy, which deviated by only 1.44 % from the system-reported value of 11.86 mGy. This minimal deviation confirms that the scanner delivers doses with a high level of precision. Similarly, for the CTDI head phantom, the central dose was 30.12 mGy, while peripheral dose measurements varied between 28.89 mGy (South) and 31.78 mGy (North). The calculated CTDIvol was 30.27 mGy, which showed a deviation of −4.35 % compared to the system-reported value of 31.65 mGy. These results highlight the accuracy and reliability of the dose measurements for both phantoms, with deviations well below the acceptable threshold of 20 % (see Table 2). For the low-dose protocol, the CTDIvol was 30.50 mGy, and the DLP was 518.5 mGy cm, indicating a reduced radiation burden. In comparison, the high-dose protocol resulted in a CTDIvol of 58.74 mGy and a DLP of 998.58 mGy cm, nearly doubling the radiation exposure. The detailed comparison of scanning parameters is presented in Table 5.

### 3.2. Absorbed organ dose measurements and image quality

This study evaluated the absorbed radiation doses in critical organs during cranial CT scans performed under high-dose (671 mAs) and low-dose (350 mAs) protocols. The results are summarized in Table 6, while Figs. 2 and 3 provide graphical representations of average doses by anatomical regions and the overall dose comparison. The absorbed doses in critical organs varied significantly between high-dose and low-dose protocols, as evident from Table 5. The thyroid exhibited the highest dose reduction among all organs, with the right thyroid receiving 76.07 ± 2.48 mGy in the high-dose protocol, compared to 25.60 ± 2.94 mGy in the low-dose protocol. This represents a 66.3 % reduction. The left thyroid followed a similar trend, with a reduction from 72.93 ± 2.95 mGy to 25.77 ± 0.15 mGy, marking a 64.8 % decrease. Fig. 2 clearly highlights the thyroid as the most exposed organ in the high-dose setting, emphasizing the importance of dose optimization to minimize unnecessary exposure. The salivary glands demonstrated moderate dose reductions under low-dose protocols. The left parotid dose decreased from 44.62 ± 1.04 mGy to 29.56 ± 1.53 mGy (33.7 % reduction), while the right parotid exhibited a similar drop of 33.1 %. Sublingual glands saw a dose reduction of 31.9 %, indicating the impact of tube current optimization on tissues located in proximity to the oral cavity. Fig. 2

**Table 6**
Critical organ doses for low and high dose protocols.

| Organ | High mAs Dose (mGy) and Standard Deviation | Low mAs Dose (mGy) and Standard Deviation | Difference (%) |
|---|---|---|---|
| Right Thyroid | 76.07 ± 2.48 | 25.60 ± 2.94 | 66.3 % |
| Left Thyroid | 72.93 ± 2.95 | 25.77 ± 0.15 | 64.8 % |
| Sublingual Gland | 30.79 ± 0.21 | 20.96 ± 3.97 | 31.9 % |
| Spinal Cord (C1-C2) | 36.95 ± 0.87 | 25.42 ± 2.68 | 31.1 % |
| Left Parotid Gland | 44.62 ± 1.04 | 29.56 ± 1.53 | 33.7 % |
| Right Parotid Gland | 40.96 ± 0.02 | 27.45 ± 2.52 | 33.1 % |
| Right Mandibular Gland | 35.85 ± 1.00 | 23.54 ± 2.93 | 34.3 % |
| Left Mandibular Gland | 33.07 ± 0.50 | 24.18 ± 0.28 | 27.0 % |
| Left Temporal Squamous | 36.62 ± 2.44 | 23.51 ± 4.13 | 35.8 % |
| Right Temporal Squamous | 42.64 ± 4.11 | 26.69 ± 5.58 | 37.6 % |
| Pituitary | 33.07 ± 2.47 | 19.13 ± 1.36 | 42.1 % |
| Ethmoid | 35.16 ± 2.67 | 18.94 ± 3.11 | 46.2 % |
| Right Lens | 38.14 ± 1.84 | 18.53 ± 0.96 | 51.7 % |
| Left Lens | 41.73 ± 3.29 | 18.94 ± 1.52 | 54.4 % |
| Left Thyroid Surface | 72.20 ± 10.05 | 36.72 ± 14.06 | 49.4 % |
| Right Thyroid Gland Surface | 72.16 ± 10.85 | 47.55 ± 19.57 | 34.3 % |

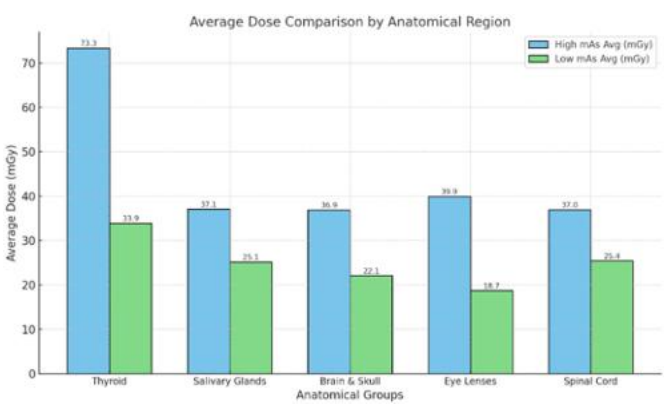


**Fig. 2.** Average dose graph for anatomical regions.

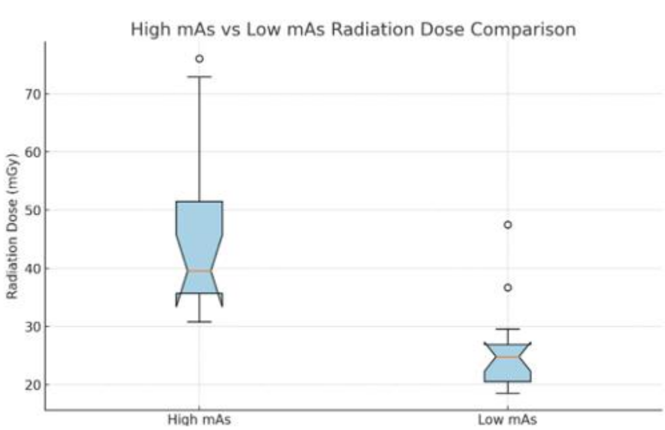


**Fig. 3.** Difference between radiation dose (mGy) as a function of high mAs and low mAs.

shows that although salivary glands receive lower doses compared to the thyroid, they remain significantly affected by radiation exposure. The eye lenses are particularly radiosensitive and demonstrated significant dose reductions. The right lens dose dropped from 38.14 ± 1.84 mGy to 18.53 ± 0.96 mGy (51.7 % reduction), while the left lens dose decreased from 41.73 ± 3.29 mGy to 18.94 ± 1.52 mGy (54.4 % reduction). The spinal cord region experienced a dose reduction of 31.1 %, with absorbed doses decreasing from 36.95 ± 0.87 mGy to 25.42 ± 2.68 mGy. Temporal squamous regions also demonstrated notable dose differences. The right temporal squamous dose dropped by 37.6 %, while the left side showed a 35.8 % reduction. Brain tissues (including the ethmoid and pituitary regions) showed dose reductions of 46.2 % and 42.1 %, respectively, further illustrating the potential for dose savings in critical head regions without compromising image quality. Fig. 3 emphasizes the overall dose disparity between high and low mAs protocols. The boxplot clearly demonstrates the reduced variability and significantly lower median doses under low-dose protocols, reinforcing the effectiveness of tube current reduction for radiation dose minimization. The results highlight that significant dose reductions can be achieved for critical organs without sacrificing diagnostic image quality (see Fig. 4). The thyroid gland and eye lenses are the most vulnerable organs in cranial CT imaging, with dose reductions exceeding 50 % when adopting low-dose protocols.

SNR values calculated from ROIs drawn over the temporal bone and cerebellum on the same axial slice were found to be 51.77 for the low-dose acquisition and 68.87 for the high-dose acquisition. Similarly, the corresponding CNR values were 51.58 and 67.90, respectively.

## 4. Discussions

The successful calibration and quality control confirmed the CT scanner's readiness for use in the dosimetry study. These validated parameters ensured precise radiation dose delivery during the cranial CT imaging of the Alderson Rando phantom, enabling an accurate comparison of absorbed doses for high-dose and low-dose imaging protocols. The reliability of these measurements is critical for evaluating dose optimization strategies and their effectiveness in reducing absorbed radiation doses in critical organs.

Cranial CT imaging generally involves lower effective doses compared to thoracic, abdominal, or pelvic scans. However, the head and neck region contain radiosensitive organs such as the eye lenses and thyroid gland, which are particularly vulnerable to the genotoxic effects of ionizing radiation [2]. Therefore, evaluating absorbed doses and optimizing imaging protocols is crucial to minimize potential risks. Our study demonstrated significant dose reductions under low-dose protocols, particularly for organs with high radiosensitivity, such as the eye lenses and thyroid, while maintaining diagnostic image quality. The results of this study, as shown in Table 6, revealed significant reductions in absorbed doses across all critical organs when switching from high-dose to low-dose protocols. The most striking reductions were observed in the eye lenses, where the left lens dose decreased by 54.4 % (from 41.73 ± 3.29 mGy to 18.94 ± 1.52 mGy) and the right lens showed a 51.7 % reduction (from 38.14 ± 1.84 mGy to 18.53 ± 0.96 mGy). These findings align with previous research emphasizing the critical need for shielding or optimized protocols to reduce cataract risk, especially for radiosensitive tissues (Seals et al., 2016). Given the established association between radiation exposure and cataract formation, these reductions are of considerable clinical importance (Günay et al., 2020). Techniques such as bismuth shielding have been explored to further reduce lens dose without degrading image quality (Santos et al., 2019). Similarly, the thyroid gland, which is highly sensitive to ionizing radiation, exhibited dose reductions of 66.3 % (right thyroid) and 64.8 % (left thyroid). These findings align with studies conducted by Santos et al., who measured thyroid doses of 24.70 mGy in male Alderson Rando phantoms during cervical CT imaging using similar protocols (120 kVp, 175 mAs, 0.8 s, 0.984 pitch) (Santos et al., 2019).

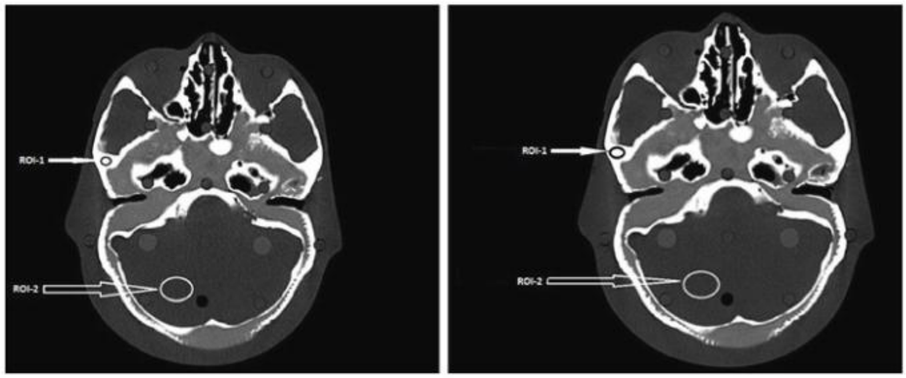


**Fig. 4.** The image on the left shows a high-dose cranial scan, while the image on the right shows a low-dose cranial scan. ROI-1:Temporal bone, ROI-2:Cerebellum.

Our study confirms comparable reductions under a 300 mAs protocol, supporting the reliability of low-dose optimization strategies for thyroid protection. In addition to the eye lenses and thyroid, dose reductions were also observed in the salivary glands and brain tissues. The left parotid gland dose decreased by 33.7 % (from 44.62 ± 1.04 mGy to 29.56 ± 1.53 mGy), while the right parotid showed a reduction of 33.1 %. Submandibular glands exhibited reductions of 34.3 % for the right side and 27.0 % for the left side. These findings are consistent with previous studies that emphasized the significance of reducing dose exposure to salivary glands to mitigate xerostomia, a common side effect of radiation exposure in the head and neck region [**6**]. Temporal squamous bones and ethmoid regions also showed significant dose reductions of 35–37.6 % and 46.2 %, respectively. Although these structures are less radiosensitive compared to soft tissues, the observed reductions demonstrate the broader impact of optimized protocols. Comparing our results with those reported in the literature further validates the effectiveness of low-dose protocols. For instance, Günay et al. investigated head and neck doses using a General Electric Optima CT520 scanner with automated exposure settings (120 kVp, 221.7 mAs), reporting lens doses of 19.83 ± 3.93 mSv and thyroid doses of 13.97 ± 3.90 mSv [**4**]. Studies using similar phantom models reported dose reductions of 30–60 % for critical organs when implementing low-dose CT protocols (Joyce et al., 2020). The significant dose savings for eye lenses and thyroid glands align with recommendations from the International Commission on Radiological Protection (ICRP), which emphasize shielding and protocol optimization to reduce risks in these regions (Barnard et al., 2016). The results highlight that significant dose reductions can be achieved for critical organs without sacrificing diagnostic integrity. Optimizing tube current (mA) and implementing advanced reconstruction techniques can effectively balance image quality and patient safety. Similarly, Anim-Sampong et al. assessed head CT doses in Ghana and reported a mean CTDIvol of 86.00 mGy for high-dose protocols, with DLP values ranging from 1037.30 mGy cm to 1699.60 mGy cm depending on tube current settings (Anim-Sampong et al., 2023). The CTDIvol and DLP values obtained in this study provide additional insights into dose optimization. Under high-dose protocols, CTDIvol increased by approximately 93 %, demonstrating the direct impact of tube current and pitch values on local dose distribution. While higher CTDIvol values may be necessary for specific clinical indications requiring enhanced image quality, low CTDIvol values are preferred for routine imaging to minimize unnecessary exposure [ (ICRU, 1989)]. Similarly, DLP, which reflects the cumulative radiation burden over the scanned region, nearly doubled under high-dose settings. Given that DLP accounts for the total volume of tissue irradiated, excessive DLP values can result in unnecessary radiation risks, particularly for patients undergoing frequent imaging (Tsapaki et al., 2006). The findings of this study align with international dose recommendations. European Commission guidelines suggest CTDIvol values of 60.0 mGy and DLP limits of 100.0 mGy cm for cranial CT examinations (European Commission, 2014). Studies conducted by Toori et al. (Toori et al., 2015) in Iran and Salama et al. (Salama et al., 2017) in Egypt also reported variations in CTDIvol and DLP values, emphasizing the importance of standardizing protocols. Toori et al. (Toori et al., 2015) identified optimized values of 59.5 mGy for CTDIvol and 750 mGy cm for DLP, while Salama et al. reported an average CTDIvol of 28.80 mGy (Salama et al., 2017). Our results further support global efforts to reduce radiation exposure through the implementation of optimized imaging protocols. By reducing tube current and pitch while leveraging advanced reconstruction techniques, substantial dose reductions can be achieved without compromising diagnostic confidence. This is particularly important for radiosensitive organs such as the thyroid and eye lenses, as well as for paediatric and at-risk populations requiring repeated imaging (Samei et al., 2018). In conclusion, the findings of this study demonstrate that low-dose protocols can effectively reduce absorbed doses to critical organs in cranial CT imaging, with reductions of up to 66 %. These results underscore the importance of adhering to the ALARA principle and implementing dose optimization strategies to enhance patient safety while maintaining diagnostic efficacy (Khong et al., 2013). By comparing our results with the existing literature, it is evident that protocol optimization offers a reliable approach to minimizing radiation exposure and achieving clinically acceptable outcomes.

When comparing patient dose values between the two protocols, dose reduction varied between 31.1 % and 64.8 % depending on the anatomical region. In the quantitative image quality assessment, the ratios of high-dose to low-dose values for SNR and CNR were calculated as approximately 33 % and 31.6 %, respectively. These findings are consistent with the dose variation ratios reported by Amasya et al. in their study on cranial cone-beam CT (Amasya et al., 2025).

## 5. Conclusions

This study demonstrated that significant dose reductions in cranial CT can be achieved by optimizing parameters such as tube current and pitch (Kalra et al., 2004). The low-dose protocol effectively lowered CTDIvol and DLP values while maintaining diagnostic image quality, especially in radiosensitive organs like the thyroid and eye lenses (Ahmed, 2022, pp. 222–230; Jeyasugiththan et al., 2023). These findings support adherence to the ALARA principle (Dudhe et al., 2024). Advanced reconstruction techniques may further improve image quality at lower doses. For future work, comparing results with IAEA simulation data could enhance dosimetric accuracy and promote broader international applicability.

## CRediT authorship contribution statement

**Duygu Tunçman Kayaokay:** Writing – original draft, Methodology, Investigation, Formal analysis. **Fahrettin Fatih Kesmezacar:** Software, Investigation, Data curation. **Osman Günay:** Methodology, Investigation. **Songül Çavdar Karaçam:** Methodology, Investigation. **Ali Demirci:** Supervision, Methodology, Investigation. **Mustafa Demir:** Methodology, Investigation. **Ghada ALMisned:** Writing – original draft, Methodology, Investigation. **Huseyin Ozan Tekin:** Writing – original draft, Supervision, Methodology, Investigation, Data curation, Conceptualization.

## Data availability Statement

The data that support the findings of this study are not openly available due to reasons of sensitivity and are available from the corresponding author upon reasonable request.

## Funding

None

## Conflicts of interest/competing interests

None.

## Acknowledgements

The authors gratefully acknowledge the valuable institutional support provided by ***Istinye University,*** Türkiye and the ***MLP Care***, which significantly contributed to the successful execution of this multicenter research study.

## References

Ahmed, F. K. (2022). *Assessment of radiation absorbed dose and cancer risk in head computed tomography examinations*. Journal of University of Babylon for Pure and Applied Sciences.
Alashban, Y., & Alghamdi, S. A. (2025). Evaluating the knowledge of radiation exposure parameters among CT technologists in Saudi Arabia: A survey-based study on adherence to ALARA principles and dose optimization. *Radioprotection, 60*(2), 168–175.
Amasya, H., Günay, O., Kesmezacar, F., Kayaokay, D. T., Yeyin, N., Kekeç, E., … Demir, M. (2025). Head and neck imaging with a dental CBCT device: Comparison of 360° and 180° rotation angles in effective dose and quantitative image quality in a phantom study head. *Current Medical Imaging, 21*(1), Article E15734056316438.
Anim-Sampong, S., Ohene-Botwe, B., Adom, E. B., et al. (2023). Dose optimization of adult head computed tomography examination in an academic hospital in Ghana. *Radiation Physics and Chemistry, 205*, Article 110735.
Barnard, S. G., Ainsbury, E. A., Quinlan, R. A., & Bouffler, S. D. (2016). Radiation protection of the eye lens in medical workers—basis and impact of the ICRP recommendations. *British Journal of Radiology, 89*(1060), Article 20151034.
Dudhe, S. S., et al. (2024). Radiation dose optimization in radiology: A comprehensive review of safeguarding patients and preserving image fidelity. *Cureus, 16*(5), Article e60846.
Edyvean, S. (2013). CT equipment and performance issues: Radiation protection 162. *Radiation Protection Dosimetry, 153*(2), 190–196.
European Commission. (2014). *Radiation protection N° 180. diagnostic reference levels in thirty-six European countries*.
Günay, O., Gündoğdu, Ö., Demir, M., Timlioğlu İper, H. S., et al. (2020). Determination of radiation dose levels absorbed by lenses, thyroid, and oral mucosa during CT imaging: A phantom study. *Kocaeli University Health Sciences Journal, 6*(1), 23–27.
Husseiny Salama, D., Vassileva, J., Mahdaly, G., et al. (2017). Establishing national diagnostic reference levels (DRLs) for computed tomography in Egypt. *Physica Medica, 39*, 16–24.
ICRU. (1989). *International commission on radiation units and measurements. Report 44: Tissue substitutes in radiation dosimetry and measurement*. Bethesda, MD: ICRU.
International Atomic Energy Agency (IAEA). (2013). Radiation protection in pediatric radiology. *Safety Reports Series*. No. 71. Vienna: IAEA.
IPEM. (2002). *Medical and dental guidance notes: A good practice guide on all aspects of ionising radiation protection in the clinical environment (York: IPEM)*.
Jensen, S. B., Vissink, A., Limesand, K. H., & Reyland, M. E. (2019). Salivary gland hypofunction and xerostomia in head and neck radiation patients. *JNCI Monographs*, (53), Article lgz016.
Jeong, D. K., Lee, S. C., Huh, K. H., Yi, W. J., Heo, M. S., Lee, S. S., & Choi, S. C. (2012). Comparison of effective dose for imaging of mandible between multi-detector CT and cone-beam CT. *Imaging science in dentistry, 42*(2), 65–70.
Jeyasugiththan, J., et al. (2023). Evaluation of radiation dose in multi-slice computed tomography protocols of head and neck regions. *Radiation Protection Dosimetry, 199*(10), 1096–1102.
Joyce, S., et al. (2020). Strategies for dose reduction with specific clinical indications during computed tomography. *Radiography, 26*, S62–S68.
Kalra, M. K., et al. (2004). Strategies for CT radiation dose optimization. *Radiology, 230*(3), 619–628.
Khong, P. L., et al. (2013). ICRP publication 121: Radiological protection in paediatric diagnostic and interventional radiology. *Annals of the ICRP, 42*(2), 1–63.
Kleinerman, R. A. (2006). Cancer risks following diagnostic and therapeutic radiation exposure in children. *Pediatric Radiology, 36*(Suppl 2), 121–125.
McCollough, C. H., Bruesewitz, M. R., McNitt-Gray, M. F., Bush, K., Ruckdeschel, T., Payne, J. T., … Zeman, R. K. (2004). The phantom portion of the American College of Radiology (ACR) computed tomography (CT) accreditation program: Practical tips, artifact examples, and pitfalls to avoid. *Medical Physics, 31*(9), 2423–2442.
Mohd, A. (2024). Optimization of CT radiation dose: Insight into DLP and CTDI. *Future Health, 2*, 148–152. https://doi.org/10.25259/FH_45_2024
Özden, I., Scheidegger, & KSA, S. (2014). P 86 the influence of scan length and collimation on the CTDIvol measurement in case of helical CT. In *Joint conference of the SSRMP, DGMP, ÖGMP* (p. 459).
Perisinakis, K., Raissaki, M., Tzedakis, A., Theocharopoulos, N., Damilakis, J., & Gourtsoyiannis, N. (2005). Reduction of eye lens radiation dose by orbital bismuth shielding in pediatric patients undergoing CT of the head: A Monte Carlo study. *Medical Physics, 32*(4), 1024–1030.
Rodrigues, F., et al. (2023). Assessment of dose heterogeneity in TBI using the thorax of the anthropomorphic Alderson-Rando phantom and TLDs in two different setups. *Brazilian Journal of Radiation Sciences, 11*(1A), 1–13. Suppl.
Salama, D. H., Vassileva, J., Mahdaly, G., et al. (2017). Establishing national diagnostic reference levels (DRLs) for computed tomography in Egypt. *Physica Medica, 39*, 16–24.
Samei, E., et al. (2018). Medical imaging dose optimisation from ground up: Expert opinion of an international summit. *Journal of Radiological Protection, 38*(3), 967.
Santos, F. S., Gomez, A. M. L., da Silva, C. A. M., do Carmo Santana, P., & Mourao, A. P. (2019). Analysis of thyroid absorbed dose in cervical CT scan with the use of bismuth shielding. *Brazilian Journal of Radiation Sciences, 7*(2A). Suppl.
Seals, K. F., Lee, E. W., Cagnon, C. H., Al-Hakim, R. A., & Kee, S. T. (2016). Radiation-induced cataractogenesis: A critical literature review for the interventional radiologist. *Cardiovascular and Interventional Radiology, 39*, 151–160.
Sodickson, A., Baeyens, P. F., Andriole, K. P., et al. (2009). Recurrent CT, cumulative radiation exposure, and associated radiation-induced cancer risks from CT of adults. *Radiology, 251*(1), 175–184.
Sohrabi, M., Parsi, M., & Sina, S. (2018). A new dual-purpose quality control dosimetry protocol for diagnostic reference-level determination in computed tomography. *Health Physics, 115*(2), 252–258.
Toori, A. J., Shabestani-Monfared, A., Deevband, M. R., et al. (2015). Dose assessment in computed tomography examination and establishment of local diagnostic reference levels in Mazandaran, Iran. *Journal of Biomedical Physics & Engineering, 5*(4), 177–182.
Tsapaki, V., Aldrich, J. E., Sharma, R., et al. (2006). Dose reduction in CT while maintaining diagnostic confidence: Diagnostic reference levels at routine head, chest, and abdominal CT. *Radiology, 240*(3), 839–845.

Available online at www.SciMedJournal.org

**SciMedicine Journal**

Vol. 2, No. 1, March, 2020

# Dosimetry Study in Head and Neck of Anthropomorphic Phantoms in Computed Tomography Scans

A. M. L. Gómez [a*], P. C. Santana [a], A. P. Mourão [a]

[a] *Department of Nuclear Engineering, Engineering School, Universidade Federal de Minas Gerais, Av. Antônio Carlos 6627, CEP: 31270-90, Pampulha, Belo Horizonte, MG, Brazil.*

Received 03 January 2020; Accepted 19 February 2020

---

**Abstract**

*Objectives:* To determine the CT absorbed dose profiles for routine adult scan parameters in adults, using male and female anthropomorphic phantoms. Compare the levels of absorbed dose of the phantoms and perform image quality analysis by making noise percentage measurements on the CT images obtained. *Methods:* Radiochromic film strips were introduced in the central region of the phantoms for to record the dose profile in head and neck in order to determine the amount of the dose deposited along the central axis of the phantoms. The scans were performedon a 64 - channel CT scanner (General Electric), programmed in helical scaning mode. In addition to the routine acquisition protocol with fixed current value, it was performed other three scans with the voltage of 80, 100 and 120 kV, using automatic exposure control. *Results:* Absorbed dose values were found between 15.54 to 24.38 mGy on average for anthropomorphic male phantom and values of 13.13 to 21.49 mGy for anthropomorphic female phantom. Noise analysis was performed, finding that all are acceptable diagnostic parameters according to ministerial order 453/98 of the Brazilian Ministry of Health. The acquisition parameters of CT images were found that deposited on average less doses in the head and neck for both phantoms, maintaining the image quality for diagnosis.

*Keywords:* Dosimetry; Computed Tomography; Anthropomorphic Phantom.

---

## 1. Introduction

Since ionizing radiations began to be used in medical applications for the diagnosis and treatment of diseases, the doses to which the population has been exposed are increasingly higher. In 2008, in the United States, the diagnose technique that showed the highest dose deposition in the population was CT scans. Studies carried out in the Unified Health System of Brazil (*SUS*) reported that, between 2001 and 2011, authorized CT head scans for inpatients and outpatients had increased 14.7% and 17.5%, respectively [1-3].

The use of anthropomorphic phantoms in CT dosimetry studies has been a great help in proposing to optimize image quality in new acquisition protocols. The female and male Alderson Rando anthropomorphic phantoms have physical properties similar to that of a patient, such as geometry, weight and equivalent materials to human body tissues. The use of radiochromic films in anthropomorphic phantoms has allowed obtaining absorbed dose profiles in different places considered as radiosensitive organs [4-9].

The radiochromic films are calibrated for different energy intensities separately, due to their energy dependence. Studies carries out with PMMA cylindrical head phantom and ionization chambers determined the calibration curves for radiochromic films GAFCHROMIC XR-AQ2 for different voltages of CT X-ray tube [10, 11].

---

* Corresponding author: amlgphys@gmail.com

http://dx.doi.org/10.28991/SciMedJ-2020-0201-6

## 2. Materials and Methods

### 2.1. Materials

The materials and equipment used for the development of this dosimetry study were:

- Anthropomorphic male and female phantoms, Anderson Rando model
- Radiochromic film strips, GAFCHROMIC XR-AQ2 model
- GE CT scanner with 64-channels, model VCT

### 2.2. Methods

The male and female anthropomorphic phantoms were positioned in isocenter of the CT scanner gantry. Radiochromic film strips with dimensions of 0.5 x 32 $cm^2$ were inserted in the longitudinal axis section of anthropomorphic male and female adult phantoms. The CT scanner was setting in helical mode for head scans to realize acquisitions with the voltages of 80, 100 and 120 kV, using the automatic exposure control to make scans of 30 cm, performing 12 phantom slices, form the top of the skull justthe phantom slice number 12 (vertebra T2.. Another CT scan was performed using the routine protocol with voltage of 120 kV with a fixed current of 200 mA.The scans were performed with a tube tine of 0.5 s, pitch of 0.984, image reconstruction of 1.25 mm and thickness beam of 40 mm. Figure 1 illustrates a frontal scouts of anthropomorphic phantoms.

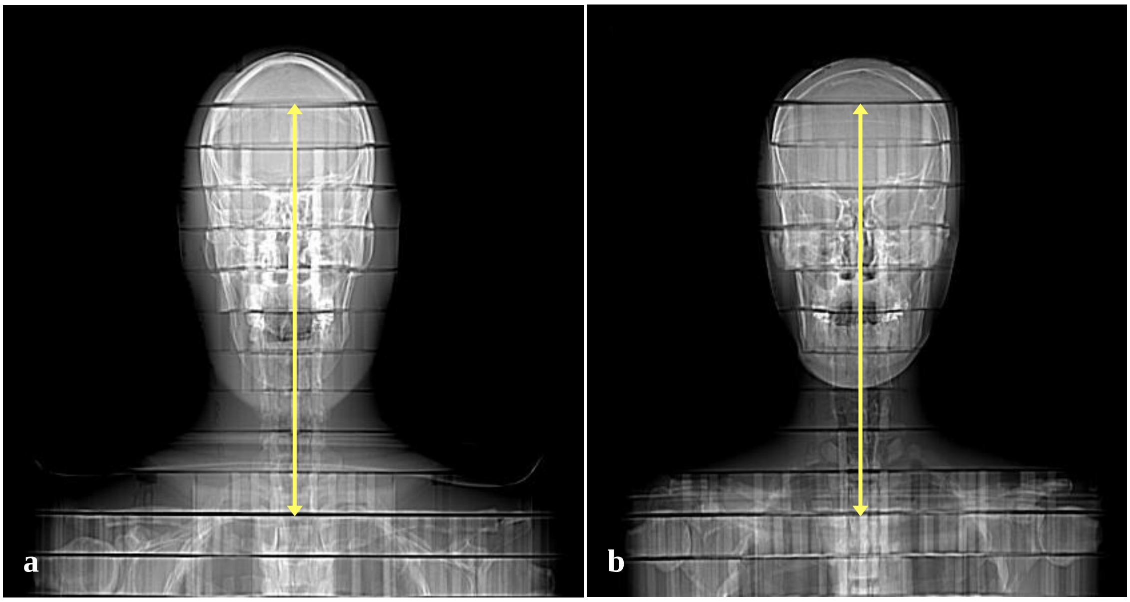


**Figure 1. Scout of male (a) and female (b) anthropomorphic phantoms**

The exposed film strips were stored of 24 hours, with temperature and humidity control. They were digitized using a HP Photosmart C4480 scanner in reflective mode and these images processed using ImageJ software to obtain the pixel intensity values of the scanned strips images with 25 cm in length, including the phantom slice 2 just to slice 12. The pixel intensity values was obtained making the RBG color split channels and the red channel was elected because it presents better response to X-ray energy variations. The red channel images were the greyscale inverted to have the intensity values. The pixel intensity values for film strips none irradiated it was considered 0 mGy (zero miligrays).

The absorbed dose values are obtained from the pixel intensity values using calibration curves for each voltage value to get air kerma values [10]. The conversion factors used to determine the dose profile for each protocol in the anthropomorphic phantoms. The calibration curves are meeting the following mathematical model: The absorbed dose values are obtained from the pixel intensity values using calibration curves for each voltage value to get air kerma values [8]. The conversion factors used to determine the absorbed dose profile for each protocol in the anthropomorphic phantoms were 1.0106, 1.0324, and 1.0418 for 80, 100 and 120 kV [12]. The noise analysis was performed electing a CT axial image in the brain using the RadAnt software of the phantom slice number 3. Four ROI´s were selected in each image and the average noise percentage calculated. Equation 1 was used to calculate the noise values.

$$y=(A\, e^{-x/B}+y_0)\times FC \tag{1}$$

Where $A$, $B$ and $Y_0$ are proportionality constants for each energy, $X$ is the intensity pixel value, $FC$ is the conversion factor from NIST [12] and $Y$ is the adsorbed dose value. The proportionality constants values are shown in Table 1. The noise analysis was performed electing a CT axial image in the brain using the RadAnt software of the phantom slice number 5. Four ROI´s were selected in each image and the average noise percentage calculated. Equation 2 was used to calculate the noise values.

$$\text{Noise }\%=100\times(SD)/(HU_{average}-HU_{air}) \quad (2)$$

Where $SD$ is the standard deviation, $HU_{average}$ is the HU average value of the ROI and $HU_{air}$ is the HU value of the air (-1000).

**Table 1. Proportionality constants for calibration films**

| kV | 120 | 100 | 80 |
|---|---|---|---|
| A | 4.45 | 5.10 | 0.93 |
| B | 48.46 | 53.18 | 27.89 |
| $y_0$ | 9.88 | 10.64 | 3.69 |
| FC | 1.10 | 1.01 | 1.09 |

## 3. Results

The curves in the graphs of the Figure 2 shown the dose variation in the central area of the phantoms for the four scans using different parameter in acquisition protocol. These scans start in the brain (0) just to the up of the lungs (25 mm). The absorbed dose in the region referring to the brain, presents little variation because there are small variations in density in the materials which the phantom was manufactured. The data recorded in the mandible region were the lowest for the image acquisition protocols used in this study. The image acquisition protocol that registered the lowest absorbed dose values in the head and neck areas was the one that used 80 kV.

As the X-ray beam begins to scan the chest region, greater attenuation is evident by the materials present in this region, causing the scanner to deposit more energy, producing a higher absorbed dose in the chest. The protocol that recorded a higher peak of absorbed dose in the chest region was 120 kV with automatic exposure control.

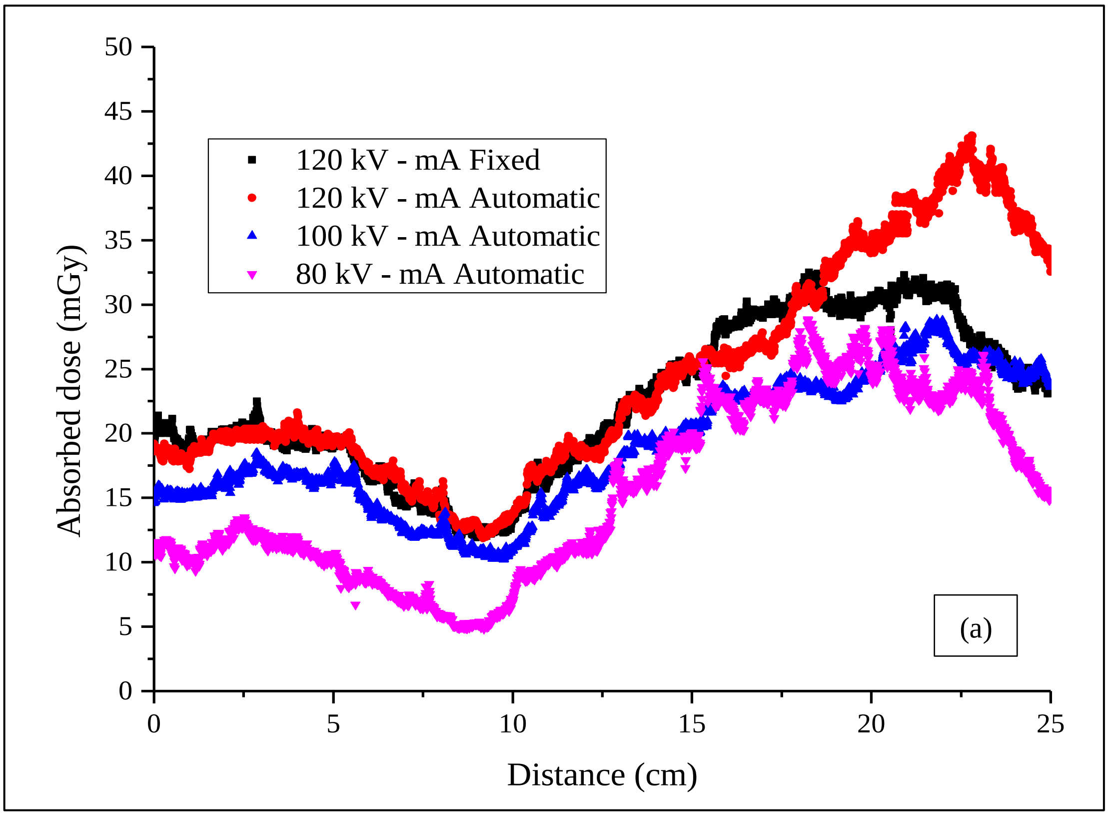

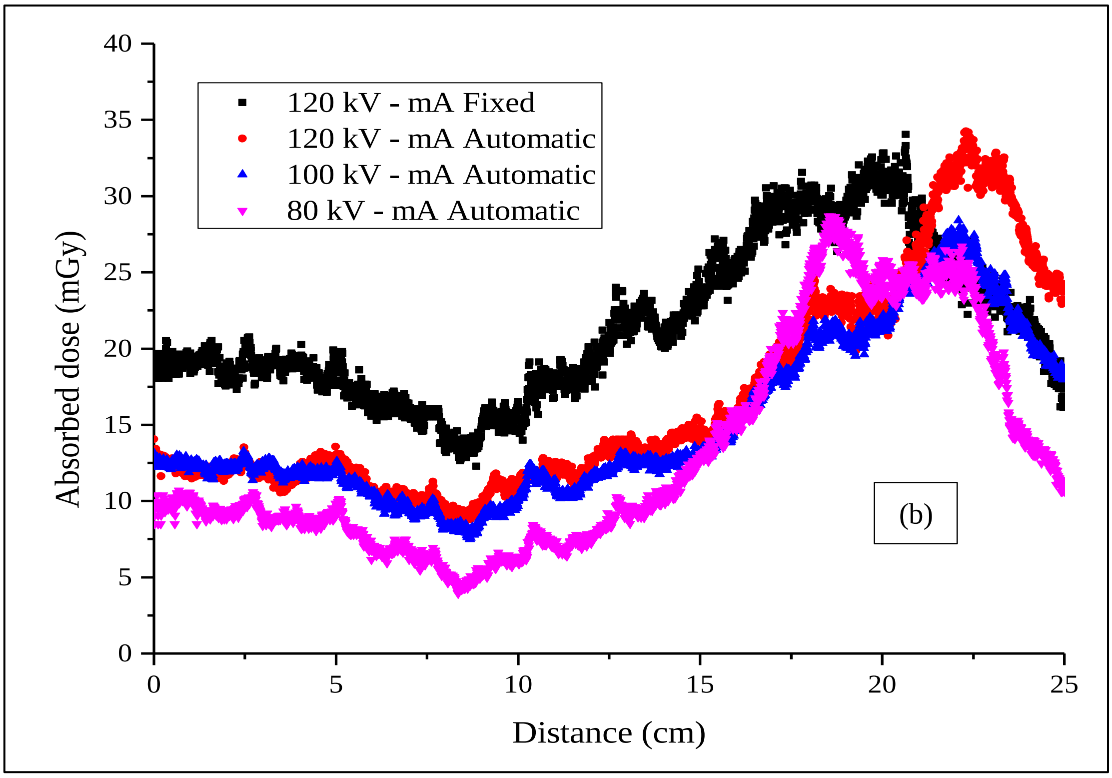


**Figure 2. Dose profile in head and neck CT scans in anthropomorphic male phantom (a) and anthropomorphic female phantom (b)**

For scans in anthropomorphic male phantom, the lowest average dose was observed for the protocol with voltage of 80 kV and automatic exposure control. Compared to the routine protocol (120 kV and fixed current), the reduction observed was of 30.62%. Figure 2a shows the absorbed dose profiles for each protocol used. The average values of absorbed dose for 100 kV had a 15.26% reduction and 120 kV with automatic exposure control had an increase of 8.66%, compared to the routine CT head scan.

For scans in anthropomorphic female phantom, the lowest average absorbed dose was observed for voltage of 80 kV and automatic exposure control, followed by protocol with voltage of 120 kV and fixed current. Figure 2b represents the absorbed dose profiles for each protocol used. The average values of absorbed dose for 80 kV and automatic exposure control had a 38.90% to reduction compared to the routine CT head scan. For voltage 100 and 120 kV used automatic exposure control, they had 29.97% and 22.61% to reduction of absorbed dose compared to the routine CT head scan.

The absorbed dose curves for the four protocols used in this study show similar variations between them. However, the registered mean dose values vary according to the acquisition parameters with which the scanner was programmed. The average values of absorbed dose and their standard deviation (SD) for phantoms and different image acquisition parameters are shown in the Table 2.

**Table 2. Average absorbed dose in mGy for anthropomorphic female and male phantoms**

| | 80 kV | | 100 kV | | 120 kV | | 120 kV* | |
|---|---|---|---|---|---|---|---|---|
| | **Absorbed dose (mGy)** | **SD** | **Absorbed dose (mGy)** | **SD** | **Absorbed dose (mGy)** | **SD** | **Absorbed dose (mGy)** | **SD** |
| Female | 13.13 | 7.02 | 15.05 | 5.39 | 16.63 | 6.86 | 21.49 | 5.03 |
| Male | 15.54 | 6.95 | 18.98 | 5.09 | 24.38 | 8.52 | 22.40 | 5.95 |

* With fixed current.

Significant differences in absorbed dose were found by comparing the two types of phantoms. The male phantom with higher absorbed dose values in all the protocols used in this study. Comparing the two phantoms, average absorbed dose difference of 15.51%, 20.71%, 44.09% and 4.06% were found for 80, 100, and 120 kV with automatic exposure control and 120 kV with fixed current respectively.

The absorbed dose peak recorder every 2.5 cm are the product of the interaction of the x-ray bean with the air present between the phantoms slices.

Noise analyzed was made for TC images of slice number 5 of the phantoms for each of the protocols used. The ROI´s selected shown the Figure 3. The values in percentage of noise found in the images are shown in Table 3.

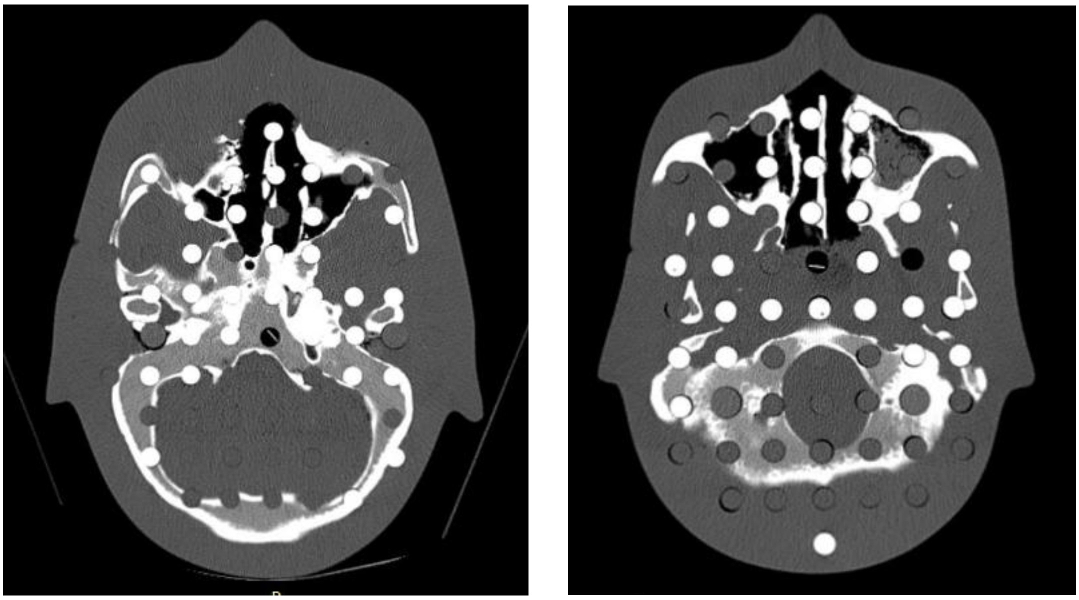

(a) (b)

**Figure 3. CT head images of (a) male and (b) female anthropomorphic phantoms**

**Table 3. Noise percent from CT images of anthropomorphic phantoms**

| | Noise % | | | |
|---|---|---|---|---|
| **Phantom** | **80 kV** | **100 kV** | **120 kV** | **120 kV*** |
| Female | 8.43 | 6.03 | 7.10 | 6.12 |
| Male | 1.42 | 1.29 | 1.62 | 1.68 |

The noise indexes in the CT images of anthropomorphic phantoms did not exceed 8.5%, which reached a value greater than 10%. The female phantom CT images have higher noise percentages than those found in the male phantom CT images.

## 4. Conclusion

The dose profile variations showed the presence of small peaks due to the air layer between the phantoms slices. The highest dose values were recorded in the chest and the lowest values near the mouth area, for all tested acquisition protocols. The use of radiochromic films as absorbed dose recording devices allows, with the recording of the dose profile, to consider the contribution in the dose of secondary radiation in CT scans. Dosimetry studies carried out with phantoms of identical characteristics, using thermo luminescent dosimeters (TLDs) located in regions close to the region where this study was conducted, and recorded lower dose values than those recorded with radiochromic films due to the use of different parameters of acquisition of CT images. The images acquisition parameters than deposited the lowest dose values in the two phantoms used were voltage 80 kV and automatic exposure control. The use of this protocol means an optimization in head and neck CT scans. The recorded absorbed dose values are lower than values suggested by the order 453/98 [13] of the Brazilian Ministry of Health that is of 50 mGy for CT head scans. The percentage of noise found in the CT images in the female phantom was higher because there is evidence of a difference in materials with which it was manufactured when compared to the CT images obtained with the male phantom.

## 5. Funding and Acknowledgements

The authors are thankful to CAPES, FAPEMIG for their support of developing this study and CDTN/CNEN for the loan of the phantoms. The funds provided for development of this study were made available by CAPES and FAPEMIG in the form of scholarship and research projects.

## 6. Declaration of Competing Interest

The authors declare that they have no known competing financial interests or personal relationships that could have appeared to influence the work reported in this paper.

## 7. Ethical Approval

All procedures performed in studies involving human participants were in accordance with the ethical standards of the institutional and/or national research committee and with the 1964 Helsinki declaration and its later amendments or comparable ethical standards.

## 8. References

[1] Bolus, N. E. (2013). NCRP Report 160 and What It Means for Medical Imaging and Nuclear Medicine. Journal of Nuclear Medicine Technology, 41(4), 255–260. doi:10.2967/jnmt.113.128728.

[2] Dovales, A. C. M., da Rosa, L. A. R., Kesminiene, A., Pearce, M. S., & Veiga, L. H. S. (2016). Patterns and trends of computed tomography usage in outpatients of the Brazilian public healthcare system, 2001–2011. Journal of Radiological Protection, 36(3), 547–560. doi:10.1088/0952-4746/36/3/547.

[3] Dovales, A. C. M., Souza, A. A. D., & Veiga, L. H. (2015). Computed tomography in Brazil: frequency and pattern of usage among inpatients of the Unified Health System (SUS). Revista Brasileira de Fisica Medica (Online), 9(1), 11-14.

[4] Nardi, C., Talamonti, C., Pallotta, S., Saletti, P., Calistri, L., Cordopatri, C., & Colagrande, S. (2017). Head and neck effective dose and quantitative assessment of image quality: a study to compare cone beam CT and multislice spiral CT. Dentomaxillofacial Radiology, 46(7), 20170030. doi:10.1259/dmfr.20170030.

[5] Santos, F. S., Gomez, A. M. L., Silva, C. A. M. da, Santana, P. D. C., & Mourao, A. P. (2019). Analysis of thyroid absorbed dose in cervical CT scan with the use of bismuth shielding. Brazilian Journal of Radiation Sciences, 7(2A). doi:10.15392/bjrs.v7i2a.614.

[6] Gomez, A. M., Santana, P. D. C., & Mourao, A. P. Dose profile study in head CT scans using a male anthropomorphic phantom. INAC 2017: International Nuclear Atlantic Conference; Belo Horizonte, MG (Brazil); 22-27.

[7] Santana, P. do C., Mourão, A. P., Oliveira, P. M. C. de, Bernardes, F. D., Mamede, M., & Silva, T. A. da. (2014). Dosimetria de pacientes submetidos a exames de PET/CT cerebral para diagnóstico de comprometimento cognitivo leve. Radiologia Brasileira, 47(6), 350–354. doi:10.1590/0100-3984.2013.1800.

[8] Hofmann, E., Schmid, M., Sedlmair, M., Banckwitz, R., Hirschfelder, U., & Lell, M. (2013). Comparative study of image quality and radiation dose of cone beam and low-dose multislice computed tomography - an in-vitro investigation. Clinical Oral Investigations, 18(1), 301–311. doi:10.1007/s00784-013-0948-9.

[9] Gharbi, S., Labidi, S., & Mars, M. (2020). Automatic Brain Dose Estimation in Computed Tomography Using Patient Dicom Images. Radiation Protection Dosimetry. doi:10.1093/rpd/ncaa006.

[10] Costa, K. C., Gomez, A. M. L., Alonso, T. C., & Mourao, A. P. (2017). Radiochromic film calibration for the RQT9 quality beam. Radiation Physics and Chemistry, 140, 370–372. doi:10.1016/j.radphyschem.2017.02.032.

[11] Giaddui, T., Cui, Y., Galvin, J., Chen, W., Yu, Y., & Xiao, Y. (2012). Characteristics of Gafchromic XRQA2 films for kV image dose measurement. Medical Physics, 39(2), 842–850. doi:10.1118/1.3675398.

[12] National Institute of Standards and Technology. Available online: www.nist.gov (accessed on 20 November 2018).

[13] Brasil (1998), Portaria 453, de 01 de junho de 1998. Estabelece as diretrizes de proteção radiológica em radiodiagnóstico médico e odontológico, Diário Oficial [da] República Federativa do Brasil, Brasília, DF, p. 7-16, 02 de junho de 1998. Seção 1. Available online: https://saude.es.gov.br/Media/sesa/NEVS/Servi%C3%A7os%20de%20sa%C3%BAde%20e%20de%20interesse/portaria453.pdf. (accessed on 21 November 2018).

IOP Publishing | Society for Radiological Protection Journal of Radiological Protection
J. Radiol. Prot. 38 (2018) 807–818 (12pp) https://doi.org/10.1088/1361-6498/aac336

# Assessment of organ dose and image quality in head and chest CT examinations: a phantom study

**S Gharbi[1], S Labidi[1], M Mars[1], M Chelli[2], S Meftah[1] and M F Ladeb[2]**

[1] Université Tunis EL Manar, Institut Supérieur des Technologies Médicales de Tunis, Laboratoire de recherche de Biophysique et de Technologies Médicales, 9, Avenue du Docteur Z. Essafi, Tunis 1006, Tunisia
[2] Service de Radiologie, Institut Kassab d'orthopédie, Ksar Saïd, Tunisia

E-mail: gharbi_souha@yahoo.com

Received 23 April 2017, revised 24 April 2018
Accepted for publication 9 May 2018
Published 5 June 2018

CrossMark

**Abstract**

The purpose of this study is to assess dose for radiosensitive organs and image quality in head and chest computed tomography (CT) examinations. Our focus was in the brain, eye lens and lung organs using two protocols; one protocol with fixed mAs and filtered back projection (FBP) and another with tube current modulation (TCM) and sinogram affirmed iterative reconstruction (SAFIRE). Measurements were performed on a 128-slice CT scanner by placing thermoluminescent dosimeters (TLDs) in an anthropomorphic adult phantom. Results were compared to a CT-Expo software. Objective image quality was assessed in terms of signal-to-noise ratio (SNR) and contrast-to-noise ratio (CNR). SPSS software was used for data analyses. Results showed that, using TCM, doses were reduced by 22.84%–25.06% for brain, by 21.82%–23.48% for eye lens and by 54%–53.22% for lung with TLD and CT-Expo respectively. The increased SNR and CNR values achieved for scans performed with TCM combined with iterative reconstruction techniques were 38.68%–58.81% and 38.91%–43.60% respectively. We conclude that, using TCM, a significant mean organ dose reduction is achieved for brain, eye lens and lung organs. Then, combined with iterative reconstruction, image quality was well maintained in terms of SNR and CNR. Thus it is highly recommended in clinical practice optimization in head and chest CT examinations.

Keywords: computed tomography, organ dose, phantoms, CT-Expo, image quality

  

(Some figures may appear in colour only in the online journal)

## 1. Introduction

Since the introduction of computed tomography (CT) in the 1970s, the CT imaging modality has become an essential examination in diagnostic radiology. Therefore, the number of CT examinations has increased significantly. While the clinical value and benefits of CT are unquestionable compared to other diagnostic modalities [1–5], radiation dose exposure from CT scans is relatively high and its potential risk should not be ignored [6–9]. In addition, over-exposure to the radiation can lead to deterministic effects, i.e. radiation-induced damage where a dose threshold exists, such as cataracts. In addition, the lens of the eye is one of the radiation sensitive organs and is considered to be at risk during CT brain procedures [10–13]. This issue is a major concern within the field, and numerous studies have tried to find an applicable way to reduce radiation exposure and minimize the health risks for patients undergoing CT diagnosis [14, 15]. Unfortunately, there are several limitations to the implementation of a standard optimized process such as operator awareness and a lack of knowledge of recent CT technology [16].

The main concern with CT scans in a clinical setting is achieving high quality images while using the most applicable low dose protocols [15]. Various studies have reported on optimal doses considering different factors, including the type of examination and justification for clinical information [15, 17, 18]. To date the most effective way to optimize radiation dose is adjusting CT scan parameters in accordance with patient characteristics [17].

Recently different approaches have been developed for dose reduction such as tube current modulation (TCM). This mode allows current to be adjusted automatically with scanning object thickness [16, 19, 20].

Unfortunately, the reduction of tube current remains limited by the use of the standard filtered back projection (FBP) reconstruction technique, because the FBP technique significantly increases the image noise when the dose reduction is too great [21]. Only recently has the introduction of iterative reconstructions in CT practice as a method that allowed a significant noise reduction in CT images made TCM clinically realistic [21–23].

Our goal in this study is to assess radiosensitive organ dose and image quality using low dose protocol in head and chest CT examinations.

## 2. Materials and methods

### *2.1. Scanning techniques*

The examination was performed on a 128-slice CT system (SOMATOM Definition Edge, Siemens Healthcare, Forchheim, Germany) using an anthropomorphic RANDO® phantom with the specific parameters given in table 1. Two head and two chest CT protocols were implemented. For each protocol, the scout was used for scan guidance. During both scans, the phantom had the same position in the gantry using helical acquisition during scans.

### *2.2. Organ dose evaluation*

*2.2.1. Anthropomorphic phantom study.* For all protocols, an anthropomorphic adult, Alderson-RANDO® Phantom (The Phantom Laboratory, Salem, NY) was used as the subject (figure 1). This phantom is made of tissue equivalent materials that simulate the radiation

**Figure 1.** The RANDO® anthropomorphic phantom in 128-slice CT scanner Definition Edge Siemens.

**Table 1.** Acquisition parameters for head and chest phantom scans with and without TCM.

| Parameters | Protocols | | | |
|---|---|---|---|---|
| | Head (Fixed mAs) | Head (TCM) | Chest (Fixed mAs) | Chest (TCM) |
| Scan length (cm) | 26.4 | 26.4 | 34.4 | 34.4 |
| Slice thickness (mm) | 1 | 1 | 1 | 1 |
| Tube potential (kVp) | 120 | 120 | 120 | 120 |
| Acquisition time (s) | 6.69 | 6.69 | 4.9 | 4.9 |
| Rotation time (s) | 1 | 1 | 0.5 | 0.5 |
| Fixed mAs | 365 | — | 200 | — |
| Quality ref. mAs | — | 365 | — | 200 |
| Eff. mAs | — | 275 | — | 102 |
| Slice collimation | 0.6 × 128 | 0.6 × 128 | 0.6 × 128 | 0.6 × 128 |
| Pitch | 0.55 | 0.55 | 1.05 | 1.05 |
| Dose modulation | Off | On | Off | On |
| Reconstruction slice thickness (mm) | 1 | 1 | 1 | 1 |
| Kernel | H30f medium smooth | J30f medium smooth | B31f medium smooth | I31f medium smooth |
| CTDIvol (mGy) | 50 | 38.2 | 13.41 | 6.93 |
| DLP (mGy cm) | 1320 | 1008.4 | 501.1 | 258.9 |

*TCM = Tube Current Modulation.

**Figure 2.** Position of TLDs in(a) lung, (b, c) brain and (d) eye lens phantom slices.

attenuation characteristics of an adult. The phantom was divided into 22 numbered slabs, each slab equipped with several small holes for TLD placement.

In our study we choose to use thermoluminescent dosimeters (TLD-100 made of LiF: Mg, Ti) to measure the dose absorbed by the phantom's radiosensitive organs. Prior to each measuring session, the TLDs were annealed for 1 h at 400 °C followed by rapid cooling using two aluminum plates. All TLDs were calibrated in a $^{60}$Co beam to a known absorbed dose. Then the TLDs were read out using a TLD Reader, Harshaw 4500, equipped with a software called WinRems in the secondary standard dosimetry laboratory (CNRP, Tunis, Tunisia). In order to assess the TLD's response under CT depending on the tube voltage used in this study (120 kV) a second step of measurement was performed using an ion chamber model Radcal® Accu-Dose® and PMMA phantom. The readout values of TLDs compared to the ion chamber value lead to a mean correction factor of 0.75.

For organ dose assessments, the main TLDs were positioned within the phantom, with guidance from a human anatomy CT atlas and clinical experience. We used thirty-three TLDs and tried to cover the whole organ utilizing a sufficient number of TLD chips in each organ—15 in the lung (slab number 16), 2 in the eye lens (slab number 3) and 16 on the brain (8 on the mid brain, slab number 2, and 8 in the occipital lobe, slab number 4); see figure 2. After reading, the mean values from the TLDs for each organ multiplied by the correction factor represent the mean organ doses.

*2.2.2. CT-Expo software.* In this study results of dose measurements done with the phantom were compared to those from the CT-Expo (V 2.4) software [24, 25]. Organ dose calculations provided by this software are measured on an adult anthropomorphic mathematical phantom (ADAM) as shown in figure 3. In addition, despite the recent development of different versions [15–18], we have chosen CT-Expo (V 2.4). This software update with TCM aims at more accurate organ-dose estimations than the earlier version, V 2.0, for which, when the examination was performed with TCM, only the average mAs per rotation could be inputted [26]. However, the CT-Expo (V 2.4) allows a correction of dose modulation effects using implemented gender-specific mAs profiles figure 4. They were based on the measured attenuation data of adult standard patients examined using Care Dose4D from Siemens (Forchheim, Germany) [25], which is the same TCM as used in this study. From these profiles, an average correction factor is calculated, which is the mean value of the relative mAs plotted in figure 4, for the selected phantom and scanned region. Then, for each position

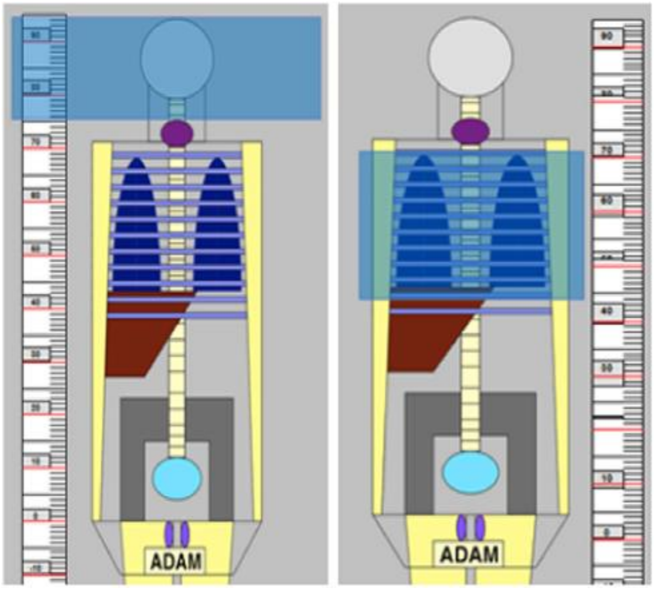


**Figure 3.** Mathematical phantom from CT-Expo, showing the range of scanning during CT head and chest examinations.

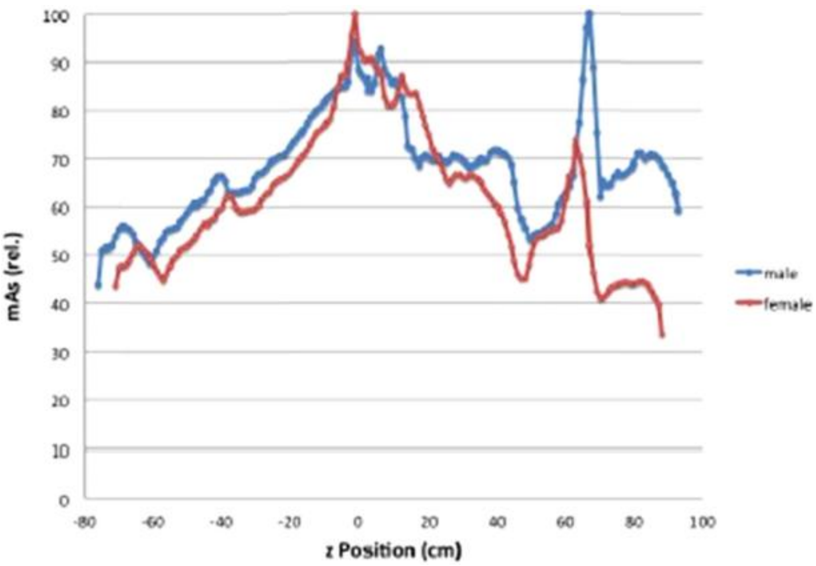


**Figure 4.** mAs profiles used in CT-Expo V 2.4 to correct for mAs modulation effects as a function of the slice location from feet to head (left to right).

in the selected scan range, the ratio between the relative mAs value of the reference profile and the average correction factor for the selected imaging range is calculated. This value is multiplied by the average mAs used in the examination to calculate the mAs per position. Finally, these local mAs values are applied to perform the dose calculations. Input steps for

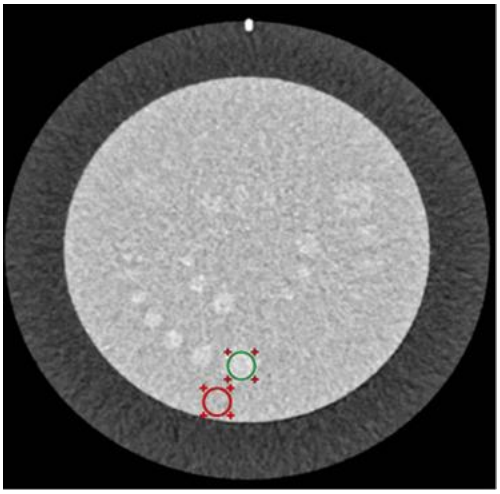

**Figure 5.** Transverse CT slices of the phantom's low-contrast module 515 ROIs placed in a 1% low-contrast target of 15 mm in diameter and in the background area.

dose calculation were as follows: patient type (adult male or female); actual (patient-specific) imaging range; model type (Siemens Definition Edge); CT mode (spiral mode); scan range; CT parameters (tube voltage, average mAs, acquisition time, pitch, reconstructed slice thickness) and whether TCM was used.

### *2.3. Objective image assessment*

The image quality was evaluated objectively in terms of signal-to-noise ratio (SNR) and contrast-to-noise ratio (CNR) in a phantom Catphan 500 (The Phantom Laboratory, Inc., Salem, NY) using the low-contrast module CTP515. The phantom was scanned using the same acquisition and reconstruction parameters tabulated in table 1. The images acquired with fixed current and TCM were reconstructed using traditional FBP reconstruction and sinogram affirmed iterative reconstruction (SAFIRE) respectively. To assess reproducible placement of a region of interest (ROI) for all acquisitions, ROI1 was positioned in a 1% low-contrast target of 15 mm in diameter, and ROI2 was located in the background area (figure 5). In order to asses SNR and CNR correctly between the two reconstruction methods ROIs were consistently placed and sized.

*2.3.1. Low-contrast detectability: SNR.* The noise corresponded to the measurement of the standard deviation of the measured Hounsfield units (HU) of ROI2. The ratio between the mean attenuation value of ROI2 and the standard deviation of ROI2 corresponded to the SNR [27].

*2.3.2. Low-contrast detectability: CNR.* The ratio between the differences of mean attenuation values of these two ROIs (ROI1 and ROI2) and the standard deviation of ROI2 corresponded to the CNR [28].

**Table 2.** Mean organ dose assessments in head and chest examinations.

| | | Mean organ dose (mGy) | | | |
|---|---|---|---|---|---|
| Protocols | Organs | TLD (Fixed mAs) | TLD (TCM) | CT-Expo (Fixed mAs) | CT-Expo (TCM) |
| Head | Brain (mGy) | 41.5 | 32.02 | 40.3 | 30.2 |
| | Eye lens (mGy) | 52 | 40.65 | 51.1 | 39.1 |
| Chest | Lung (mGy) | 20 | 9.18 | 18.6 | 8.7 |

*TCM = Tube Current Modulation.

**Table 3.** Image quality assessments in terms of signal-to-noise ratio (SNR) and contrast-to-noise ratio (CNR) using acquisition and reconstruction parameters of head and chest protocols performed in the low contrast module of a phantom Catphan 500.

| Protocol | SNR | CNR |
|---|---|---|
| Head (Fixed mAs + FBP) | 9.5 | 1.46 |
| Head (TCM + SAFIRE) | 15.51 | 2.39 |
| Chest (Fixed mAs + FBP) | 4.18 | 1.5 |
| Chest (TCM + SAFIRE) | 10.15 | 2.66 |

*TCM = Tube Current Modulation,
SAFIRE = Sinogram Affirmed Iterative Reconstruction.

## 3. Statistical analysis

The statistical analysis was performed with *t*-test using SPSS software (V 15.0). P values of less than (0.05) were used to indicate significance.

## 4. Results

In this study, organ dose was measured directly for each protocol using TLDs inserted in an anthropomorphic adult phantom and indirectly using a computer simulation phantom by CT-Expo. The mean organ dose values are listed in table 2.

It is evident from these results that including a dose modulation system significantly contributes to changes in organ absorbed dose. In addition, in the case of the Alderson phantom for head CT scans the measurement showed a significant difference ($p = 0.01 < 0.05$) between brain dose values with and without TCM. Similarly, eye lens results were significantly different when including TCM ($p = 0.01 < 0.05$). For chest protocol, the result for mean lung dose using fixed mAs was significantly different ($p = 0.01 < 0.05$) to those with CARE Dose 4D. When comparing results between direct measurements and CT-Expo there is a close agreement between the results ($p > 0.05$) with a mean percentage difference of $4.3 \pm 2\%$, $2.8 \pm 1\%$ and $6 \pm 1\%$ observed for brain dose, eye lens and lung dose respectively.

For image quality assessments, table 3 shows different values of SNR and CNR depending on acquisition and reconstruction methods when using settings on the two different protocols in the case of head and chest CT acquisition. In addition, the SNR has increased for images acquired with TCM and reconstructed with SAFIRE by 38.68%–58.81%

accompanied by an improvement of the CNR by 38.91%–43.60% respectively compared to those with fixed current combined with FBP.

## 5. Discussion

In this study, the organ dose values were obtained by indirect measurement using the CT-Expo calculator and by direct measurement using TLDs on the Alderson phantom. The two methods were compared for each scan protocol. When analyzing by examination, results showed that the mean brain dose without TCM are 41.5 mGy and 40.3 mGy using phantom and CT-Expo software respectively. This is in agreement with a similar result reported by Emine *et al* [29] that brain dose varies between 37 mGy and 38 mGy using ImPACT software and Rando phantom respectively with helical acquisition and fixed current. Another study demonstrated that the dose range for the brain in different conventional scanners was 25.8–61 mGy [30]. Regarding those results, our optimized protocol leads to a low brain dose using TCM. In addition, the estimated mean brain dose gives a lower mean dose by 22.84% and 25.06% using TLD measurements and CT-Expo respectively. Similar efficiency of TCM is observed for mean eye lens dose reduction; the obtained results for eye lens mean dose with fixed mAs protocol either with phantom or CT-Expo were higher than those using TCM. The mean eye dose values are 52 mGy and 51.1 mGy without TCM using phantom and CT Expo respectively. Similar results were found by Breiki *et al* [30] who demonstrated that the dose for the eye lens ranges between 40.5 mGy–97.9 mGy for conventional acquisition. Also, in accordance with Emine *et al* [29] the eye dose values were 45 mGy using impact calculator and 47.8 mGy with the Rando phantom. However, our optimized protocol leads to a mean eye dose reduction of 21.82% and 23.48% using phantom and CT-Expo respectively.

These findings are of paramount importance with regard to the optimization process of our current practice. Enabling the TCM function significantly reduces lung dose by 54% and 53.22% using phantom and CT-Expo respectively. The mean lung absorbed dose when compared between TLD and CT-Expo was found to be 20 mGy and 18.6 mGy for fixed mAs scan respectively. Our results are in the broad range of those reported by Emine *et al* [30]. They showed that the range of radiation dose resulting from chest exams which were obtained from conventional scanners was 14.00–75.94 mGy for the lung. However, enabling TCM mean lung dose values are 9.18 mGy and 8.7 mGy using phantom and CT-Expo respectively. Our results are in good agreement with those found by Hashim *et al* [31] using TLD thoracic measurement for organ dose with routine protocol compared to a modified protocol using mAs modulation technique. The lung dose is 9.2 mGy and 23.2 mGy with TLD and CT-Expo respectively using TCM. But when TCM is switched off, the values are 21.5 mGy and 12.1 mGy using TLD and CT-Expo respectively. In spite of these results, it is difficult to compare the estimated dose reduction values obtained in this study with values reported in the literature. This wide range variation can be explained by the differences between scan protocols depending on several variables, including tube potential, slice collimation, and pitch factor even when using a scanner from the same manufacturer [20, 32, 33].

Regarding the measurements of organ dose between TLD and CT-Expo, results showed no significant difference between mean organ dose values: a mean percentage difference of 4.3% $\pm$ 2%, 2.8% $\pm$ 1% and 6% $\pm$ 1% for brain, eye lens and lung respectively. Moreover, mean organ dose values, measured directly, were slightly higher than those obtained with CT-Expo. It has already been shown by several studies that the direct dose measuring values were higher than the computer simulated ones [34–36]. These considerable differences are justified by the organ's position in the Alderson phantom at the border or inside the body region being directly irradiated, while in the mathematical model it may be located completely inside or outside of this region. One major cause in the difference in the organ dose measured directly by TLD and estimated by CT-Expo is the distinctions between organ composition in the Rando phantom and the conditions considered for mathematical phantoms.

In addition to these results demonstrating organ dose reduction, we have results on the objective assessment of image quality. Comparing FBP and iterative reconstructions generated from the same data sets, the results showed that SNR and CNR were increased by 38.68%–58.81% and 38.91%–43.60% respectively in the case of two protocol sets. These results confirm what has been already suggested in the literature concerning the use of SAFIRE [22, 23, 37–42].

In accordance with the present results, Korn *et al* [43] showed that in reduced dose CT examinations the use of SAFIRE as opposed to FBP resulted in a 47% increase in CNR (2.49 versus 1.69; $p < 0.0001$). Regarding the SNR values, in a study by Maciej Guzinski *et al* [44] the SNR increases by 34% and 36% respectively for white and gray matter for iterative reconstruction compared to FBP. A similar result by François Pontana *et al* where the image noise was significantly reduced with iterative reconstruction compared to FBP ($p < 0.0001$) for chest CT examinations showed a mean noise reduction of 34.3% on lung images [45].

However, comparing our results with other types of iterative reconstruction is difficult because their implementation is different for each manufacturer. Nonetheless, maintaining image quality at radiosensitive lower organ dose compared to fixed mAs protocols still represents a considerable step in terms of patient dose reduction and may particularly benefit the large number of patients with serial follow-up examinations.

The present study has some obvious limitations. First, in our study only a standard size represented by the adult anthropomorphic phantom and the stylized mathematical phantom with CT-Expo was considered which may not be applicable to a larger patient. Second, an ideal comparison for this type of study is to utilize protocols performed on the same patient. However, ethical principles make this impractical. Radiologists and technologists still need to decide which parameters are useful to their clinical application before accepting the changes described in these protocols. On the other hand, the TLD measurements are not very practical and unavailable for routine use in CT imaging procedures in spite of their advantages over indirect computer simulated measurement techniques. This study then suggests a potential for dose modulation and iterative reconstruction and encourages future use of simulation to estimate dose for radiosensitive organs in chest and head CT examinations.

## 6. Conclusion

In conclusion, in our study we found advantages in using TCM combined with SAFIRE in head and chest CT scans in terms of radiosensitive organ dose reduction and image quality improvement. In addition, a mean dose reduction of up 25.06%, 23.82% and 54% for brain, eye lens and lung were achieved respectively with no compromise on the image quality. Thus they are highly recommended in clinical practice optimization in head and chest CT examinations.

## Acknowledgments

Special thanks to the staff of Clinique El Manar (Tunis, Tunisia) in allowing us to perform this study using their CT equipment.

## ORCID iDs

S Gharbi https://orcid.org/0000-0002-8677-6031

## References

[1] Edyvean S 2013 CT equipment and performance issues: radiation protection 162 *Radiat. Prot. Dosim.* **153** 190–6
[2] Ripolles T, Errando J, Agramunt M and Martínez M J 2004 Ureteral colic: US versus CT *Abdom Imaging* **29** 263–6
[3] Hamaoka T, Madewell J E, Podoloff D A, Hortobagyi G N and Ueno N T 2004 Bone imaging in metastatic breast cancer *J. Clin. Oncol.* **22** 2942–53
[4] Stuhlfaut J W, Soto J A, Lucey B C, Ulrich A, Rathlev N K, Burke P A and Hirsch E F 2004 Blunt abdominal trauma: performance of CT without oral contrast material *Radiology* **233** 689–94
[5] Rao P, Rhea J T, Novelline R A, McCabe C J, Lawrason J N, Berger D L and Sacknoff R 1997 Helical CT technique for the diagnosis of appendicitis: prospective evaluation of a focused appendix CT examination *Radiology* **202** 139–44
[6] Dawson P 2004 Patient dose in multislice CT: why is it increasing and does it matters? *J. Radiol.* **77** S10–3
[7] David J B, Carl D E, Eric J H and Walter E B 2001 Estimated risks of radiation-induced fatal cancer from pediatric CT *AJR* **176** 289–96
[8] Berrington A and Darby S 2004 Risk of cancer from diagnostic X-rays: estimates for the UK and 14 other countries *Lancet.* **363** 345–51
[9] Pearce M S *et al* 2012 Radiation exposure from CT scans in childhood and subsequent risk of leukaemia and brain tumours: a retrospective cohort study *Lancet.* **380** 499–505
[10] Ciarmatori A, Nocetti L, Mistretta G, Zambelli G and Costi T 2016 Reducing absorbed dose to eye lenses in head CT examinations: the effect of bismuth shielding *Australas. Phys. Eng. Sci. Med.* **39** 583–9
[11] Tan J S, Tan K L, Lee J C, Wan C M, Leong J L and Chan L L 2009 Comparison of eye lens dose on neuroimaging protocols between 16- and 64-section multidetector CT: achieving the lowest possible dose *AJNR Am. J. Neuroradiol.* **30** 373–7
[12] Ibrahim M, Parmar H, Christodoulou E and Mukherji S 2014 Raise the bar and lower the dose: current and future strategies for radiation dose reduction in head and neck imaging *AJNR Am. J. Neuroradiol.* **35** 619–24
[13] ICRP 2007 The recommendations of the international commission on radiological protection *ICRP Publication 103* **37** 2–4
[14] Kalra M K, Maher M M, Rizzo S, Kanarek D and Shepard J A 2004 Radiation exposure from chest CT: issues and strategies *Korean Med Sci.* **19** 159–66
[15] Kalra M K, Maher M M, Toth T L, Hamberg L M, Blake M A, Shepard J A and Saini S 2004 Strategies for CT radiation dose optimization *Radiology* **230** 619–28
[16] Foley S J, Evanoff M G and Rainford L A 2013 A questionnaire survey reviewing radiologists' and clinical specialist radiographers' knowledge of CT exposure parameters *Insights Imaging* **4** 637–46
[17] Kalender W A, Wolf H and Suess C 1999 Dose reduction in CT by anatomically adapted tube current modulation: II. Phantom measurements *Med. Phys.* **26** 2248–53
[18] Gonzaga N B, Mourão A P, Magalhães M J and Silva T A 2014 Organ equivalent doses of patients undergoing chest computed tomography: measurements with TL dosimeters in an anthropomorphic phantom *Appl. Radiat. Isot.* **83** 242–4
[19] Ludlow J B and Walker C 2013 Assessment of phantom dosimetry and image quality of i-CAT FLX cone-beam computed tomography *Am. J. Orthod. Dentofac. Orthop.* **144** 802–17
[20] Akmal S, Zakira M, Khadijah M N, Hamzaini A H and Zhonghua S 2015 Radiation dose reduction in chest and abdomen—pelvic CT using tube current modulation: a phantom study *J. Appl. Clin. Med. Phys.* **16** 319–28
[21] Xu J, Mahesh M and Tsui B M 2009 Is iterative reconstruction ready for MDCT? *J. Am. Coll. Radio.* **l 6** 274–6

[22] Hara A K, Paden R G, Silva A C, Kujak J L, Lawder H J and Pavlicek W 2009 Iterative reconstruction technique for reducing body radiation dose at CT: feasibility study *AJR Am. J. Roentgenol.* **193** 764–71

[23] Beister M, Kolditz D and Kalender W A 2012 Iterative reconstruction methods in x-ray CT *Phys. Med.* **28** 94–108

[24] Stamm G and Nagel H 2002 CT-Expo–a novel program for dose evaluation in CT *Rofo.* **174** 1570–6

[25] Stamm G and Nagel H D 2014 User's Guide for CT-Expo V 2.4: A tool for dose evaluation in computed tomography

[26] Stamm G and Nagel H D 2011 User's Guide for CT-Expo V 2.0: A tool for dose evaluation in computed tomography

[27] Gupta A K, Nelson R C, Johnson G A, Paulson E K, Delong D M and Yoshizumi T T 2003 Optimization of eight-element multi-detector row helical CT technology for evaluation of the abdomen *Radiology* **745** 227–739

[28] Pontana F, Duhamel A, Pagniez J, Flohr T, Faivre J B, Hachulla A L, Remy J and Remy-Jardin M 2011 Chest computed tomography using iterative reconstruction versus filtered back projection (part 2): image quality of low-dose CT examinations in 80 patients *Eur Radiol.* **21** 636–43

[29] Emine D C, Nina T and Bora S 2015 Assessment of organ dose by direct and indirect measurements for a wide bore x-ray computed tomography unit that used in radiotherapy *International Journal of Medical Physics. Clinical Engineering and Radiation Oncology* **4** 132–42

[30] Breiki G, Abbas Y, EL-Ashry M and Diyab H 2008 Evaluation of Radiation Dose and Image Quality for Patients Undergoing Computed Tomography (CT) Examinations. *IX Radiation Physics & Protection Conference* 15–19

[31] Suhairul H, Karim M K A, Bakar K A, Sabarudin A, Chin A W, Saripan M I and Bradley D A 2016 Evaluation of organ doses and specific k effective dose of 64-slice CT thorax examination using an adult anthropomorphic phantom *Radiat. Phys. Chem.* **126** 14–20

[32] Muhogora W E, Nyanda A M, Ngoye W M and Shao D 2006 Radiation doses to patients during selected CT procedures at four hospitals in Tanzania *Eur. J. Radiol.* **57** 461–7

[33] Suliman I I, Abdalla S E, Ahmed N A, Galal M A and Salih I 2011 Survey of computed tomography technique and radiation dose in Sudanese hospitals *Eur. J. Radiol.* **80** 544–51

[34] Groves A M, Owen K E, Courtney H M, Yates S J, Goldstone K E, Blake G M and Dixon A K 2004 16-detector multislice CT: dosimetry estimation by TLD measurement compared with Monte Carlo simulation *The British Journal of Radiology* **77** 662–5

[35] Fearon F, Xie H, Cheng J Y, Ning H, Zhuge Y and Miller R W 2011 Patient-specific CT dosimetry calculation: a feasibility study *Journal of Applied Clinical Medical Physics* **12** 196–209

[36] Struelens Lara, Vanhavere Filip and Smans Kristien 2008 Experimental validation of Monte Carlo calculations with a voxelized Rando-Alderson phantom: a study on influence parameters *Phys. Med. Biol.* **53** 5831–44

[37] Greffier J, Macri F and Larbi A 2016 Dose reduction with iterative reconstruction in multidetector CT: what is the impact on deformation of circular structures in phantom study? *Diagn. Interv. Imaging* **97** 187–96

[38] Mieville F A, Gudinchet F, Brunelle F, Bochud F O and Verdun F R 2013 Iterative reconstruction methods in two different MDCT scanners: physical metrics and 4-alternative forced-choice detectability experiments–a phantom approach *Phys. Med.* **29** 99–110

[39] Baker M E *et al* 2012 Contrast-to-noise ratio and low-contrast object resolution on full- and low-dose MDCT: SAFIRE versus filtered back projection in a low-contrast object phantom and in the liver *AJR Am. J. Roentgenol.* **199** 8–18

[40] Alban G, Benoît O, Sophie L, Alain N, Emilien M, Jacques F and Alain B 2012 CT image quality improvement using adaptive iterative dose reduction with wide-volume acquisition on 320-detector CT *Eur. Radiol.* **22** 295–301

[41] Hyun J S, Yong E C, Young H L, Jin-Young C, Mi-Suk P, Myeong-Jin K and Ki Whang K 2013 Radiation dose reduction via sinogram affirmed iterative reconstruction and automatic tube voltage modulation (CARE kV) in abdominal CT *KJR* **14** 886–93

[42] Greffier J, Pereira F, Francesco M, Beregi J P and Ahmed L 2016 CT dose reduction using automatic exposure control and iterative reconstruction: a chest paediatric phantoms study *Phys. Med.* **32** 582–9

[43] Korn A *et al* 2013 Sinogram affirmed iterative reconstruction in head CT: improvement of objective and subjective image quality with concomitant radiation dose reduction *Eur. J. Radiol.* **82** 1431–5
[44] Maciej G, Lukasz W and Marek J S 2016 Head CT: image quality improvement of posterior fossa and radiation dose reduction with ASiR—comparative studies of CT head examinations *Eur. Radiol.* **26** 3691–6
[45] François P, Julien P, Thomas F, Jean B F, Alain D, Jacques R and Martine R J 2011 Chest computed tomography using iterative reconstruction versus filtered back projection (Part 1): evaluation of image noise reduction in 32 patients *Eur. Radiol.* **21** 627–35

Original Research

# Radiation exposure during computerized tomography-based neuroimaging for acute ischemic stroke: a case-control study

Subhash C Kapur[1], Jeevesh Kapur[1], Vijay K Sharma[2,3,*]

[1] Department of Diagnostic Imaging, National University Health System, 119228 Singapore, Singapore

[2] Division of Neurology, National University Health System, 119228 Singapore, Singapore

[3] YongLoo Lin School of Medicine, National University of Singapore, 119077 Singapore, Singapore

*Correspondence: mdcvks@nus.edu.sg (Vijay K Sharma)

DOI:10.31083/j.jin2003064



Submitted: 4 May 2021 Revised: 11 June 2021 Accepted: 30 June 2021 Published: 30 September 2021

Patients and clinicians often raise concerns about radiation exposure to various organs during computerized tomography-based imaging. We evaluated radiation exposure during standard and low-dose imaging protocols for non-contrast computerized tomography, computerized tomography angiography and computerized tomography perfusion of the head. Whether reducing the radiation dose affected the image quality was also evaluated. Radiation data were retrieved for computerized tomography-based imaging studies performed for acute ischemic stroke patients during 2015. The volume-weighted computerized tomography dose index, dose-length product, scan length, effective dose and whole-body integral dose for brain, skin, eye, thyroid and red bone marrow were extracted from dose-tracking software. Dose metrics for low-dose protocols data were compared with standard protocols. The calculated effective doses for non-contrast computerized tomography, computerized tomography angiography and computerized tomography perfusion were $2.56 \pm 0.67$ mSv, $4.45 \pm 2.5$ mSv, and $4.47 \pm 0.85$ mSv, respectively for 391 acute ischemic stroke patients. Corresponding radiation exposures for low-dose protocol (n = 31) were non-contrast computerized tomography ($2.36 \pm 0.65$ mSv), computerized tomography angiography ($1.57 \pm 0.74$ mSv) and computerized tomography perfusion ($2.20 \pm 0.55$ mSv). Overall, the effective dose for one complete stroke imaging protocol (non-contrast computerized tomography + computerized tomography angiography + computerized tomography perfusion) for the standard-dose protocol was 11.48 mSv, which was reduced to 6.13 mSv (46.6% reduction) using a low-dose protocol ($p < 0.001$). Reduced radiation exposure was noted for other radiosensitive organs. Radiation exposures of sensitive organs are within acceptable limits with standard neuroimaging protocols for acute ischemic stroke. Lower-dose computerized tomography imaging protocols reduced the radiation doses without appreciable deterioration in image quality.

*Keywords*

Neuroimaging; Acute ischemic stroke; Radiation; Radiation dose; Computerized tomography

## 1. Introduction

Acute ischemic stroke (AIS) is a leading cause of mortality and permanent disability [1]. Computerized tomography (CT) based neuroimaging techniques continue to be the mainstay for selecting patients eligible for thrombolytic therapy. Non-contrast CT (NCCT) and CT angiography (CTA) of cervico-cerebral vessels are routinely performed for AIS, while CT perfusion (CTP) of the brain is performed in selected patients. One important reason for selecting CT-based imaging is the fast data acquisition in multi-detector row CT systems [2]. Recent clinical trials have demonstrated that CTP imaging of the brain using an increased detector width can detect additional potentially salvageable ischemic lesions even in the extended therapeutic time window [2, 3].

American Heart Association recommends NCCT to evaluate patients presenting with stroke-like symptoms to exclude various mimicking conditions [2]. An NCCT of the head excludes intracranial hemorrhage with high reliability. However, multimodal imaging with NCCT, CTA and CTP significantly increase diagnostic accuracy compared to NCCT alone. CTA depicts the presence and site of arterial occlusion as well as various collateral flow patterns. CTP further helps in cases with an uncertain time of symptom-onset, especially to evaluate the amount of salvageable penumbra and eligibility for various endovascular procedures in AIS [2, 3]. Importantly, whole-brain perfusion measurement can be achieved very fast and avoid any significant delays in the initiation of definitive therapy [2, 3].

CT scanners are the significant contributors to the radiation exposure received by patients in radiology departments, predisposing them to an increased risk of somatic and genetic effects of ionizing radiation [4–7]. In addition to the brain, red bone marrow, thyroid, and the eyes' lens are the most radiosensitive tissues for these CT procedures. Patients and clinicians often raise concerns about radiation exposure to various organs during computerized tomography (CT) based imaging. Therefore, various strategies are employed to minimize the radiation exposure associated with CT protocols

**Table 1. Stroke protocol scanning parameters.**

| Variable | NCCT | | CTA | | CTP | |
|---|---|---|---|---|---|---|
| | Standard dose | Low dose | Standard dose | Low dose | Standard dose | Low dose |
| Scan type | Helical | Helical | Helical | Helical | Axial | Axial |
| Detector Configuration | 64 × 0.625 | 64 × 0.625 | 128 × 0.625 | 128 × 0.625 | 64 × 0.625 | 64 × 0.625 |
| Pitch | 0.4 | 0.4 | 0.4 | 0.4 | - | - |
| FOV (mm) | 250 | 250 | 260 | 250 | 250 | 250 |
| kVp | 120 | 120 | 120 | 100 | 80 | 80 |
| mAs/SLICE | 330 | 280 | 300 | 200 | 150 | 100 |
| Rotation Time (sec) | 0.5 | 0.5 | 0.5 | 0.5 | 0.5 | 0.5 |
| Section thickness (mm) | 3 | 3 | 1 | 1 | 5 | 5 |
| CTDI vol (mGy) | 54.4 | 44.4 | 38.3 | 15.6 | 120 | 72 |

CTA, computerized tomographic angiography; CTDI vol, computerized tomographic dose index volume; CTP, computerized tomographic perfusion; FOV, field of view; NCCT, non-contrast computerized tomography.

for brain imaging. Some of these strategies involve changes in the acquisition parameters (kVp, mill-ampere, pitch, etc.) [5, 6]. Although described scarcely, the risks due to the radiation exposure are believed to be related to the dose received by various radiosensitive organs. Hence, evaluating patient doses during various imaging procedures is essential to justify repeated exposure and optimize them to balance the benefit against radiation risk [7–9]. We evaluated the amount of radiation exposure to the brain and various organs in our stroke patients during various CT-based imaging studies. We created a low-dose protocol to hypothesize that a low-dose protocol would be associated with less radiation exposure, specifically to individual organs, without reducing diagnostic accuracy. We compared radiation exposure between the low-dose protocol and the standard protocol used at our institution using the low-dose protocol. Additionally, we compared to control the image quality between low-dose and standard protocol.

## 2. Material and methods

### *2.1 Patients and scanning parameters*

This retrospective study included 391 consecutive AIS patients admitted to our tertiary center between January and December 2015. The institutional review board approved it. An additional prospective study was performed on the low-dose protocol in 32 consecutive patients. We used Brilliance iCT 256-slice CT scanner (Philips Medical Systems, Eindhoven, Netherlands) that made it possible to shorten the acquisition time, improve image quality with iDose4 algorithms technology and scan a larger anatomical volume during NCCT, CTA, and CTP. The radiometric software was used for tracking the individual as well as a cumulative dose for patients. The dose records were used to audit radiation dose awareness and patient safety at our radiology department. Radimetrics Enterprise (Bayer Healthcare LLC, Whippany, NJ, USA), a web-based dose monitoring solution, allowed the institution to monitor patients' radiation doses and ensure they were kept as low as reasonably achievable (ALARA). This software integrated with our CT units provided several dose matrices from CT procedures such as organ doses, effective dose and whole body integral dose, calculated from Monte Carlo simulations using a library of Cristy phantoms. It is based on scanner-specific values. It uses mathematical descriptions or voxels from scan images. It calculates organ dose and effective dose estimates from the volume-weighted CT dose index CTDI vol (as mGy) and dose length product DLP (as mGy.cm) provided in the DICOM data. The effective dose (E) represents the sum of equivalent doses from all organs, weighted by tissue factors [9, 10]. Effective doses, whole body integral dose and radiation dose to brain, skin, eye, thyroid and red bone marrow doses were extracted for analyses. For the head scan, DLP was measured on the head phantom of 16cm made up of polymethyl-methacrylate (PMMA). This software estimated a size-specific dose estimate (SSDE) based on the water equivalent diameter (WED) according to AAPM calculations [11]. Phillips iDose4 iterative reconstruction technique was employed to maintain image quality after applying dose reduction parameters in NCCT, CTA, and CTP protocols.

The CTDI vol (mGy) and the DLP (mGy.cm) were recorded from the console and tested for their reliability within the 10% range. Under our institution's quality assurance and control program, we developed a low-dose radiation stroke protocol for NCCT and CTP optimized by reducing tube current (mAs) only. In contrast, in CTA, both mAs and kVp were reduced, keeping other exposure factors unchanged (Table 1). We optimized exposure factors for head CT imaging protocols on two Philips CT units, Brilliance 64 slice and i256 slice CT, with iDOSE4 and IMR techniques. We used an anthropomorphic complete angiographic head phantom for making CT images, as it was moulded in tissue-equivalent material. CT image quality could be evaluated quantitatively and qualitatively with actual measurements of details and contrast under the same exposure conditions, repeated many times. For each examination, the weighted CTDI vol and DLP were recorded, and the noise was measured by placing an ROI on two areas in the image on the selected slice for measurements of Hounsefield

**Table 2. Patient metrics.**

| Variable | NCCT | | | CTA | | | CTP | | |
|---|---|---|---|---|---|---|---|---|---|
| | Standard dose (n = 391) | Low dose (n = 32) | *p* value | Standard dose (n = 149) | Low dose (n = 32) | *p* value | Standard dose (n = 61) | Low dose (n = 32) | *p* value |
| Mean Age in years (± SD) | 62 (17) | 63 (17) | 0.098 | 59 (14) | 63 (17) | 0.087 | 60 (17) | 63 (17) | 0.082 |
| Mean Skull Diameter in mm (± SD) | 171.4 (6.9) | 171.3 (7.3) | 0.092 | 186.8 (17.6) | 186.3 (24.3) | 0.074 | 172.7 (23.1) | 172.6 (30.1) | 0.95 |
| Water Equivalent Diameter in mm | 164.9 (7.9) | 164.3 (7.9) | 0.022 | 186.8 (17.6) | 192.5 (38.5) | 0.067 | 172.4 | 176.2 | 0.068 |
| Scan length in mm | 202.8 (52.1) | 204.5 (54.8) | 0.091 | 558.1 (364.9) | 395.1 (320.8) | <0.001 | 2114.4 (278.1) | 1912.4 (418.9) | <0.001 |

CTA, computerized tomographic angiography; CTP, computerized tomographic perfusion; NCCT, non-contrast computerized tomography.

units. Each study was also reviewed for image quality by two technologists, a medical physicist and two radiologists. Continuous variables (CTDI vol, DLP, noise) were compared. Finally, the optimized data for low-dose scanning regimens were compared with the standard protocols. All scans were reviewed by experienced neuroradiologists and stroke neurologists for image quality. The NCCT and the CTA protocol were performed in spiral mode, while CTP was done on axial mode without gantry angulation. For CTA, scanning was performed from the arch of the aorta to the vertex. Scan lengths in both sets of protocols of NCCT, CTA, and CTP were kept similar. We calculated patients' skull diameter and water equivalent diameter to avoid the possible confounding effect of anthropometric variables. Although the effective skull diameter can be calculated automatically, the calculations only in the lateral or anterior-posterior direction may result in a high variability. In addition, such calculations from scout images may vary according to patient centering. We measured the diameter only for axial images to avoid over-estimation, which is not affected by patient centering and produces high accuracy. In addition, we measured water equivalent diameter as this value reflects the x-ray attenuation of the patient and is a good descriptor of patient size.

### 2.2 Radiation dose calculations

Radimetrics software platform (Radimetrics, Bayer Healthcare, Germany), a web-based dose monitoring solution, was used to estimate the organ-specific radiation dose. Monte-Carlo-Simulation was employed for individual organs such as the brain, eyes, skin, red bone marrow and thyroid, ICRP 103 dose equivalent and whole body integral dose [10].

The interrater and interrater reliability for NCCT, CTA and CTP was assessed using intraclass correlation coefficients. The scan quality was graded as 'reasonable' and 'poor'. All measurements performed by 2 blinded investigators (JK and VKS) showed an inter- and intra-observer agreement for NCCT, CTA, and CTP were 0.87/0.90, 0.90/0.93, and 0.86/0.89, respectively (n = 10 samples for each from standard and low dose scanning protocols).

### 2.3 Statistical analysis

All statistical tests were performed with Statistical Package for the Social Sciences (Version 12.0; SPSS, Chicago, Ill, USA). Mann-Whitney U test was used for statistical analysis to compare the means for various quantitative parameters. Customarily distributed quantitative indices were compared using unpaired *t*-test, and means of various radiation exposure values for standard and low-dose radiation protocols were compared. All tests were two-tailed, and a *p*-value of <0.05 was considered statistically significant. All data are presented as the mean ± standard deviation (SD) unless stated otherwise.

## 3. Results

The radiation data for standard-dose protocol for brain imaging for NCCT (n = 391), CTA (n = 149) and CTP (n = 61) were retrieved from the institutional dose tracking system attached to a dedicated CT scanner (Phillips iCT256 with iDose4). Data for the optimized low-dose protocol for NCCT, CTA, and CTP were obtained prospectively for 32 adult AIS patients (mean age 63 ± 17 years vs. 62 ± 17 years for standard-dose patients; $p = 0.098$). Details of various scan parameters such as kVp, mAs, collimation, scan length, rotation time and pitch for standard dose scanning of the head (AAPM) [11] and low-dose optimized stroke protocols for NCCT, CTA and CTP procedures are summarized in Table 1.

### 3.1 NCCT

The patient dose metrics age (years), skull diameter (mm), water equivalent diameter (mm) and scan-length (mm) for NCCT in the standard protocol and low dose protocol are shown in Table 2. Briefly, there were no significant differences in patient metrics in both groups.

The radiation dose parameters such as CTDI vol, DLP, effective dose and whole-body integral dose of the two groups are shown in Table 3. Briefly, the low-dose protocol showed a 10% decrease in dose metrics than the standard protocol, mainly due to the 12.5% decrease in tube current. Similarly, the low-dose protocol showed reduced radiation dose to various radiosensitive organs ($p < 0.001$), as shown in Table 4. There were no significant differences in patient metrics such as skull diameter, water equivalent diameter and scan length between the two radiation dose protocols of NCCT but significant reduction ($p < 0.001$) in dose exposure to all radiosensitive organs except thyroid ($p < 0.58$) in the low-dose protocol.

**Table 3. Radiation dose metrics.**

| Variable | NCCT | | CTA | | CTP | |
|---|---|---|---|---|---|---|
| | Standard dose | Low dose | Standard dose | Low dose | Standard dose | Low dose |
| | (n = 391) | (n = 32) | (n = 149) | (n = 32) | (n = 61) | (n = 32) |
| Mean CTDI vol in mGy (SD) | 52.4 (0.3) | 47.4 (0.05) | 28.7 (8.1) | 14.7 (2.4) | 93.0 (0.9) | 72.0 (1.4) |
| Mean DLP in mGy.cm (SD) | 1061.9 (272.8) | 972.9 (260.2) | 1415.5 (471.1) | 584.6 (281.6) | 1916.2 (339.7) | 995.1 (233.2) |
| Mean ED ICRP 103 in mGy (SD) | 2.6 (0.7) | 2.4 (0.6) | 4.5 (2.5) | 1.6 (0.7) | 4.5 (0.9) | 2.2 (0.5) |
| Whole Body integral in mGy (SD) | 0.4 (0.1) | 0.39 (0.1) | 0.6 (0.2) | 0.2 (0.02) | 0.8 (0.14) | 0.4 (0.09) |

CTA, computerized tomographic angiography; CTDI vol, computerized tomographic dose index; CTP, computerized tomographic perfusion; DLP, dose length product; ED ICRP, Effective dose International commission of radiation protection; NCCT, non-contrast computerized tomography.

**Table 4. Radiation dose to various sensitive organs.**

| Variable | NCCT | | CTA | | CTP | |
|---|---|---|---|---|---|---|
| | Standard dose | Low dose | Standard dose | Low dose | Standard dose | Low dose |
| | (n = 391) | (n = 32) | (n = 149) | (n = 32) | (n = 61) | (n = 32) |
| Mean Brain dose in mGy (SD) | 57.7 (12.1) | 43.1 (9.1) | 101.8 (17.8) | 20.7 (5.7) | 82.1 (3.2) | 55.7 (4.5) |
| Mean Skin dose in mGy (SD) | 8.5 (3.1) | 5.8 (1.6) | 11.6 (2.2) | 2.6 (1.8) | 11.2 (1.7) | 6.1 (1.5) |
| Mean Red Bone Marrow dose in mGy (SD) | 7.4 (2.9) | 5.2 (1.5) | 9.7 (2.9) | 2.6 (1.5) | 8.7 (0.9) | 4.7 (1.3) |
| Mean Eye dose in mGy (SD) | 83.4 (17.4) | 63.6 (17.8) | 159.1 (26.7) | 33.6 (11.7) | 152 (3.2) | 100.3 (24.6) |
| Mean Thyroid dose in mGy (SD) | 26.6 (9.4) | 8.7 (3.8) | 13.4 (5.8) | 11.9 (3.9) | 5.1 (0.9) | 3.3 (0.8) |

CTA, computerized tomographic angiography; CTP, computerized tomographic perfusion; NCCT, non-contrast computerized tomography.

### 3.2 CTA

Patient dose metrics with standard and low-dose CTA protocol are presented in Table 2, while the organ-specific radiation doses for both groups are shown in Table 3. The low-dose protocol was optimized for lower kVp (120 kVp to 100 kVp) and mAs (300 mAs to 200 mAs), maintaining an optimum image quality using the iterative reconstruction of iDose4 similar to the standard protocol. CTDI vol (14.71 $\pm$ 2.39 mGy vs. 28.72 $\pm$ 8.02 mGy) and DLP (584.61 $\pm$ 281.63 mGy.cm vs. 1415.45 $\pm$ 471.01 mGy.cm) were lower in the low-dose imaging protocol ($p < 0.001$).

The brain, skin, red bone marrow, eyes and thyroid received relatively higher radiation doses during CTA than NCCT. However, the effective doses ICRP (103) evaluated in CTA with standard and low-dose protocols were 4.45 $\pm$ 2.5 mSv and 1.57 $\pm$ 0.74 mSv, respectively, showing a reduction of approximately 64% ($p < 0.001$) as well as the advantage of reducing kVp and mAs with low-dose protocols (Table 3). Similarly, dose metrics parameters and organ doses were also reduced (48–50%) considerably ($p < 0.001$) in the low-dose protocol.

### 3.3 CTP

CTP was performed on the same CT machine using the iDose4 iterative reconstruction imaging technique. As suggested by AAPM [11], modified CTP protocol was used, where tube current was reduced to 100 mAs at 80 kVp compared to standard protocol using tube current of 150 mAS at 80 kVp. The patient metrics and dose metrics of both groups are shown in Table 2 and Table 3. In both groups, the scan lengths used in CTP (2114.35 $\pm$ 278.01 mm and 1912.39 $\pm$ 418.99 mm, respectively) are 4–5 times higher than NCCT and CTA protocols. Comparing to the standard protocol of CTP, the optimized low-dose protocol reduced the dose metrics parameters by 45–47% ($p < 0.001$) with a similar reduction of 36–72% in specific organ doses.

### 3.4 The radiation dose for overall stroke protocol in standard and optimized exposure settings

In addition to improving the diagnostic capability of NCCT, CTP and CTA provide important information about cerebral hemodynamics. While CTA demonstrates the patency of the cervico-cranial arterial tree and various intracranial collaterals, CTP estimates the ischemic core and salvageable penumbra in AIS. Most comprehensive acute stroke centers perform one emergent NCCT and CTA at presentation and one NCCT on day 2 (especially in thrombolysis patients). CTP is often performed in patients with the undetermined time of stroke onset, for example, wake-up stroke. CTP is a functional study that utilizes continuous CT acquisition over the same slab of tissue during the dynamic administration of a small contrast bolus. It certainly exposes patients' radiosensitive organs with a higher than usual radiation dose. We employed a low-dose protocol for CTP and could reduce the total effective dose and whole-body equivalent dose by approximately 43% and 46%, respectively, compared to the standard stroke imaging protocol ($p < 0.001$). The corresponding decrease in CTDI vol (134.07 $\pm$ 1.23 mGy vs. 174.08 $\pm$ 3.05 mGy) and DLP (2552.65 $\pm$ 258.33 mGy.cm vs. 4393.56 $\pm$ 361.18 mGy.cm) showed 22.9% and 41.9% reduction in radiation exposure, respectively. Importantly, the image quality of NCCT, CTA, and CTP did not show any appreciable deterioration, confirmed by independent neuroradiologists and stroke neurologists blinded to the clinical and radiation data. All evaluations performed by the two blinded investigators showed inter-and intra-observer agreement for NCCT, CTA and CTP of 0.88/0.92, 0.92/0.94 and 0.89/0.91, respectively (n = 32 samples for each).

The total effective dose for comprehensive stroke imaging (NCCT + CTA + CTP) by standard protocol was 11.48 mSv, while the low-dose protocol delivered a radiation dose of 6.13 mSv, a reduction of 46.6% (Table 3). Patients' age, length of scan coverage, maximum transverse skull diameters, and water equivalent diameter did not differ between the standard dose and low-dose imaging protocols (Table 2).

### 3.5 Organ dose

The software calculated the organ-specific dose for the brain, eye lens, thyroid, red bone marrow and skin for standard and low-dose protocols. All radiosensitive organs showed lower radiation exposure with the low-dose scanning protocol ($p < 0.001$). Table 4 summarizes the organ-specific radiation dose results.

## 4. Discussion

Our findings demonstrate that radiation exposure to the sensitive organs during standard dose neuroimaging protocols employed in AIS patients is within acceptable limits. However, the radiation doses to these organs may be reduced further by using low-dose CT imaging protocols and dose tracking software, without any significant deterioration in the image quality.

The preferred neuroimaging in AIS remains CT-based, mainly due to the widespread availability, rapid acquisition, and acceptable image quality [2, 3]. An NCCT is the first diagnostic test for rapid exclusion of a hemorrhagic stroke, identifying early ischemic signs as well as a quick estimation of tissue damage. Intravenous thrombolysis is often initiated in eligible patients immediately after the completion of NCCT. In patients without any contraindications to radiocontrast, CTA is performed according to the 'bolus tracking' technique and shows the arterial tree from the aortic arch to the circle of Willis. Identification of thrombotic occlusion of a relevant artery helps in early prognostication, prediction of response to intravenous thrombolysis, and early planning for endovascular treatment. Most comprehensive stroke centers employ additional parenchymal imaging to estimate the amount of salvageable penumbra, especially in patients presenting beyond the thrombolysis window. The preferred imaging in this subset of AIS patients is CTP [2]. Furthermore, additional CT scans may be needed in patients with clinical fluctuations, elevating the cumulative radiation dose exposure. Therefore, various radiation dose reduction strategies are often explored, such as modifying exposure factors like tube voltage, lowering tube current, and applying iterative reconstruction of CT images [12–15]. Such strategies may carry a risk of degrading the image quality. This work estimated the radiation dose delivered to various radiosensitive organs in the head and neck region. Furthermore, we demonstrated that employing low-dose imaging protocols for NCCT, CTA, and CTP can reduce the radiation dose delivered to sensitive organs without compromising the image quality. An example of the image quality with standard radiation dose protocol and the low dose protocol for plain CT, CTA and CTP is shown in Fig. 1.

Decreasing the peak voltage (kV) results in a lower dose exposure to the imaged tissues proportional to the square of the change in tube voltage. Furthermore, CT manufacturers have also introduced new techniques of dose reduction, such as dose modulation and iterative reconstruction (iDose4, ADMIRE, and ASIR) to achieve these aims [15–17]. While evaluating the feasibility of low-dose imaging protocol by reducing tube current or current and tube voltage together. We ensured that the level of image quality remained acceptable for diagnostic purposes. We decreased the tube current during stroke imaging protocols for NCCT, CTA as well as CTP. Additionally, we decreased kVp with lower mAs for CTA only to increase the effectiveness of contrast enhancement [15–17].

CTDI vol and DLP are routinely reported on scanner consoles in clinical practice. They do not quantify the patients' dose metrics and provide only the output radiation of the CT scanners determined by many factors, including kVp, mAs, collimation, pitch, slice thicknesses and reconstruction techniques, etc. CTDI vol is a good index when comparing protocols and technical parameter settings. However, it overestimates skin dose if the scan is performed without table movement. We estimated that the CTDI vol value was less than the reference value of 60 mGy for NCCT brain set by ACR guidelines based on AAPM and ICRP recommendations [10, 11, 18]. We used lower mAs in the low-dose protocols (decrease tube current from 330 to 280 mAs) that resulted in a 15% reduction (2.36 mSv) of the radiation dose during NCCT. While trying the low-dose scanning protocols, we found acceptable image quality for CTP at 80 kV and 100 mAs, whereas CTA required100 kV and 200 mAs for similar results. All CT protocols at our center used the iDose4 iterative reconstruction algorithm as a standard scanning procedure, which has been described[1] to ensure the better image quality of CTA and CTP in dynamic enhancing imaging within a reduced radiation dose [16].

Our work provides detailed organ-specific radiation dose values associated with the standard and low-dose scanning protocol for CT-based studies in AIS. Doses to individual organs may be more appropriate in estimating cancer risk from CT exposure [17–19]. Eye lenses are susceptible to radiation as they are directly in the radiation beam and exposed to higher radiation doses. ICRP (2012) has recently set the thresholds in absorbed dose to 500 mGy for the eye lens [19].

1 ACR Practice Guideline for the Performance of Computed Tomography (CT) Perfusion in Neuroradiologic Imaging 2017 (https://www.acr.org/-/media/ACR/Files/Practice-Parameters/ct-perfusion.pdf); accessed on 16 May 2020.

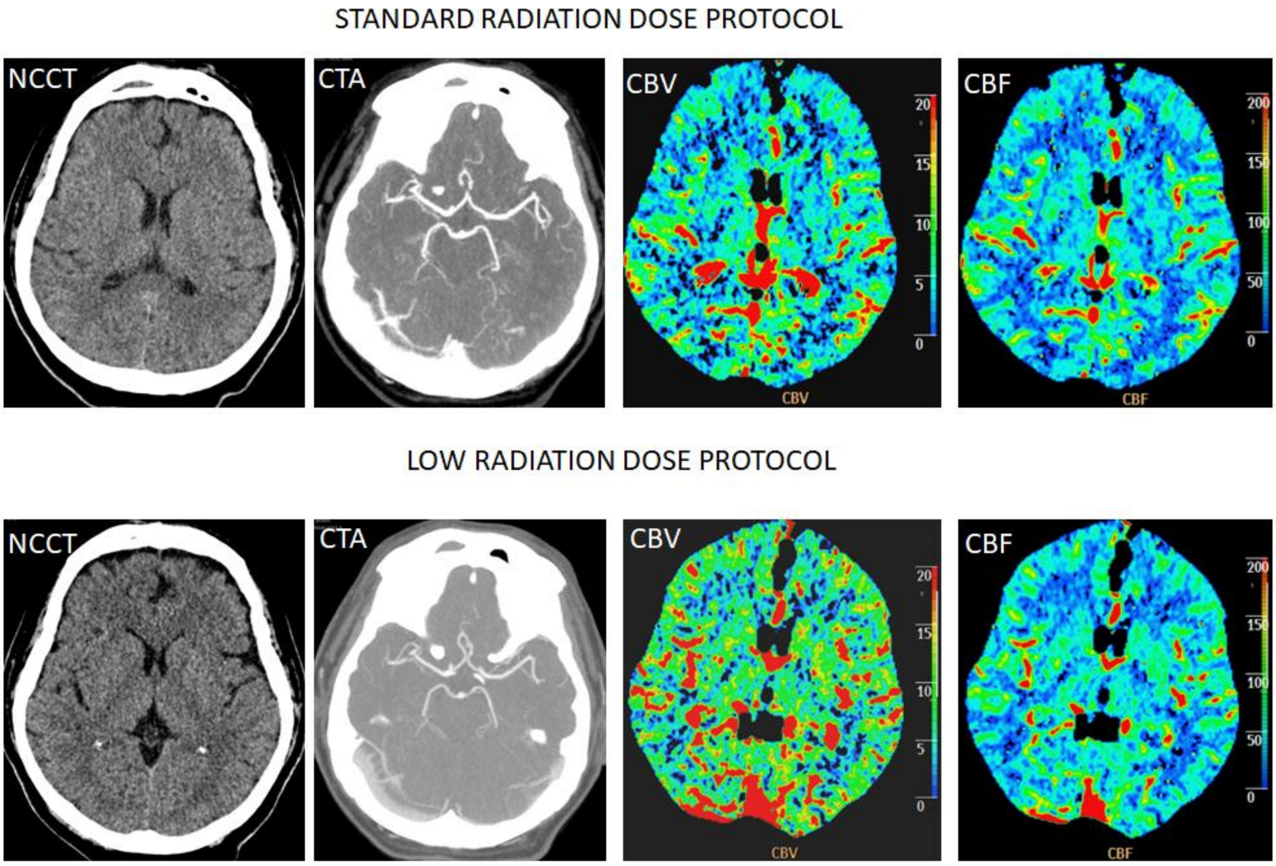


**Fig. 1. Comparative Image quality with standard radiation dose protocol and the low dose protocol for non-contrast-enhanced computed tomography (NCCT), CT angiography (CTA) and CT perfusion (CTP) in a 62 years old patient who presented with acute ischemic stroke.** The top panel shows NCCT, CTA and CTP images performed using the standard radiation dose protocol. As a part of a research project, this patient underwent repeat imaging studies using the low radiation dose protocol. The resultant representative images are shown in the lower panel.

The radiation exposure to eye lens was only 197.58 mGy in the low-dose group when NCCT, CTA, and CTP were performed in a patient. Other sensitive organs such as skin and red bone marrow showed significantly reduced exposure in the low-dose protocol. For example, the estimated dose exposure to the thyroid gland was 25.35 mGy, which is similar to the reported literature [19, 20]. Importantly, the total effective dose during comprehensive scanning (NCCT + CTA + CTP) was 6.128 mSv in the low-dose protocol as compared 11.48 mSv in the standard scanning, a reduction of 46.6%. Furthermore, we used the statistical Iterative Reconstruction IDose4 algorithm for CT reconstruction, which ramps the image clarity and reduces noise compared to the standard filtered back projection (FBP) technique. This enabled comparable image quality even with significantly reduced radiation dose in all CT-based imaging protocols.

Some limitations need to be acknowledged. First, the standard dose and low-dose CT scans were not acquired in the same patient. Standard dose CT studies would have served as a reference against which the diagnostic quality and imaging findings of low-dose scans could have been assessed. However, it would have been unethical to expose the human subjects to additional radiation exposure. Second, the blinded neuroradiologists and stroke neurologists had a good agreement in reading various imaging studies. The low-dose CT studies might have failed to detect tiny parenchymal lesions in some patients. Last, there was no reference standard for CTP studies. We strongly feel that faster MRI brain perfusion studies (with no ionizing radiation) in a smaller subset of the study population could have served as the standard control to evaluate the scan quality for CTP. However, this approach would have exposed our patients to an additional dose of a nephrotoxic contrast agent. Acute stroke care had changed considerably since this research work was performed. An increasing number of endovascular interventions are being performed, especially among patients with large vessel occlusions. This certainly increases the amount of radiation exposure. However, we cannot comment on this aspect since no acute stroke interventions were performed.

Furthermore, reduction of radiation exposure in CTP did not degrade the quality of images. However, one should be careful in optimizing the post-processing of the source images since the reduced dose might lead to clinically relevant infarct core overestimation in individual cases [21]. Lastly, Dose Area Product (DAP) size or Kerma Area Product (KAP) size are currently used to represent patient exposure during diagnostic X-ray examinations and interventional procedures. DAP is greatly affected due to scattered radiation being the primary source of exposure (mostly during interventional procedures). However, this information was not collected.

## 5. Conclusions

Radiation dose is a significant concern for clinicians and patients with the increased use of CT-based examination. Our data show that although the standard dose techniques deliver an acceptable radiation dose, a low-dose scanning protocol may be adopted while maintaining acceptable image quality. Continuous radiation monitoring, controlling and optimizing stroke CT protocols with dose tracking software will help implement best practices for the safe use of ionizing radiation in medical imaging.

## Abbreviations

AIS, acute ischemic stroke; ALARA, as low as reasonably achievable; CT, computerized tomography; CTA, computerized tomographic angiography; CTP, computerized tomographic perfusion; DLP, dose length product.

## Author contributions

SCK and VKS conceived and designed the study; SCK and JK performed the radiation dose measurements; SCK wrote the initial draft of the paper; JK and VKS provided critical revision and final approval.

## Ethics approval and consent to participate

The study was approved by institutional ethics committee (NHG DSRB 2012/00517).


## Acknowledgment

We thank Arvind K Sinha for technical guidance during the study. We also thank the anonymous reviewers for their constructive comments and suggestions.

## Funding

The study was supported by a research grant from National Medical Research Council, Singapore (NMRC//CSA/037/2012).


## Conflict of interest

The authors declare no conflict of interest.

## References


[1] Go AS, Mozaffarian D, Roger VL, Benjamin EJ, Berry JD, Borden WB, *et al.* Heart disease and stroke statistics–2013 update: a report from the American Heart Association. Circulation. 2013; 127: e6–e245.

[2] Powers WJ, Rabinstein AA, Ackerson T, Adeoye OM, Bambakidis NC, Becker K, *et al.* 2018 Guidelines for the early management of patients with acute ischemic stroke: A guideline for healthcare professionals from the American Heart Association/American Stroke Association. Stroke. 2018; 49: e46–e110.

[3] Powers WJ, Derdeyn CP, Biller J, Coffey CS, Hoh BL, Jauch EC, *et al.* Focused Update of the 2013 Guidelines for the Early Management of Patients With Acute Ischemic Stroke Regarding Endovascular Treatment: A Guideline for Healthcare Professionals From the American Heart Association/American Stroke Association. Stroke. 2015; 46: 3020–3035.

[4] Smith AB, Dillon WP, Gould R, Wintermark M. Radiation dose-reduction strategies for neuroradiology CT protocols. American Journal of Neuroradiology. 2007; 28: 1628–1332.

[5] Kalra MK, Maher MM, Toth TL, Hamberg LM, Blake MA, Shepard JA, *et al.* Strategies for CT radiation dose optimization. Radiology. 2004; 230: 619–628.

[6] Faulkner K, Moores BM. Radiation dose and sometic risk from computed radiography. Acta Radiologica. 1987; 28: 483–438.

[7] McCollough CH, Primak AN, Braun N, Kofler J, Yu L, Christner J. Strategies for reducing radiation dose in CT. Radiologic Clinics of North America. 2009; 47: 27–40.

[8] The 2007 Recommendations of the International Commission on Radiological Protection. ICRP publication 103. Annals of the ICRP. 2007; 37: 1–332.

[9] Valentin J. International Commission on Radiation Protection. Managing patient dose in multi-detector computed tomography (MDCT). ICRP Publication 102. Annals of the ICRP. 2007; 37: 1–79.

[10] Huda W, Magill D, He W. CT effective dose per dose length product using ICRP 103 weighting factors. Medical Physics. 2011; 38: 1261–1265.

[11] McCollough C, Bakalyar DM, Bostani M, Brady S, Boedeker K, Boone JM, *et al.* Use of Water Equivalent Diameter for Calculating Patient Size and Size-Specific Dose Estimates (SSDE) in CT: The Report of AAPM Task Group 220. AAPM Report. 2014; 2014: 6–23.

[12] Wintermark M, Maeder P, Verdun FR, Thiran JP, Valley JF, Schnyder P, Meuli R. Using 80 kVp vs. 120 kVp in perfusion CT measurement of regional cerebral blood flow. American Journal of Neuroradiology. 2000; 21: 1881–1884.

[13] Hirata M, Sugawara Y, Fukutomi Y, Oomoto K, Murase K, Miki H, *et al.* Measurement of radiation dose in cerebral CT perfusion study. Radiation Medicine. 2005; 23: 97–103.

[14] Lin CJ, Wu TH, Lin CH, Hung SC, Chiu CF, Liu MJ, *et al.* Can iterative reconstruction improve imaging quality for lower radiation CT perfusion? Initial experience. American Journal of Neuroradiology. 2013; 34: 1516–1521.

[15] Huda W, Lieberman KA, Chang J, Roskopf ML. Patient size and x-ray technique factors in head computed tomography examinations. II. Image quality. Medical Physics. 2004; 31: 595–601.

[16] Padole A, Ali Khawaja RD, Kalra MK, Singh S. CT radiation dose and iterative reconstruction techniques. American Journal of Roentgenology. 2015; 204: W384–W392.

[17] Cohnen M, Wittsack HJ, Assadi S, Muskalla K, Ringelstein A, Poll LW, *et al.* Radiation exposure of patients in comprehensive computed tomography of the head in acute stroke. American Journal of Neuroradiology. 2006; 27: 1741–1745.

[18] Rehani MM. ICRP and IAEA actions on radiation protection in computed tomography. Annals of the ICRP. 2012; 41: 154–160.

[19] Stewart FA, Akleyev AV, Hauer-Jensen M, Hendry JH, Kleiman NJ, Macvittie TJ, *et al.* ICRP publication 118: ICRP statement on tissue reactions and early and late effects of radiation in normal tissues and organs–threshold doses for tissue reactions in a radiation protection context. Annals of the ICRP. 2012; 41: 1–322.

[20] Omer H, Alameen S, Mahmoud WE, Sulieman A, Nasir O, Abolaban F. Eye lens and thyroid gland radiation exposure for patients undergoing brain computed tomography examination. Saudi Journal of Biological Sciences. 2021; 28: 342–346.

[21] Karwacki GM, Vögele S, Blackham KA. Dose reduction in perfusion CT in stroke patients by lowering scan frequency does not affect automatically calculated infarct core volumes. Journal of Neuroradiology. 2019; 46: 351–358.

Radiology and Diagnostic Imaging

Research Article ISSN: 2515-0200

# CT radiation dose optimization and reduction for routine head, chest and abdominal CT examination

**Lama Sakhnini***

Department of Physics, College of Science, University of Bahrain, Sakhir, Kingdom of Bahrain

## Abstract

The purpose of this study is to find an optimization approach to minimize the absorbed dose to adult patients undergoing CT examination, while maintain the diagnostic image quality. A single detector CT was considered, to represent typical practice in King Hamad University Hospital. We included 626 patients in this study and investigated radiation dose for three anatomical regions, head, chest and abdomen and pelvis. For each type of CT examination, two groups of patients were considered. 383 patients in Group I: were imaged according to the protocols set by the manufacturer. Group II: 243 patients were imaged according to the protocols set by our team after optimization. We were able to adjust the adjustable factors such as noise index, scan time, pitch, rotation time and slice thickness. For each examination the weighted volume CT dose index (CTDIvol) and dose length product (DLP) were recorded and noise is measured. Each study was also reviewed for image quality. Measured (CTDIvol, DLP) were compared to international reference levels. For Group I, the CTDIvol and DLP values were higher than the reference levels. After Dose optimization the CTDIvol and DLP values were significantly reduced to have lower values than the reference levels. The results of our study showed that the CTDIvol and DLP values taken from images done using the protocols set by the Ct machine developers are higher than the reference levels which indicate that manufacturers are focusing their efforts toward improving image quality rather than the minimizing the dose that can be given to the patient.

## Introduction

The use of helical, multislice CT (MSCT) is rapidly growing due to technological improvements in the modern machines. Advances in CT imaging techniques have resulted in a significant increase in the frequency of CT examinations in both adult and children, replacing more and more radiographic examinations. However, CT can be responsible for the increase of carcinogenesis [1-4]. But we have to accept the fact that with the vast improvement of technology, patients benefited from a quicker and more accurate diagnosis and precise anatomic information for planning therapeutic procedures. This lead to a substantial increase in the collective dose, as reported by international organizations (ICRP 2000 and United Nations Scientific Committee 2000) [5]. In spite of this constructive contributions of CT to modern healthcare, attention must also be given to the health risk associated with the ionizing radiation received during a CT exam. Because of this potential radiation risk from this increased use of CT makes it important that CT doses be kept as low as reasonably achievable. However, modern CT scanners have a wide variety of exposure factors and involve techniques that allow dose optimization to the patient [6-9]. Guidelines to optimize the protection of patients during CT procedures have been provided by various international organizations [10-13]. All implemented guidelines include reference doses that are defined as diagnostic reference levels (DRLs) or guidance levels. These guidelines assist in the optimization and reduction of patient protection and allow comparisons between the different CT scanners and techniques. The dose parameters suggested in the guidelines are the volume CT dose index (CTDIvol) and dose length product (DLP) for the entire examination.

Although there is still adequate room for improvement, CT dose reduction requires a combination of different approaches or strategies. These include optimization of scanning protocols according to age- or weight-based adjustments, justification of CT use by referring physicians and emergency departments, decrease of unnecessary examinations, development of better exposure protocols by manufacturers, and better training and education for radiological technologists. However, to our knowledge, no reports are available in Bahrain with regard to the investigation of CT scanning protocols. There are no standardized procedures for CT imaging across hospitals in Bahrain, as each hospital has its own specific protocol, which are not necessarily optimized in terms of dose reduction.

The purpose of this study was to assess the adult CT practice, analyze CT scanning parameters used in routine head, chest and abdomen and pelvis imaging in the radiology department at King Hamad University Hospital. Moreover, our practical goal was to find an optimization approach to minimize the absorbed dose to adult patients undergoing CT examination, while maintain the diagnostic image quality.

We hope that the results of this study could be used by radiologists and medical imaging technologists to modify their existing practice and serve as one of the basis for optimization of CT imaging. Additionally, the medical community in Bahrain needs to better educate the public to the risks and benefits associated with CT, such that they can make conscience decisions based on scientific facts regarding their healthcare.

## Materials and methods

### Patient examinations

In this study, medical images taken by Optima CT660 system (GE Health Care, WI, USA) are considered. Adult head, chest, and

***Correspondence to:*** Lama Sakhnini, Department of Physics, College of Science, University of Bahrain, Sakhir, Kingdom of Bahrain; E-mail: l_sakhnini@yahoo.com

**Received:** November 1, 2017; **Accepted:** December 12, 2017; **Published:** December 15, 2017

abdominal and pelvis CT examinations were chosen for the evaluations because they are most common procedures performed in the radiology department. The hospital ethics committees of King Hamad University Hospital approved the study protocol.

### Radiation dose

Radiation dose to the patient was monitored for each study by means of the two standard dose indicators, volume CT dose index (CTDIvol) and dose length product (DLP), that were calculated by the CT scanner for each CT study. The CTDIvol parameter is representative of the average dose delivered within the reconstructed section. The CTDIvol represents the weighted CT dose index divided by the pitch and describes the average dose throughout a 160-mm-diameter circular Plexiglas phantom, incorporating the central dose weighted by a 1/3 factor and the peripheral dose weighted by a 2/3 factor. The DLP can be related to energy imparted to organs and can thus be used to assess the overall radiation burden of a given examination. It is equal to the product of the CTDIvol and the length of the scan in centimeters (Huda and Mettler 2011 [14]).

### Effective dose estimate

The effective dose estimate was determined by using a DLP-based method in which CT dose estimates are calculated by multiplying a DLP value and an appropriate conversion factor. Accordingly, conversion factors for the DLP-based method should be updated (ICRP 2007, Deak et al 2010 [15]) (Table 1).

### Statistical analysis

For each type of CT study, differences between the two groups of patients in terms of radiation dose values were evaluated for statistical significance. Differences were considered significant at $P < 0.05$ and 0.01.

### Data collected

The studied data included patient sex, and age; tube voltage and tube current settings; pitch; section thickness; number of sections; volume CT dose index (CTDIvol) and dose length product (DLP). Patients in Group I was imaged according to the protocols set by the GE. Group II were imaged according to the protocols set by our team after optimization.

## Results

We evaluated our three most frequent types of CT studies: adult brain CT performed without contrast material (unenhanced CT), abdomen and pelvis CT, chest CT in adult patients. Data from 626 examinations for the two studied groups of patients who underwent routine head, chest, abdominal and pelvic CT were collected. Group I was for patients before optimization, while Group II for the patients after optimization. These subjects included 152 patients who underwent head CT, 422 who underwent chest CT, and 52 who underwent abdominal CT.

Prior to the introduction of dose optimization, and to evaluate the dose, patients' data were collected, analyzed and compared with the international standards [16-18]**.** The general results are shown in Table 2.

The CTDIvol and DLP values were higher than the reference levels given by of the international standards. Dose reduction through optimization of the examination protocol was then considered. We were able to adjust the adjustable factors such as noise index, scan time, pitch, rotation time and slice thickness. However, we limited the pitch to ≤ 1.37, as sampling gaps occur if higher pitch values are used that lead to image reconstruction artifacts. In planning the scan, issues that are related to quality had to be considered include image noise and image contrast. For the purpose of minimizing radiation dose exposure, noisier images, if sufficient for radiological diagnosis, should be accepted. Dose reduction efforts were matched with this critical component in order to maximize the quality/dose ratio. For chest examination we restricted our protocol for a slice thickness of 5mm, while we allowed the value to be 2.5 or 5mm for abdominal and pelvic examination. We initially tried 5 mm, but this section thickness was judged sometimes to be insufficient by our radiologists in terms of spatial resolution. Hence, for abdomen and pelvis CT the slice thickness was chosen to be either 2.5 mm for renal or 5 mm for routine evaluation. However, a thinner section thickness (1.25 or 0.625mm) was required in few cases to achieve better spatial resolution and enable assessment of fine anatomic details in these studies.

The range of the modulated tube current in milliamperes was decided subjectively by a registered radiology technologist, in a range set by the technologist, on the basis of different factors. The noise index NI was initially set at its lowest value and slowly increased until the image quality was determined to be sufficient by the radiologists. A lower NI leads to lower noise and thus into an improved image. However, a lower NI (better image quality) requires higher tube current for a given pitch and tube rotation time and therefore delivers higher patient radiation dose. The rotation time for most types of scans was lowered from 1 second to 0.5 second.

The important technical factors and radiation doses, including volumetric CT dose index and DLP values, at routine head, chest, and abdominal CT for Group I and group II are listed in Tables 3, 4, and 5, respectively.

Both CTDIvol and DLP were significantly lowered from for unenhanced female adult brain from (79 to 40 mGy) and for male adult from (79 to 46 mGy) (Table 3). Regarding adult abdomen and pelvis CT (Table 4), CTDIvol were lowered from (20.7 to 19.0) for adult females and for adult males from (37.3 to 17.8 mGy) when dose optimization was considered compared with CTDIvol and DLP when dose optimization was not used. Regarding chest CT in adult patients (Table 5), CTDIvol and DLP were lowered from (21.4 to 14.2 mGy) and from (22.3 to 14.3 mGy) for adult males.

## Discussion and conclusion

In this study we investigated the DRLs for three anatomical regions, head, chest and abdomen and pelvis for both females and male patients. Two groups were considered, in Group I patients were imaged according to the protocols set by the GE and in Group II patients were imaged according to the protocols set by our team after optimization.

The results of our study demonstrate that the radiation doses for Group I were higher than the international guidelines. This indicates that manufacturers are focusing their efforts toward improving image quality regardless to the radiation limits and guidelines. After optimization (Group II) radiation doses were lower than the DRLs for the head, abdomen and chest CT examinations.

The mean weighted CT dose index CTDIvol for head after optimization (Group II) (43.8 mGy) for head CT in the entire sample (Female and Male patients) was comparable to values reported by other authors (34–56 mGy) [19,20] (58-66) [8], and in the range of the value reported by the IAEA coordinated research project (19-51 mGy) [11]. The mean DLP (760 mGy.cm) for head CT was comparable also to

**Table 1.** Adult Conversion Factors for Dose-Length Product-Based CT Dosimetry Based on International Commission on Radiological Protection (ICRP) Publication 103, (ICRP 2007) and summarized by [15].

| Age | kVp | Male | | | | | Female | | | | |
|---|---|---|---|---|---|---|---|---|---|---|---|
| | | Head | Neck | Chest | Abdomen | Pelvis | Head | Neck | Chest | Abdomen | Pelvis |
| Adult | 80 | 0.0017 | 0.005 | 0.0107 | 0.0132 | 0.01 | 0.0019 | 0.0055 | 0.0188 | 0.017 | 0.0157 |
| | 100 | 0.0018 | 0.0049 | 0.0104 | 0.0132 | 0.0099 | 0.002 | 0.0053 | 0.0183 | 0.017 | 0.0155 |
| | 120 | 0.0018 | 0.0049 | 0.0105 | 0.0134 | 0.01 | 0.002 | 0.0053 | 0.0185 | 0.0173 | 0.0157 |
| | 140 | 0.0018 | 0.005 | 0.0107 | 0.0134 | 0.0102 | 0.002 | 0.0055 | 0.0188 | 0.0173 | 0.016 |

**Table 2.** Comparison of Head, Chest, and Abdominal CT Dose Values with DRLs given in the international standards [16,17,18]. Group I was imaged according to the protocols set by the GE. Group II were imaged according to the protocols set by our team after optimization.

| *Examination* | *Dose Parameter* | *Group I* | *Group II* | *EU 2004* | *UK 2003* | *IAEA 2006* |
|---|---|---|---|---|---|---|
| **Head CT** | **CTDIvol (mGy)** | 79 | 44 | 60 | 100 | 47 |
| | **DLP (mGy·cm)** | 1218 | 760 | 1050 | 1050 | 1050 |
| **Chest CT** | **CTDIvol (mGy)** | 22 | 14 | 30 | 14 | 9.5 |
| | **DLP (mGy·cm)** | 794 | 401 | 650 | 580 | 447 |
| **Abdominal CT** | **CTDIw (mGy)** | 31 | 18 | 35 | 13 | 10.9 |
| | **DLP (mGy·cm)** | 1097 | 831 | 780 | 560 | 696 |

**Table 3.** The important technical factors and radiation doses, at routine head, for Group I and group II. Group I was imaged according to the protocols set by the GE. Group II were imaged according to the protocols set by our team after optimization.

| **Head** | **Group I** | | **Group II** | |
|---|---|---|---|---|
| | **Adult Females** | **Adult males** | **Adult Females** | **Adult males** |
| **No of Patients** | 44 | 50 | 25 | 33 |
| **Average Age** | 53.4 | 54.4 | 53.2 | 53.9 |
| **Milliampere** | 224-322 | 202-385 | 157-344 | 202-409 |
| **$CTDI_{vol}$ (mGy)** | 79 | 79 | 40 | 46 |
| **DLP (mGy.cm)** | 1198 | 1207 | 655 | 831 |
| **Slice thickness (mm)** | 2.5 | 2.5 | 5 | 5 |
| **Rotation time (second)** | 1.2 | 1 | 0.5 | 0.5 |
| **pitch** | 0.78 | 0.76 | 0.98 | 0.98 |
| **Conversion factor** | 0.002 | 0.0018 | 0.002 | 0.0018 |
| **E (mGy)** | 2.4 | 2.2 | 1.3 | 1.5 |

**Table 4.** The important technical factors and radiation doses, at routine abdomen and pelvis, for Group I and group II. Group I was imaged according to the protocols set by the GE. Group II were imaged according to the protocols set by our team after optimization.

| **Abdomen and pelvis** | **Group I** | | **Group II** | |
|---|---|---|---|---|
| | **Adult Females** | **Adult males** | **Adult Females** | **Adult males** |
| **No of Patients** | 95 | 167 | 70 | 90 |
| **Average Age** | 44.5 | 44.1 | 39 | 42.2 |
| **Milliampere** | 308-429 | 303-410 | 304-403 | 299-408 |
| **$CTDI_{vol}$ (mGy)** | 20.7 | 37.3 | 19.0 | 17.8 |
| **DLP (mGy.cm)** | 1090 | 1100 | 814 | 838 |
| **Slice thickness (mm)** | 2.5 | 2.5 | 2.5-5 | 2.5-5 |
| **Rotation time (second)** | 0.85 | 0.85 | 0.5 | 0.5 |
| **pitch** | 1.35 | 1.35 | 1.37 | 1.37 |
| **Conversion factor** | 0.0173 | 0.0134 | 0.0173 | 0.0134 |
| **E (mGy)** | 18.9 | 14.7 | 14.1 | 11.2 |

**Table 5.** The important technical factors and radiation doses, at routine chest, for Group I and group II. Group I was imaged according to the protocols set by the GE. Group II were imaged according to the protocols set by our team after optimization.

| **Chest** | **Group I** | | **Group II** | |
|---|---|---|---|---|
| | **Adult Females** | **Adult males** | **Adult Females** | **Adult males** |
| **No of Patients** | 14 | 13 | 12 | 13 |
| **Average Age** | 60.7 | 57.2 | 59.1 | 46.5 |
| **Milliampere** | 342-426 | 218-376 | 330-425 | 250-380 |
| **$CTDI_{vol}$ (mGy)** | 21.4 | 22.3 | 15.2 | 14.29 |
| **DLP (mGy.cm)** | 770 | 819 | 480 | 401 |
| **Slice thickness (mm)** | 2.2 | 2.1 | 5 | 5 |
| **Rotation time (second)** | 1.25 | 1.13 | 0.5 | 0.5 |
| **pitch** | 0.85 | 0.88 | 1.37 | 1.37 |
| **Conversion factor** | 0.0185 | 0.0105 | 0.0185 | 0.0105 |
| **E (mGy)** | 14.2 | 8.6 | 8.9 | 4.2 |

the results reported by other authors such as [21] (740 mGy .cm) and [22] (587 mGy. cm) (31), and [17] (787 mGy.cm). It should be noted, however, that all of these authors reported values that were much lower than the European and IAEA DRL (1050 mGy.cm).

The mean weighted CT dose index for abdominal CT after optimization was 18.2 mGy, which is in the range of values (16–29 mGy) reported by a number of other authors [17,19,23]. On the other hand, the mean DLP for abdominal CT (830 mGy. cm) is higher than the values reported by [23] (493–551 mGy.cm). It should be noted, however, that the above values were taken in the upper part of the abdomen and not in the entire abdominal region, so the scanned region in the patient was substantially decreased. On the other hand, all of the abdominal CT examinations performed in the KHUH were in fact abdominal-pelvic examinations, and this partially explains why the mean DLP for abdominal CT (696 mGy.cm) at our hospital was higher than the mean DLP for our entire sample (549 mGy.cm).

Moreover, the mean weighted CT dose index (14.3 mGy) for chest CT was lower than the value reported in the previous IAEA-coordinated research project (16.2 mGy) (IAEA 2004) [10]. The mean DLP (401 mGy. cm) for chest CT was lower than the IAEA-reported value (455 mGy.cm) [11].

Our study was limited by the decision to examine only adult patients from our hospital, so the results did not include smaller health centers or private hospitals in the country.

We found that dose optimization resulted in significant reductions in radiation dose to adults ($P \leq 0.001$). As our study was performed in one center only and with one type of CT scanner, hence these obtained data and results should be confirmed in studies that evaluate CT scanners from other manufacturers. In conclusion, we recommend routine use of dose optimization for all CT examinations, because this approach affords a significant dose reduction while preserving image quality. Implementation of dose optimization requires a fine-tuning process to identify optimal signal-to-noise level for each type of CT study performed. Although, we investigated the effect of dose optimization on all our CT protocols, but this study is limited to our radiology department and further investigation should be done in other hospitals in the country.

## References

1. Committee to assess health risks from exposure to low levels of ionizing radiation NRC (2006) Health risks from exposure to low levels of ionizing radiation: BEIR VII Phase 2. Washington, DC: National Academies Press: 2006.

2. Hall EJ, Brenner DJ (2008) Cancer risks from diagnostic radiology. *Br J Radiol* 81: 362-378. [Crossref]

3. Berrington de González A, Mahesh M, Kim KP, Bhargavan M, Lewis R (2009) Projected cancer risks from computed tomographic scans performed in the United States in 2007. *Arch Intern Med* 169: 2071-2077. [Crossref]

4. Mathew JD, Forsythe AV, Brady Z, Butler MW, Goergen SK, et al. (2013) Cancer risk in 680,000 people exposed to computed tomography scans in childhood or adolescence: data linkage study of 11 million Australians. *BMJ* 346: f2360. [Crossref]

5. United Nations Scientific Committee on the Effects of Atomic Radiation (2000) Report to the general assembly, annex D: medical radiation exposures. New York, NY: United Nations.

6. McCollough CH, Primak AN, Braunc N, Kofler J, Yu L, et al. (2009) Strategies for Reducing Radiation Dose in CT. *Radiol Clin North Am* 47: 27-40. [Crossref]

7. Graser A, Wintersperger BJ, Suess C, Reiser MF, Becker CR (2006) Dose reduction and image quality in MDCT colonography using tube current modulation. *AJR Am J Roentgenol* 187: 695-701. [Crossref]

8. Foley SJ, McEntee MF, Rainford LA (2012) Establishment of CT diagnostic reference levels in Ireland. *Br J Radiol* 85: 1390-1397. [Crossref]

9. Yates SJ, Pike LC, Goldstone KE (2014) Effect of multislice scanners on patient dose from routine CT examinations in East Anglia. *Br J Radiol* 77: 472-478. [Crossref]

10. IAEA, International Atomic Energy Agency (2004) Optimisation of the radiological protection of patients undergoing radiography, fluoroscopy and computed tomography. Document no. IAEA-TECDOC-1423. Vienna, Austria: International Atomic Energy Agency.

11. Tsapaki V, Aldrich JE, Sharma,R, Staniszewska MA, Krisanachinda A, et al. (2006) Dose Reduction in CT while Maintaining Diagnostic Confidence: Diagnostic Reference Levels at Routine Head, Chest, and Abdominal CT—IAEA-coordinated Research Project. *Radiology* 240: 828-834. [Crossref]

12. International Commission on Radiological Protection 2000: managing patient dose in computed tomography. In: Annals of International Commission on Radiological Protection. ICRP 84. Didcot, Oxfordshire, England: Pergamon, 2000.

13. European Guidelines on Quality Criteria for Computed Tomography. Report EUR 16262. Brussels, Belgium: European Commission, 1999.

14. Huda W, Mettler FA (2011) Volume CT Dose Index and Dose-Length Product Displayed during CT: What Good Are They? *Radiology* 258: 236-242. [Crossref]

15. Deak PD, Smal Y, Kalender WA (2010) Multisection CT Protocols: Sex- and Age-specific Conversion Factors Used to Determine Effective Dose from Dose-Length Product. *Radiology* 257: 158-166. [Crossref]

16. Bongartz G, Golding SJ, Jurik AG, Leonardi M, van Persijn van Meerten E, et al. (2004) Quality criteria for multislice computed tomography. Results from a European concerted action on CT (FIGM-CT-2000-20078) Appendix B: European field survey on MSCT

17. Shrimpton PC, Hillier MC, Lewes MA, Dunn M (2005) National Radiological Protection Board (NRPB): doses from computed tomography examinations in the UK—2003 review. Document NRPB-W67. Chilton, England: National Radiological Protection Board.

18. Shrimpton PC, Hillier MC, Lewis MA, Dunn M (2006) National survey of doses from CT in the UK: 2003. *Br J Radiol* 79: 968-980. [Crossref]

19. Fridberg E, Borretzen I, Olerud M (2003) Dual and multidetector-row CT: what about the doses?" Presented at the Radiation Protection Symposium of the North West European Radiation Protection Societies, Utrecht, the Netherlands.

20. Prokop M, Galanski M (Eds.) Spiral and Multislice Computed Tomography of the Body, Thieme, New York, NY (2003), pp. 131-16.

21. Torp C, Olerud H, Einarson G, Gron P, Leitz W, et al. (2001) Use of the EC quality criteria as a common method of inspecting CT laboratories: a pilot study by the Nordic Radiation Protection Authorities—radiological protection of patients in diagnostic and interventional radiology, nuclear medicine and radiotherapy. Document IAEA-CN-85-175. Vienna, Austria: International Atomic Energy Agency.

22. Hidajat N, Wolf M, Nunnemann A, Liersch P, Gebauer B, et al. (2001) Survey of conventional and spiral ct doses. *Radiology* 218: 395-401. [Crossref]

23. Papadimitriou D, Perris A, Manetou A, Molfetas M, Panagiotakis N, et al. (2003) A survey of 14 computed tomography scanners in Greece and 32 scanners in Italy. Examination frequencies, dose reference values, effective doses and doses to organs. *Radiat Prot Dosimetry* 104: 47-53. [Crossref]

Dose-Response:
An International Journal
January-March 2020:1-8

DOI: 10.1177/1559325820909778
journals.sagepub.com/home/dos
SAGE

# Benefits of Low-Dose CT Scan of Head for Patients With Intracranial Hemorrhage

**Dan Wu[1], Gang Wang[2], Bingyang Bian[1], Zhuohang Liu[1], and Dan Li[1]**

## Abstract

**Objectives:** For patients with intracranial hemorrhage (ICH), routine follow-up computed tomography (CT) scans are typically required to monitor the progression of intracranial pathology. Remarkable levels of radiation exposure are accumulated during repeated CT scan. However, the effects and associated risks have still remained elusive. This study presented an effective approach to quantify organ-specific radiation dose of repeated CT scans of head for patients with ICH. We also indicated whether a low-dose CT scan may reduce radiation exposure and keep the image quality highly acceptable for diagnosis.

**Methods:** Herein, 72 patients with a history of ICH were recruited. The patients were divided into 4 groups and underwent CT scan of head with different tube current–time products (250, 200, 150, and 100 mAs). Two experienced radiologists visually rated scores of quality of images according to objective image noise, sharpness, diagnostic acceptability, and artifacts due to physiological noise on the same workstation. Organ-/tissue-specific radiation doses were analyzed using Radimetrics.

**Results:** In conventional CT scan group, signal to noise ratio (SNR) and contrast to noise ratio (CNR) of ICH images were significantly higher than those in normal brain structures. Reducing the tube current–time product may decrease the image quality. However, the predilection sites for ICH could be clearly identified. The SNR and CNR in the predilection sites for ICH were notably higher than other areas. The brain, eye lenses, and salivary glands received the highest radiation dose. Reducing tube current–time product from 250 to 100 mA can significantly reduce the radiation dose.

**Discussion:** We demonstrated that low-dose CT scan of head can still provide reasonable images for diagnosing ICH. The radiation dose can be reduced to ~45% of the conventional CT scan group.

## Keywords

repeated computed tomography, radiation dose, intracranial hemorrhage, Monte Carlo simulation

## Introduction

Since invention of computed tomography (CT) in the 1970s, it has remarkably influenced medical researches.[1,2] There is a considerable literature questioning the use of CT, or the use of multiple CT scans, in a variety of contexts, including management of blunt trauma, seizures, and chronic headaches, and particularly questioning its use as a primary diagnostic tool for acute appendicitis in children.[3] Specially for intracerebral hemorrhage (ICH), CT scan can accurately display location of ICH and distinguish the type of hemorrhage.[4] However, increasing use of the brain CT scan has aroused public concerns about radiation exposure.[5,6] Although CT represents only 11% of radiologic procedures, it accounts for as much as 70% of the total effective dose from all diagnostic radiologic studies.[7,8] A previous study demonstrated that radiation dose via multiple CT scans in the same patient could be accumulated compared with a single CT scan.[9] Several studies reported a significant association between exposure to high-dose radiation and

[1] Department of Radiology, The First Hospital of Jilin University, Changchun, Jilin, People's Republic of China
[2] Department of Orthopedics, The Third Hospital of Jilin University, Changchun, Jilin, People's Republic of China

Received 24 August 2019; received revised 23 October 2019; accepted 16 January 2020

**Corresponding Author:**
Dan Li, Department of Radiology, The First Hospital of Jilin University, Changchun, Jilin 130021, People's Republic of China.
Email: 13604430730@126.com

increased risk of cortical and posterior subcapsular cataract formation or other lenticular changes.[10,11]

A CT scan protocol is typically designed to reliably achieve high-quality images for diagnosing all types of brain diseases. Hence, development of low-dose CT scans can reduce patient radiation exposure, which is particularly important for the diagnosis of ICH. To date, there is no specific guideline for diagnosing ICH using CTs. In the present study, we demonstrated that low-dose CT scan can offer images with acceptable quality for diagnosis and reduce the radiation exposure. We also quantified organ-specific radiation dose for repeated head CT scan. Our data may assist physicians to select a more effective CT scan protocol for follow-up CT scans.

## Patients and Methods

### Patients' Selection

This study was approved by the ethics committee of the First Hospital of Jilin University (Changchun, China), and all patients signed the written informed consent form prior to start of the study. Inclusion criterion was verified ICH through initial CT scanning conducted by GE ADW4.6 CT Workstation (GE Healthcare, New York, New York). Patients who admitted to the emergency department were excluded. A total of 72 patients (41 males and 31 females) who underwent CT of head at our institution from January 2017 to December 2017 were included in this study.

### Computed Tomography Protocol

*Helical CT protocol:* In group of $CON_{250}$, CT scan of head was performed using a 64-slice multidetector computed tomography scanner (Brilliance 64; Philips Healthcare, Cleveland, Ohio), which contains single source, 64 detector rows. The details of CT protocol were as follows: tube voltage of 120 kVp, scanning during 9.6 seconds, slice thickness of 5 mm, gantry rotation time of 0.75 seconds, a collimation of $64 \times 0.625$ mm, and field of view of 250 mm, image matrix of $512 \times 512$ pixels, pixel spacing of $0.44 \times 0.44$ mm$^2$, and tube current–time product of 250 mAs.

In 3 low-dose groups, the tube current–time products were set to 100, 150, and 200 mAs, respectively. All the other parameters remained unchanged.

### Evaluation of Quality of Images

Radiologists who analyzed the images were blinded to the patients' data and scan protocol. In order to evaluate the quality of images, the same image was taken from each patient. The window and level settings used for CT scan were as follows: window width = 80 and window level = 40.

Quality of image was evaluated via signal intensity (SI) measured in Hounsfield units (HU). Eight 4 to 6 mm$^2$ circular regions of interest (ROIs) were selected as follows: basal ganglia (ROI1), frontal white matter (WM; ROI2), frontal cortical layer (ROI3), lateral ventricles (ROI4), internal capsule (ROI5), cortical layer of cerebellum (ROI6), WM of middle cerebellar peduncle (ROI7), and vermis (ROI8). The ROIs were placed in the normal brain parenchyma; if the bleeding foci was existed, the circle was put on the contralateral side.[12]

The signal to noise ratio (SNR) was calculated according to Equation 1:

$$\mathrm{SNR} = \frac{\mathrm{SI}_{\mathrm{ROIa}}}{\mathrm{SD}_{\mathrm{ROIa}}}. \tag{1}$$

The contrast to noise ratio (CNR) was calculated according to Equation 2:

$$\mathrm{CNR} = \frac{\Delta(\mathrm{SI}_{\mathrm{ROIa}}, \mathrm{SI}_{\mathrm{ROIb}})}{\sqrt[2]{(\mathrm{SD}_{\mathrm{ROIa}})^2 + (\mathrm{SD}_{\mathrm{ROIb}})^2}.} \tag{2}$$

It is noteworthy that CNR was calculated in the supratentorial (ST) region between ROI3/ROI2 (ST-CNR C/WM) and between ROI1/ROI2 (ST-CNR NL/WM). For the infratentorial (IT) region, CNR was calculated between ROI6/ROI7 (IT-CNR C/WM) and ROI8/ROI7 (IT-CNRV/WM).

### Evaluation of Quality of ICH Images

Since the aim of CT scan is to monitor the ICH, we quantified the predilection sites for ICH images. A 4 to 6 mm$^2$ circular ROI was selected.

Similar to that mentioned earlier, SNR was calculated according to Equation 1.

The CNR was calculated using Equation 3[13]:

$$\mathrm{CNR} = \frac{\mathrm{SI}_{\mathrm{ROI9}}, \mathrm{SI}_{\mathrm{ROI3}}}{\mathrm{SD}_{\mathrm{ROI3}}}, \tag{3}$$

where $\mathrm{SI}_{\mathrm{ROI9}}$ denotes the mean HU value of the ROI in the center of the ICH image, $\mathrm{SI}_{\mathrm{ROI3}}$ represents the mean HU of frontal cortical layer, and a denominator in Equation 3 denotes the standard deviation of the distribution of HU values in ROI3.

### Evaluation of Quality of Images by Physicians

Two independent radiologists, who were expert in diagnosis of head and neck diseases with >10 years of experience, were employed to assess the quality of images. The radiologists were blinded to the patient's data. The radiologists evaluated image noise, artifacts due to physiological noise, and anatomical structures and lesions using the European Guidelines on Quality Criteria for Computed Tomography[14] (see Table 1). The final score of an image was the average score of the 3 parameters. An image quality score of $\geq$3 was considered as a qualified image.

To assess differences in diagnosis between 2 images, the Cohen $\kappa$ coefficient was used. A Cohen $\kappa$ coefficient equal to 0 demonstrates disagreement. A Cohen $\kappa$ coefficient in the range of 0.1 to 0.4 indicates poor agreement. A strong correlation is achieved when Cohen $\kappa$ coefficient is between 0.41 and 0.6.[15]

**Table 1.** Grating Scale of Subjective Images Quality.

| Image Quality | | | |
|---|---|---|---|
| Grade Scale | Noise | Artifacts | Anatomical Details and Lesions |
| 5 | No noise | No or minimal artifacts | Clearly |
| 4 | Less than average noise | Less artifacts | Clearly |
| 3 | Average image noise | Noise and artifacts were obvious but acceptable | Better anatomical detail, lesions appeared well |
| 2 | Above average noise | Considerable artifacts make diagnosis difficult | Structures cannot be visualized; lesions shown were blurred |
| 1 | Unacceptable image noise | Not applicable | Unable to identify anatomical detail and lesion |

### Organ-/Tissue-Specific Radiation Doses

The effective radiation doses of specific organs/tissues were analyzed with Radimetrics Enterprise Platform (Radimetrics; Bayer Healthcare, Whippany, New Jersey). It merges and mobilizes patient dose histories and current examination details across all enterprise sites, bringing analysis and quality solutions to the point of care. This platform provides both radiation dose management and contrast dose analytics management and rapid access to patient dose history. In the present study, 10 different organs/tissues (brain, eye lenses, esophagus, muscles, red marrow, salivary glands, skeleton, skin, thymus, and thyroid) were analyzed and simulated using the mentioned platform.

### Statistical Analysis

All statistical analyses were performed using SPSS 22.0 software (IBM Corp, Armonk, New York). Continuous variables were analyzed using unpaired $t$ test, and categorical variables were analyzed by Mann-Whitney $U$ test.[16] The Tukey-Kramer post hoc analysis was employed to evaluate the difference among different groups.[17] One-way analysis of variance (ANOVA) was employed to compare variables among more than 2 groups. Value of $P \leq .05$ was considered statistically significant.

## Results

### Quality of Conventional CT ɪmages of Head

In this study, the tube current was set to 250 mA. Figure 1A shows an example of conventional CT image of head. The score of image quality graded by radiologists was 5 (the mean score of image quality, 4.68 $\pm$ 0.44). In this image, the cortical structure could be clearly distinguished. We further evaluated the quality of the image by measuring the SNR of 8 ROIs located at different structures (Figure 1B). In normal brain area, the greatest SNR was observed in ROI3 and ROI7, with average SNR of 9.76 $\pm$ 2.94 and 9.62 $\pm$ 3.64, respectively. However, the SNR in the hemorrhage spot was 21.90 $\pm$ 9.72. One-way ANOVA indicated that the SNR was significantly different ($P < .001$, $F = 28.17$, degrees of freedom [DOF] = 143). The Tukey-Kramer post hoc analysis revealed that the SNR in hemorrhage spot was remarkably higher than that in the other groups ($P < .001$).

We also investigated CNR in different areas (Figure 1C). It was noted that CNR in normal brain areas (ST C/WM, ST NL/WM, IT C/WM, and IT V/WM) was notably lower than that in the ICH. One-way ANOVA unveiled that SNR was significantly different ($P < .001$, $F = 86.18$, DOF = 79). The Tukey-Kramer post hoc analysis indicated that CNR in hemorrhage spot was markedly higher than that in normal brain areas ($P < .001$).

Since the purpose of follow-up CT scan was to monitor the ICH in the present study, the conventional CT of head was found overqualified. Computed tomography scan of head with a lower dose CT scan may still provide high-quality images for diagnosis.

### Low-Dose CT Scan

We assessed whether low-dose CT scan could generate qualified images. In 3 groups of patients, the tube current–time products were reduced to 200, 150, and 100 mAs, respectively. The other parameters remained unchanged. First, we investigated the score of quality of image determined by independent radiologists (Figure 2B). Although the scores of quality of image were all $\geq$3, the scores decreased with reducing of tube current–time product. One-way ANOVA demonstrated that the SNRs were significantly different ($P < .001$, $F = 25.34$, DOF = 71). The Tukey-Kramer post hoc analysis indicated that the score of convention group (tube current–time product of 250 mA) was noticeably higher than that in other groups ($P < .001$ for 100 and 150 mA groups, $P = .007$ for 200 mA group). Similarly, the SNR in the majority of ROIs slightly reduced with attenuating the tube current–time product (Figure 2C), while no significant difference was detected. The CNRs also slightly decreased with decline of tube current–time product (Figure 2D). Our data indicated that the lower tube current–time product may decrease the image quality. The conventional CT scan parameters may guarantee an image with acceptable quality for detecting the normal brain structures, and reducing the tube current–time product may decrease the quality of images.

However, the aim of the follow-up CT scan is to diagnosis the predilection sites for ICH. Hence, we attempted to study

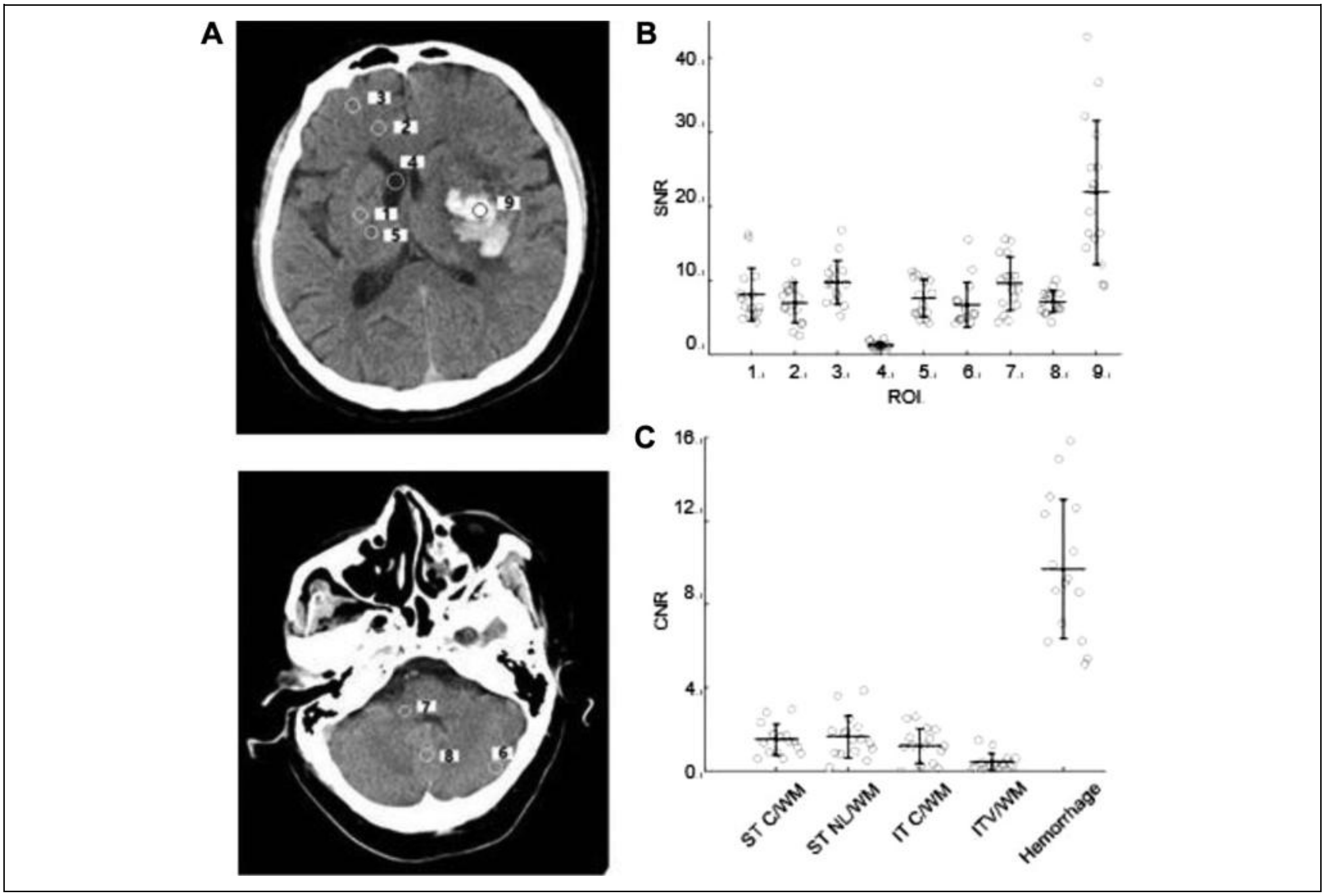


**Figure 1.** Sites of ROIs for analysis of image quality. A, An example of conventional CT image of head. Supratentorial ROIs included the lentiform nucleus (ROI1), frontal white matter (ROI2), temporal cortical layer (ROI3), ventricle (ROI4), and internal capsule (ROI5). Infratentorial ROIs included the cortical layer of the cerebellum (ROI6), WM of the middle cerebellar peduncle (ROI7), and the vermis (ROI8). ROI9 indicates the center of hemorrhage in supratentorial or infratentorial region. B, The mean SNR values of 9 ROIs were shown in conventional CT scan group. C, The mean CNR values of 4 ROIs in normal brain structures and center of hemorrhage were presented in conventional CT scan group. CNR, contrast to noise ratio; CT, computed tomography; IT-CNR C/WM, infratentorial CNR (cortex/white matter); IT-CNR V/WM, infratentorial CNR (vermis/white matter); ST-CNR C/WM, supratentorial CNR (cortex/white matter); ST-CNR NL/WM, supratentorial CNR (lentiform nucleus/white matter); ROI, region of interest; SNR, signal to noise ratio; WM, white matter.

whether the predilection sites for ICH can be clearly differentiated in different images. As shown in Figure 2A, the predilection sites for ICH can be clearly identified. The predilection sites for ICH is illustrated as an area with high brightness from the surrounding brain structure. We also compared the SNR of the predilection sites for ICH and other brain areas. The SNRs of predilection sites for IHC recorded in 4 different groups were remarkably higher than other ROIs ($ROI_9$ in Figure 2C). One-way ANOVA indicated that the SNRs were significantly different ($P < .001$, $F = 32.64$, DOF $= 647$). The Tukey-Kramer post hoc analysis showed that the SNRs of predilection sites for IHC in 4 groups were all markedly higher than SNR recorded in each group individually ($P < .001$).

Similarly, the CNR was also higher in predilection sites for ICH than other areas. One-way ANOVA demonstrated that the CNRs were different among these groups ($F = 70.38$, $P < .00$, DOF $= 356$). The Tukey-Kramer post hoc analysis indicated that the CNRs of the ICH groups were significantly higher than other groups ($P < .001$).

## *Benefits of Radiation Absorption*

We then investigated the organ-specific radiation dose of conventional CT scans. The organ-specific radiation dose of the 16 patients is presented in Figure 3A. Of all the 10 organs/tissues, brain, eye lenses, and salivary glands received higher radiation dose than other organs/tissues. Reducing the radiation dose may be remarkably advantageous for these organs.

We also assessed whether reducing the tube current–time product is highly beneficial for brain, eye lens, and salivary glands (Figure 3B). These organs received lower radiation dose with the decreasing tube current–time product. The radiation doses in group of 100 mA were only 45.65% (brain), 44.46% (eye lens), and 45.65% (salivary glands) in the conventional CT

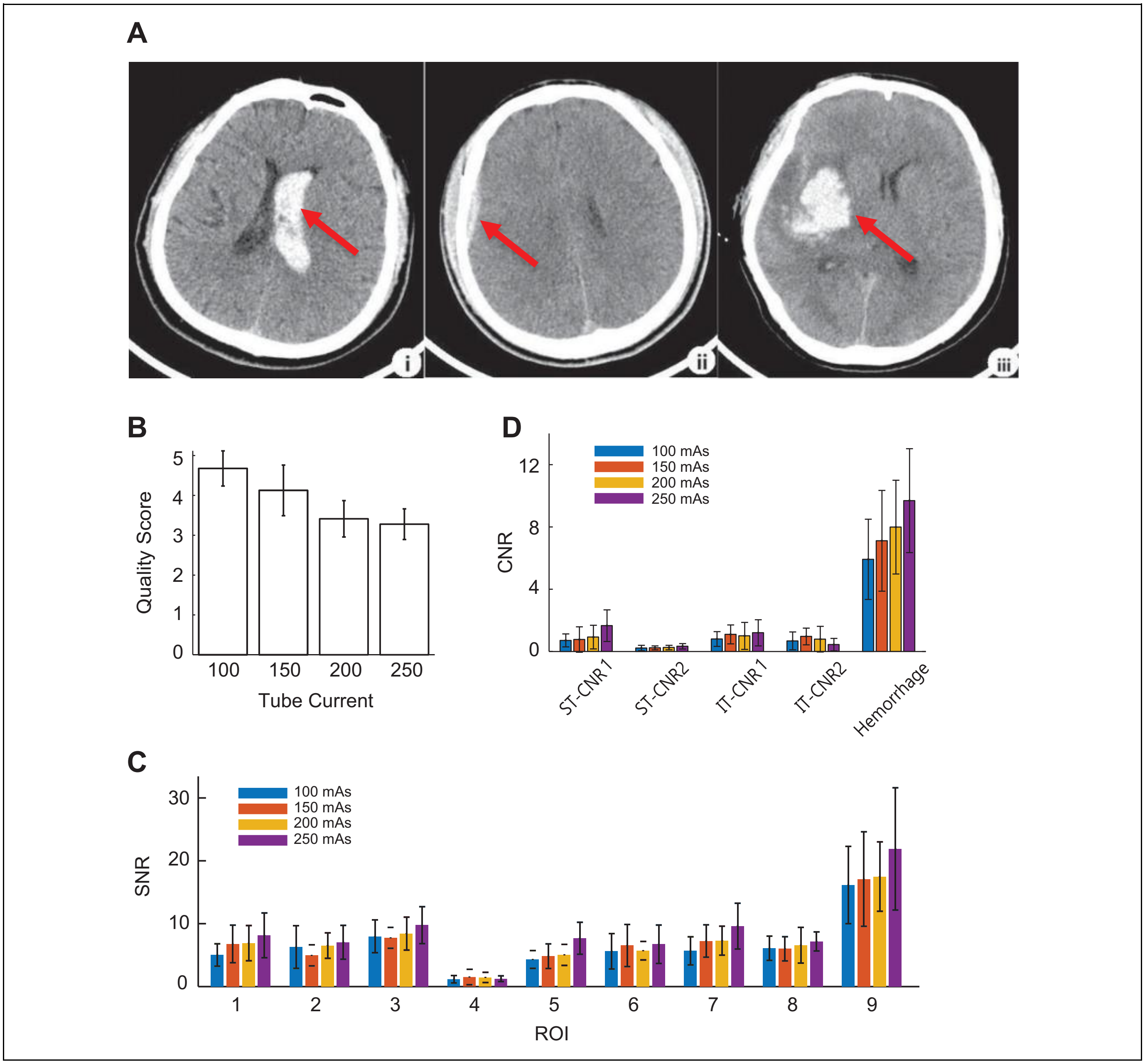


**Figure 2.** A, The representative images acquired from CT scans with different radiation doses: (i) 100 mAs dose; (ii) 150 mAs dose; (iii) 200 mAs dose. The red arrow indicates the predilection sites for ICH. B, The bar graph compares image quality under different tube current–time products. C, The bar graph shows the SNR of 9 ROIs in 4 groups. D, The bar graph shows the CNR in 4 groups. CNR indicates contrast to noise ratio; CT, computed tomography; ICH, intracranial hemorrhage; ROI, regions of interest; SNR, signal to noise ratio.

scan group. For CT scan of brain, 1-way ANOVA unveiled that the radiation doses were significantly different ($F = 75.56$, $P < .001$, DOF $= 71$). The Tukey-Kramer post hoc analysis indicated that the radiation doses were noticeably different ($P < .001$). For eye lenses, 1-way ANOVA revealed that the radiation doses were remarkably different ($F = 98.44$, $P < .001$, DOF $= 71$). The Tukey-Kramer post hoc analysis indicated that the radiation doses were significantly different ($P < .001$). For salivary glands, 1-way ANOVA showed that the radiation doses were significantly different ($F = 29.16$, $P < .001$, DOF $= 71$). The Tukey-Kramer post hoc analysis demonstrated that the radiation dose in group of 100 mA was significantly different compared with other groups ($P < .001$), and the radiation dose in group of 200 mA group was considerably lower than that in the conventional CT scan (250 mA) group ($P = .0249$). Our findings expressed that less tube current–time product can greatly advantageous for patients in the follow-up CT scan of brain.

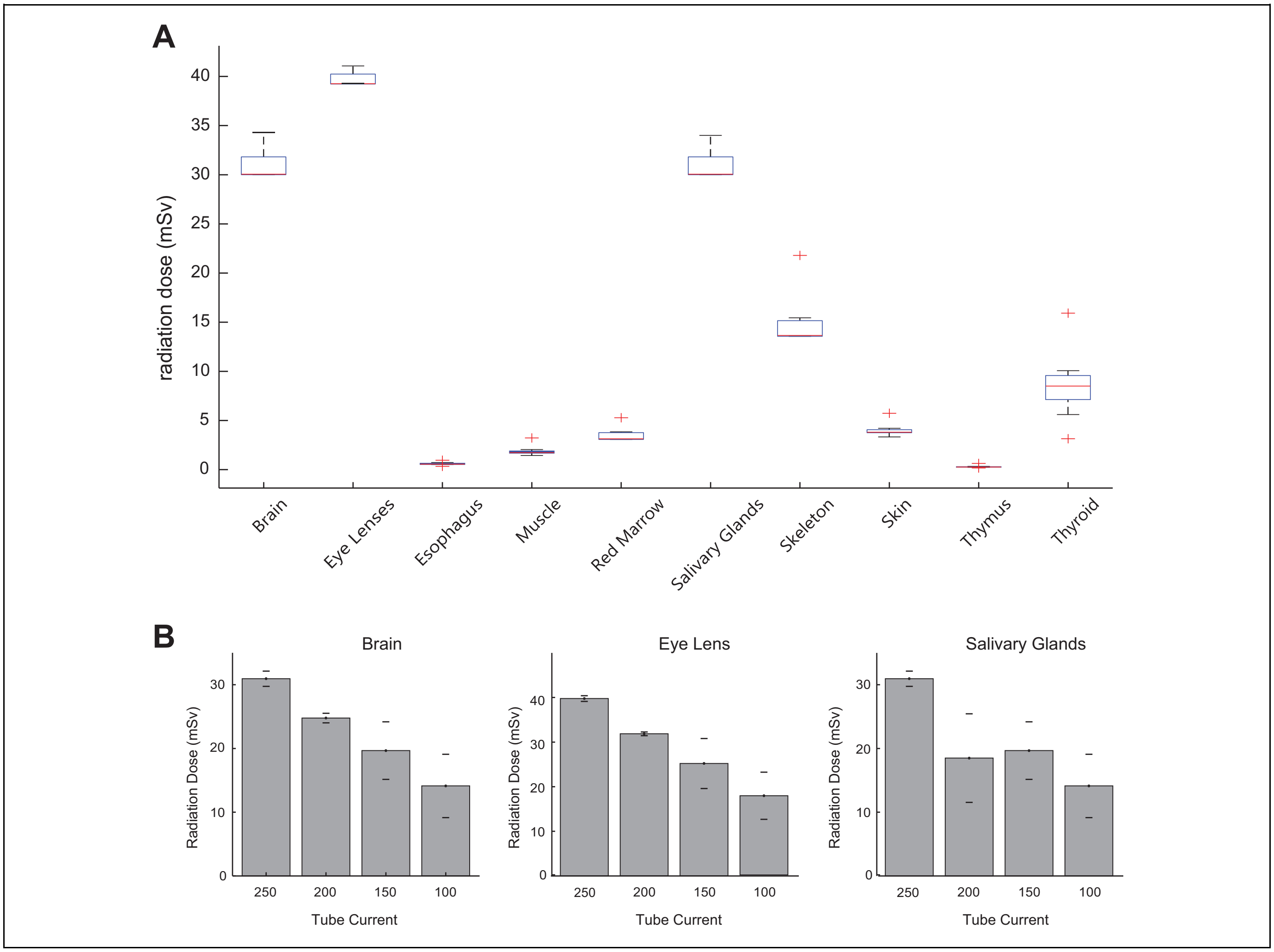


**Figure 3.** A, The bar graph shows that effective dose of 9 specific organs/tissues for 4 different CT scans of head in (B-D). The bar graph compares 3 sensitive organs. CT, computed tomography.

## Discussion

The ultimate goal of CT development is to reduce the radiation dose and maintain the quality of CT images. In the present study, for the first time, we used Radimetrics to quantify the radiation dose in different organ/tissues with a systemic reduction of tube current–time product. We found that decreasing the tube current–time product to 100 mAs may attenuate the radiation dose by more than 50% and the quality of image is satisfactory enough for the diagnosis of ICH. We, in the present study, for the first time, assessed both image quality and radiation dose. Our findings may assist physicians to better interpret the quality of CT images for different cases.

### *Image Quality*

The ultimate goal of CT scan is to provide a more clear brain structure for diagnosis. In the majority of the brain diseases, such as vertigo, skull fracture, and cerebral infarction, CT images aim to distinguish abnormalities in the structure. In the majority of brain regions, SNR and CNR remain acceptable (Figure 2). In our ICH case, there is a high contrast between the normal brain area and the hemorrhagic area, and a conventional CT protocol is overqualified as well. In the present research, the SNR and CNR in predilection sites for ICH were significantly higher than other brain regions (Figure 1B, C).

### *Low-Dose CT Scan*

A limited number of scholars attempted to study the quality of images in low-dose CT scan of head.[18] However, in those studies, organ-/tissue-specific radiation doses were not estimated.

Previous researches reported the application of low-dose CT scan of chest,[19,20] in addition to study of low-dose CT scan of head and abdomen.[21,22] The study of low-dose CT scan of brain is limited, mainly due to the thicker skull and absorption. Dose reduction is not conducive to observe intracranial structures, and in the present study, we assessed the balance relationship between radiation dose and quality of image in ICH. Other studies used iterative reconstruction techniques to reduce the tube voltage or tube current–time product, and so on, to attenuate the radiation dose.[23] The current research did not use iterative reconstruction techniques, and only the tube current–time product was adjusted to reduce the radiation dose. A number of scholars suggested that low levels of ionizing radiation are beneficial[24]; a recently conducted study by Calabrese et al reported over 37 000 patients who were treated with low levels of ionizing radiation.[25]

In the present study, the tube current–time product was reduced by 60% (from 250 to 100 mAs), and the SNR and CNR of ICH were remarkably higher than those of normal brain area in conventional CT scan. However, we couldn't further reduce the tube current–time product. A clear image of other brain regions was also found to be valuable to identify other complications. A number of images in the low-dose CT scan group reached a score of 3, and further deduction of tube current–time product might result in unqualified images.

### *Benefits of Low-Dose CT Scan for Patients With ICH*

Our data showed that less tube current–time product (mAs) may significantly reduce the radiation dose in brain, eye lenses, and salivary glands by 100, 150, and 200 mAs, respectively (Figure 3B). The quality of image of hemorrhagic area was higher than the normal brain area ($ROI_9$ in Figure 1A). In general, radiation exposure may increase the risk of salivary gland cancers.[26] The present research showed that the radiation exposure can be markedly reduced for patients with ICH, decreasing the risk of salivary gland cancers.

### *Application of Low-Dose CT Scan*

Although low-dose CT scan may be beneficial for patients with IHC, the application of affiliated protocol should be highly taken into consideration. For patients with IHC, the purpose of the initial CT scan is to identify the hemorrhage focus, in addition to potential damage to other areas. Thus, convention CT protocol is required to detect any potential damage in the whole brain. During the follow-up CT scans, the major target is to detect the progression of hematoma in the brain. The anatomical structure of other brain areas is less important unless some new clinical symptoms occur. Thus, reducing the tube current–time product may significantly decrease the accumulated radiation dose and attenuate the carcinogenic risk, especially for young patients.[27]

In summary, we presented a quantified method to estimate the benefits of undergoing follow-up CT scans for patients with ICH. We have evaluated the image quality at different tube current–time products. Our data may assist physicians to effectively design a CT scan protocol for patients with ICH.

## Declaration of Conflicting Interests

The author(s) declared no potential conflicts of interest with respect to the research, authorship, and/or publication of this article.

## Funding

The author(s) disclosed receipt of the following financial support for the research, authorship, and/or publication of this article: This work was supported by the Jilin Province Science and Technology Development Plan Item (No. 20191102001YY) and the First Hospital of Jilin University (No. JDYYJC008).

## ORCID iDs

Dan Wu https://orcid.org/0000-0003-0626-4245
Bingyang Bian https://orcid.org/0000-0001-6444-1698
Zhuohang Liu https://orcid.org/0000-0003-0033-3852
Dan Li https://orcid.org/0000-0002-4425-0242

## References

1. Brenner DJ, Hall EJ. Computed tomography—an increasing source of radiation exposure. *N Engl J Med*. 2007;357(22):2277-2284.
2. Esses D, Birnbaum A, Bijur P, Shah S, Gleyzer A, Gallagher EJ. Ability of CT to alter decision making in elderly patients with acute abdominal pain. *Am J Emerg Med*. 2004;22(4):270-272.
3. Bata SC, Yung M, Role of routine repeat head imaging in paediatric traumatic brain injury. *ANZ J Surg*. 2014;84(6):438-441.
4. Cellina M, Panzeri M, Floridi C, Martinenghi C. Overuse of computed tomography for minor head injury in young patients: an analysis of promoting factors. *La Radiologia Medica*. 2018;123(7):507-514.
5. Namasivayam S, Kalra MK, Pottala KM, Waldrop SM, Hudgins PA. Optimization of Z-axis automatic exposure control for multidetector row CT evaluation of neck and comparison with fixed tube current technique for image quality and radiation dose. *AJNR Am J Neuroradiol*. 2006;27(10):2221-2225.
6. Kilic K, Erbas G, Guryildirim M, et al. Quantitative and qualitative comparison of standard-dose and low-dose pediatric head computed tomography: a retrospective study assessing the effect of adaptive statistical iterative reconstruction. *J Comput Assist Tomogr*. 2013;37(3):377-381.
7. Paolicchi F, Faggioni L, Bastiani L, et al. Optimizing the balance between radiation dose and image quality in pediatric head CT: findings before and after intensive radiologic staff training. *AJR Am J Roentgenol*. 2014;202(6):1309-1315.
8. Power SP, Moloney F, Twomey M, James K, O'Connor OJ, Maher MM. Computed tomography and patient risk: facts, perceptions and uncertainties. *World J Radiol*. 2016;8(12):902.
9. Boning G, Kahn JF, Kaul D, et al. CT follow-up in patients with neuroendocrine tumors (NETs): combined radiation and contrast dose reduction. *Acta Radiol*. 2017;59(5):517-526.
10. Ogino H, Fujimichi Y, Sasaki M, et al. Quantitative assessment of provability of radiation-related cancers considering unavoidable existence of unadjusted risk factors. *J Radiol Prot*. 2016;36(4):865-884.
11. Law M, Ma WK, Lau D, et al. Cumulative effective dose and cancer risk for pediatric population in repetitive full spine follow-up imaging: how micro dose is the EOS microdose protocol? *European J Radiol*. 2018;101:87-91.

12. Kaul D, Kahn J, Huizing L, et al. Reducing radiation dose in adult head CT using iterative reconstruction—a clinical study in 177 patients. *Rofo*. 2016;188(2):155-162.
13. Li Y, Li Y, Jackson A, et al. Comparison of virtual unenhanced CT images of the abdomen under different iodine flow rates. *Abdom Radiol*. 2017;42(1):312-321.
14. Jurik AG, Bongartz G, Golding SJ, Leonardi M. The quality criteria for computed tomography. *Radiat Prot Dosim*. 1998; 80(1-3):49-53.
15. Reichelt A, Zeckey C, Hildebrand F, et al. Imaging of the brain in polytraumatized patients comparing 64-row spiral CT with incremental (sequential) CT. *Eur J Radiol*. 2012;81(4):789-793.
16. Wang W, Liu L, Zeng H, Sun C, Huang N, Zhang M. Utility of virtual unenhanced images and split-bolus injection using spectral multidetector CT for the assessment of renal cell carcinoma conspicuity and radiation dose. *Int J Clin Pract*. 2016;70(9B): B56-B63.
17. Tamhane AC, Hochberg Y, Dunnett CW. Multiple test procedures for dose finding. *Biometrics*, 1996;52(1):21-37.
18. Lim D, Lee SH, Kim DH, et al. The possibility of application of spiral brain computed tomography to traumatic brain injury. *Am J Emerg Med*. 2014;32(9):1051-1054.
19. Saltybaeva N, Krauss A, Alkadhi A. Effect of localizer radiography projection on organ dose at chest CT with automatic tube current modulation. *Radiology*. 2017;282(3):842-849.
20. Paul J, Banckwitz R, Krauss B, Vogl TJ, Maentele W, Bauer RW. Estimation and comparison of effective dose (E) in standard chest CT by organ dose measurements and dose-length-product methods and assessment of the influence of CT tube potential (energy dependency) on effective dose in a dual-source CT. *Eur J Radiol*. 2012;81(4):e507-e512.
21. Scharf M, Brendel S, Melzer K, et al. Image quality, diagnostic accuracy, and potential for radiation dose reduction in thoracoabdominal CT, using Sinogram Affirmed Iterative Reconstruction (SAFIRE) technique in a longitudinal study. *PLoS One*. 2017; 12(7):e0180302.
22. Udayasankar U.K, Braithwaite K, Arvaniti M, et al. Low-dose nonenhanced head CT protocol for follow-Up evaluation of children with ventriculoperitoneal shunt: reduction of radiation and effect on image quality. *Am J Neuroradiol*. 2008;29(4):p802-806.
23. Bricout N, Estrade L, Boustia F, Kalsoum E, Pruvo JP, Leclerc X. Reduced-dose CT protocol for the assessment of cerebral vasospasm. *Neuroradiology*. 2015;57(12):1211-1218.
24. Cuttler JM. Commentary on Fukushima and beneficial effects of low radiation. *Dose-Response*. 2013;11(4):447-458.
25. Calabrese EJ, Dhawan G, Kapoor R, Kozumbo WJ. Radiotherapy treatment of human inflammatory diseases and conditions: optimal dose. *Hum Exp Toxicol*. 2019;38(8):888-898.
26. Fetterly K, Schueler B, Grams M, Sturchio G, Bell M, Gulati R. Head and neck radiation dose and radiation safety for interventional physicians. *JACC Cardiovas Interv*. 2017;10(5): 520-528.
27. Siegel JA, Sacks B, Pennington CW, Welsh JS. Dose optimization to minimize radiation risk for children undergoing CT and nuclear medicine imaging is misguided and detrimental. *J Nucl Med*. 2017;58(6):865-868.

scientific reports

Check for updates

OPEN

# Impact of dose reduction and iterative model reconstruction on multi-detector CT imaging of the brain in patients with suspected ischemic stroke

Karolin J. Paprottka[1]✉, Karina Kupfer[1], Isabelle Riederer[1], Claus Zimmer[1,2], Meinrad Beer[3], Peter B. Noël[4], Thomas Baum[1], Jan S. Kirschke[1,2] & Nico Sollmann[1,2,3,5]

Non-contrast cerebral computed tomography (CT) is frequently performed as a first-line diagnostic approach in patients with suspected ischemic stroke. The purpose of this study was to evaluate the performance of hybrid and model-based iterative image reconstruction for standard-dose (SD) and low-dose (LD) non-contrast cerebral imaging by multi-detector CT (MDCT). We retrospectively analyzed 131 patients with suspected ischemic stroke (mean age: 74.2 ± 14.3 years, 67 females) who underwent initial MDCT with a SD protocol (300 mAs) as well as follow-up MDCT after a maximum of 10 days with a LD protocol (200 mAs). Ischemic demarcation was detected in 26 patients for initial and in 64 patients for follow-up imaging, with diffusion-weighted magnetic resonance imaging (MRI) confirming ischemia in all of those patients. The non-contrast cerebral MDCT images were reconstructed using hybrid (Philips "iDose4") and model-based iterative (Philips "IMR3") reconstruction algorithms. Two readers assessed overall image quality, anatomic detail, differentiation of gray matter (GM)/white matter (WM), and conspicuity of ischemic demarcation, if any. Quantitative assessment included signal-to-noise ratio (SNR) and contrast-to-noise ratio (CNR) calculations for WM, GM, and demarcated areas. Ischemic demarcation was detected in all MDCT images of affected patients by both readers, irrespective of the reconstruction method used. For LD imaging, anatomic detail and GM/WM differentiation was significantly better when using the model-based iterative compared to the hybrid reconstruction method. Furthermore, CNR of GM/WM as well as the SNR of WM and GM of healthy brain tissue were significantly higher for LD images with model-based iterative reconstruction when compared to SD or LD images reconstructed with the hybrid algorithm. For patients with ischemic demarcation, there was a significant difference between images using hybrid versus model-based iterative reconstruction for CNR of ischemic/contralateral unaffected areas (mean ± standard deviation: SD_IMR: 4.4 ± 3.1, SD_iDose: 3.5 ± 2.3, $P < 0.0001$; LD_IMR: 4.6 ± 2.9, LD_iDose: 3.2 ± 2.1, $P < 0.0001$). In conclusion, model-based iterative reconstruction provides higher CNR and SNR without significant loss of image quality for non-enhanced cerebral MDCT.

**Abbreviations**

| | |
|---|---|
| CNR | Contrast-to-noise ratio |
| CT | Computed tomography |
| CTDIvol | Volumetric CT dose index |
| DLP | Dose-length product |
| DWI | Diffusion-weighted imaging |

[1]Department of Diagnostic and Interventional Neuroradiology, School of Medicine, Klinikum rechts der Isar, Technical University of Munich, Munich, Germany. [2]TUM-Neuroimaging Center, Klinikum rechts der Isar, Technical University of Munich, Munich, Germany. [3]Department of Diagnostic and Interventional Radiology, University Hospital Ulm, Ulm, Germany. [4]Department of Radiology, Perelman School of Medicine, University of Pennsylvania, Philadelphia, PA, USA. [5]Department of Radiology and Biomedical Imaging, University of California, San Francisco, CA, USA. ✉email: Karolin.Paprottka@tum.de

| | |
|---|---|
| FBP | Filtered back projection |
| FOV | Field of view |
| GM | Gray matter |
| HU | Hounsfield Units |
| κ | Cohen's kappa |
| LD | Low dose |
| MDCT | Multi-detector CT |
| MRI | Magnetic resonance imaging |
| PACS | Picture archiving and communication system |
| R1 | Reader 1 |
| R2 | Reader 2 |
| ROI | Region of interest |
| SD | Standard dose |
| SNR | Signal-to-noise ratio |
| StdDev | Standard deviation |
| WM | White matter |

Non-contrast cerebral computed tomography (CT) is one of the most frequently performed radiological examinations and the first-line diagnostic approach for emergency evaluation of patients with suspected stroke[1–4]. It is recommended by the American Heart Association as the initial emergency modality for investigation[5], which is mostly thanks to the high speed, wide availability, and feasibility of CT in most institutions.

Due to attenuation differences of healthy brain parenchyma, the absence of the gray matter (GM)/white matter (WM) interface is a well-known and notable early CT sign for delineation of the infarct in patients with ischemic stroke[6,7]. Yet, image noise in cerebral CT data is particularly problematic for assessment of this characteristic feature of ischemic stroke and can aggravate detection of infarcted areas[8–10], because the difference in attenuation of normal brain tissue at the GM/WM boundary is as low as 5 to 10 Hounsfield Units (HU)[11]. Therefore, image noise has to be kept as low as possible in order to improve the visualization of the normal GM/WM interface.

As the photoelectric component for GM is roughly about 5% higher than the value of WM[12], brain tissue represents therefore an optimal tissue for improving image quality by alternating dose parameters for CT acquisitions. Raising of the tube current during CT acquisitions results in an increase of the contrast-to-noise-ratio (CNR)[12], which can also facilitate a reduction of image noise[13]. However, this would lead to an increased radiation exposure for the patient. Against the background of ever-increasing numbers of CT examinations and related cancer risk ratios, CT-based radiation exposure should be kept as low as possible to prevent harm to the patient[14–16].

As another useful tool to improve image quality by reducing image noise, various CT scanner vendors have developed different image reconstruction algorithms as alternatives to the traditionally used filtered back projection (FBP)[17–20]. The concept of iterative reconstruction was first described decades ago. Until today, most commercially available algorithms are not fully iterative but use a combination of iterative reconstruction and a conventional reconstruction algorithm such as FBP, commonly referred to as hybrid iterative reconstruction[18–20]. Comparable to FBP, a backward projection step is used for such hybrid algorithms, but they are more advanced given that they can iteratively filter the raw data to reduce artifacts, and after the backward projection, the image data are iteratively filtered to reduce image noise[18–20]. A fully iterative method is more demanding, using raw data that are backward projected into the cross-sectional image space, which is followed by forward projection to compute artificial raw data[18–20]. Importantly, this data forward projection step is crucial to the algorithms, given that it establishes a physically correct modulation of the acquisition process[18–20]. Artificial raw data are then systematically compared to the initial true raw data to revise the cross-sectional images, while, simultaneously, a regularization step is implemented to remove image noise[18]. Backward and forward projections are repeated so that discrepancies between true and artificial raw data can be minimized[18–20]. With advancements in CT technique and increased computational power, fully iterative reconstruction methods become increasingly available. Although distinct technical details and names for reconstruction algorithms can vary between manufacturers, it is generally acknowledged that iterative model-based approaches provide images with improved noise and artifact reduction whilst requiring prolonged reconstruction speed, which should, however, not be a clinically relevant issue with modern CT systems[18]. Specifically, model-based iterative algorithms may help to increase the visibility of anatomical details of brain structures and the GM/WM interface. Consequently, these algorithms may have the potential to increase the sensitivity for detection of parenchymal brain lesions in ischemic stroke.

The aim of our study was to evaluate the impact of a model-based iterative image reconstruction algorithm for non-contrast cerebral multi-detector CT (MDCT) in patients with suspected ischemic stroke. We therefore compared the image quality and diagnostic value of scans with model-based iterative image reconstruction with those of scans using hybrid reconstruction considering MDCT acquisitions with standard dose (SD) and low dose (LD), respectively.

## Material and methods

**Study design and patient inclusion.** All image acquisitions were performed at one institution and according to clinical indications, which were based on (1) the requirement for initial imaging due to suspected ischemic stroke, or (2) follow-up imaging in the context of a control scan after mechanical recanalization and/or thrombolytic therapy. Eligible patients who had both initial and follow-up imaging by non-contrast cerebral MDCT available at our department were identified in our hospital's picture archiving and communication system (PACS).

| | Standard-dose (SD) imaging | Low-dose (LD) imaging |
|---|---|---|
| Scan increment (in mm) | 10.0 | |
| Cycle time (in s) | 2.5 | |
| No. of cycles | 18 | |
| Scan angle | 420 | |
| Rotation time | 0.75 | |
| Tube voltage (in kV) | 120 | 120 |
| Tube current (in mA) | 343 | 229 |
| Exposure (in mAs) | 300 | 200 |
| Volumetic CT dose index (in mGy) | 46.6 ± 1.2 (range: 38.5–47.6) | 31.2 ± 1.8 (range: 20.1–46.8) |
| Collimation width | 16 × 0.625 | |
| Slice thickness (axial, in mm) | 5 | |
| Image reconstruction | IMR3 and iDose4 | |
| Windowing | Standard setting of window width of 80 HU and window length of 40 HU, individually adjustable | |

**Table 1.** Scanning details and image reconstruction for scanning with standard dose (SD) and low dose (LD).

Inclusion criteria were (1) MDCT according to the hospital-intern standard stroke protocol (non-contrast cerebral CT with SD, CT angiography of supraaortal and intracranial vessels, and CT perfusion), (2) follow-up cerebral MDCT (non-contrast cerebral CT with LD) on the same MDCT system, (3) follow-up cerebral magnetic resonance imaging (MRI) according to a hospital-intern standard stroke protocol (including diffusion-weighted imaging [DWI] sequences), and (4) diagnosis of cerebral ischemia or no intracranial pathology according to all available imaging data. The exclusion criteria were (1) interval between the initial and follow-up MDCT examination of more than 10 days, (2) incomplete coverage of the neurocranium or artifacts due to foreign bodies or motion, (3) age below 18 years, and (4) an intracranial pathology other than ischemia (e.g., bleeding or tumor). Overall, 131 patients were eligible and included in this study, with an interval of study enrollment from November 2018 to September 2020.

**Imaging by multi-detector computed tomography.** Image acquisition was performed in supine position using a 128-slice MDCT scanner (Ingenuity Core 128, Philips Healthcare) in all patients. An initial scout scan was used for planning of the field of view (FOV), and subsequent helical scanning was acquired with implicit tube current modulation for non-enhanced cerebral MDCT examinations. Initial SD and follow-up LD scans were performed with a tube voltage of 120 kV, while the tube current was decreased in the LD protocol (343 mA versus 229 mA).

The datasets derived from SD and LD scanning were both reconstructed with an axial slice thickness of 5 mm using two different image reconstruction algorithms, which were provided by the vendor (hybrid algorithm: iDose4, iterative model-based algorithm: IMR3, Philips Healthcare). The distinct regularization level for the iterative model-based algorithm was determined for clinical routine scanning by a consensus decision (reached by six board-certified neuroradiologists) directly after implementation of this method at our institution (in 2018) and used consistently thereafter as a hospital-intern standard. The volumetric CT dose index (CTDIvol) and dose-length product (DLP) were extracted from the automatically generated dose reports. Table 1 provides an overview of scanning details for MDCT imaging.

**Qualitative image analysis.** Qualitative image evaluation was performed using a standard PACS viewer (IDS7, Sectra AB). Two radiologists (reader 1 [R1], board-certified radiologist with 8 years of experience and reader 2 [R2], resident with 4 years of experience in stroke imaging) systematically assessed all imaging data in all patients. Evaluations were performed after patient pseudonymization, and the readers had no access to the clinical reports for original imaging as generated during clinical routine and were unaware of the distinct clinical indication that resulted in MDCT imaging.

All imaging data were assessed separately, with the readers being strictly blinded to the ratings of each other. Furthermore, the order of patient cases was randomized per reading round (four reading rounds: SD_IMR, LD_IMR, SD_iDose, and LD_iDose), with an interval of at least two weeks between single rounds to minimize recall bias. Overall image quality, anatomic detail, and differentiation of GM/WM were evaluated based on 5-point Likert scales for all datasets (Table 2). In case of ischemic demarcation, both readers rated the conspicuity of such demarcation on another 5-point Likert scale.

**Quantitative image analysis.** Similar to previous studies on CT scan quality assurance[21–24], R1 used the following approach to perform quantitative image analysis. An axial slice at the level of the basal ganglia and third ventricle was chosen and measurements were taken in three regions of interest (ROIs) of identical size per patient (Fig. 1). One ROI was used to measure the attenuation (in HU) of WM in the left (or in case of ischemia unaffected) frontal lobe. Additional ROIs were placed to measure thalamic GM as well as WM of the posterior limb of the internal capsule on the left side (or, if affected by ischemic demarcation, on the unaffected right side). In case of ischemic demarcation another axial CT slice was chosen at the level of demarcation and two further

| Item | Score | | | | |
|---|---|---|---|---|---|
| | 1 | 2 | 3 | 4 | 5 |
| Overall image quality | Poor | Fair | Medium | Good | Excellent |
| Anatomic detail | | | | | |
| GM/WM differentiation | | | | | |
| Conspicuity of ischemic demarcation | | | | | |

**Table 2.** Scoring scheme for qualitative image analysis.

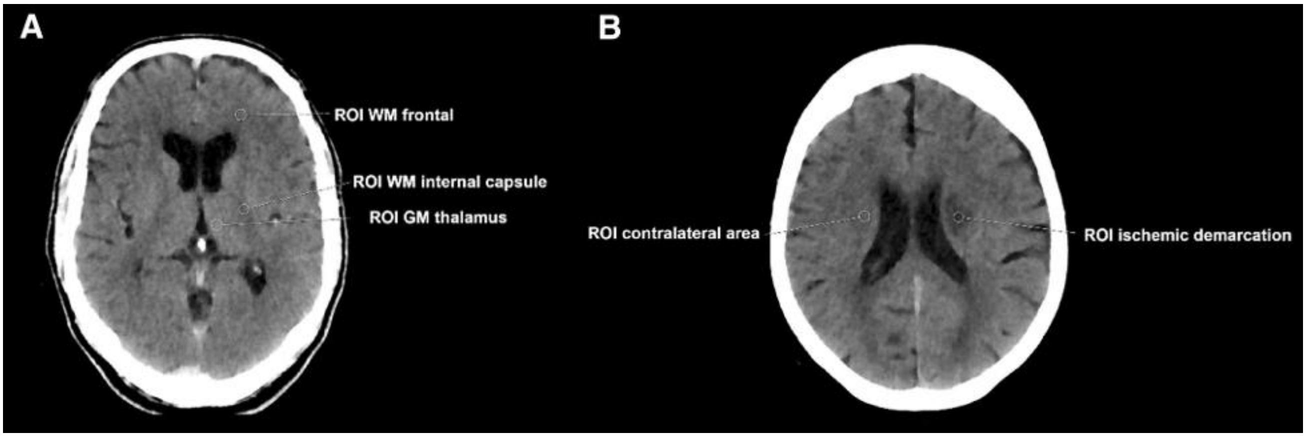


**Figure 1.** Placement of regions of interest (ROIs). (**A**) Placement of circular ROIs for the white matter (WM) of the left frontal lobe, WM of the left internal capsule, and gray matter (GM) of the left-sided thalamus (using axial slices at the level of the basal ganglia/third ventricle); (**B**) Placement of circular ROIs within ischemic demarcation (adjacent to the left lateral ventricle) and within a homologue, unaffected area of the contralateral hemisphere (using axial slices at the level of ischemic demarcation).

ROIs were set: one in the core of the demarcated ischemic area and one within the same region of the unaffected contralateral hemisphere (Fig. 1).

Based on the values obtained, the signal-to-noise ratio (SNR) was calculated for the thalamus, the frontal WM, and the posterior limb of the internal capsule of the left or unaffected hemisphere using the following formula:

$$\mathrm{SNR} = \frac{\text{mean attenuation ROI}}{\text{StdDev of mean attenuation ROI}}$$

Additionally, the CNR was calculated for the GM/WM differentiation using the following formulas for all patients together as well as only for patients with ischemic demarcation:

$$\mathrm{CNR}_{\text{all\_patients}} = \frac{\text{mean attenuation ROI GM} - \text{mean attenuation ROI WM}_{\text{frontal}}}{\left(\frac{\text{StdDev of mean attenuation ROI GM}+\text{StdDev of mean attenuation ROI WM}_{\text{frontal}}}{2}\right)}$$

$$\mathrm{CNR}_{\text{patients\_ischemia}} = \frac{\text{mean attenuation ROI within ischemic area} - \text{mean attenuation ROI contralateral}}{\left(\frac{\text{StdDev of mean attenuation ROI ischemic area}+\text{StdDev of mean attenuation ROI contralateral}}{2}\right)}$$

**Statistical data analysis.** GraphPad Prism (version 6.0; GraphPad Software Inc.) and SPSS (version 25.0; IBM SPSS Statistics for Windows, IBM Corp.) were used for statistical data analyses. The level of statistical significance was set at $P<0.05$.

For patient details, scanning parameters, dose characteristics, and values derived from quantitative and qualitative evaluations, descriptive statistics including mean ± standard deviation (StdDev), median, range, and absolute frequencies were calculated. Friedman tests were conducted between the SNR derived from SD_IMR, LD_IMR, SD_iDose, and LD_iDose data for GM as measured in the thalamus as well as for frontal WM and the internal capsule, respectively, followed by Dunn's multiple comparisons test as a post-hoc analysis. Similarly, Friedman tests were performed for the CNR of GM/WM between SD_IMR, LD_IMR, SD_iDose, and LD_iDose data for all included patients, again using Dunn's multiple comparisons test as a post-hoc test. In patients with detected ischemic demarcation, Wilcoxon matched-pairs signed rank tests were conducted for the CNR of unaffected/demarcated parenchyma for SD_IMR versus SD_iDose and for LD_IMR versus LD_iDose data, respectively.

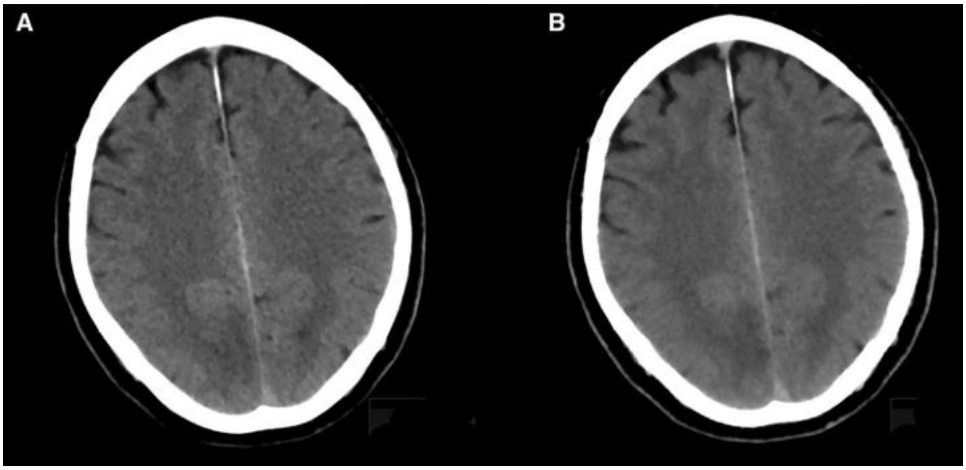


**Figure 2.** Exemplary patient case with ischemic demarcation (63-year-old male with visual disturbances). (**A**) Axial slices derived from scanning with low dose (LD) using a hybrid reconstruction algorithm (LD_iDose); (**B**) Corresponding axial slices from scanning with LD combined with a model-based iterative image reconstruction algorithm (LD_IMR). The demarcated area (parieto-occipital, right hemisphere) is more markedly depicted in (**B**), corresponding to a higher contrast-to-noise ratio (CNR).

Inter-reader agreements for qualitative evaluation regarding overall image quality, depiction of anatomic detail, and differentiation of GM/WM, considering all enrolled patients, and for conspicuity of demarcated ischemic parenchyma against healthy tissue only in patients with detected ischemic demarcation were assessed by weighted Cohen's kappa (κ). Specifically, κ was calculated between the ratings of R1 and R2 for SD_IMR, LD_IMR, SD_iDose, and LD_iDose separately. Further, Wilcoxon matched-pairs signed rank tests were performed to compare scorings for SD_IMR versus SD_iDose and LD_IMR versus LD_iDose for each reader separately. Wilcoxon matched-pairs signed rank tests were also performed to investigate differences in the CTDIvol or the DLP between SD and LD images.

**Ethical approval.** The study was approved by the ethics committee of the Faculty of Medicine of the Technical University of Munich and performed in accordance with the Declaration of Helsinki.

**Informed consent.** The requirement for written informed consent was waived by the ethics committee of the Technical University of Munich due to the study's retrospective design.

## Results

**Cohort characteristics.** Data of 131 patients (mean age: 74.2 ± 14.3 years; age range: 26.8–95.6 years; 67 females) met our inclusion criteria. The mean interval between initial SD and follow-up LD imaging was 1.4 ± 1.7 days (range: 0–10 days), and the mean interval between initial SD MDCT and MRI was 2.3 ± 2.3 days (range: 2–13 days). Vessel occlusion in the CT angiography of initial MDCT examinations was identified in 80 patients, perfusion deficits according to CT perfusion were detected in 83 patients.

Ischemic demarcation was detected initially in 26 patients, and it was present in 64 patients for follow-up LD imaging according to both readers (Fig. 2). Ischemic affection in these patients was confirmed by DWI sequences as derived from MRI. Characteristics of ischemia are shown in Table 3.

**Qualitative image analysis.** According to qualitative evaluation, overall image quality was excellent on average for SD_IMR, LD_IMR, SD_iDose, and LD_iDose, respectively, with almost perfect inter-reader agreement (range of κ: 0.82–0.93) and without a statistically significant difference between SD_IMR versus SD_iDose for both readers and between LD_IMR versus LD_iDose for R1 only ($P > 0.05$; Table 4). Furthermore, high anatomic detail was depicted by all investigated data with substantial to almost perfect inter-reader agreement (range of κ: 0.61–0.89). Of note, while there was no statistically significant difference between SD_IMR versus SD_iDose ($P > 0.05$), the reconstruction algorithm had impact on anatomic detail for LD images, with statistically significantly better scores assigned by both readers for data reconstructed with IMR ($P < 0.01$; Table 4).

Very good differentiation between GM and WM was observed for all investigated data, with at least moderate to almost perfect inter-reader agreement (range of κ: 0.44–0.89). No statistically significant difference was observed between SD_IMR versus SD_iDose ($P > 0.05$) according to assessments of both readers, while statistically significantly better scores were obtained for LD data reconstructed with IMR when compared to iDose ($P < 0.01$; Table 4). In patients with demarcated ischemic parenchyma, conspicuity of ischemic demarcation was very good for all investigated data, and the agreement between scorings of both readers was substantial to almost perfect (range of κ: 0.72–0.96). Statistically significantly better conspicuity was observed for LD_IMR compared to LD_iDose according to evaluations of R2 ($P < 0.01$; Table 4).

| | Standard-dose (SD) imaging | Low-dose (LD) imaging |
|---|---|---|
| **Ischemic demarcation** (total number of patients) | 26 | 64 |
| Territory middle cerebral artery | 18 | 27 |
| Territory anterior cerebral artery | 0 | 1 |
| Territory posterior cerebral artery | 2 | 4 |
| Basal ganglia | 0 | 13 |
| Disseminated | 0 | 1 |
| Infratentorial | 4 | 10 |
| Multiple territories | 2 | 8 |
| **Side of demarcation** | | |
| Right hemisphere | 11 | 20 |
| Left hemisphere | 11 | 35 |
| Bihemispheric | 4 | 9 |

**Table 3.** Overview of detected ischemic stroke characteristics.

| | R1 (median, range) | R2 (median, range) | κ | p (SD_iDose vs. SD_IMR) R1 | p (SD_iDose vs. SD_IMR) R2 | p (LD_iDose vs. LD_IMR) R1 | p (LD_iDose vs. LD_IMR) R2 |
|---|---|---|---|---|---|---|---|
| **Overall image quality** | | | | | | | |
| SD_iDose | 5 (3 – 5) | 5 (3 – 5) | 0.82 | 0.99 | 0.99 | 0.50 | 0.02 |
| SD_IMR | 5 (3 – 5) | 5 (3 – 5) | 0.82 | | | | |
| LD_iDose | 5 (3 – 5) | 5 (3 – 5) | 0.86 | | | | |
| LD_IMR | 5 (3 – 5) | 5 (3 – 5) | 0.93 | | | | |
| **Anatomic detail** | | | | | | | |
| SD_iDose | 5 (3 – 5) | 5 (4 – 5) | 0.83 | 0.06 | 0.99 | < 0.01 | < 0.01 |
| SD_IMR | 5 (3 – 5) | 5 (4 – 5) | 0.61 | | | | |
| LD_iDose | 5 (2 – 5) | 5 (3 – 5) | 0.89 | | | | |
| LD_IMR | 5 (2 – 5) | 5 (3 – 5) | 0.86 | | | | |
| **GM/WM differentiation** | | | | | | | |
| SD_iDose | 5 (4 – 5) | 5 (4 – 5) | 0.65 | 0.38 | 0.75 | < 0.01 | < 0.01 |
| SD_IMR | 5 (4 – 5) | 5 (4 – 5) | 0.44 | | | | |
| LD_iDose | 5 (3 – 5) | 5 (3 – 5) | 0.89 | | | | |
| LD_IMR | 5 (3 – 5) | 5 (4 – 5) | 0.79 | | | | |
| **Conspicuity of ischemic demarcation** | | | | | | | |
| SD_iDose | 5 (3 – 5) | 5 (4 – 5) | 0.72 | 0.50 | 0.99 | 0.13 | < 0.01 |
| SD_IMR | 5 (3 – 5) | 5 (3 – 5) | 0.96 | | | | |
| LD_iDose | 5 (2 – 5) | 5 (3 – 5) | 0.87 | | | | |
| LD_IMR | 5 (2 – 5) | 5 (3 – 5) | 0.86 | | | | |

**Table 4.** Results of qualitative image evaluation from both readers (R1 and R2) using median and ranges for assigned scores. Images derived from scanning with standard dose (SD; SD_iDose & SD_IMR) and low dose (LD; LD_iDose & LD_IMR).

**Quantitative image analysis.** Regarding the SNR of GM as measured in the thalamus as well as for the SNR of frontal WM and the internal capsule, SD_IMR showed the highest values, respectively (mean ± StdDev: GM: 24.7 ± 7.9; WM frontal: 17.1 ± 4.2; WM internal capsule: 20.2 ± 7.5), followed by LD_IMR, SD_iDose, and LD_iDose (Table 5). Comparison of SNRs between SD_IMR, LD_IMR, SD_iDose, and LD_iDose for the SNRs measured in the different structures revealed a statistically significant difference ($P < 0.01$), yet the comparison between images using IMR was not significant according to post-hoc testing (Table 5).

Similarly, for the CNR of GM/WM in all enrolled patients, highest values were obtained for SD_IMR (mean ± StdDev: 5.9 ± 2.0), followed by the results for LD_IMR, SD_iDose, and LD_iDose (Table 5; Fig. 3). The comparison of SD_IMR, LD_IMR, SD_iDose, and LD_iDose yielded a statistically significant difference ($P < 0.01$), however post-hoc testing of SD_IMR versus LD_IMR was not statistically significant (Table 5). For patients with ischemic stroke and detected ischemic demarcation, there was a statistically significant difference

| | | | | Dunn's post-hoc test | | |
|---|---|---|---|---|---|---|
| | Mean ± StdDev | Range | *P* | Comparison | Rank sum diff | Sign |
| **SNR–GM thalamus** | | | | | | |
| SD_iDose | 20.6 ± 6.2 | 10.2–48.8 | < 0.01 | SD_iDose vs. SD_IMR | − 88.0 | * |
| | | | | SD_iDose vs. LD_iDose | 116.0 | * |
| SD_IMR | 24.7 ± 7.9 | 11.9–64.3 | | SD_iDose vs. LD_IMR | − 78.0 | * |
| | | | | SD_IMR vs. LD_iDose | 204.0 | * |
| LD_iDose | 16.1 ± 6.9 | 7.7–58.7 | | SD_IMR vs. LD_IMR | 10.0 | n.s |
| LD_IMR | 23.3 ± 5.8 | 13.4–50.3 | | LD_iDose vs. LD_IMR | − 194.0 | * |
| **SNR–WM frontal** | | | | | | |
| SD_iDose | 14.9 ± 5.3 | 6.7–54.0 | < 0.01 | SD_iDose vs. SD_IMR | − 104.0 | * |
| | | | | SD_iDose vs. LD_iDose | 102.0 | * |
| SD_IMR | 17.1 ± 4.2 | 8.2–29.7 | | SD_iDose vs. LD_IMR | − 88.0 | * |
| | | | | SD_IMR vs. LD_iDose | 206.0 | * |
| LD_iDose | 12.2 ± 4.1 | 5.1–35.8 | | SD_IMR vs. LD_IMR | 16.0 | n.s |
| LD_IMR | 16.8 ± 4.5 | 4.9–27.9 | | LD_iDose vs. LD_IMR | − 190.0 | * |
| **SNR–WM internal capsule** | | | | | | |
| SD_iDose | 16.9 ± 5.4 | 7.8–33.4 | < 0.01 | SD_iDose vs. SD_IMR | − 97.0 | * |
| | | | | SD_iDose vs. LD_iDose | 116.0 | * |
| SD_IMR | 20.2 ± 7.5 | 3.7–73.3 | | SD_iDose vs. LD_IMR | − 57.0 | * |
| | | | | SD_IMR vs. LD_iDose | 213.0 | * |
| LD_iDose | 13.3 ± 4.4 | 6.7–31.6 | | SD_IMR vs. LD_IMR | 40.0 | n.s |
| LD_IMR | 18.6 ± 5.5 | 6.1–39.7 | | LD_iDose vs. LD_IMR | − 173.0 | * |
| **CNR–GM/WM** | | | | | | |
| SD_iDose | 4.8 ± 1.6 | 0.8–10.6 | < 0.01 | SD_iDose vs. SD_IMR | − 105.0 | * |
| | | | | SD_iDose vs. LD_iDose | 111.0 | * |
| | | | | SD_iDose vs. LD_IMR | − 84.0 | * |
| SD_IMR | 5.9 ± 2.0 | 1.4–15.7 | | SD_IMR vs. LD_iDose | 216.0 | * |
| LD_iDose | 3.8 ± 1.4 | 0.5–10.6 | | SD_IMR vs. LD_IMR | 21.0 | n.s |
| LD_IMR | 5.6 ± 1.9 | 1.2–11.5 | | LD_iDose vs. LD_IMR | − 195.0 | * |

**Table 5.** Results of quantitative image evaluation. Results of quantitative image evaluation using mean ± standard deviation (StdDev) for measurements. Images derived from scanning with standard dose (SD; SD_iDose & SD_IMR) and low dose (LD; LD_iDose & LD_IMR). *n.s* not statistically significant. *Statistically significant.

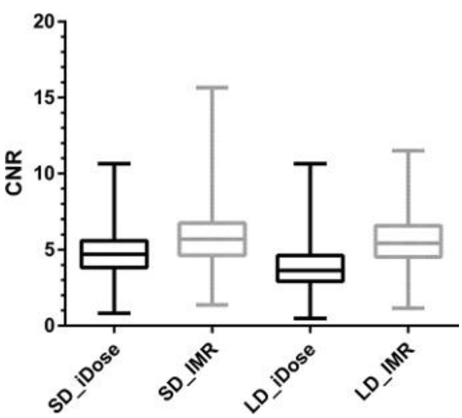


**Figure 3.** Contrast-to-noise ratio (CNR) of gray matter (GM)/white matter (WM) for all included patients. Box plots with minimum-to-maximum whiskers for the CNR of GM/WM using data from scanning with standard dose (SD; SD_iDose & SD_IMR) and low dose (LD; LD_iDose & LD_IMR).

between images using iDose and IMR for both SD imaging (mean ± StdDev: SD_IMR: 4.4 ± 3.1; SD_iDose: 3.5 ± 2.3; $P < 0.0001$) and LD imaging (mean ± StdDev: LD_IMR: 4.6 ± 2.9; LD_iDose: 3.2 ± 2.1; $P < 0.0001$), with application of IMR leading to significantly higher CNR (Fig. 4).

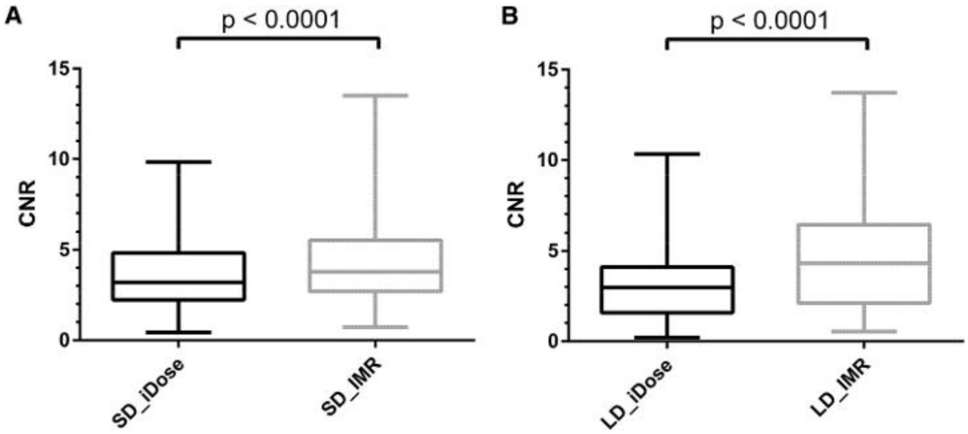


**Figure 4.** Contrast-to-noise ratio (CNR) in patients with ischemic demarcation. Box plots with minimum-to-maximum whiskers for the CNR ischemic demarcation/contralateral healthy parenchyma using data from scanning with standard dose (SD; SD_iDose & SD_IMR; **A**) and low dose (LD; LD_iDose & LD_IMR; **B**).

**Radiation dose.** The mean CTDIvol for SD images amounted to 46.6 ± 1.2 mGy (range: 38.5–47.6 mGy), and it was 31.2 ± 1.8 mGy (range: 20.1–46.8 mGy) for LD images. Correspondingly, the mean DLP amounted to 673.6 ± 48.6 mGy*cm (range: 571.0–857.5 mGy*cm) for SD data and 441.9 ± 33.0 mGy*cm (range: 381.0–666.3 mGy*cm) for LD images. The difference between SD and LD data was statistically significant for the CTDIvol and the DLP, respectively ($P < 0.01$).

## Discussion

Our results indicate higher SNR and CNR for SD as well as LD imaging by non-contrast cerebral MDCT when a model-based iterative algorithm is used for image reconstruction, as compared to a hybrid reconstruction algorithm. This was observed for both unaffected brain parenchyma as well as for demarcated areas due to ischemia in initial SD and follow-up LD imaging, respectively. More specifically, a model-based iterative image reconstruction algorithm could provide better anatomic detail, GM/WM differentiation, and conspicuity of ischemic demarcation for non-enhanced cerebral MDCT using LD imaging. Except for evaluations of GM/WM differentiation using MDCT data acquired with SD and reconstructed with the model-based iterative algorithm, inter-reader agreement was substantial to almost perfect.

Head CT has most commonly been performed at a tube voltage of 120 to 140 kVp[25]. Up to now, the American Association of Physicists in Medicine recommends a peak tube voltage in conventional cerebral CT studies of 120 to 140 kVp, depending on the manufacturer as well as on the system[27]. In accordance with this recommendation, we performed our non-contrast cerebral MDCT scans with a tube voltage of 120 kV while reducing tube currents from 343 mA for SD to 229 mA for LD imaging (exposure of 300 mAs versus 200 mAs). To the best of our knowledge, no studies with comparable low tube currents have been performed in-vivo for cerebral non-enhanced MDCT considering patients with suspected ischemic stroke. In this regard, previous studies on the matter have demonstrated reductions of exposure to values in the range of about 350 mAs to 260 mAs[28,29]. The range of potential relative dose reduction for head CT is thus similar to the range reported throughout the body: paranasal sinus[30], chest[31], coronary arteries[32], and abdomen[33]. As a result of tube current reduction, the image quality was lower for LD compared to SD imaging, but still showed mostly sufficient values for LD MDCT according to our assessments.

The application of fully iterative reconstruction approaches has potential to compensate for increases in image noise and artifacts with tube current reductions to a certain degree[18–20]. Bodelle et al. compared cranial CT scans of 51 patients with infarction performed with either a LD (260 mAs; n = 21) or SD (340 mAs; n = 30) protocol, which were reconstructed with a hybrid reconstruction algorithm as well as FBP considering, amongst other items, the conspicuity of infarcted areas[34]. They concluded that hybrid reconstruction makes possible a dose reduction (− 24%) without relevant constraints regarding imaging of the demarcation of ischemic lesions[34]. Results seem to correspond to those of Bricout et al., who showed that a LD protocol (using a hybrid reconstruction algorithm) enables a significant reduction of radiation dose without relevant image quality impairment as overall image quality was judged as good or excellent in patients with a suspicion of delayed cerebral ischemia after aneurysmal subarachnoid hemorrhage[28]. Ben-David et al. investigated the effect of dose reduction in non-contrast cerebral CT scans with regard to GM/WM contrast by reducing tube voltage from 120 to 80 kV[25]. As in our study they compared two CT scans with different doses acquired for the same patients at two different time points and assessed attenuation, noise, and CNR for different ROIs, concluding that the CNR of GM/WM per dose is increased by 40%[25].

In general, model-based iterative reconstruction algorithms seem to offer higher noise reduction than previously used reconstruction methods[18,35]. For cerebral CT, this is proposed by two studies performed by Inoue and colleagues, who investigated the impact of model-based iterative reconstruction on the accuracy of stroke diagnosis for the posterior fossa and the territory of the middle cerebral artery, comparing 5 mm axial slices of cerebral CT reconstructed with FBP or model-based iterative reconstruction with regard to image noise and

CNR[36,37]. The authors concluded that model-based iterative reconstruction provides a better diagnostic performance as well as a better image quality and improved hypo-attenuation detection in patients with acute stroke as image noise was significantly lower and the difference in CNR between the infarcted and non-infarcted areas was significantly higher for the model-based iterative reconstructions[36,37]. Their results are in accordance with those presented by Iyama et al., who also compared FBP and model-based reconstructions for cerebral CT[38]. They postulated that model-based reconstruction may improve not only the image quality but also the performance for the detection of parenchymal hypo-attenuation in patients with acute ischemic stroke[38]. While these studies investigated previously used FBP but not a more recently applied hybrid approach, Lombardi et al. compared the diagnostic value of a model-based iterative reconstruction algorithm with that of a hybrid algorithm for identifying the hyperdense artery sign as one of the earliest signs of ischemic stroke on non-enhanced CT[39]. The authors found that a model-based iterative approach significantly increased sensitivity in detecting a hyperdense artery sign, offering higher SNR and CNR in comparison with hybrid reconstruction algorithms[39]. Furthermore, Liu et al. evaluated the image quality and lacunar lesion detection of thin-slice head CT images with three different reconstruction algorithms (FBP, hybrid reconstruction, and iterative model-based reconstruction) by comparing routine images with FBP to those with hybrid and iterative model-based reconstructions, analyzing CT attenuation using CNR and noise measurements, an artifact index of the posterior cranial fossa, and subjective analysis of overall image quality[40]. They concluded that iterative model-based reconstruction can lead to better image quality[40]. However, their study excluded patients with ischemic stroke (except for lacunar infarcts), and they did not specifically investigate the impact of tube current reduction in combination with an iterative model-based reconstruction algorithm[40]. Hence, to date we are not aware of another study that compared hybrid versus model-based iterative image reconstruction for non-enhanced cerebral CT in patients with suspected acute stroke and ischemic demarcation. Thus, the results of the present study may provide relevant evidence for significantly improved image quality when using a model-based iterative image reconstruction approach for this very common use case in clinical routine. On the long run, this may potentially allow to decrease the radiation exposure during MDCT scanning even further, with aggravated image noise having greater chances to be compensated for by a model-based iterative approach.

Even though the differences regarding imaging quality and conspicuity of ischemic areas are minor, the inter-reader agreement in the blinded rating of both raters was substantial to almost perfect for most evaluated items and scans, except for evaluations of GM/WM differentiation using SD imaging data with model-based iterative reconstruction. In this regard, previous research has already suggested that the performance of human readers for assessing ischemic demarcation can depend on the algorithm used for MDCT image reconstruction, with a trend towards better agreement for more established reconstruction algorithms (i.e., hybrid algorithms) with the experience of the reader[41]. Thus, a comparable result may be present for ratings of GM/WM differentiation in SD imaging data with model-based iterative reconstruction, which might be interpreted as an analogous trend to higher variation between readers for the more recently introduced model-based iterative image reconstruction algorithm over the more established hybrid algorithm.

There are some limitations to our study. First, this was a retrospective study, and experienced readers might be able to detect whether model-based iterative or hybrid reconstruction was used for image reconstruction in selected cases. However, subjective qualitative and objective quantitative results seem in agreement, supporting potential benefits of iterative model-based reconstructions particularly for LD data. Second, this study only used tube current reduction with two levels for radiation dose reduction and a fixed level of regularization, which was based on a consensus decision at the time of introduction of iterative model-based reconstruction at our institution. Yet, the reconstruction parameters of iterative model-based algorithms can be tuned to improve visibility of objects with a low contrast and to further decrease image noise (e.g., by using other or multiple levels of regularization related to the clinical indication for imaging)[18]. Other approaches such as sparse sampling may be performed in the future on cerebral MDCT data to further exploit possibilities of further radiation dose restrictions. Yet, to date, potential benefits of this technique have been shown for other applications or body regions than non-enhanced cerebral MDCT[42–45]. Third, for ethical reasons, we could not perform a paired study with one patient undergoing two cerebral MDCT exams with different doses at the same time point. Yet, phantom studies that can apply multiple settings within the same scanning session could follow up on the results of this study. Fourth, for the LD examination that was performed up to 10 days after the initial SD exam, any ischemic area would naturally appear with clearer demarcation and would therefore be easier to detect than in the first hours after symptom onset. Importantly, in this study we did not directly compare initial SD to follow-up LD imaging for demarcated areas to avoid bias due to aggravated demarcation over time.

## Conclusion

A model-based iterative image reconstruction algorithm could provide better anatomic detail, GM/WM differentiation, and conspicuity of ischemic demarcation for non-contrast cerebral MDCT using a LD imaging protocol. On a similar note, the CNR of ischemic demarcation/contralateral healthy parenchyma could be improved by model-based iterative image reconstruction. Future studies including advanced acquisition schemes (e.g., sparse sampling) or other approaches for image reconstruction (e.g., fine-tuned iterative model-based reconstructions by using different dedicated regularization levels, or artificial intelligence-based image reconstruction algorithms) could facilitate additional decreases in radiation exposure without clinically relevant impact on image quality and diagnostic use.

Received: 6 July 2021; Accepted: 25 October 2021
Published online: 15 November 2021

## References


1. Bernick, C. *et al.* Silent MRI infarcts and the risk of future stroke: the cardiovascular health study. *Neurology* **57**, 1222–1229. https://doi.org/10.1212/wnl.57.7.1222 (2001).
2. El-Koussy, M., Schroth, G., Brekenfeld, C. & Arnold, M. Imaging of acute ischemic stroke. *Eur. Neurol.* **72**, 309–316. https://doi.org/10.1159/000362719 (2014).
3. Gonzalez, R. G. Current state of acute stroke imaging. *Stroke J. Cereb. Circ.* **44**, 3260–3264. https://doi.org/10.1161/STROKEAHA.113.003229 (2013).
4. Young, J. Y. & Schaefer, P. W. Acute ischemic stroke imaging: a practical approach for diagnosis and triage. *Int. J. Cardiovasc. Imaging* **32**, 19–33. https://doi.org/10.1007/s10554-015-0757-0 (2016).
5. Go, A. S. *et al.* Heart disease and stroke statistics–2013 update: a report from the American Heart Association. *Circulation* **127**, e6–e245. https://doi.org/10.1161/CIR.0b013e31828124ad (2013).
6. Moulin, T. *et al.* Early CT signs in acute middle cerebral artery infarction: predictive value for subsequent infarct locations and outcome. *Neurology* **47**, 366–375. https://doi.org/10.1212/wnl.47.2.366 (1996).
7. Truwit, C. L., Barkovich, A. J., Gean-Marton, A., Hibri, N. & Norman, D. Loss of the insular ribbon: another early CT sign of acute middle cerebral artery infarction. *Radiology* **176**, 801–806. https://doi.org/10.1148/radiology.176.3.2389039 (1990).
8. Kucinski, T. *et al.* Correlation of apparent diffusion coefficient and computed tomography density in acute ischemic stroke. *Stroke J. Cerebr. Circ.* **33**, 1786–1791. https://doi.org/10.1161/01.str.0000019125.80118.99 (2002).
9. Dzialowski, I., Weber, J., Doerfler, A., Forsting, M. & von Kummer, R. Brain tissue water uptake after middle cerebral artery occlusion assessed with CT. *J. Neuroimaging Off. J. Am. Soc. Neuroimaging* **14**, 42–48 (2004).
10. Schriger, D. L., Kalafut, M., Starkman, S., Krueger, M. & Saver, J. L. Cranial computed tomography interpretation in acute stroke: physician accuracy in determining eligibility for thrombolytic therapy. *JAMA* **279**, 1293–1297. https://doi.org/10.1001/jama.279.16.1293 (1998).
11. Barber, P. A., Demchuk, A. M., Zhang, J. & Buchan, A. M. Validity and reliability of a quantitative computed tomography score in predicting outcome of hyperacute stroke before thrombolytic therapy. ASPECTS Study Group. Alberta Stroke Programme Early CT Score. *Lancet* **355**, 1670–1674. https://doi.org/10.1016/s0140-6736(00)02237-6 (2000).
12. Alvarez, R. E. & Macovski, A. Energy-selective reconstructions in X-ray computerized tomography. *Phys. Med. Biol.* **21**, 733–744. https://doi.org/10.1088/0031-9155/21/5/002 (1976).
13. Ogawa, A. *et al.* Randomized trial of intraarterial infusion of urokinase within 6 hours of middle cerebral artery stroke: the middle cerebral artery embolism local fibrinolytic intervention trial (MELT) Japan. *Stroke J. Cerebr. Circ.* **38**, 2633–2639. https://doi.org/10.1161/STROKEAHA.107.488551 (2007).
14. Brenner, D. J. & Hall, E. J. Computed tomography–an increasing source of radiation exposure. *N. Engl. J. Med.* **357**, 2277–2284. https://doi.org/10.1056/NEJMra072149 (2007).
15. Fazel, R. *et al.* Exposure to low-dose ionizing radiation from medical imaging procedures. *N. Engl. J. Med.* **361**, 849–857. https://doi.org/10.1056/NEJMoa0901249 (2009).
16. Richards, P. J. & George, J. Diagnostic CT radiation and cancer induction. *Skeletal Radiol.* **39**, 421–424. https://doi.org/10.1007/s00256-009-0819-2 (2010).
17. Tamm, E. P. *et al.* Quality initiatives: CT radiation dose reduction: how to implement change without sacrificing diagnostic quality. *Radiographics* **31**, 1823–1832. https://doi.org/10.1148/rg.317115027 (2011).
18. Willemink, M. J. & Noel, P. B. The evolution of image reconstruction for CT-from filtered back projection to artificial intelligence. *Eur. Radiol.* **29**, 2185–2195. https://doi.org/10.1007/s00330-018-5810-7 (2019).
19. Willemink, M. J. *et al.* Iterative reconstruction techniques for computed tomography Part 1: technical principles. *Eur. Radiol.* **23**, 1623–1631. https://doi.org/10.1007/s00330-012-2765-y (2013).
20. Willemink, M. J. *et al.* Iterative reconstruction techniques for computed tomography part 2: initial results in dose reduction and image quality. *Eur. Radiol.* **23**, 1632–1642. https://doi.org/10.1007/s00330-012-2764-z (2013).
21. Kalender, W. A., Deak, P., Kellermeier, M., van Straten, M. & Vollmar, S. V. Application- and patient size-dependent optimization of x-ray spectra for CT. *Med. Phys.* **36**, 993–1007. https://doi.org/10.1118/1.3075901 (2009).
22. Pomerantz, S. R. *et al.* Virtual monochromatic reconstruction of dual-energy unenhanced head CT at 65–75 keV maximizes image quality compared with conventional polychromatic CT. *Radiology* **266**, 318–325. https://doi.org/10.1148/radiol.12111604 (2013).
23. Bechara, B. *et al.* Contrast-to-noise ratio difference in small field of view cone beam computed tomography machines. *J. Oral. Sci.* **54**, 227–232. https://doi.org/10.2334/josnusd.54.227 (2012).
24. Rozeik, C. *et al.* Cranial CT artifacts and gantry angulation. *J. Comput. Assist. Tomogr.* **15**, 381–386. https://doi.org/10.1097/00004728-199105000-00007 (1991).
25. Ben-David, E. *et al.* Significance of enhanced cerebral gray-white matter contrast at 80 kVp compared to conventional 120 kVp CT scan in the evaluation of acute stroke. *J. Clin. Neurosci.* **21**, 1591–1594. https://doi.org/10.1016/j.jocn.2014.03.008 (2014).
26. Brooks, R. A., Di Chiro, G. & Keller, M. R. Explanation of cerebral white–gray contrast in computed tomography. *J. Comput. Assist. Tomogr.* **4**, 489–491. https://doi.org/10.1097/00004728-198008000-00016 (1980).
27. Kanal, K. How to develop CT protocols for children. Image gently: the alliance for radiation safety in pediatric imaging. *Sci. Rep.* **2**, 109 (2007).
28. Bricout, N. *et al.* Reduced-dose CT protocol for the assessment of cerebral vasospasm. *Neuroradiology* **57**, 1211–1218. https://doi.org/10.1007/s00234-015-1585-6 (2015).
29. Bodelle, B. *et al.* Acute intracranial hemorrhage in CT: benefits of sinogram-affirmed iterative reconstruction techniques. *AJNR Am. J. Neuroradiol.* **35**, 445–449. https://doi.org/10.3174/ajnr.A3801 (2014).
30. Schulz, B. *et al.* Performance of iterative image reconstruction in CT of the paranasal sinuses: a phantom study. *AJNR Am. J. Neuroradiol.* **34**, 1072–1076. https://doi.org/10.3174/ajnr.A3339 (2013).
31. Pourjabbar, S. *et al.* Dose reduction for chest CT: comparison of two iterative reconstruction techniques. *Acta Radiol* **56**, 688–695. https://doi.org/10.1177/0284185114537256 (2015).
32. Schindler, A. *et al.* Iterative image reconstruction techniques for CT coronary artery calcium quantification: comparison with traditional filtered back projection in vitro and in vivo. *Radiology* **270**, 387–393. https://doi.org/10.1148/radiol.13130233 (2014).
33. Park, M. *et al.* Intraindividual comparison of diagnostic performance in patients with hepatic metastasis of full-dose standard and half-dose iterative reconstructions with dual-source abdominal computed tomography. *Invest. Radiol.* **49**, 195–200. https://doi.org/10.1097/RLI.0000000000000014 (2014).
34. Bodelle, B. *et al.* Iterative reconstruction leads to increased subjective and objective image quality in cranial CT in patients with stroke. *AJR Am. J. Roentgenol.* **205**, 618–622. https://doi.org/10.2214/AJR.15.14389 (2015).
35. Park, H. J. *et al.* Comparison of knowledge-based iterative model reconstruction and hybrid reconstruction techniques for liver CT evaluation of hypervascular hepatocellular carcinoma. *J. Comput. Assist. Tomogr.* **40**, 863–871. https://doi.org/10.1097/RCT.0000000000000455 (2016).
36. Inoue, T. *et al.* Brain computed tomography using iterative reconstruction to diagnose acute middle cerebral artery stroke: usefulness in combination of narrow window setting and thin slice reconstruction. *Neuroradiology* **60**, 373–379. https://doi.org/10.1007/s00234-018-1982-8 (2018).

37. Inoue, T. *et al.* Diagnosis of small posterior fossa stroke on brain CT: effect of iterative reconstruction designed for brain CT on detection performance. *Eur. Radiol.* **27**, 3710–3715. https://doi.org/10.1007/s00330-017-4773-4 (2017).
38. Iyama, Y. *et al.* Iterative reconstruction designed for brain CT: a correlative study with filtered back projection for the diagnosis of acute ischemic stroke. *J. Comput. Assist. Tomogr.* **41**, 884–890. https://doi.org/10.1097/RCT.0000000000000626 (2017).
39. Lombardi, S. *et al.* "Hyperdense artery sign" in early ischemic stroke: diagnostic value of model-based reconstruction approach in comparison with standard hybrid iterative reconstruction algorithm. *Neuroradiology* **60**, 1273–1280. https://doi.org/10.1007/s00234-018-2092-3 (2018).
40. Liu, X. *et al.* Thin-slice brain CT with iterative model reconstruction algorithm for small lacunar lesions detection: Image quality and diagnostic accuracy evaluation. *Medicine (Baltimore)* **96**, e9412. https://doi.org/10.1097/MD.0000000000009412 (2017).
41. Loffler, M. T. *et al.* Improved reliability of automated ASPECTS evaluation using iterative model reconstruction from head CT scans. *J. Neuroimaging Offic. J. Am. Soc. Neuroimaging* **31**, 341–347. https://doi.org/10.1111/jon.12810 (2021).
42. Mookiah, M. R. K. *et al.* Multidetector computed tomography imaging: effect of sparse sampling and iterative reconstruction on trabecular bone microstructure. *J. Comput. Assist. Tomogr.* **42**, 441–447. https://doi.org/10.1097/RCT.0000000000000710 (2018).
43. Sollmann, N. *et al.* Multi-detector CT imaging: impact of virtual tube current reduction and sparse sampling on detection of vertebral fractures. *Eur. Radiol.* **29**, 3606–3616. https://doi.org/10.1007/s00330-019-06090-2 (2019).
44. Sollmann, N. *et al.* Low-Dose MDCT of Patients With Spinal Instrumentation Using Sparse Sampling: Impact on Metal Artifacts. *AJR Am J Roentgenol.* **216**, 1308-1317. https://doi.org/10.2214/AJR.20.23083 (2021).
45. Sollmann, N. *et al.* Effects of virtual tube current reduction and sparse sampling on MDCT-based femoral BMD measurements. *Osteoporos. Int.* **29**, 2685–2692. https://doi.org/10.1007/s00198-018-4675-6 (2018).


## Author contributions

Conception and design: K.J.P., T.B., J.S.K, and N.S. Acquiring data: K.J.P., K.K., and N.S. Analysing data: K.J.P., K.K., and N.S. Drafting manuscript: K.J.P. and N.S. Revising the manuscript: All authors. Approving the final content of the Manuscript: All authors.

## Funding

Open Access funding enabled and organized by Projekt DEAL. We acknowledge support by the B. Braun Foundation (Project No BBST-D-19-00106), Dr.-Ing. Leonhard Lorenz Foundation, and the Joachim Herz Foundation (awarded to N.S.).

## Competing interests

The authors declare no competing interests.

## Additional information

**Correspondence** and requests for materials should be addressed to K.J.P.

**Reprints and permissions information** is available at www.nature.com/reprints.

**Publisher's note** Springer Nature remains neutral with regard to jurisdictional claims in published maps and institutional affiliations.

PATIENT SAFETY

# Lowering the Dose in Head CT Using Adaptive Statistical Iterative Reconstruction

K. Kilic
G. Erbas
M. Guryildirim
M. Arac
E. Ilgit
B. Coskun

FELLOWS' JOURNAL CLUB

**BACKGROUND AND PURPOSE:** While CT has found wide use in medical practice, it is also a substantial source of radiation exposure and is associated with an increased lifetime risk of cancer. There is an urgent need for new approaches to reduce the radiation dose in CT. In this regard, ASIR is an alternative method to FBP. We assessed the effect of ASIR on dose reduction in adult head CT.

**MATERIALS AND METHODS:** We retrospectively evaluated a sample of 149 adult head CT examinations that were divided into 2 groups, STD and LD. We lowered the tube current and used ASIR in the LD group. SNR and CNR were analyzed. Dose parameters were recorded while subjective image noise, sharpness, diagnostic acceptability, and artifacts were graded. The Student *t* test, the Mann-Whitney *U* test, and $\kappa$ statistics were used for statistical analyses.

**RESULTS:** We achieved a dose reduction of 31% in the LD group (STD, 2.3 $\pm$ 0.1 mSv; LD, 1.6 $\pm$ 0.1 mSv; $P < .001$). There was no significant difference in the noise measured in the air between the 2 comparison groups ($P = .273$). Noise in the CSF was higher in the STD group ($P < .001$), while the noise in the WM was higher in the LD group ($P < .001$). Differences in the CNR between groups were insignificant, but the STD group displayed better SNR values. There was no significant difference in the modal scores of diagnostic acceptability ($P = .062$) and the artifacts ($P = .148$) between the 2 groups. Better scores for subjective image noise ($P < .001$) and sharpness ($P = .04$) were observed in the STD group.

**CONCLUSIONS:** ASIR appears to be useful in reducing the dose in adult head CT examinations. While the effect of ASIR on noise reduction observed in the present study of head CT is less than that reported previously in abdomen and chest CT, these findings encourage further prospective studies in larger patient samples.

**ABBREVIATIONS:** ASIR = adaptive statistical iterative reconstruction; CNR = contrast-to-noise ratio; CTDI = CT dose index; $CTDI_{vol}$ = volume CT dose index; $CT_n$ = CT number; DLP = dose-length product; ED = effective dose; FBP = filtered back-projection; GM = gray matter; LD = low dose; SNR = signal-to-noise ratio; STD = standard dose; WM = white matter

With recent advances and availability of biotechnology, CT has become a major source of medical radiation exposure.[1] At present, CT-derived dose accounts for 75% of the dose given at medical imaging. Given the past reports[2] pointing to the major contribution of CT in the increased risk of lifetime cancer associated with medical radiation, there is an urgent need for new approaches to reduce the dose in CT. To date, some of the dose-reduction strategies that have been investigated and proved to be efficient include, for example, in-plane and longitudinal automatic tube-current modulation, lowering tube potential especially in iodinated examinations, bismuth shields, filters, x-ray shutters for over-ranging, increasing detector efficiency, and low-dose techniques.[3-5]

Recently, some of the mathematic methods for reconstruction that have been known since the 1970s have been used for CT research and practice. These methods remove the noise from the image by means of iterations. Notably, iterative reconstruction has been used in positron-emission tomography but could not be implemented in CT until now because calculations required for these methods can only be performed with recently developed high-performance computer processors.

Noise is inversely proportional to the square root of the dose. By lowering image noise, these methods can, conceivably, be used to reduce radiation dose. Indeed, clinical studies supporting this hypothesis have been reported, describing the use of iterative reconstruction methods such as ASIR—a name given by the vendor (GE Healthcare, Milwaukee, Wisconsin)—in abdomen[6-8] and chest CT[9-11] and coronary CT angiography.[12-14] On the other hand and most important, the role of ASIR in head CT has never been reported to date, to our knowledge. The aim of the present study was to assess the effect of ASIR on dose reduction in adult head CT by using a 16-section multidetector row CT scanner. While the reported observations herein derive from a retrospective examination, we submit that they contribute to the emerging knowledge base on the utility of iterative methods to achieve CT dose reduction.

## Materials and Methods

### *Study Description and Patient Sample*

This retrospective study was reviewed and approved by the Gazi University Institutional Review Board.

From July 1, 2010, to August 31, 2010, 149 consecutive patients who underwent head CT with a 16-section multidetector row CT scanner (BrightSpeed, GE Healthcare) were examined retrospectively in the present study.

There were 2 groups of patients: 1) the STD group comprising 51 patients (28 men, 23 women; mean age, 52.0 years; range, 20–

Received November 15, 2010; accepted after revision February 5, 2011.

From the Department of Radiology, School of Medicine, Gazi University, Ankara, Turkey.

Please address correspondence to Koray Kilic, MD, Gazi University School of Medicine, Department of Radiology, 06510 Besevler, Ankara, Turkey; e-mail: koraykilic@yahoo.com

http://dx.doi.org/10.3174/ajnr.A2585

91 years) who went through the STD and standard reconstruction algorithm (FBP) head CT protocol before implementation of ASIR in our protocols; and 2) the LD group comprising 98 patients (44 men, 54 women; mean age, 55.5 years; range, 19–94 years) who were examined with LD and a mixture of ASIR and FBP reconstruction algorithm head CT protocols after implementation of ASIR as a departmental policy.

Only adult patients were examined in the present study because, in our department, different protocols are used for children of different age groups. Hence, our focus on adult patients ensured consistency in the protocol used in the present study sample. Moreover, to have adequate noise measurements, patients with images with severe streak artifacts caused by foreign bodies, metallic surgical materials, and movement of the head were excluded from the study. Emergency patients, who were scanned with a faster helical mode protocol, were also excluded. Only noncontrast studies were included, while patients' follow-up examinations were excluded.

### Scan Protocol

A lateral scout image with 100 kV (peak) and 20 mA was obtained to define the scan area prior to axial imaging. Scanning parameters of the STD group wre 170-mA tube current, 2-second tube-rotation time, 140-kVp tube voltage, $4 \times 2.5$ mm section thickness, 25-cm FOV, a standard reconstruction algorithm for the posterior fossa; and 270-mA tube current, 1-second tube rotation time, 120-kVp tube voltage, $2 \times 5$ mm section thickness, 25-cm FOV, a standard reconstruction algorithm for the cerebrum. A routine reconstruction algorithm of FBP was used. The same protocol except with lowered mA settings (125 mA for the posterior fossa, 190 mA for the cerebrum) and the addition of ASIR (30%) was used in the LD group. Thirty percent ASIR means a blend of 30% ASIR and 70% FBP. ASIR percentage can be selected in a spectrum of 0%–100%, where 0% means all FBPs and 100% means all ASIRs. With the increase in the percentage, noise decreases. At higher levels, contours of the structures begin to blur.[6,11] With the vendor's suggestions (30%–50%) and our initial experience, we chose 30% by consensus in our department.

### Dose Parameters

The $CTDI_{vol}$ and DLP were derived from the result page of each examination, which was automatically prepared by the system. ED (mSv) was estimated by multiplying DLP (mGy.centimeter) by a conversion factor ($0.0021$ mSv $\times$ mGy$^{-1}$ $\times$ cm$^{-1}$).[15]

### Quantitative Analysis

Image noise, defined by a percentage SD of the mean $CT_n$ within a region of interest, was measured in the air, CSF, and WM. A region of interest (60 mm$^2$) was placed in the air on the 3 consecutive sections at the level of the posterior fossa, and an average of the measurement of 3 sections was used for comparison. A place with minimum streak artifacts and maximum 1-cm distance away from the patient was chosen. We measured noise in the CSF in a subgroup of patients (82/98, 84%, LD group; 38/51, 75%, STD group) whose lateral ventricles were suitable for drawing a region of interest of $\geq$15 mm$^2$. A third region of interest of 40 mm$^2$ was placed in the WM at the level of centrum semiovale.

Moreover, the CNR and SNR were analyzed as described in the literature.[16-18] For CNR, 3 regions of interest of 4 mm$^2$ were placed in the WM and 3 regions of interest of 4 mm$^2$ were placed in the GM at the level of centrum semiovale without causing partial volume effects. $CT_n$ and SD values were recorded and averaged for each part. CNR was calculated by using a standard equation: (mean GM $CT_n$ − mean WM $CT_n$)/[(SD GM)$^2$ + (SD WM)$^2$]$^{1/2}$. For SNR, 3 regions of interest of 20 mm$^2$ were placed in the WM at the level of centrum semiovale. $CT_n$ and SD values were recorded and averaged. SNR was calculated by dividing the $CT_n$ by the SD.

### Qualitative Analysis

Examinations were reviewed in a random manner at the same workstation (Advantage Windows 4.4, GE Healthcare) by 2 radiologists working independently (G.E., 10 years' experience; K.K. 8 years' experience) who were blinded to the protocol, ASIR usage, and date. Image noise, sharpness, diagnostic acceptability, and artifacts were graded. A second-year resident (M.G.) helped in the interpretation process by removing all the information on the monitor and anonymizing the patients. Window level (40–60 HU for the posterior fossa, 40–50 HU for the cerebrum) and window width (80–100 for the posterior fossa, 50–70 for the cerebrum) were kept within predefined limits for all images.

Subjective noise was graded on a 4-point scale: 1, little, best noise; 2, optimum noise; 3, noisy but permits evaluation; and 4, too much, which degrades the image so that no information can be gathered.

Sharpness was graded on a 5-point scale according to WM and GM differentiation; visualization of the basal ganglia, pons, and ventricular system; and CSF space around the mesencephalon and over the brain: 1, Structures are well-defined with sharp contours; 2, better seen but contours are not fully sharp; 3, structures can be seen, contours are sharp enough, diagnostic information can be retrieved; 4, structures can be visualized but not enough for diagnostic reporting; contours are blurred; and 5, structures cannot be defined.

Diagnostic acceptability was graded on a 4-point scale: 1, fully acceptable; 2, probably acceptable; 3, only acceptable under limited conditions; and 4, unacceptable. The presence of artifacts was graded on a 4-point scale: 1, no artifacts; 2, minor artifacts; 3, major artifacts; and 4, artifacts that make interpretation impossible. The grading method was constructed around the European Guidelines on Quality Criteria for Computed Tomography.[19]

### Statistical Analysis

We compared the STD and LD groups by using quantitative measurements and qualitative modal scores. For modal score comparison, the average of the scores of the 2 readers was used.

An unpaired Student *t* test was used for continuous variables, and a Wilcoxon rank sum (Mann-Whitney *U*) test was used for categoric variables. A statistically significant difference was $P < .05$. The degree of interobserver agreement was determined by using $\kappa$ statistics (Statistical Package for the Social Sciences, Version 13.0; SPSS, Chicago, Illinois).

## Results

The differences in the ages and number of images were not significant ($P > .05$).

After lowering the tube current, we achieved a significant dose reduction of 26% in the CTDI of the posterior fossa, 35% in the CTDI of the cerebrum, and 31% in the DLP and ED ($P < .001$) (Table 1).

The quantitative and qualitative measures are presented in Table 2.

Noise measured in the air and CSF in the LD group was less than that of in STD group, with insignificant difference in the former ($P = .273$) and a significant difference in the latter

**Table 1: Dose parameters**

| Mean Parameter | STD Group | LD Group | $P$ |
|---|---|---|---|
| $CTDI_{vol}$ posterior fossa (mGy) | 93.49 ± 2.26 | 69.14 ± 1.48 | <.001 |
| $CTDI_{vol}$ cerebrum (mGy) | 59.40 ± 1.44 | 38.55 ± 0.83 | <.001 |
| No. of images | 39.5 ± 2.5 | 39.8 ± 2.7 | .470 |
| DLP (mGy×cm) | 1081.28 ± 66.57 | 748.61 ± 51.78 | <.001 |
| Effective dose (mSv) | 2.3 ± 0.1 | 1.6 ± 0.1 | <.001 |

**Table 2: Quantitative and qualitative measures**

| Mean Measure | STD Group | LD Group | $P$ |
|---|---|---|---|
| Measured noise in the air (HU) | 3.40 ± 0.50 | 3.32 ± 0.43 | .273 |
| Measured noise in the WM (HU) | 3.60 ± 0.33 | 4.07 ± 0.52 | <.001 |
| Measured noise in the CSF (HU) | 3.46 ± 0.48 | 2.92 ± 0.46 | <.001 |
| CNR | 2.29 ± 0.61 | 2.40 ± 0.74 | .349 |
| SNR | 6.77 ± 0.86 | 5.52 ± 0.80 | <.001 |
| Subjective image noise | 1.53 ± 0.50 | 1.86 ± 0.40 | <.001 |
| Sharpness | 1.43 ± 0.45 | 1.63 ± 0.57 | .04 |
| Diagnostic acceptability | 1.16 ± 0.41 | 1.24 ± 0.42 | .062 |
| Artifacts | 2.09 ± 0.30 | 2.02 ± 0.31 | .148 |

($P < .001$). On the other hand, when we measured noise in the WM, we found higher noise values and lower SNR in the LD group than in the STD group ($P < .001$). The difference in the CNR values was insignificant ($P = .349$).

There was no significant difference in the diagnostic acceptability ($P = .062$) and artifacts ($P = .148$) between groups. None of the images of the patients were graded as diagnostically unacceptable. Two patients (1 from the LD group, 1 from the STD group) had scores of 3 (Fig 1), and 2 patients (both from the LD group) had scores of 2.5. The rest of the patients (97%, 95/98, of the LD group; 98%, 50/51, of the STD group) had scores ≤2 (Fig 2). None of the patients had artifacts that impeded evaluation.

Modal scores for subjective image noise ($P < .001$) and sharpness ($P = .04$) were better in the STD group. However, all patients in both groups were considered suitable for reporting, thus having scores of ≤3 for both criteria.

Interobserver agreements were moderate for image noise ($\kappa = 0.556$), sharpness ($\kappa = 0.539$), and diagnostic acceptability ($\kappa = 0.540$) and substantial for artifacts ($\kappa = 0.613$). The differences between the scores of the readers never exceeded 1 in any criteria. The visual scores for both readers are given in Table 3.

## Discussion

With the increasing public awareness of the radiation dose burden of radiologic examinations, dose-reduction strategies for CT have attracted marked interest among the research community. In pursuit of such new approaches to reduce the radiation dose in CT, relatively old iterative reconstruction algorithms have been increasingly revisited in this research field. Most of the scanners that are in use currently have analytic reconstruction algorithms called "FBP." While FBP is fast as an algorithm, it is also sensitive to noise and artifacts because it ignores the system optics and statistical fluctuations of photons. On the other hand, with iterative reconstruction methods, the focal spot size, image voxel, and detector size (namely system optics) are taken into consideration.[7,20]

Iterative reconstruction starts with an initial estimate and forward projection. Subsequently, this projection is updated to minimize the difference between the actual image and the forward projection. Photon statistics are also put into this estimation, updating flow. Abnormal measurements, which are deviated far from the adjacent ones, are considered statistical fluctuations and are removed. This process is repeated until the difference between the successive iterations gets smaller. The largest part of the extensive calculations required is mostly for the modeling of the system optics. On the other hand, the modeling of system statistics is not as demanding as the modeling of system optics. The reconstruction algorithm used in our system (ASIR) deals only with the system statistics; by doing so, it allows faster reconstruction.[7,20]

The vendors tend to implement their own iterative image reconstruction methods to achieve dose reduction without image-quality degradation (GE: ASIR; Siemens, Erlangen, Germany: Iterative Reconstruction in Image Space[21-23]; Toshiba Medical Systems, Tokyo, Japan: Adaptive Iterative Dose Reduction; and Philips Healthcare, Best, the Netherlands: iDose.[24] With these methods, 30%–80% dose reduction is expected.

By adapting ASIR into our protocols, we observed a reduction in the head CT dose by 31% in the LD group without compromising the CNR and diagnostic acceptability. Similar reductions were reported in abdomen CT by Hara et al (29%–65%),[6] Prakash et al (25.1%),[7] and Sagara et al (33%)[8] and in chest CT by Prakash et al (27.6%).[10] Notably, Flicek et al[25] were able to reduce the dose by 50% in their study, in which they compared an STD supine set with an LD prone set with ASIR in a CT colonoscopy examination without degrading image quality.

We achieved different levels of noise reduction across the image plane. Noise measurements in the air revealed insignificant differences between the LD and STD groups. We found lower noise levels in the CSF of the LD group than of the STD group. However, unlike the above-mentioned studies, with these reduced levels of dose, WM measurements (noise and SNR) and visual scores of noise were better in the STD group. Our results were in concordance with those of Marin et al.[26] By using the noise power spectrum curve, they showed that the effect of ASIR on the noise reduction was more noticeable in the smoother areas than in the grainy areas. In light of these findings, we propose that less aggressive noise reduction (<30%) should be aimed at head CT examinations if keeping the noise at routine levels is desired. Because 97% (95/98) of the examinations in the LD group were considered fully or probably acceptable for diagnosis, we have kept using LD settings as our routine head CT protocol.

We observed better image sharpness scores in the STD group than in the LD group. Sagara et al[8] also reported the same finding without affecting the diagnostic acceptability. We attributed this to the oversmoothing effect of ASIR as well as to the noise. At higher levels of ASIR, contours of structures begin to blur and sharpness decreases.[6] Even if we chose a low ASIR percentage (30%), we could not prevent the sharpness from degrading.

Minor artifacts seen in both groups were expected such as beam-hardening artifacts at the posterior fossa. Higher tube settings were used in the posterior fossa to decrease the magnitude of artifacts. We did not observe any artifacts in either group that made interpretation impossible.

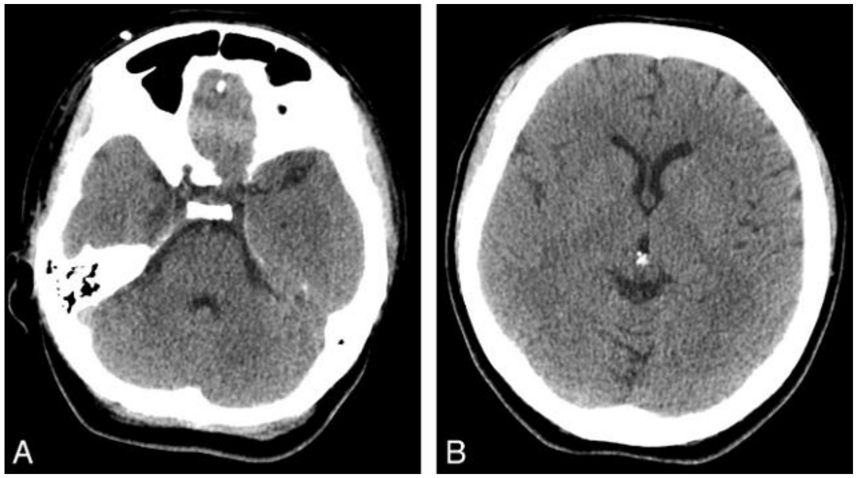


**Fig 1.** Axial images of a 34-year-old woman with normal findings at the level of the posterior fossa (*A*) and basal ganglia (*B*). The patient belongs to the LD group (DLP, 832 mGy×cm). Note that the WM and GM differentiation is decreased. This is 1 of the 2 examinations that are considered diagnostically acceptable only under limited conditions (score of 3 for diagnostic acceptability criterion).

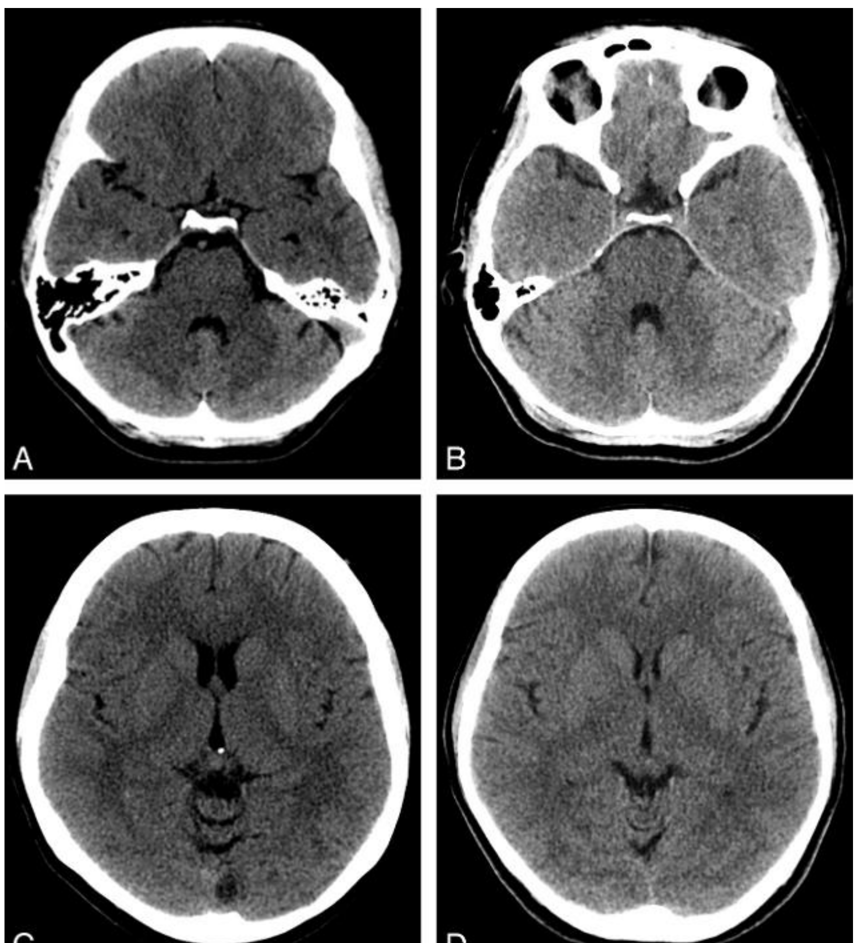


**Fig 2.** Axial images of a 45-year-old woman (*A* and *C*) from the STD group (DLP, 1100 mGy×cm) and a 37-year-old man (*B* and *D*) from the LD group (DLP, 713 mGy×cm) are compared. Both examinations have good WM and GM differentiation and are considered fully acceptable (score of 1 for diagnostic acceptability criterion). *A* and *B*, Posterior fossa. *C* and *D*, Basal ganglia.

There are limitations to our study. First, we disregarded patients with images with severe artifacts caused by foreign bodies, metallic surgical materials, and movement of the head, which might have also been compared. They were too small in number for a healthy comparison to be made; thus, larger series are needed. Second, we used a small region of interest (60 $mm^2$ for air and 40 $mm^2$ for WM). This could not be prevented because of a lack of space in and around the cranium. Therefore, to overcome this, we made measurements on 3 consecutive sections and averaged them. Third, we did

**Table 3: Visual scores for readers 1 and 2**

| Mean of Criteria | Reader 1 STD Group | Reader 1 LD Group | Reader 2 STD Group | Reader 2 LD Group |
|---|---|---|---|---|
| Subjective image noise | 1.53 ± 0.58 | 1.92 ± 0.42 | 1.53 ± 0.58 | 1.81 ± 0.47 |
| Sharpness | 1.45 ± 0.50 | 1.65 ± 0.56 | 1.41 ± 0.50 | 1.57 ± 0.56 |
| Diagnostic acceptability | 1.16 ± 0.42 | 1.28 ± 0.51 | 1.16 ± 0.42 | 1.21 ± 0.44 |
| Artifacts | 2.06 ± 0.31 | 2.02 ± 0.38 | 2.12 ± 0.33 | 2.01 ± 0.30 |

not verify our results with different scanning and reconstruction settings. Our findings should be validated on a head phantom and should be correlated with different detector configurations. Fourth, we did not assess the diagnostic accuracy or the effect of ASIR on the different disease subgroups in this study. Larger prospective series are warranted for this.

For the future studies, ASIR can be used in conjunction with other dose-reduction methods, such as automatic tube-current modulation. Smith et al[5] proposed that automatic tube-current modulation could be used as an effective dose-reduction tool for head CT. Therefore, when incorporated with ASIR, more dose reduction would be possible. In addition, although we did not assess the diagnostic accuracy or the effect of ASIR on the different disease subgroups in the present study with a limited sample size, we suggest that future studies in a larger sample might consider such further stratified analyses.

## Conclusions

ASIR appears to reduce the dose in adult head CT examinations performed on a 16-section multidetector row CT scanner without compromising the diagnostic acceptability. While the effect of ASIR on the noise reduction observed in the present study of head CT is less than that reported previously in abdomen and chest CT, these findings encourage further prospective studies in larger patient samples.

## References


1. Hall EJ, Brenner DJ. **Cancer risks from diagnostic radiology.** *Br J Radiol* 2008;81:362–78
2. Brenner DJ, Hall EJ. **Computed tomography: an increasing source of radiation exposure.** *N Engl J Med* 2007;357:2277–84
3. Gunn MLD, Kohr JR. **State of the art: technologies for computed tomography dose reduction.** *Emerg Radiol* 2010;17:209–18
4. Rogalla P, Kloeters C, Hein PA. **CT technology overview: 64-slice and beyond.** *Radiol Clin North Am* 2009;47:1–11
5. Smith B, Dillon WR, Gould R, et al. **Radiation dose-reduction strategies for neuroradiology CT protocols.** *AJNR Am J Neuroradiol* 2007;28:1628–32
6. Hara AK, Paden RG, Silva AC, et al. **Iterative reconstruction technique for reducing body radiation dose at CT: feasibility study.** *AJR Am J Roentgenol* 2009;193:764–71
7. Prakash P, Kalra MK, Kambadakone AK, et al. **Reducing abdominal CT radiation dose with adaptive statistical iterative reconstruction technique.** *Invest Radiol* 2010;45:202–10
8. Sagara Y, Hara AK, Pavlicek W, et al. **Abdominal CT: comparison of low-dose CT with adaptive statistical iterative reconstruction and routine-dose CT with filtered back projection in 53 patients.** *AJR Am J Roentgenol* 2010;195:713–19
9. Prakash P, Kalra MK, Ackman JB, et al. **Diffuse lung disease: CT of the chest with adaptive statistical iterative reconstruction technique.** *Radiology* 2010;256:261–69
10. Prakash P, Kalra MK, Digumarthy SR, et al. **Radiation dose reduction with chest computed tomography using adaptive statistical iterative reconstruction technique: initial experience.** *J Comput Assist Tomogr* 2010;34:40–45
11. Yanagawa M, Honda O, Yoshida S, et al. **Adaptive statistical iterative reconstruction technique for pulmonary CT: image quality of the cadaveric lung on standard- and reduced-dose CT.** *Acad Radiol* 2010;17:1259–66
12. Heilbron BG, Leipsic J. **Submillisievert coronary computed tomography angiography using adaptive statistical iterative reconstruction: a new reality.** *Can J Cardiol* 2010;26:35–36
13. Leipsic J, Labounty TM, Heilbron B, et al. **Adaptive statistical iterative reconstruction: assessment of image noise and image quality in coronary CT angiography.** *AJR Am J Roentgenol* 2010;195:649–54
14. Gosling O, Loader R, Venables P, et al. **A comparison of radiation doses between state-of-the-art multislice CT coronary angiography with iterative reconstruction, multislice CT coronary angiography with standard filtered back-projection and invasive diagnostic coronary angiography.** *Heart* 2010;96:922–26
15. American Association of Physicists in Medicine. **The measurement, reporting, and management of radiation dose in CT: report of AAPM Task Group 23 of the Diagnostic Imaging Council CT Committee.** AAPM report no. 96; 2008. http://www.aapm.org/pubs/reports/rpt_96.pdf. Accessed November 20, 2010
16. Mullins ME, Lev MH, Bove P, et al. **Comparison of image quality between conventional and low-dose nonenhanced head CT.** *AJNR Am J Neuroradiol* 2004;25:533–38
17. Udayasankar UK, Braithwaite K, Arvaniti M, et al. **Low-dose nonenhanced head CT protocol for follow-up evaluation of children with ventriculoperitoneal shunt: reduction of radiation and effect on image quality.** *AJNR Am J Neuroradiol* 2008;29:802–06
18. Murakami Y, Kakeda S, Kamada K, et al. **Effect of tube voltage on image quality in 64-section multidetector 3D CT angiography: evaluation with a vascular phantom with superimposed bone skull structures.** *AJNR Am J Neuroradiol* 2010;31:620–25
19. Bongartz G, Golding SJ, Jurik AG, et al, for the European Study Group of Radiologists and Physicists. **European guidelines on quality criteria for computed tomography.** EUR 16262 EN; 1999. http://www.drs.dk/guidelines/ct/quality/mainindex.htm. Accessed November 20, 2010
20. Silva AC, Lawder HJ, Hara A, et al. **Innovations in CT dose reduction strategy: application of the adaptive statistical iterative reconstruction algorithm.** *AJR Am J Roentgenol* 2010;194:191–99
21. Pontana F, Pagniez J, Flohr T, et al. **Chest computed tomography using iterative reconstruction vs filtered back projection. Part 1. Evaluation of image noise reduction in 32 patients.** *Eur Radiol* 2011;21:627–35. Epub 2010 Nov 5
22. Pontana F, Duhamel A, Pagniez J, et al. **Chest computed tomography using iterative reconstruction vs filtered back projection. Part 2. Image quality of low dose CT examinations in 80 patients.** *Eur Radiol* 2011;21:636–43. Epub 2010 Nov 16
23. Bittencourt MS, Schimdt B, Seltman M, et al. **Iterative reconstruction in image space (IRIS) in cardiac tomography: initial experience.** *Int J Cardiovasc Imaging* 2010 Dec 1. [Epub ahead of print]
24. Lee T, Chhem RK. **Impact of new technologies on dose reduction in CT.** *Eur J Radiol* 2010;76:28–35
25. Flicek KT, Hara AK, Silva AC, et al. **Reducing the radiation dose for CT colonography using adaptive statistical iterative reconstruction: a pilot study.** *AJR Am J Roentgenol* 2010;195:126–31
26. Marin D, Nelson RC, Schindera ST, et al. **Low-tube-voltage, high-tube-current multidetector abdominal CT: improved image quality and decreased radiation dose with adaptive statistical iterative reconstruction algorithm—initial clinical experience.** *Radiology* 2010;254:145–53